LBL-25824 c.2

RECEIVED
LAWRENCE
BERKELEY LABORATORY

JUN 14 1989

LIBRARY AND
DOCUMENTS SECTION

Center for Advanced Materials

CAM

The Role of Adatoms (C,S) and Surface Structure in Thiophene Hydrodesulfurization over Transition Metal Surfaces: A Surface Science and Catalytic Study

M.E. Bussell
(Ph.D. Thesis)

August 1988

TWO-WEEK LOAN COPY

This is a Library Circulating Copy
which may be borrowed for two weeks.

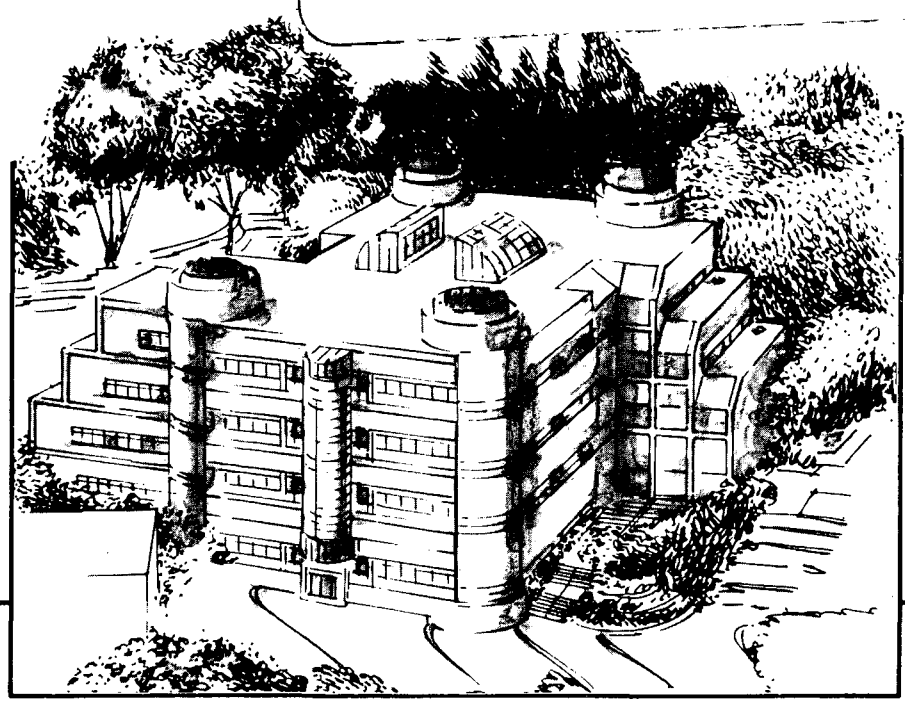

Materials and Chemical Sciences Division

Lawrence Berkeley Laboratory • University of California

ONE CYCLOTRON ROAD, BERKELEY, CA 94720 • (415) 486-4755

Prepared for the U.S. Department of Energy under Contract DE-AC03-76SF00098

LBL-25824 c.2

DISCLAIMER

This document was prepared as an account of work sponsored by the United States Government. While this document is believed to contain correct information, neither the United States Government nor any agency thereof, nor the Regents of the University of California, nor any of their employees, makes any warranty, express or implied, or assumes any legal responsibility for the accuracy, completeness, or usefulness of any information, apparatus, product, or process disclosed, or represents that its use would not infringe privately owned rights. Reference herein to any specific commercial product, process, or service by its trade name, trademark, manufacturer, or otherwise, does not necessarily constitute or imply its endorsement, recommendation, or favoring by the United States Government or any agency thereof, or the Regents of the University of California. The views and opinions of authors expressed herein do not necessarily state or reflect those of the United States Government or any agency thereof or the Regents of the University of California.

LBL-25824

THE ROLE OF ADATOMS (C,S) AND SURFACE STRUCTURE IN THIOPHENE HYDRODESULFURIZATION OVER TRANSITION METAL SURFACES: A SURFACE SCIENCE AND CATALYTIC STUDY

Mark Edward Bussell
Ph.D. Thesis

Department of Chemistry
University of California at Berkeley
and
Center for Advanced Materials
Materials and Chemical Sciences Division
Lawrence Berkeley Laboratory
Berkeley, California 94720

August, 1988

This work was supported by the Director, Office of Energy Research, Office of Basic Energy Sciences, Chemical Sciences Division, of the U.S. Department of Energy under Contract No. DE-AC03-76SF00098.

The Role of Adatoms (C, S) and Surface Structure in Thiophene Hydrodesulfurization over Transition Metal Surfaces: A Surface Science and Catalytic Study

Mark Edward Bussell

Department of Chemistry
University of California
and
Materials and Chemical Sciences Division
Lawrence Berkeley Laboratory
Berkeley, California 94720

Abstract

Thiophene Hydrodesulfurization (HDS) has been studied over transition metal single crystal (Mo, Re) and polycrystalline foil (Co, Mo, Re) surfaces using a combined ultrahigh vacuum/catalytic reactor apparatus. The metal surfaces were cleaned, modified and characterized in ultrahigh vacuum (1×10^{-9} Torr) prior to high pressure (1 atm) catalytic reactions carried out in an in-situ isolation cell. The influence of catalyst surface structure on thiophene HDS was investigated by carrying out reactions over surfaces of different crystallographic orientation and the role of adsorbates examined using radiotracer ^{14}C and ^{35}S isotopes.

Thiophene HDS is a structure insensitive reaction over molybdenum surfaces, but a structure sensitive reaction over rhenium surfaces. The HDS reaction over

molybdenum occurs on a strongly bound adsorbate overlayer composed primarily of carbidic carbon. In contrast, HDS of thiophene over rhenium surfaces occurs directly on the metal surface. The ability of the rhenium surfaces to remain free of strongly bound deposits of carbon and/or sulfur makes them more active (by a factor of 1-6 times) than the molybdenum surfaces studied. For both metals, deactivation at high conversions is caused by product inhibition (H_2S).

Thiophene HDS studies over Co, Mo and Re foils reveal a trend in catalytic activity similar to that found in the literature for the sulfides of these metals. This suggests that metal single crystals and polycrystalline foils are suitable catalysts for model studies of HDS.

Contents

List of Figures vi

List of Tables x

Acknowledgements xi

1 Introduction 1

1.1 General Introduction 1

1.2 The Hydrodesulfurization Process 2

1.3 Catalytic and Bulk Structure Studies of Hydrodesulfurization . . . 6

1.4 Surface Science Studies of Hydrodesulfurization on Single Crystal Surfaces 14

1.5 Combined Surface Science and Catalytic Studies of Hydrodesulfurization 19

2 Experimental Methods 23

2.1 Introduction 23

2.2 Ultrahigh Vacuum Surface Analysis/Catalytic Reactor System . . 23

2.2.1 Ultrahigh Vacuum Chamber 26

2.2.2 Sample Manipulator and High Pressure Isolation Cell . . . 27

2.2.3 Catalytic Reactor System 30

2.2.4 Electrochemical Sulfur Source 30
2.3 Surface Analytical Techniques 32
2.3.1 Auger Electron Spectroscopy 35
2.3.2 Low Energy Electron Diffraction 44
2.4 Detection of Radiotracer ^{14}C and ^{35}S Overlayers 50
2.5 Materials 53
2.5.1 Single Crystals and Polycrystalline Foils 53
2.5.2 Reagents 56
2.5.3 Radioactively Labelled Reagents 57
2.6 Procedures 58
2.6.1 Sample Cleaning 58
2.6.2 Preparation of Carbon and Sulfur Overlayers 59
2.6.3 Preparation of ^{35}S and ^{14}C Labelled Overlayers 60
2.6.4 High Pressure Reactions 61

3 Structure of Clean and Adsorbate (C, S) covered Molybdenum and Rhenium Single Crystal Surfaces 65

3.1 Introduction 65
3.2 Structure of Clean Mo and Re Surfaces 66
3.3 Structure of Carbon and Sulfur Overlayers on the Mo(100) Single Crystal Surface 72
3.3.1 Carbon on Mo(100) 72
3.3.2 Sulfur on Mo(100) 75
3.3.3 STM Study of the p(2×1) Mo(100)–S System 78
3.4 Structure of Carbon and Sulfur Overlayers on the Re(0001) and Re(10$\bar{1}$0) Single Crystal Surfaces 83

3.4.1 Carbon on Re(0001) 84
3.4.2 Carbon on Re($10\bar{1}0$) 86
3.4.3 Sulfur on Re(0001) 86
3.4.4 Sulfur on Re($10\bar{1}0$) 91
3.5 Discussion 91

4 Thiophene Hydrodesulfurization over Molybdenum Single Crystal Surfaces 95

4.1 Introduction 95
4.2 Thiophene HDS over Initially Clean Mo Surfaces 96
4.3 Thiophene HDS over sulfided Mo(100) Surfaces 99
4.3.1 Effect of Adsorbed Sulfur on HDS Activity 99
4.3.2 Radiotracer (^{35}S) Labelling Studies 99
4.4 Thiophene HDS over Carbided Mo(100) Surfaces 109
4.4.1 Effect of Adsorbed Carbon on HDS Activity 109
4.4.2 Radiotracer (^{14}C) Labelling Studies 111
4.5 The Influence of Products (H_2S, cis-2-butene) on HDS Activity of Mo(100) Surfaces 118
4.6 Discussion 118
4.6.1 Thiophene Hydrodesulfurization over Clean Molybdenum Single Crystal Surfaces 120
4.6.2 The Role of Adsorbed Sulfur in Thiophene HDS over the Mo(100) Surface 122
4.6.3 Evidence that the Active Surface is Covered with Adsorbed Carbon 128

4.6.4 Explanation of the Different Effects of C and S on Thiophene HDS over the Mo(100) Surface 129
4.6.5 Hydrogenation of Adsorbed Carbon and Sulfur on the Mo(100) Surface: The Effect of Hydrocarbons 131
4.6.6 Deactivation of the Mo(100) Surface at High Conversions . 134
4.6.7 Nature of the Active Site for Thiophene HDS on Mo(100) . 135

5 Thiophene Hydrodesulfurization over Rhenium Surfaces 138

5.1 Introduction 138
5.2 Thiophene HDS over Initially Clean Rhenium Surfaces 140
5.3 Thiophene HDS over Sulfided Rhenium Single Crystal Surfaces . . 150
5.4 Thiophene HDS over Carbon Covered Rhenium Single Crystal Surfaces 150
5.5 The Influence of Products (H_2S, cis-2-butene) on the HDS Activity of a Rhenium Foil 153
5.6 Discussion 155
5.6.1 Thiophene HDS over Initially Clean Rhenium Surfaces . . . 155
5.6.2 Effect of Adsorbed Sulfur on HDS Activity 158
5.6.3 Effect of Adsorbed Carbon on HDS Activity 160
5.6.4 Deactivation of a Rhenium Foil at High Conversions 164
5.6.5 Kinetics and Mechanism of Thiophene HDS over Rhenium Surfaces 164
5.6.6 Explanation of the Structure Sensitivity 166

6 Thiophene Hydrodesulfurization over Transition Metal Foils 172

6.1 Introduction 172
6.2 Thiophene HDS over Co, Mo and Re Foils 174

6.3 Discussion 176

6.3.1 Trend of HDS Activities of Co, Mo and Re foils 176

6.3.2 Importance of Surface Defects in Thiophene HDS over Metal Surfaces 177

List of Figures

1.1 Chemical structures of thiophene and dibenzothiophene 3

1.2 Hydrodesulfurization of thiophene 4

1.3 Structure of molybdenum disulfide. 7

1.4 Schematic drawing of MoS_2 platelets on Al_2O_3 8

1.5 Schematic drawing of a Co-Mo/Al_2O_3 catalyst 9

1.6 Proposed mechanisms for thiophene HDS 13

1.7 Decomposition pathways of thiophene on Mo(100) 16

2.1 Photograph of the UHV surface analysis/catalytic reactor system. 24

2.2 Schematic drawing of the UHV surface analysis/catalytic reactor system. 25

2.3 Photograph of the manipulator and high pressure cell. 28

2.4 Schematic drawing of the manipulator and high pressure cell. . . . 29

2.5 Schematic drawing of the batch reactor used for HDS reactions. . . 31

2.6 Schematic diagram of sulfur source 33

2.7 Mean free paths of electrons in solids 34

2.8 Energy distribution of scattered electrons 36

2.9 De-excitation pathways for ions with core holes 38

2.10 Retarding field analyzer for AES 40

2.11 AES spectra of the Mo(100) surface 41

2.12 AES spectra of the Re(0001) surface 42
2.13 AES lineshapes for carbon 45
2.14 Schematic diagram of a LEED experiment 47
2.15 LEED pattern of S on Mo(100) 49
2.16 Schematic diagram of the β^- detector 52
2.17 Drawing of the β^- detector mounting flange 54
2.18 β^- spectrum from ^{14}C on Mo(100) 55

3.1 Perspective drawings of Mo surfaces 67
3.2 Top view drawings of Mo surfaces 68
3.3 Perspective drawings of Re surfaces 69
3.4 Top view drawings of Re surfaces 70
3.5 Schematic drawing of C and S on Mo(100) 73
3.6 AES calibration of C on Mo(100) 74
3.7 Carbon AES peak shapes on Mo(100) 76
3.8 AES spectra of p(2×1) Mo(100)–S system 79
3.9 LEED patterns of p(2×1) Mo(100)–S system 80
3.10 An STM image of the p(2×1) Mo(100)–S surface 81
3.11 Models proposed for the p(2×1) structure 82
3.12 Carbon AES peak shapes on Re(0001) 85
3.13 Carbon AES peak shapes on Re(10$\bar{1}$0) 87
3.14 AES spectra of Re(0001) covered with 0.5 ML of sulfur 89
3.15 LEED patterns of Re(0001) covered with 0.5 ML of sulfur 90

4.1 Thiophene HDS activities of Mo Surfaces 97
4.2 Product accumulation curves for thiophene HDS over Mo(100) . . 98
4.3 Effect of adsorbed sulfur on HDS Activity 100

4.4 ^{35}S hydrogenation on Mo(100) 102
4.5 Temperature dependence of sulfur hydrogenation 103
4.6 Hydrogen pressure dependence of sulfur hydrogenation 104
4.7 Coverage dependence of sulfur hydrogenation 105
4.8 Temperature dependence of ^{35}S removal in HDS conditions 107
4.9 Pressure dependencies of ^{35}S removal in HDS conditions 108
4.10 Thiophene HDS over carbided Mo(100) 110
4.11 HDS Activity of Mo(100) surfaces of different composition 112
4.12 Carbon hydrogenation on Mo(100) 113
4.13 H_2 pressure dependence of carbon hydrogenation on Mo(100) . . . 115
4.14 ^{14}C removal under HDS conditions 116
4.15 ^{14}C removal in different gas mixtures 117
4.16 Effect of products on HDS activity 119
4.17 Comparison of rates of ^{35}S removal and thiophene HDS 125
4.18 Thiophene desulfurization mechanisms 126

5.1 HDS activities of Re surfaces 141
5.2 Product accumulation curves for thiophene HDS over Re(0001) . . 142
5.3 Temperature dependence of HDS over rhenium 144
5.4 Arrhenius plot of individual products 145
5.5 Dependence of the HDS rate on thiophene pressure 146
5.6 Dependence of the HDS rate on hydrogen pressure 147
5.7 Thiophene partial pressure dependence of the individual products . 148
5.8 Hydrogen partial pressure dependence of the individual products . 149
5.9 Effect of C and S on HDS over Re(0001) 151
5.10 Effect of C and S on HDS over Re($10\bar{1}0$) 152

5.11 Effect of annealing temperature on the HDS activity of carbon covered Re(0001) 154

5.12 Effect of products on HDS over a Re foil 156

5.13 Correlation of HDS activity with coordination number 168

6.1 HDS activities of Co, Mo and Re foils 175

List of Tables

1.1 Sulfur Content of Various Crude Oils 3

1.2 Thermodynamic Data for Thiophene HDS 5

2.1 Beta Emission Data for ^{14}C and ^{35}S 51

2.2 Reagents Used in this Research 56

2.3 Retention Times of Thiophene and its HDS Products 62

3.1 Surface Atomic Densities 71

3.2 AES Attenuation Factors for C and S on Rhenium 83

4.1 Product Distributions for Mo(100) and MoS_2 121

5.1 Comparison of Product Distributions 143

6.1 Comparison of Product Distributions 174

6.2 Comparison of HDS acitivites 176

Acknowledgments

In the five years since I graduated from college I often thought that this day would never come and it is only with the help of many people that it has. I would like to thank my advisor, Professor Gabor Somorjai, for giving me the freedom to make my own decisions (and mistakes) with timely advice to keep me moving in the right direction (France). Stimulating collaboration with Andrew Gellman, David Kelly and Colette Knight helped to make each day an "adventure in science". I would especially like to thank Miquel Salmeron and Bruno Marchon for the opportunity to work with them on the scanning tunnelling microscopy project. Additional thanks go to Jim Powers, Kevin Williams, Raymond Hadden, Colette Knight and Roger Nix for critical reading of this thesis.

On the personal side, I would like to thank everyone in the Somorjai Group for their friendship and interesting conversations. The opportunity to work with people from all over the world and from different cultures is something I will always cherish. Lastly and most importantly, I would like to thank my wife, Tamsin, and the rest of my family for their constant love and support.

Chapter 1

Introduction

1.1 General Introduction

The concept of catalysis was first considered by Berzelius in 1836 when he observed that certain substances accelerate chemical reactions without undergoing a visible chemical change [1]. In the mid 1870's, heterogeneous catalysis was first introduced into industrial practice with the use of platinum metal as a catalyst for the oxidation of sulfur dioxide (SO_2) to sulfur trioxide (SO_3), a precursor to sulfuric acid [2]. Since that time, heterogeneous catalysis has played an integral role in the chemical and petroleum industries, yet the development of catalysts has been largely empirical. The advent of ultrahigh vacuum technology over the last twenty years has made available a wealth of techniques for examining catalyst surfaces at the atomic level. Using these techniques, many advances have been made on understanding the role of surface structure and composition in determining the properties of catalysts [3]. The focus of this thesis project has been to investigate an industrially important process, hydrodesulfurization, which employs complex heterogenous catalysts. In this work, the techniques of surface science and catalysis have been used together to study the molecular level surface chemistry of the thiophene hydrodesulfurization reaction.

1.2 The Hydrodesulfurization Process

Hydrodesulfurization (HDS) is a catalytic process in which sulfur containing compounds in crude oil are treated with hydrogen to produce hydrocarbons and hydrogen sulfide (H_2S).

$$sulfur\ \ compound \quad + \quad x\ H_2 \longrightarrow hydrocarbon \quad + \quad H_2S$$

Hydrogen Sulfide is readily removed from the product stream and converted to elemental sulfur via the Claus process. In this process, a fraction of the H_2S is oxidized by reaction with air, and then reacted with the remaining H_2S to give elemental sulfur and water.

$$2\ H_2S \quad + \quad SO_2 \longrightarrow 3\ S\downarrow \quad + \quad 2\ H_2O$$

Sulfur must be removed from crude oil for a number of reasons. Most importantly, sulfur poisons noble metal catalysts used to convert crude oil to gasoline and therefore sulfur levels must be reduced to one part per million or less ($\leq$ 1 ppm) before the oil is passed over the sulfur-sensitive catalysts. In addition, high sulfur contents in motor fuels deleteriously affect the stability, color, odor and corrosion properties of the fuels. Finally, it has become increasingly important to lower emissions of sulfur dioxide (SO_2) into the atmosphere. This sulfur dioxide originates from the combustion of hydrocarbon fuels and the regeneration of sulfur contaminated catalysts by the burning of coke deposits and has been implicated as a precursor to "acid rain". In the last few years, the harmful effects of acid rain on the environment have increased at an alarming rate resulting in severely damaged forests, lakes and soil.

The decline of petroleum feedstocks has necessitated processing crude oils containing greater amounts of sulfur and other impurities (S, N, metals). Typical sulfur contents of crude oils currently available are shown in Table 1.1 [2]. Sulfur

Table 1.1: Sulfur Content of Various Crude Oils

Crude Oil	*Sulfur Content (wt %)*
Light Arabian crude	1.5
Kuwait Crude	2.5-4.
Mid-continent U. S. crude	0.2-2.5
Venezuelan crude	2-4

is present in crude oil primarily in the form of thiols (R-SH), sulfides (R-S-R′), disulfides (R-S-S-R′), thiophenes and thiophene derivatives. Thiophene is the simplest aromatic compound containing sulfur and is shown in Figure 1.1 along with dibenzothiophene. Thiophene and its derivatives are the most difficult sulfur com-

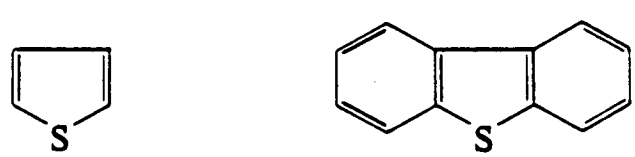

(a) (b)

Figure 1.1: Chemical structures of (a) thiophene and (b) dibenzothiophene.

pounds to desulfurize and are therefore used most often in catalytic studies of HDS.

Concentrating on thiophene, the test molecule used in this work, it is seen in Figure 1.2 that hydrodesulfurization involves the selective cleavage of the C-S bonds and hydrogenation to produce H_2S and C_4 hydrocarbons.

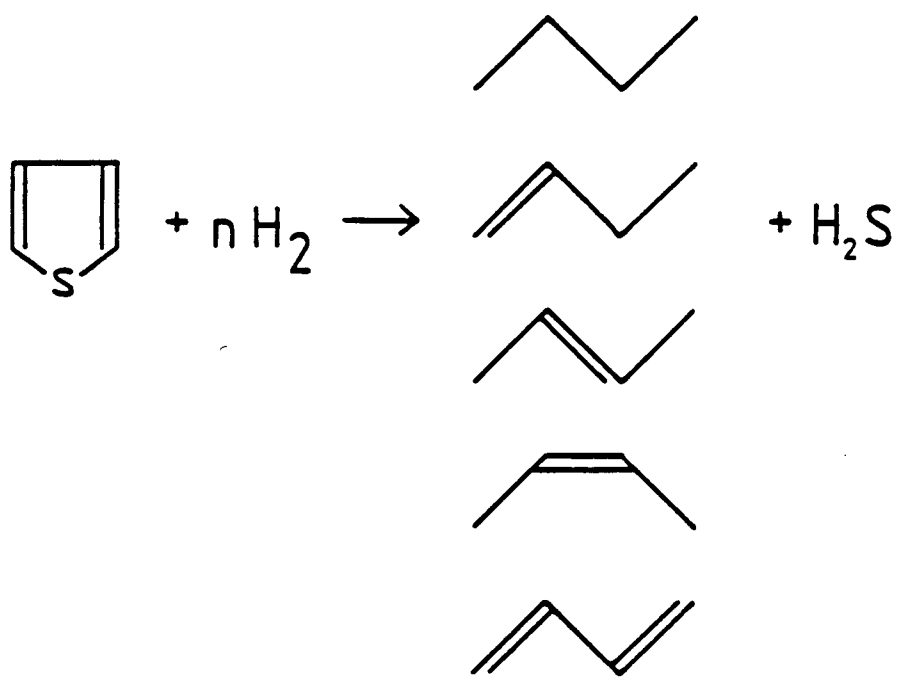

Figure 1.2: Hydrodesulfurization reaction for thiophene.

As indicated by the thermodynamic data listed in Table 1.2, the hydrodesulfurization of thiophene is a thermodynamically favorable reaction and almost complete reaction can be achieved over a wide range of temperatures. The thermodynamic driving force does, however, decrease as the reaction temperature is increased. The primary difficulty with the hydrodesulfurization process is that

Table 1.2: Thermodynamic Data for Thiophene HDS

Reaction	ΔH°_{298} *(kcal/mole)*	ΔS *(cal/mole-K)*	ΔG°_{298} *(kcal/mole)*
$C_4H_4S + 2\ H_2 \rightarrow$ butadiene $+ H_2S$	-5.9	-13.3	-1.9
$C_4H_4S + 3\ H_2 \rightarrow$ 1-butene $+ H_2S$	-32.2	–37.6	-21.0
$C_4H_4S + 3\ H_2 \rightarrow$ t-2-butene $+ H_2S$	-35.0	-40.2	-22.9
$C_4H_4S + 3\ H_2 \rightarrow$ c-2-butene $+ H_2S$	-34.0	-39.2	-22.2
$C_4H_4S + 4\ H_2 \rightarrow$ butane $+ H_2S$	-62.4	-68.2	-41.9

the rate of reaction is impractically slow. To overcome this limitation, heterogeneous catalysts are employed and have been used with considerable success for over fifty years. The catalysts used in the HDS process have their origin in catalysts developed by German scientists for the liquefaction of coal. The HDS catalysts used currently in the petroleum industry are comprised of molybdenum or tungsten dispersed on γ–alumina and promoted with cobalt or nickel. A typical Co–Mo/Al_2O_3 catalyst is prepared by pore volume impregnation of γ–Al_2O_3 with aqueous solutions of ammonium heptamolybdate ($(NH_4)_6Mo_7O_{24}$) and cobalt nitrate ($Co(NO_3)_2$). The catalyst is dried and calcined which converts the aqueous metal complexes to MoO_3 and CoO. To produce the actual working catalyst, the oxide precursor is heated in a mixture of H_2S and H_2 or in a liquid feed of sulfur containing molecules and H_2 [2]. The ratio of Mo/Co is always greater than one and a representative metal loading in an industrial catalyst is 3 wt % CoO and 12

wt % MoO_3 [4]. Normal operating conditions for the HDS process are 10-200 atm of hydrogen and temperatures between 570-700 K, but conditions vary depending on the boiling range and sulfur content of the crude oil feed [5].

1.3 Catalytic and Bulk Structure Studies of Hydrodesulfurization

The study of hydrodesulfurizaton and HDS catalysts has been an active area of research for many years, yet there remains considerable controversy with respect to both the structure of the catalyst as well as the interaction between the two metals in the sulfided catalysts. There is general agreement, however, that molybdenum is fully sulfided to form molybdenum disulfide on the surface of the support. MoS_2 has a layer lattice as depicted schematically in Figure 1.3 with successive MoS_2 sandwich planes bound weakly together by van der Waals interactions between adjacent sulfur layers. Crystals of MoS_2 grow in the form of dimensions parallel to the sulfur planes and a small dimension in the perpendicular direction. Recent work by Hayden and Dumesic has shown that crystallites of MoS_2 can be oriented in both a parallel and perpendicular manner on an alumina support as shown in Figure 1.4 [6]. At a sulfiding temperature of 770 K, in the range of temperatures used industrially, the majority of MoS_2 platelets were bonded to the support via Mo-O-Al linkages along the edge planes of MoS_2 , causing the crystallites to be oriented with the sulfur planes perpendicular to the surface of the support. Upon sulfiding at higher temperatures, the size of the crystallites increased and they became oriented parallel to the plane of the alumina surface. In an unrelated study, Topsoe et al. determined with EXAFS that the average size of the MoS_2 crystallites is about 10 Å on both Mo/Al_2O_3 and $Co\text{-}Mo/Al_2O_3$ catalysts which had been sulfided at 675 K [7]. Infrared spectroscopy studies indicate that the

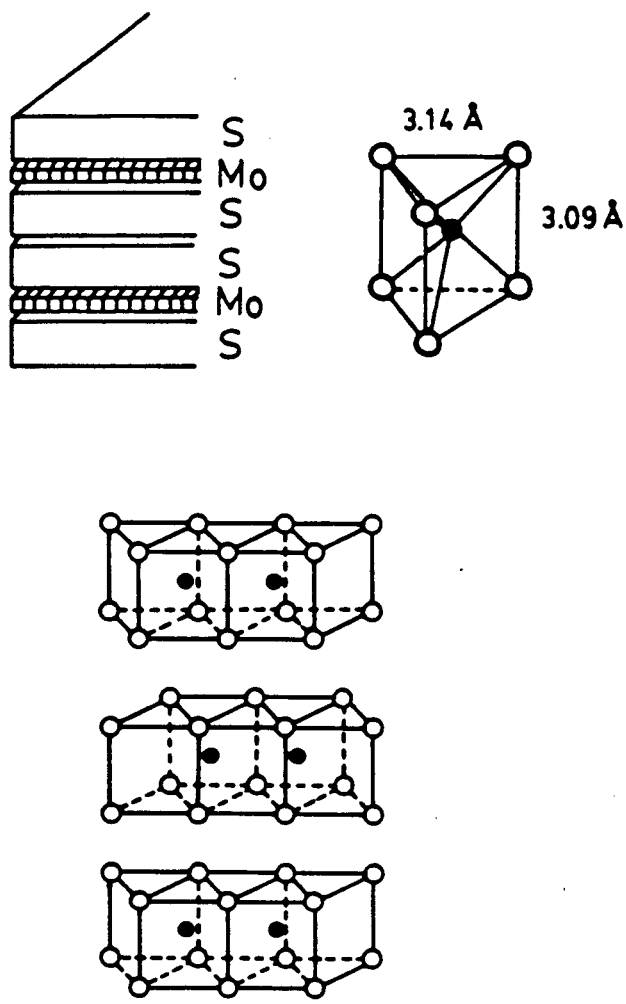

Figure 1.3: Structure of molybdenum disulfide.

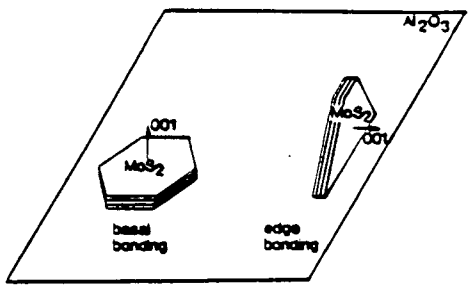

(a)

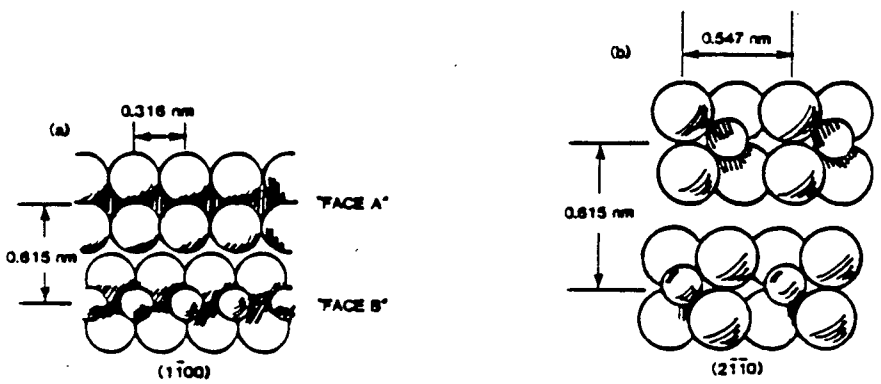

(b)

Figure 1.4: (a) Molybdenum disulfide platelets on alumina, (b) Structure of molybdenum disulfide edge planes (Mo: small atoms, S: large atoms).

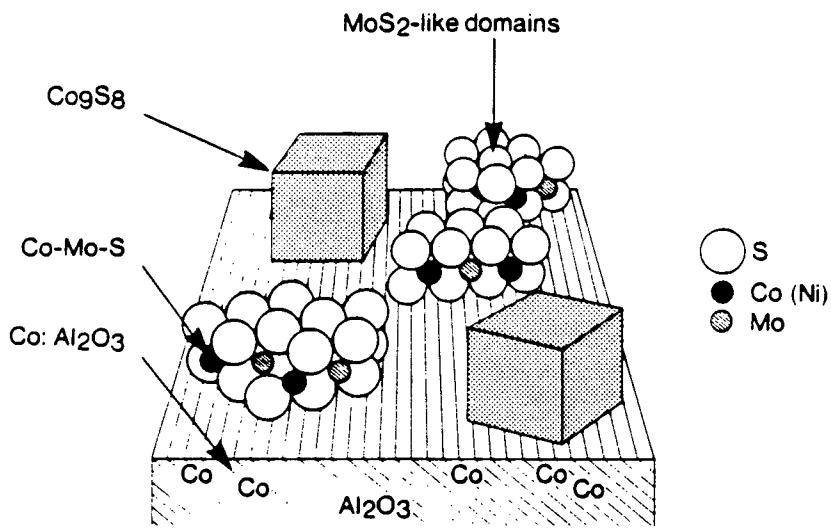

Figure 1.5: A schematic representation of the phases present in a Co-Mo/Al_2O_3 catalyst.

MoS_2 crystallites are present on the surface of the support as single slabs (i.e. one MoS_2 sandwich thick) [8].

Cobalt can exist in a number of different forms in a Co-Mo/Al_2O_3 catalyst, only one of which appears to promote the catalyst. Topsoe and coworkers have investigated cobalt promotion of HDS catalysts using Mossbauer emission spectroscopy (MES) and determined that as many as three different cobalt phases exist in a sulfided Co-Mo/Al_2O_3 catalyst [9]. They have identified the three phases to be Co_9S_8, the thermodynamically predicted Co species under reaction conditions, Co atoms located in the lattice of the alumina support (Co:Al_2O_3), and a mixed Co-Mo-S phase whose Mossbauer spectrum does not correspond to any bulk compound. The three cobalt containing species are shown schematically in Figure 1.5. Co_9S_8

is catalytically active for HDS but not at a level which would explain the promotional effect of cobalt. Instead, the increased activity of the Co promoted catalysts is associated with the mixed Co-Mo-S species whose structure is not well understood. The phase appears to be similar to MoS_2 in structure as it can be prepared by doping bulk MoS_2, thus indicating that the Al_2O_3 support is unnecessary [10]. Using scanning Auger microscopy (SAM), Chianelli et al. showed that Co is preferentially located at the edge planes of MoS_2 crystallites [11]. Furthermore, infrared absorption studies of NO adsorbed on a Co-Mo/Al_2O_3 catalyst showed that the Co atoms occupy surface sites on the edge planes of MoS_2 [12]. In summary, the structural studies of Co-Mo/Al_2O_3 catalysts indicate that MoS_2 crystallites are oriented on the alumina support in both a parallel and perpendicular manner and that the cobalt atoms responsible for the promotion effect are located at the edge planes of the MoS_2 . The local structure of this Co-Mo-S phase, however, remains largely unknown.

As sources of crude oil become increasingly scarce, it will be necessary to process lower quality crude oils and coal derived liquids containing higher levels of sulfur and other impurities. To meet these requirements, a significant amount of research has been performed to develop a new generation of HDS catalysts which are more active and less susceptible to poisoning. Chianelli and coworkers have carried out pioneering work in this area through the investigation of the catalytic properties of the transition metal sulfides [13]. Pecoraro and Chianelli measured the activities of unsupported sulfides of the transition metals for HDS of dibenzothiophene [14]. The first row sulfides were found to be relatively inactive, while the second and third row transition metal sulfides showed variations in activities of three orders of magnitude. Similar trends were observed by Ledoux et al. for the HDS of thiophene over transition metal sulfides supported on activated car-

bon [15]. Chianelli found the maximum activities for ruthenium and osmium while Ledoux observed the highest activities for rhodium and iridium; in both cases the most active sulfides were between one to two orders of magnitude more active than MoS_2 and WS_2, the sulfides used in the industrial catalysts. If the activity of the second and third row transition metal sulfides is plotted as a function of the heat of formation (ΔH_f) of the sulfide, a volcano plot results with a maximum at $\Delta H_f \approx 40$ kcal/mole [14]. Chianelli et al. conclude that transition metal sulfides with metal–sulfur bonds of intermediate strength are the most active as they are capable of inducing C–S bond cleavage but do not bind the sulfur so strongly that it cannot be removed from the active site. In addition, the authors conclude that these results are consistent with the model in which the active HDS sites of the different sulfides are sulfur vacancies. Chianelli and coworkers extended their work to include binary sulfides composed of MoS_2 or WS_2 with each of the first row transition metal sulfides. As with the individual sulfides, a volcano type dependence was observed for HDS activity as a function of the average heat of formation of the binary sulfides [16]. Once again, the maximum in the volcano plot corresponded to heat of formation of approximately 40 kcal/mole, where in this case the heat of formation is the average of the heats of formation of the two sulfides in the catalyst. Theoretical calculations by Harris and Chianelli indicate that the variation in HDS activity is due to electronic differences in the sulfides [17]. Their calculations show that the HDS activity of the sulfides correlates with a parameter which takes into account the number of d electrons in the highest occupied molecular orbital (HOMO) of the sulfide as well as the strength and degree of covalency of the metal-sulfur bond.

To complement the structural and compositional studies of HDS described above, other researchers have investigated the kinetics and mechanism of thio-

phene HDS. Numerous mechanisms have been proposed in the literature including the one-point mechanism suggested by Lipsch and Schuit which is shown in Figure 1.6. The main features of this mechanism are one-point adsorption of thiophene at a sulfur vacancy through the sulfur atom, desulfurization to produce butadiene, and hydrogenation of the sulfur atom to H_2S which regenerates the active site [18]. Butenes and butane are produced by subsequent hydrogenation of butadiene. The proposal of butadiene as an intermediate has been supported by the work of Amberg and coworkers in which butadiene appeared in the product stream at low hydrogen pressures [19]. An alternative mechanism has been proposed by Kolboe and is also shown in Figure 1.6 [20]. It involves an intramolecular dehydrosulfurization step to produce diacetylene and H_2S on the catalyst surface. The primary difference between this mechanism and the Lipsch and Schuit mechanism is that sulfur is removed from thiophene by β-elimination and is never present on the catalyst surface as atomic sulfur. The Kolboe mechanism is supported by two unrelated studies which showed that HDS of deuterated thiophene (C_4D_4S) in pure H_2 produced only D_2S and that HDS of normal thiophene (C_4H_4S) in D_2 produced only H_2S [21,22]. Satterfield and Roberts carried out an extensive study of the kinetics of thiophene HDS and found that the disappearance of thiophene could be represented by the following Langmuir-Hinshelwood rate equation [23].

$$r = k \cdot \frac{K_T P_T K_H P_H}{(1 + K_T P_T + K_S P_S)^2}$$

In this equation k is a rate constant, K is an equilbrium constant, and T, H and S represent thiophene, hydrogen and H_2S respectively. The form of this kinetic expression and others in the literature indicate that H_2S competes with thiophene for adsorption sites and that H_2 adsorbs on different sites. Butenes do not compete with thiophene for adsorption sites, indicating that desulfurization and hydrogena-

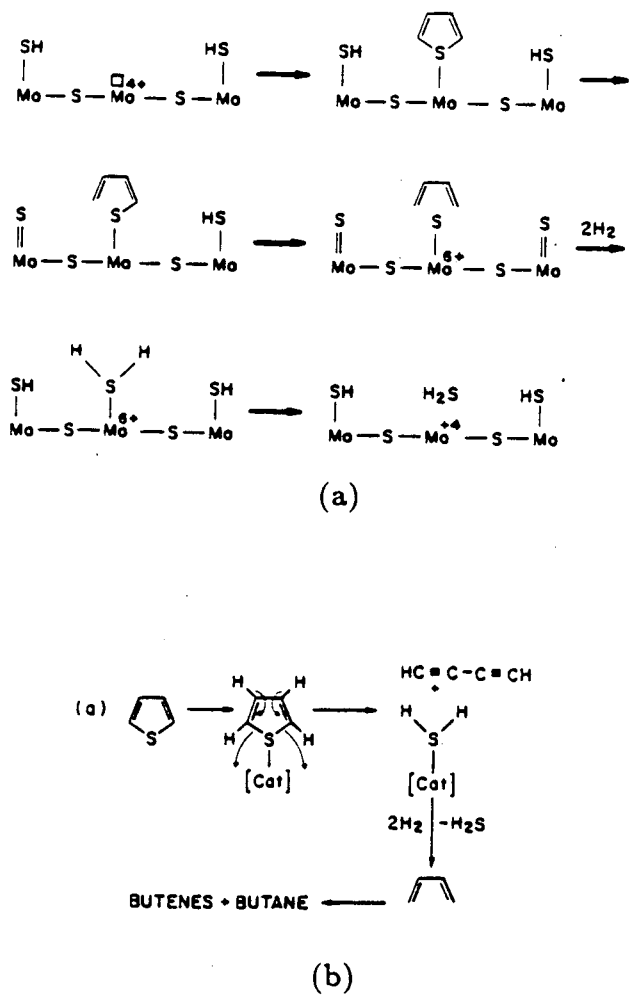

Figure 1.6: (a) Lipsch and Schuit mechanism for thiophene HDS, and (b) Kolboe mechanism for thiophene HDS.

tion occur on different sites.

1.4 Surface Science Studies of Hydrodesulfurization on Single Crystal Surfaces

The development of ultrahigh vacuum technology and surface analytical techniques in recent years has opened the door to molecular level investigation of the surface chemistry of catalytic processes. Study of the HDS of thiophene was initiated in this laboratory with the investigation of the adsorption and bonding of thiophene and its desulfurization products on a single crystal of MoS_2 in ultrahigh vacuum (UHV) [24]. As discussed earlier, MoS_2 crystals have large dimensions parallel to the sulfur plane and a small dimension in the perpendicular direction. Therefore, the adsorption experiments were carried out on the basal plane of MoS_2 which consists of a close packed layer of sulfur atoms. The basal plane was found to be chemically inert toward chemisorption of thiophene, butadiene and H_2S in agreement with the catalytic results described above (Section 1.3) in which the basal plane was found to be inactive for HDS. The adsorption of O_2 was also investigated on this surface [25]. The annealed MoS_2 surface was inert to O_2 but the introduction of defects into the basal plane by Ar^+ sputtering resulted in a marked uptake of O_2. This result verified the conclusions of Tauster et al. that HDS activity can be correlated with the uptake of O_2 by the MoS_2 catalysts because it selectively chemisorbs on defect sites in the sulfide, the active sites for HDS [26]. Unfortunately, it is very difficult to prepare MoS_2 single crystals which expose a significant area of the edge planes which contain the active sites, so this material is inappropriate for single crystal studies of thiophene HDS. As a result, surface science studies have focussed on the use of transition metal single crystals for model studies of thiophene HDS.

The chemisorption of thiophene on metal surfaces has been investigated with a variety of surface science techniques, yielding information on the adsorption geometry and reaction pathways of thiophene on these surfaces [25,27,28,29,30,31,32,33,34,35,36]. Of particular interest to the work described in this thesis has been the study of thiophene on molybdenum and rhenium single crystals. The adsorption of thiophene on the Mo(100) surface has been studied in detail using temperature programmed desorption (TPD), X-ray photoelectron spectroscopy (XPS), ultraviolet photoelectron spectroscopy (UPS), and high resolution electron energy loss spectroscopy (HREELS) [25,27,28,29]. An HREELS study by Zaera et al. indicates that some carbon–sulfur bond breaking occurs at temperatures as low as 90 K on Mo(100) [29]. Heating of the crystal to higher temperatures results in complete thiophene decomposition leaving the metal surface covered with strongly bound deposits of carbon and sulfur. TPD experiments indicate that at thiophene coverages below the saturation value (0.3 thiophene molecules/surface Mo atom), only H_2 desorbs from the surface during thiophene decomposition. The mechanism of thiophene decomposition on Mo(100) has been found to be a coverage dependent process. Zaera et al. have proposed two decomposition pathways based upon their HREELS and TPD results; the mechanisms are shown schematically in Figure 1.7 [29]. At low coverages, thiophene is proposed to be adsorbed parallel to the metal surface. Cleavage of the C–S bonds begins at 90 K and is followed by stepwise dehydrogenation of the parallel bound ring, leaving only adsorbed carbon and sulfur on the surface at 450 K. At higher coverages, thiophene is believed to be bound perpendicular to the surface through the sulfur atom, and a new decomposition route is observed. The perpendicularly bound thiophene undergoes dehydrogenation at the α-position at 230 K, leaving the thiophene ring bound to the surface through both sulfur and an α-carbon. Upon further heating to 400-

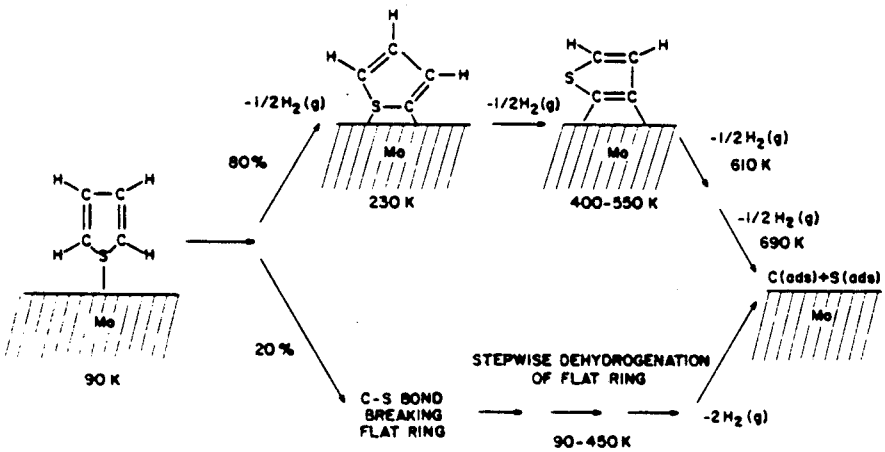

Figure 1.7: Proposed thiophene decomposition pathways on the Mo(100) surface.

550 K, this species undergoes further dehydrogenation at the β-position to give a complex bound to the surface at the α- and β-positions. Total hydrogenation is achieved in two steps by annealling to 610 K and 690 K.

Gellman et al. have proposed a slightly different mechanism for thiophene decomposition at high coverages [28]. They propose formation of an α-thiophenyl species following the initial dehydrogenation at the α-position upon heating to 235 K instead of the doubly coordinated species of Zaera et al. at 230 K. Both mechanistic pathways are supported by TPD studies of 2,5-dideuterothiophene at high coverages on Mo(100) by Kelly et al. in which dehydrogenation was observed in the sequence D_2, H_2, H_2 and D_2 at temperatures of 270, 360, 610 and 690 K respectively [27]. These results indicate that bond breaking is regiospecific, occurring first at the α-position and then at the β-position. At low thiophene coverages, H_2 and D_2 desorb in a single peak at 340 K indicating that thiophene is bound parallel to the metal surface and therefore undergoes indiscriminate C–H and C–D bond breaking. Roberts and Friend studied 2,5-dideuterothiophene decompsition on the Mo(110) surface using TPD and observed similar regiospecific bond breaking at high thiophene coverages. They also proposed formation of an α-thiophenyl species which then undergoes further decomposition.

Kelly et al. have also investigated thiophene chemisorption on sulfided and carbided Mo(100) surfaces [27]. As discussed in Section 1.3, industrial HDS catalysts are sulfided prior to use so it is of obvious interest to investigate thiophene adsorption on sulfided surfaces. Carbided surfaces are of interest because it is likely that some decomposition of hydrocarbons occurs on the surface of industrial HDS catalysts, leading to formation of carbonaceous overlayers. Adsorbed sulfur on the Mo(100) surface strongly decreases its reactivity toward thiophene; as the coverage of sulfur is increased, the fraction of adsorbed thiophene that

decomposes decreases. TPD of a saturation coverage layer of thiophene from a clean Mo(100) surface results in desorption of a small amount of reversibly adsorbed thiophene in the temperature range 190-250 K. The amount of reversibly bound thiophene increases dramatically as the sulfur coverage is increased and decomposition is completely blocked at sulfur coverages of 0.5 monolayer (ML) and higher. Instead, thiophene interacts very weakly with the sulfided surface and desorbs below 200 K, indicative of physisorption. Once again, similar results were observed by Roberts and Friend for sulfided Mo(110) surfaces. Clearly, the addition of sulfur to the Mo surfaces weakens their interaction with thiophene in the UHV environment to the extent that thiophene desorption is favored over bond cleavage.

Adsorbed carbon on the Mo(100) surface blocks thiophene decomposition as well, but the carbided surfaces also have new molecular chemisorption sites for thiophene. Thiophene desorbs from a carbided Mo(100) surface ($\theta_c = 0.84$ ML) at temperatures of 300 K and 360 K, well above the temperature of $\sim$ 170 K as observed from the sulfided Mo(100) surface. The differences in the influence of the adsorbates were explained in terms of physical blocking of metal sites at the surface. Sulfur is a larger adsorbate than carbon and therefore is more effective at blocking decomposition sites on the metal, leading to its passivation.

The chemistry of thiophene on the clean and sulfided Re(0001) surface is similar to that of thiophene on the Mo(100) surface, but differences are observed for thiophene on the carbon covered surfaces [37]. Thiophene adsorbs irreversibly on the clean Re(0001) surface to produce adsorbed C, S and H_2 which desorbs from the surface. Adsorbed sulfur blocks the decomposition pathway and thiophene desorbs from the surface in a peak of maximum desorption at 180 K, similar to the temperature of 170 K on Mo(100). In contrast to these similarities, the carbon

covered Re(0001) and Mo(100) surfaces show differences in their interactions with thiophene. Adsorbed carbon blocks thiophene decomposition on Re(0001) and thiophene desorbs at 180 K and 230 K, well below the temperatures of 310 K and 360 K on the carbon covered Mo(100) surface. These differences in the binding of thiophene were attributed to the carbon overlayer being graphite-like on rhenium while carbon on Mo(100) is carbidic in nature.

1.5 Combined Surface Science and Catalytic Studies of Hydrodesulfurization

If a molecular level description of thiophene HDS is to be developed, it is necessary to relate information gained from surface science investigation of thiophene on well characterized surfaces to catalytic studies of HDS at high pressures. UHV chemisorption experiments yield insight on the bonding and elementary reaction steps of thiophene on metal surfaces, but these experiments are conducted at pressures 10^{12}-10^{14} orders of magnitude lower than those typical of HDS reactors. As a result, the primary reaction pathway for thiophene in UHV is C–S bond cleavage and dehydrogenation while C–S bond cleavage and hydrogenation are favored in a catalytic reactor. High pressure catalytic studies of HDS, however, also have disadvantages; the major one being that the studies are carried out over catalysts whose surfaces are poorly characterized due to the lack of surface sensitive techniques which can be used in environments other than UHV.

To facilitate correlations between data obtained from high pressure catalytic reactions and UHV surface science studies, Somorjai and coworkers developed a combined UHV surface analysis/high pressure catalytic reactor system [38]. Using such a system, the surface of a small area catalyst (1 cm^2) can be characterized and modified in UHV before and after high pressure reactions carried out in an

in-situ isolation cell.

This thesis project has involved the use of a combined UHV/high pressure system to investigate the role of catalyst surface structure and composition in the thiophene hydrodesulfurization reaction. Thiophene HDS has been carried out over molybdenum and rhenium single crystals of different crystallographic orientation and the effects of carbon and sulfur overlayers determined on these surfaces. The remainder of this thesis is devoted to describing this work and has been organized into five chapters. Chapter 2 describes the experimental apparatus and techniques employed in this study, while Chapter 3 concentrates on the surface structure of the Mo and Re single crystals, both clean and when modified by adsorbate overlayers. Chapters 4 and 5 discuss thiophene HDS over the Mo and Re single crystals, and lastly, Chapter 6 discusses thiophene HDS over polycrystalline Mo, Re and Co foils.

References

[1] J. Berzelius. *Jahres-Bericht uber die Fortschritte der Physichen Wissenchaften* (1836) 243.

[2] C. N. Satterfield. *Heterogeneous Catalysis in Practice.* McGraw-Hill Book Co., New York, 1980.

[3] G. A. Somorjai. *Chemistry in Two Dimensions: Surfaces.* Cornell University Press, Ithaca, 1981.

[4] R. Prins, V. H. J. de Beer, and G. A. Somorjai.

[5] M. L. Vrinat. *Appl. Catal.* **6** (1983) 137.

[6] T. F. Hayden and J. A. Dumesic. *J. Catal.* **103** (1987) 366.

[7] B. S. Clausen, H. Topsoe, R. Candia, J. Villadsen, B. Lengler, J. Als-Nielsen, and F. Christensen. *J. Chem. Phys.* **85** (1981) 3868.

[8] N. Topsoe. *J. Catal.* **64** (1980) 235.

[9] H. Topsoe and B. S. Clausen. *Catalysis and Surface Science*, pages 95–120. Volume 21, Marcel Dekker, New York, 1985.

[10] B. S. Clausen, S. Morup, H. Topsoe, and H. Candia. *J. Phys. Colloq.* **37** (1976) c6–249.

[11] R. Chianelli, A. F. Rupert, S. K. Behal, B. H. Kear, A. Wold, and R. Kershaw. *J. Catal.* **92** (1985) 56.

[12] N. Y. Topsoe and H. Topsoe. *J. Catal.* **84** (1983) 386.

[13] R. Chianelli. *Catalysis and Surface Science*, pages 61–93. Volume 21, Marcel Dekker, New York, 1985.

[14] T. A. Pecoraro and R. R. Chianelli. *J. Catal.* **67** (1981) 430.

[15] M. J. Ledoux, O. Michaux, G. Agostini, and P. Panissod. *J. Catal.* **102** (1986) 275.

[16] R. R. Chianelli, T. A. Pecoraro, T. R. Halpert, W. H. Pan, and E. I. Stiefel. *J. Catal.* **86** (1984) 226.

[17] S. Harris and R. R. Chiannelli. *J. Catal.* **86** (1984) 400.

[18] J. G. Lipsch and G. L. A. Schuit. *J. Catal.* **15** (1969) 179.

[19] P. J. Owens and C. H. Amberg. *Adv. Chem. Ser.* **33** (1961) 182.

[20] S. Kolboe. *Can J. Chem.* **47** (1969) 352.

[21] R. J. Mikovsky, A. J. Silvestri, and H. Heinemann. *J. Catal.* **34** (1974) 324.

[22] K. F. McCarty and G. L. Schrader. *J. Catal.* **103** (1987) 261.

[23] C. N. Satterfield and G. W. Roberts. *AICHE J.* **14** (1968) 159.

[24] M. Salmeron, G. A. Somorjai, A. Wold, R. R. Chianelli, and K. S. Liang. *Chem. Phys. Lett.* **90** (1982) 105.

[25] A. J. Gellman, M. H. Farias, M. Salmeron, and G. A. Somorjai. *Surf. Sci.* **136** (1984) 217.

[26] S. J. Tauster, T. A. Pecoraro, and R. R. Chianelli. *J. Catal.* **63** (1980) 515.

[27] D. G. Kelly, M. Salmeron, and G. A. Somorjai. *Surf. Sci.* **175** (1986) 465.

[28] A. J. Gellman, W. T. Tysoe, and G. A. Somorjai. *Surf. Sci.,* (to be published)

[29] F. Zaera, E. B. Kollin, and J. L. Gland. *Surf. Sci.* **184** (1987) 75.

[30] J. Stohr, J. L. Gland, E. B. Kollin, R. J. Koestner, A. L. Johnson, E. L. Meutterties, and F. Sette. *Phys. Rev. Lett.* **53** (1984) 2161.

[31] J. Stohr, E. B. Kollin, D. A. Fischer, J. B. Hastings, F. Zaera, and F. Sette. *Phys. Rev. Lett.* **55** (1985) 1468.

[32] J. F. Lang and R. I. Masel. *Surf. Sci.* **183** (1987) 44.

[33] G. R. Schoofs, R. E. Preston, and J. B. Benziger. *Lang.* **1** (1985) 313.

[34] F. Zaera, E. B. Kollin, and J. L. Gland. *Lang.* **3** (1987) 555.

[35] N. V. Richardson and J. C. Campuzano. *Vacuum* **31** (1981) 449.

[36] B. A. Sexton. *Surf. Sci.* **163** (1985) 99.

[37] D. G. Kelly, J. A. Odriozola, and G. A. Somorjai. *J. Phys. Chem.* **91** (1987) 5695.

[38] D. W. Blakely, E. I. Kozak, B. A. Sexton, and G. A. Somorjai. *J. Vac. Sci. Technol.* **13** (1976) 1091.

Chapter 2

Experimental Methods

2.1 Introduction

In order to learn about the chemistry of clean metal surfaces and to modify them in a controlled fashion, it is necessary to study them in ultrahigh vacuum (UHV). At ambient pressure, metal surfaces are contaminated by layers of oxide, hydrocarbons and adsorbed gases which alter their surface chemistry. At a pressure of 1×10^{-9} Torr, however, a metal surface can be kept free of contaminants for a sufficient period of time ($<$ 1 monolayer in 15 minutes) to carry out experiments on the clean surface. For this reason, the use of an ultrahigh vacuum chamber, in combination with a high pressure catalytic reactor, has been of fundamental importance to this research project.

2.2 Ultrahigh Vacuum Surface Analysis/Catalytic Reactor System

All of the experiments described in this thesis were conducted in a combined UHV surface analysis/catalytic reactor system which was designed and built at the Lawrence Berkeley Laboratory. A photograph of the system is shown in Figure 2.1 and a schematic drawing in Figure 2.2. The system is composed of an ultrahigh

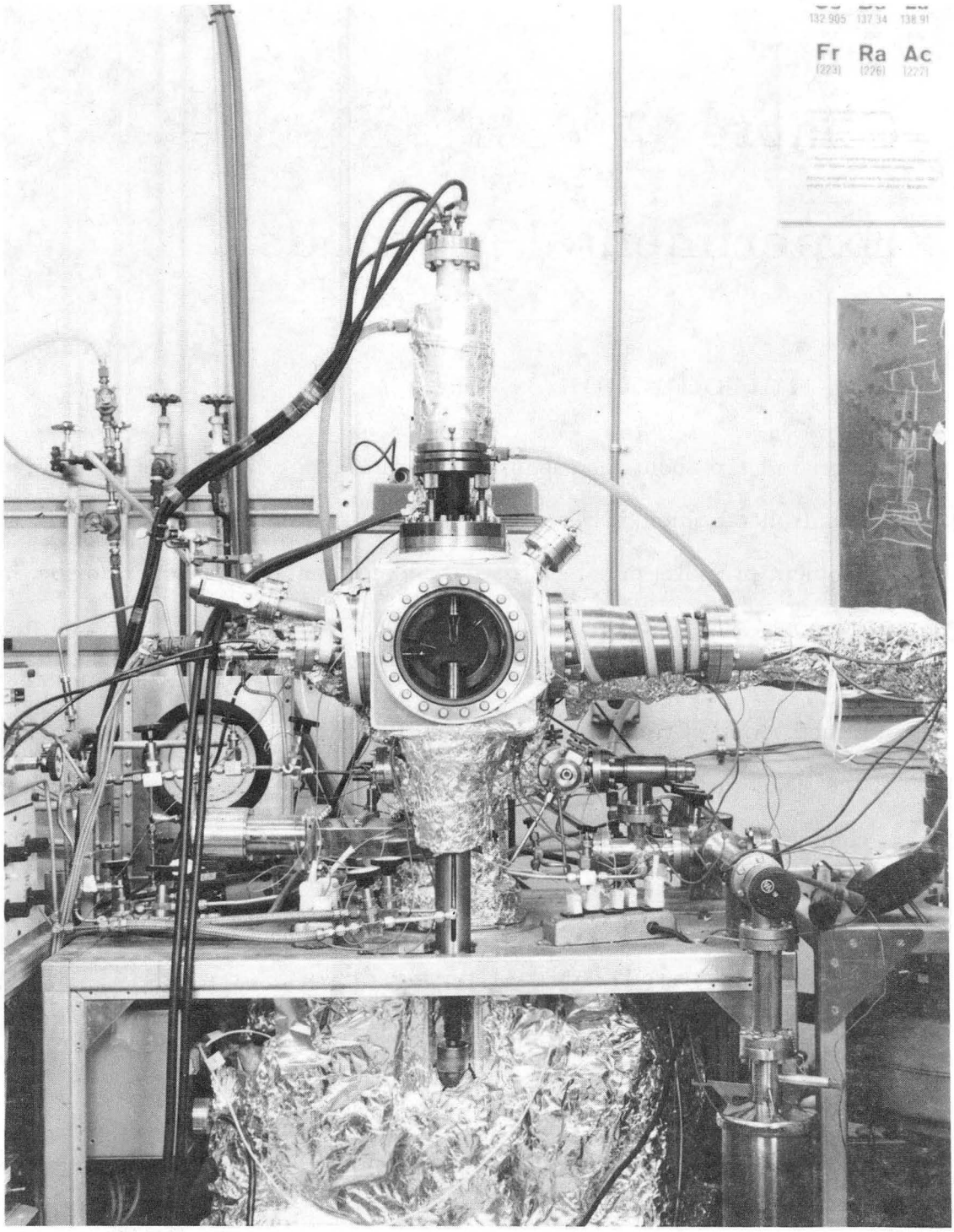

XBB 887-7308

Figure 2.1: Photograph of the UHV surface analysis/catalytic reactor system.

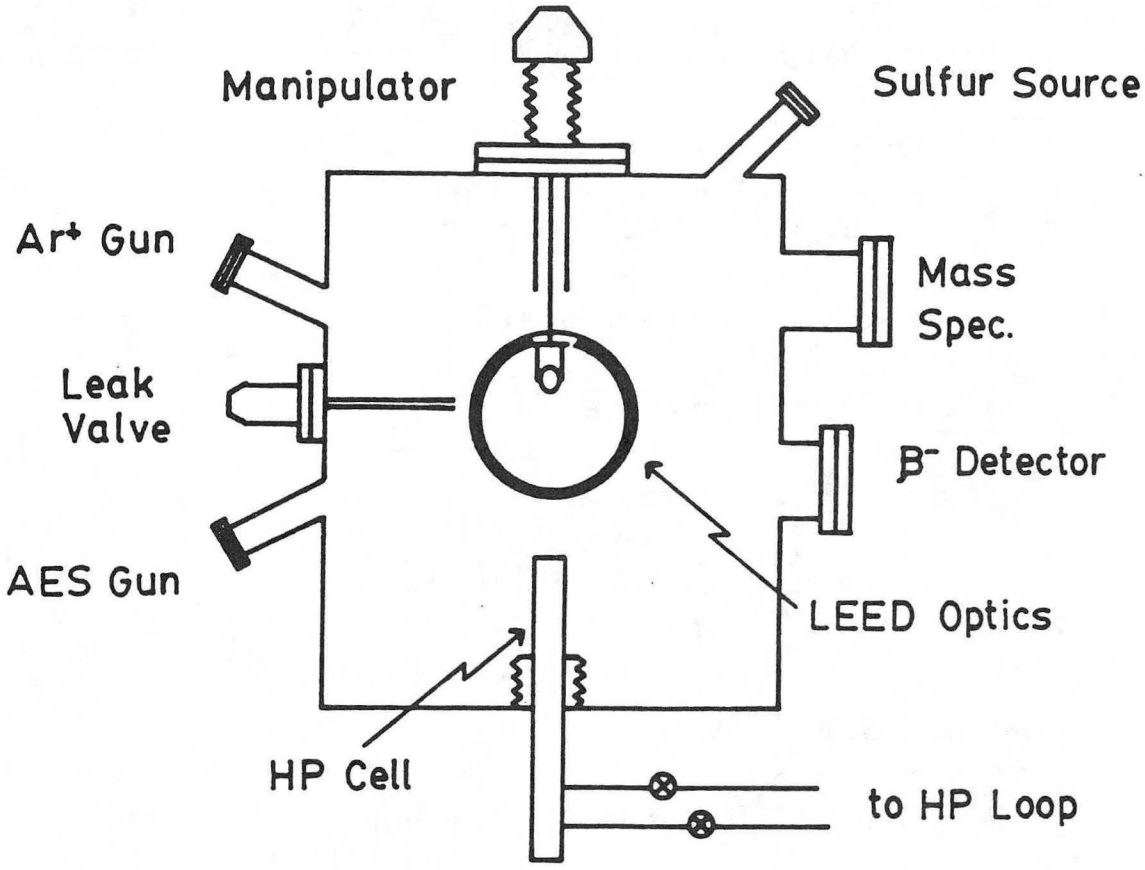

Figure 2.2: Schematic drawing of the UHV surface analysis/catalytic reactor system.

vacuum chamber outfitted with the following pieces of equipment:

- sample manipulator
- high pressure isolation cell
- three stainless steel leak valves
- electrochemical sulfur source
- Bayard-Alpert type ionization gauge
- argon ion (Ar^+) sputtering gun
- grazing angle electron gun for AES
- four-grid LEED optics assembly
- quadrupole mass spectrometer
- solid state beta particle detector

The most important pieces of equipment will be described in greater detail in the following sections.

2.2.1 Ultrahigh Vacuum Chamber

The ultrahigh vacuum chamber used in this study was constructed of stainless steel and its normal operating pressure was 1×10^{-9} Torr. The system was pumped with a 500 liter/second triode ion pump (Varian), a liquid nitrogen trapped, six inch oil diffusion pump (Varian) and a water cooled titanium sublimation pump. Following exposure of the interior of the chamber to the ambient atmosphere it was "baked-out" at a temperature of 120-140° C for 12-48 hours to restore the vacuum to its normal operating pressure. Chamber pressures in the 10^{-4}-10^{-10} torr range

were measured using a Bayard-Alpert type ionization gauge and the composition of the gas phase was monitored with a quadrupole mass spectrometer (UTI). The chamber was equipped with three stainless steel leak valves for controlled dosing of gases into the system. One of the leak valves was outfitted with a length of one-eighth inch stainless steel tubing which extended to within two inches of the single crystal or foil sample to maximize exposure of the sample to the dosing gas while minimizing the exposure of the rest of the chamber.

2.2.2 Sample Manipulator and High Pressure Isolation Cell

The single crystals and polycrystalline foils employed in this work were spot-welded to a sample manipulator which was modified for use with a high pressure cell. Figure 2.3 is a close-up photograph of the sample manipulator and high pressure cell while Figure 2.4 shows the two pieces schematically. The manipulator allowed free rotation of the sample through an angle of 270° around its axis and limited motion in the x, y and z directions. As shown in Figure 2.4, samples were mounted to the manipulator feed-throughs via twenty mil (0.020 inch) tantalum or rhenium wires spot-welded to one-eighth inch tantalum rods. The temperature of the single crystals and polycrystalline foils was measured using a platinum-platinum 10 % rhodium thermocouple spot-welded to the edge of the samples. The single crystals and foils were heated resistively over the temperature range of 300-1900 K. The mounting geometry shown in Figure 2.4 was found to be the best for minimizing heating of the support rods during both UHV experiments and catalytic reactions.

The high pressure isolation cell was mounted on a linear motion feedthrough and could be raised until a UHV-tight seal was made between the Viton O-ring of the high pressure cell and the knife edge of the manipulator. The high pressure cell had an internal volume of $\sim$ 35 cm^3 and was attached via a gas inlet and

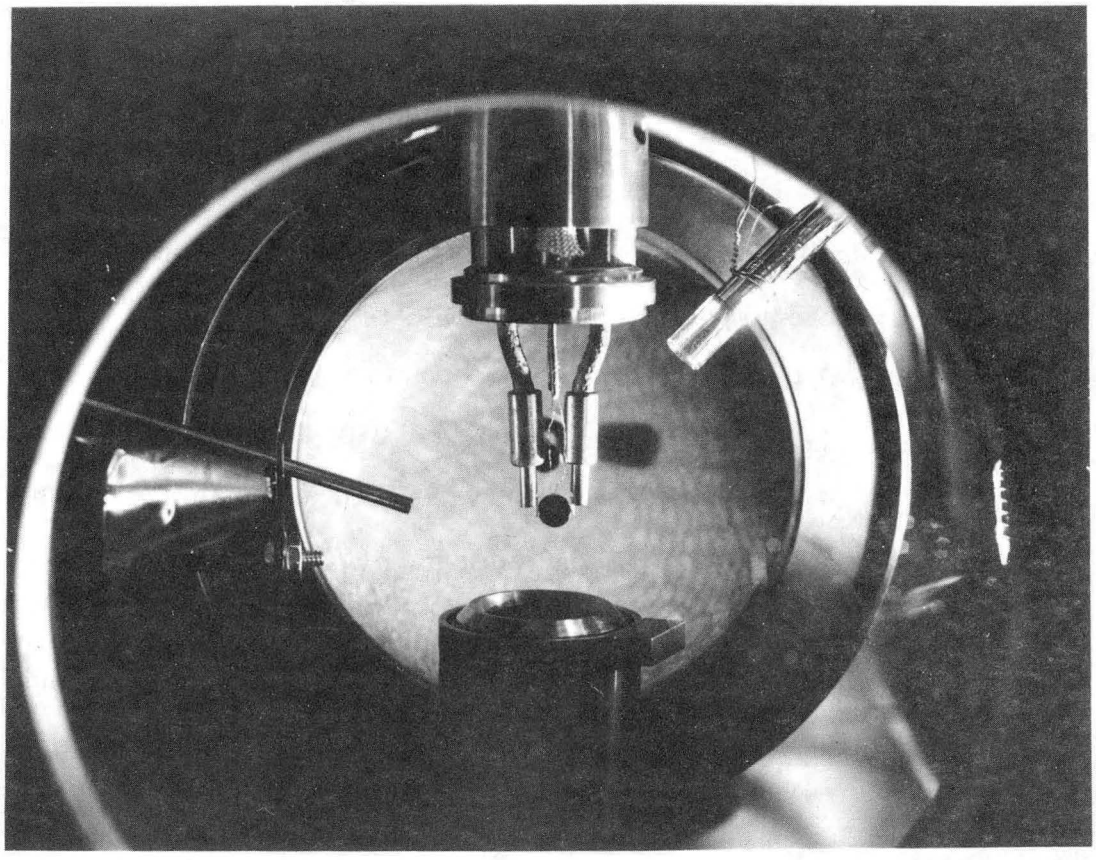

XBB 887-7309

Figure 2.3: Photograph of the manipulator and high pressure cell.

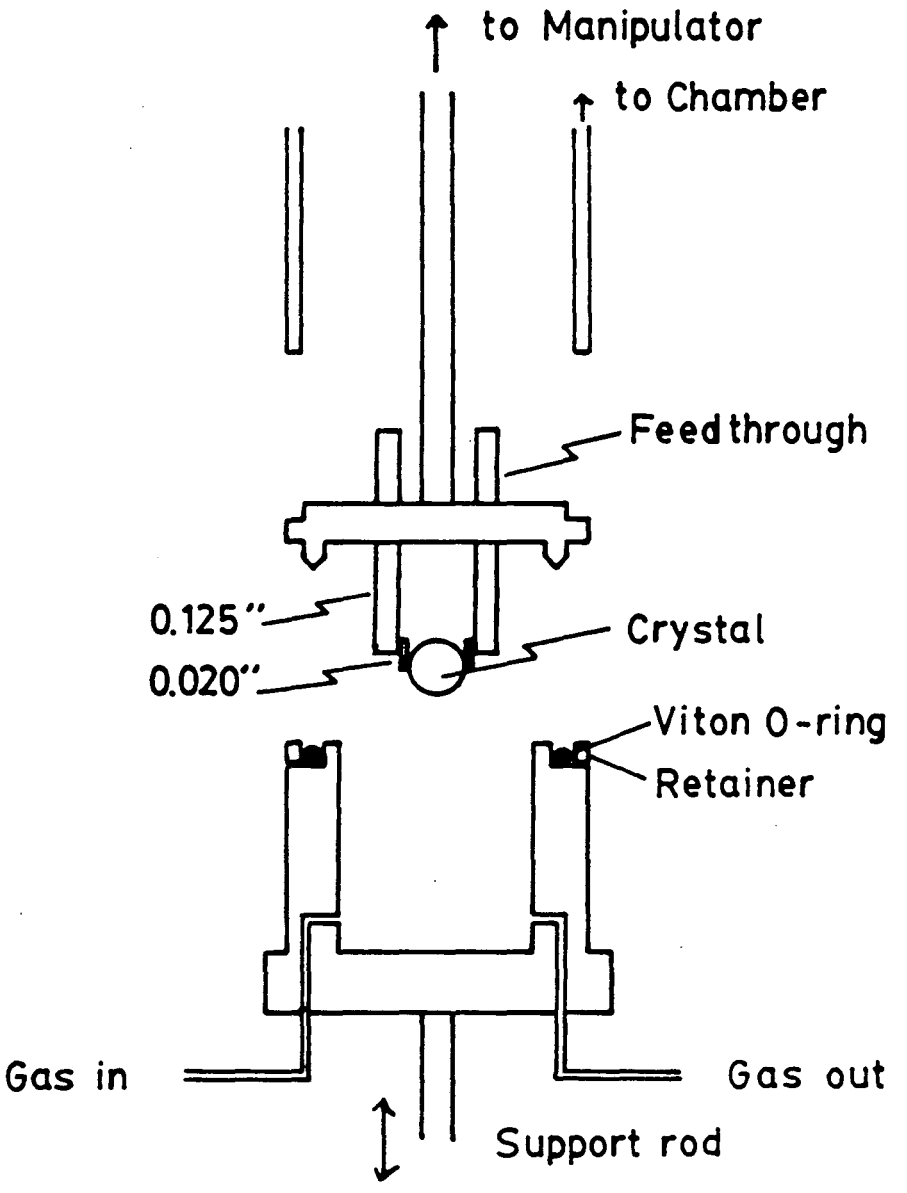

Figure 2.4: Schematic drawing of the manipulator and high pressure cell.

outlet to a reaction loop described in the next section.

2.2.3 Catalytic Reactor System

The batch reactor used to carry out catalytic reactions is shown in Figure 2.5. The reactor is comprised of a closed loop constructed out of one-quarter inch stainless steel tubing and the high pressure cell, and has a total volume of 130 cm^3. The high pressure cell could be isolated from the reaction loop by ultrahigh vacuum compatible valves (Nupro) located at the gas inlet and outlet of the cell. The reactor is equipped with a small pump (Micropump) for circulating gases and a sampling valve for injecting gas samples into a gas chromatograph (Perkin-Elmer 3920 B). The gas pressure in the reactor system was monitored over the range 1-800 Torr with a differential pressure gauge (Wallace & Tiernan) operated in the absolute mode and over the range 10^{-3}-1 Torr with a thermocouple pressure gauge (Granville-Phillips). Gases were evacuated from the system to pressures $\leq$ 100 mTorr with a liquid nitrogen trapped, rotary mechanical pump (Sargent-Welch) and to pressures $\leq 10^{-3}$ Torr with a liquid nitrogen trapped, 2 in. oil diffusion pump (Varian).

2.2.4 Electrochemical Sulfur Source

Deposition of sulfur overlayers onto sample surfaces in UHV was carried out using an electrochemical sulfur source which has been described previously in the literature [1]. This method of sulfur deposition was chosen over the more commonly used procedure of exposing the surface of interest to hydrogen sulfide (H_2S) because it minimizes contamination of the UHV chamber with sulfur. The electrochemical source produces a collimated beam of S_2 molecules which can be dosed onto sample surfaces at a rate of $\sim$ 1 monolayer/minute without producing a noticeable

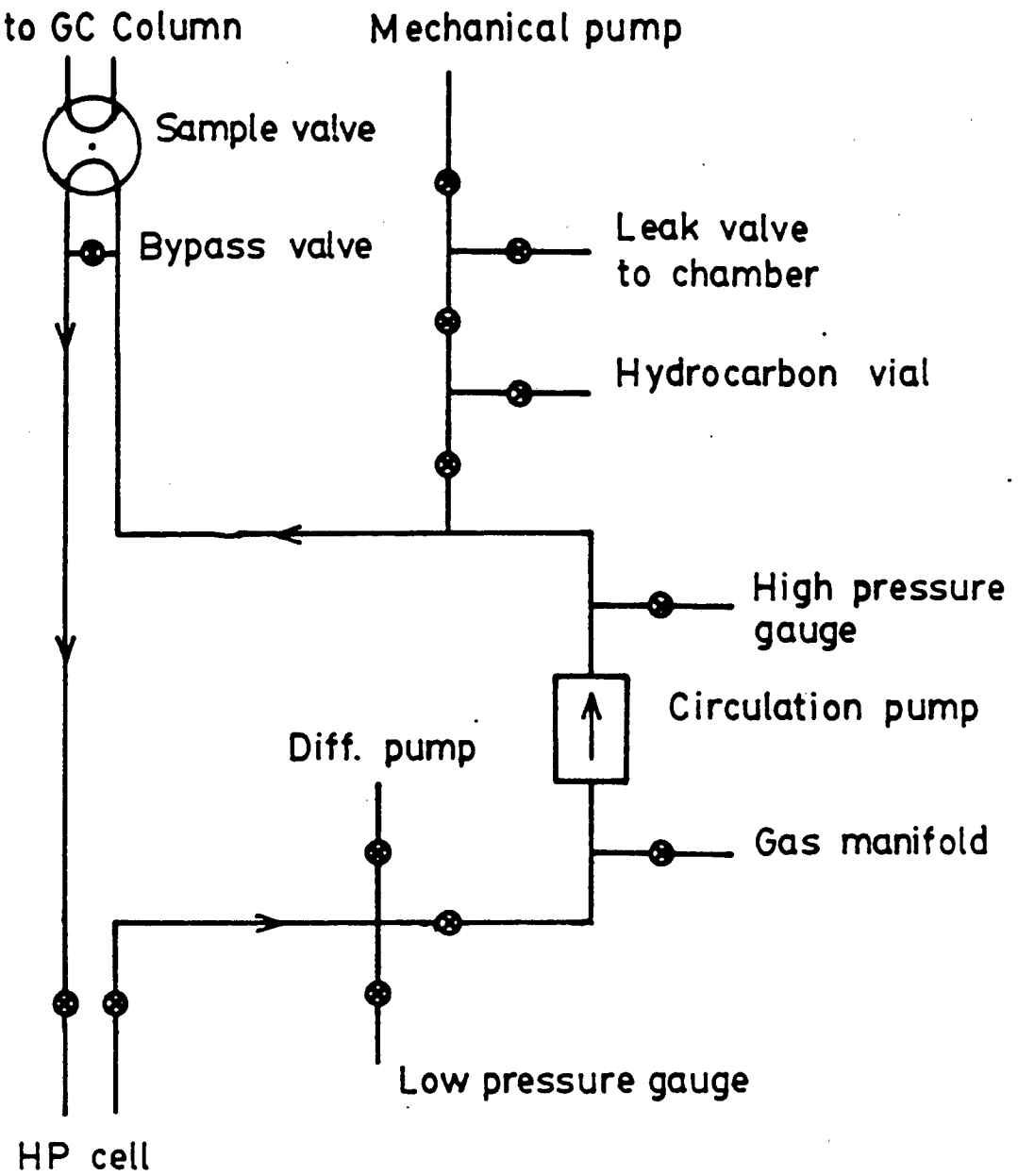

Figure 2.5: Schematic drawing of the batch reactor used for HDS reactions.

increase in the chamber pressure (1×10^{-9} Torr).

The electrochemical sulfur source is depicted in Figure 2.6 and the half cell reactions are shown below.

$$Ag_2S \longrightarrow 2\,Ag^+ + 1/2\,S_2 + 2\,e^- \qquad anode$$

$$2\,Ag^+ + 2\,e^- \longrightarrow 2\,Ag \qquad cathode$$

The two half cell reactions add to give the overall cell reaction to produce silver metal and S_2 from Ag_2S.

$$Ag_2S \longrightarrow 2\,Ag + 1/2\,S_2 \qquad E^\circ = -0.197\,V$$

The source is operated by warming the cell to a temperature of $\sim$ 150°C by passing a current (0-4 A) through the heating coil, and applying a voltage greater than 0.2 V across the cell electrodes. Heating of the cell is necessary to increase the conductivity of the solid AgI electrolyte, while application of the voltage causes electrolytic decomposition of Ag_2S.

2.3 Surface Analytical Techniques

There exist numerous experimental techniques for investigating the structure and composition of surfaces in ultrahigh vacuum [2,3]. The surface sensitivity of many of these techniques can be traced to the fact that the mean free path of low energy electrons in solids is of the order of a few atomic layers. The mean free path of electrons in metallic solids as a function of their kinetic energy is shown in Figure 2.7. The curve clearly indicates that electrons with kinetic energies in the range of 10-1000 eV have mean free paths of less than 20 Å. Both Auger electron

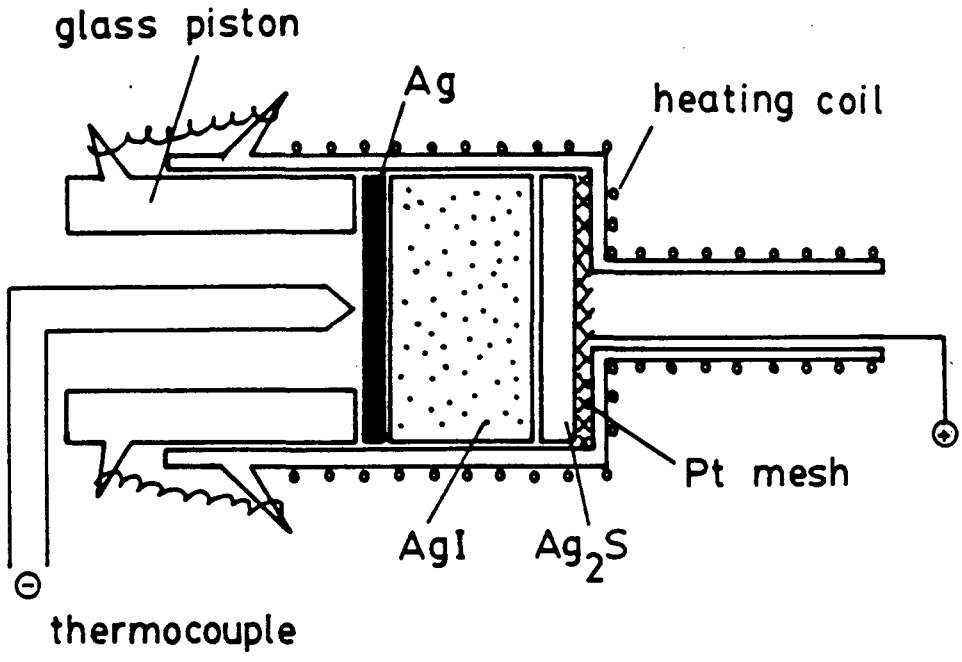

Figure 2.6: Schematic diagram of the electrochemical sulfur source

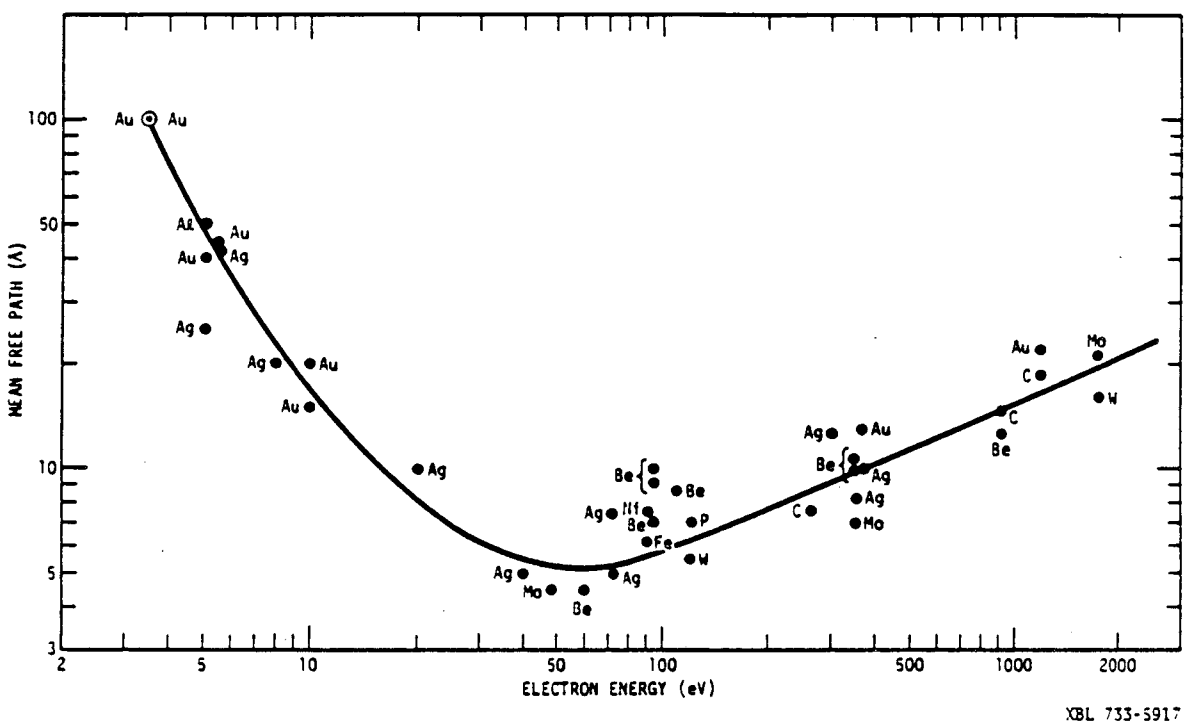

Figure 2.7: The universal curve of electron mean free paths in metallic solids as a function of their kinetic energy.

spectroscopy (AES) and low energy electron diffraction (LEED), two techniques used extensively in this work, involve collection and analysis of electrons emitted from a solid into vacuum with energies in the range of 10-1000 eV, and therefore yield information about the topmost 2-3 atomic layers of the material. LEED and AES are complimentary techniques; LEED gives information on the two dimensional order of the surface and AES provides information on the elemental composition of the surface.

When a monoenergetic beam of electrons impinges onto a solid surface, several different processes occur as suggested by Figure 2.8. A small fraction of the electrons ($\leq 5\%$) are elastically back-scattered from the surface. If the scattering surface is a single crystal, diffraction of the elastically scattered electrons can occur and this process is the basis for low energy electron diffraction. Alternately, the primary beam electrons can undergo inelastic scattering due to collisions in which energy is transferred to electrons bound in the solid. These inelastic collisions create secondary electrons which originate from within the solid (as opposed to primary beam electrons) and are emitted from its surface. The dashed curve in Figure 2.8 is the yield of secondary electrons while the solid curve is the total number of electrons scattered from the solid. As shown in the figure, one of the processes which produces secondary electrons is the Auger process, and these are the electrons detected in Auger electron spectroscopy.

2.3.1 Auger Electron Spectroscopy

Auger electron spectroscopy (AES) is a widely used technique in surface science for the determination of the elemental composition of the near surface region of materials. Both the theoretical and practical aspects of AES have been discussed in detail in the literature and the AES spectra of the different elements have been

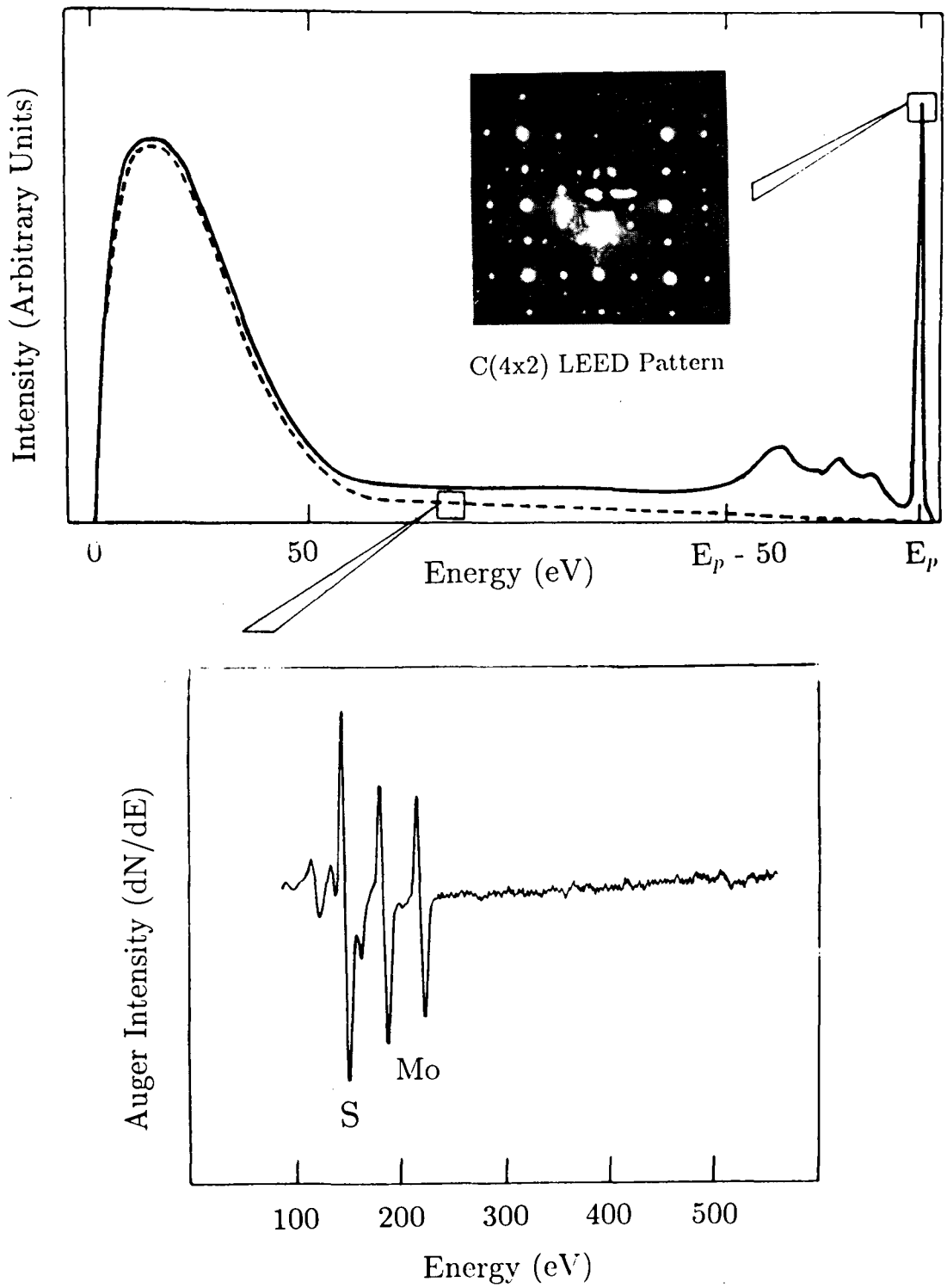

Figure 2.8: Energy distribution of scattered electrons from a sulfur covered ($\theta_s = 0.75$) Mo(100) surface. (XBB 881-598A)

tabulated [3,4,5]. In this thesis work, Auger electron spectroscopy has been used to determine the cleanliness of metal surfaces, to calibrate the surface coverage of sulfur and carbon adlayers on metals, and also to investigate the structure of adsorbed carbon overlayers.

Auger electrons are produced by the relaxation of an ionized atom that has an electron vacancy in a core energy level. Electron holes can be produced in the core energy levels of an atom by bombardment with a high energy electron beam (E_p = 1-5 kV) or by a suitable X-ray source. As depicted in Figure 2.9, there are two de-excitation pathways available for an ion which has a core hole: 1) demotion of a higher level electron accompanied with emission of a photon; and 2) demotion of a higher shell electron accompanied by ejection of a second electron from a bound state into the continuum. This latter mode of relaxation is the Auger process and analysis of the kinetic energy of the ejected electrons can be used to identify all of the elements with the exception of hydrogen and helium. These latter two elements do not have enough electrons for the Auger process to occur. The kinetic energy of an Auger electron depends upon the energy levels of the atom (and its ionized states) from which the electron is ejected and is independent of the type and energy of the ionizing source. In the case of a solid material, the kinetic energy of an Auger electron is described by the expression below.

$$E_{Auger} = E_1 - E_2 - (E_3 + e\phi_{sp})$$

In this equation, E_1 is the binding energy of the core level electron, E_2 is the binding energy of the higher level electron demoted to the core hole, E_3 is the binding energy of the Auger electron in its bound state, ϕ_{sp} is the work function of the spectrometer and e is the electron charge [3]. Clearly, the energy levels E_1, E_2 and E_3 will be different for each element of the periodic table so that the

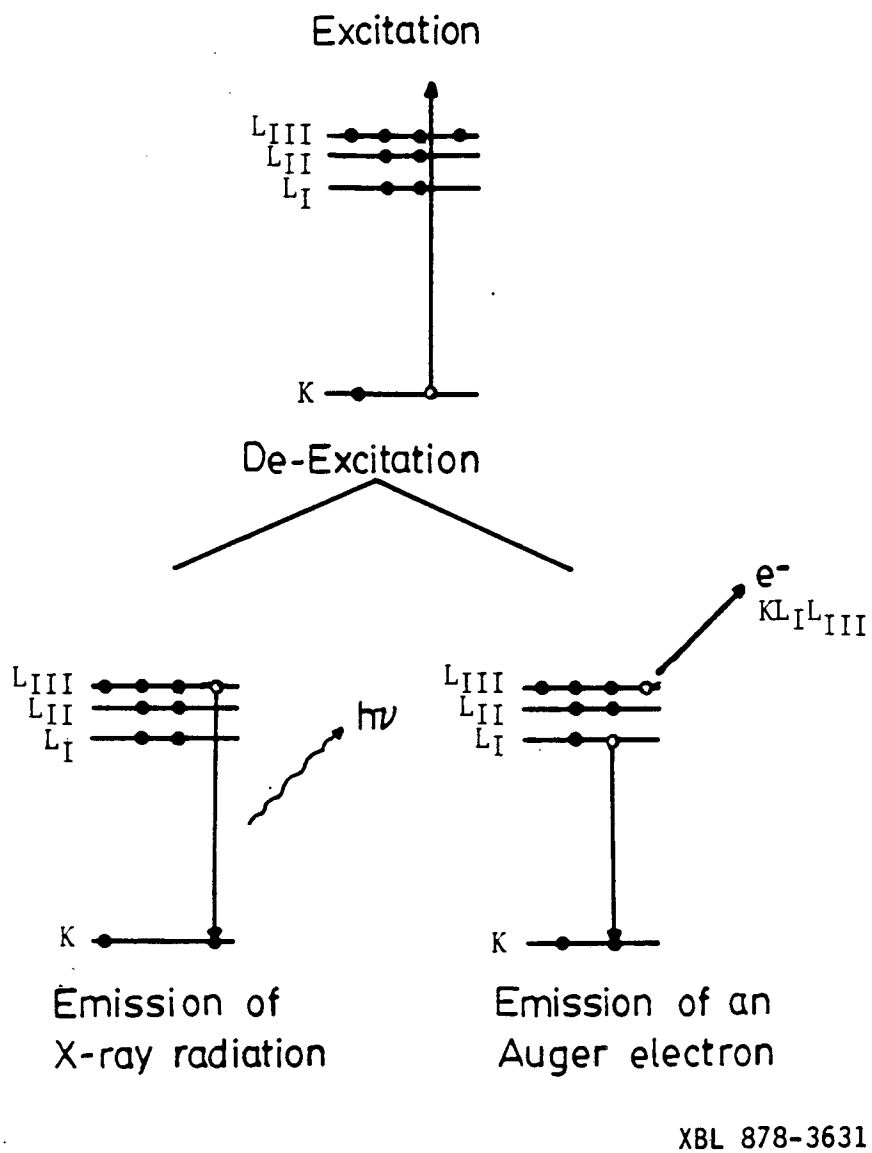

Figure 2.9: The de-excitation pathways for ionized atoms with a core vacancy.

kinetic energies of emitted Auger electrons will be distinct for each element which undergoes this relaxation process.

In this work, ionization of atoms in the single crystal and foil samples was accomplished with a grazing incidence electron gun (70° off the sample normal). The scattered electrons produced by electron bombardment were collected using the LEED optics assembly as a retarding field analyzer (RFA) as depicted in Figure 2.10 along with the signal amplification electronics. AES spectra were obtained using a primary beam voltage V_p = 2000 V, a beam currrent i_b = 7-10 μA, a retarding voltage ramped over the range 90-550 volts and a modultation voltage of 15 volts. The retarding voltage is a negative voltage applied to the second and third grids to limit the number of electrons which reach the collecter. The modulation voltage is superimposed on the retarding voltage so that phase sensitive detection can be used to increase the signal-to-noise ratio. Auger peaks appear as small steps on a slowly decreasing background and to improve the sensitivity, the spectra are normally plotted in the derivative mode. The AES spectra of clean and contaminated Mo and Re single crystals shown in Figures 2.11 and 2.12 exhibit the characteristic first derivative peakshape.

In addition to being a useful technique for identifying what elements are present at the surface of a material, Auger spectroscopy can be used to determine the relative coverage of an adsorbate on a surface. If the undifferentiated (N(E)) Auger peak of an element is of any constant shape, then the peak-to-peak height in the derivative mode (dN(E)/dE) is proportional to the quantity of the element at the surface. The amount of adsorbate is quantified in terms of the relative surface coverage, θ. In this thesis work, the adsorbate coverage (θ) is defined to be the ratio of the density of adatoms in the overlayer (no. of atoms/cm^2) to the density of substrate atoms in the top layer of the substrate.

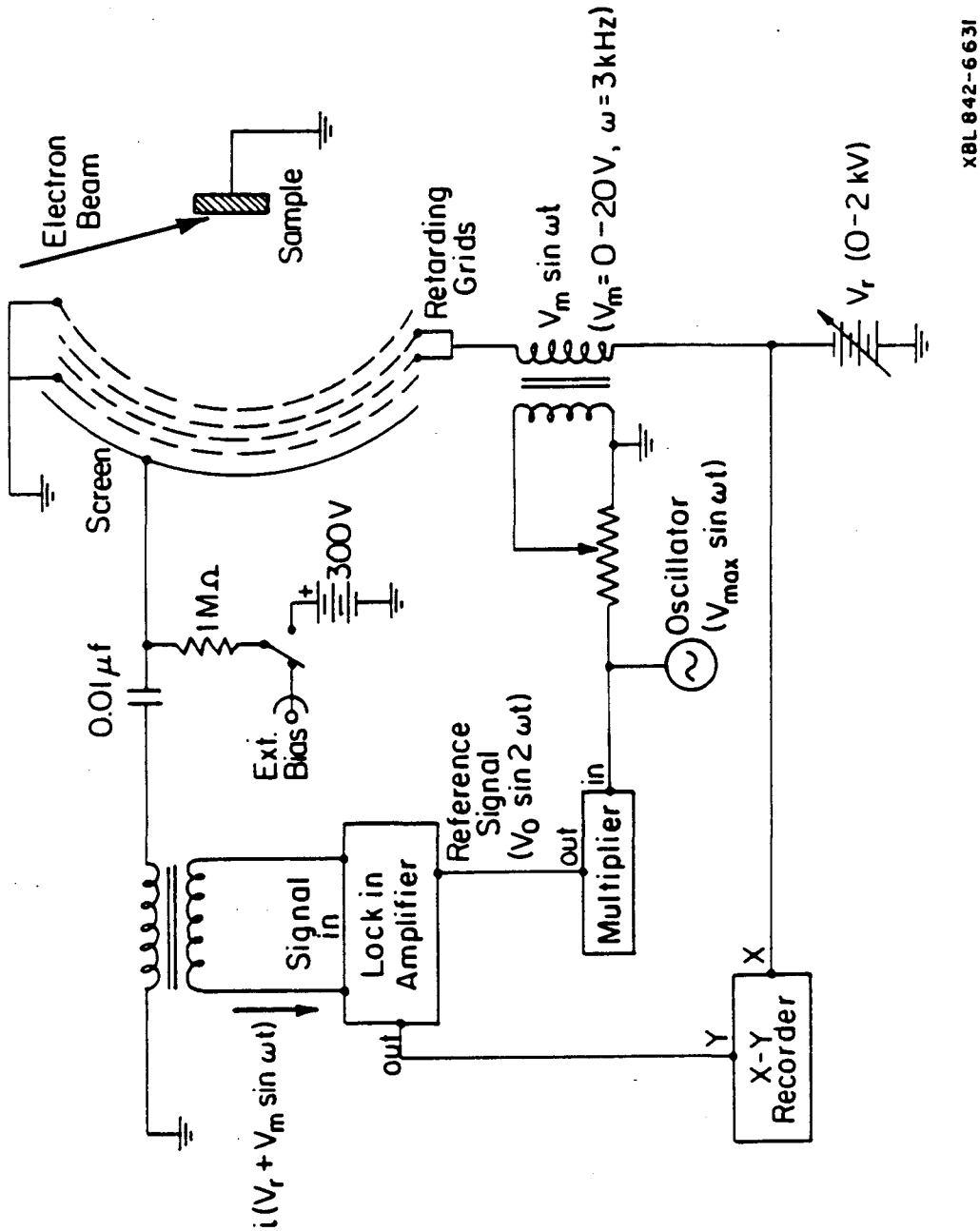

Figure 2.10: A schematic diagram of the retarding field analyzer and signal amplification circuit.

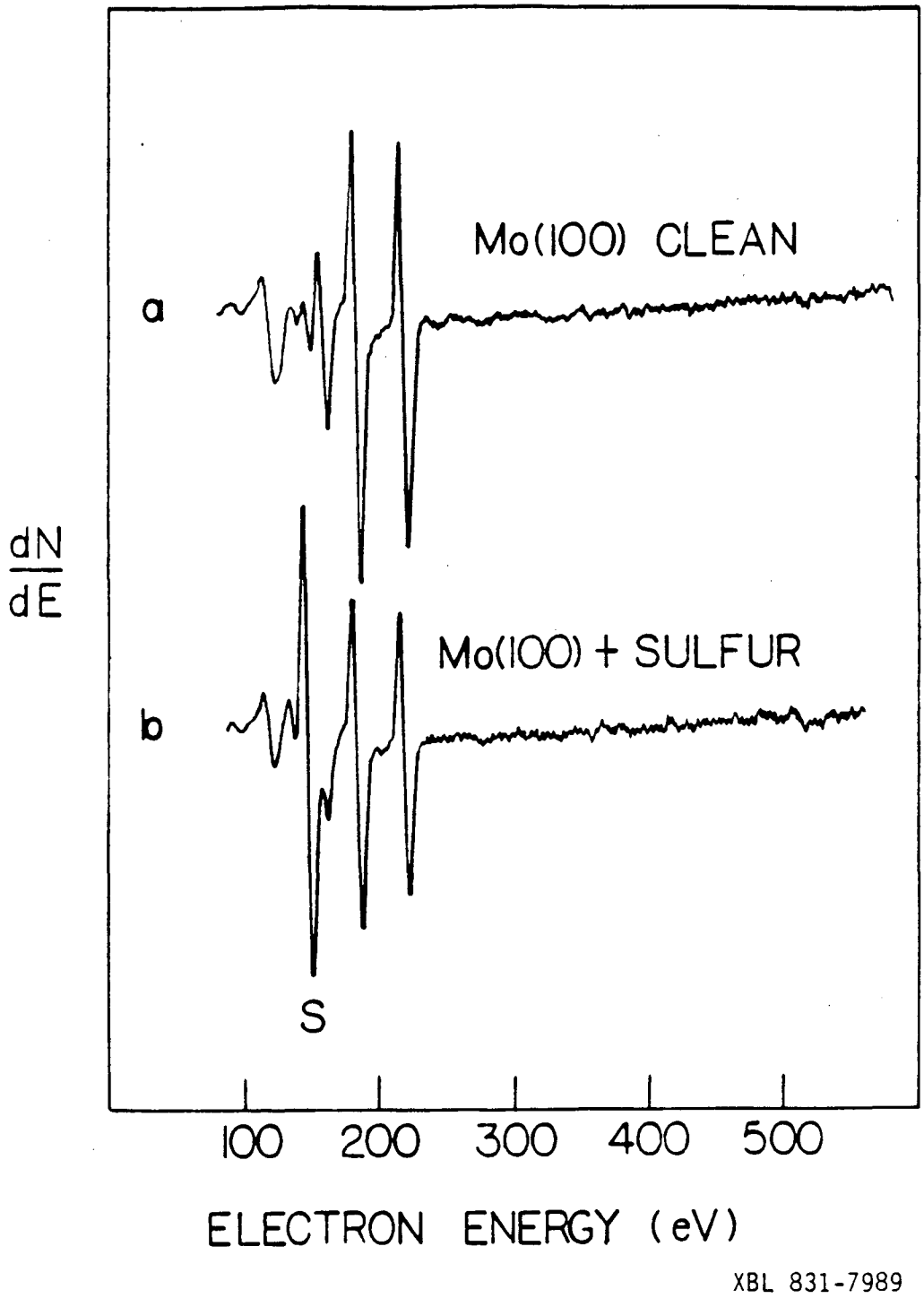

Figure 2.11: AES spectra of the clean and contaminated Mo(100) surface.

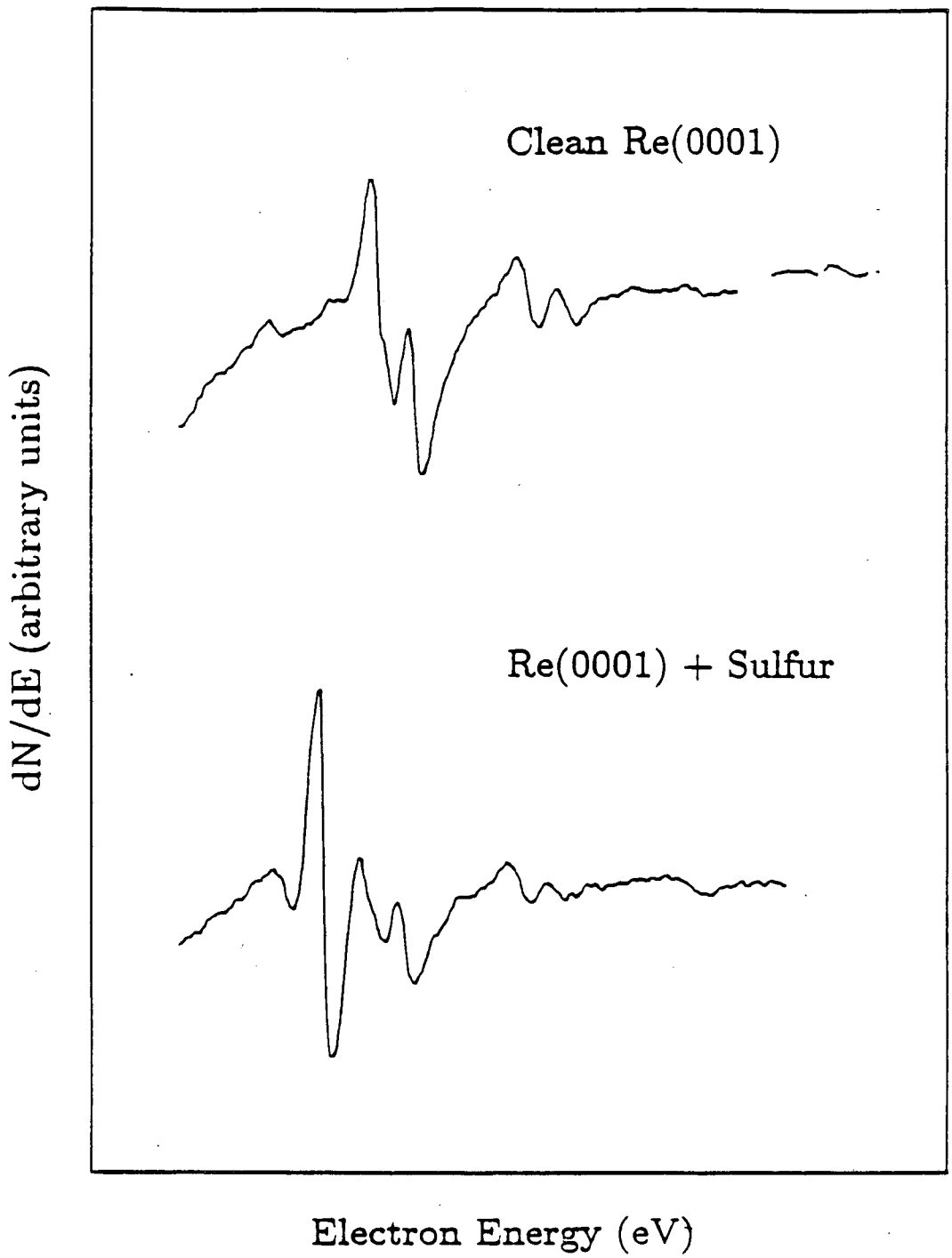

Figure 2.12: AES spectra of the clean and contaminated Re(0001) surface.

To calibrate the coverage of an adsorbate on a substrate, the ratio of the AES peak heights of the adsorbate to the substrate is related to the coverage of the adsorbate. The peak height of the adsorbate AES peak is assumed to increase linearly with coverage while the peak height of the substrate decreases linearly with coverage. In general, this is true for two-dimensional growth of an overlayer on a substrate.

Therefore

$$I_a(\theta) = \theta \cdot I_a(1)$$

$$I_s(\theta) = \theta \cdot I_s(1) + (1 - \theta) \cdot I_s(0)$$

where $I_a(\theta)$ and $I_s(\theta)$ are the AES peak heights for the adsorbate and substrate respectively at any particular adsorbate coverage, $I_a(1)$ and $I_s(1)$ are the peak heights at an adsorbate coverage of 1 monolayer (ML), and $I_s(0)$ is the substrate AES peak height for the clean surface.

Then

$$r = \frac{I_a(\theta)}{I_s(\theta)} = \frac{\theta \cdot I_a(1)}{\theta \cdot I_s(1) + (1 - \theta) \cdot I_s(0)}$$

$$= \frac{\theta \cdot I_a(1)}{I_s(0) + \theta \cdot [I_s(1) - I_s(0)]}$$

and

$$\theta(r) = \frac{r}{1 + I_a(1)/I_s(0) - I_s(1)/I_s(0)}$$

where $(I_s(1)/I_s(0))$ is called the AES attenuation factor for the adsorbate on the substrate. In practice, all that is necessary to generate an AES calibration curve for the coverage of an adsorbate is the absolute AES peak heights for the clean

substrate and for the adsorbate and substrate at a known adsorbate coverage. Normally, an additional surface science technique (e. g. LEED) is employed to accurately determine an adsorbate coverage for the AES calibration.

Finally, Auger spectroscopy can be used to investigate the chemical form of an adsorbate on a surface. The core and valence energy levels of an atom can shift depending on its chemical environment and the loss mechanisms can change as well [3]. All of these can affect the line shape of the AES transition of an element. Despite the fact that the dependence of AES line shapes upon the chemical environment of an atom is not well understood, numerous cases of changes in peak shape have been documented [6]. Figure 2.13 shows the AES line shapes for carbon in the form of graphite and tungsten carbide (W_2C) to be distinctly different [6]. In this thesis research, the lineshape of the carbon AES transition has been used to characterize adsorbed carbon overlayers as carbidic-like or graphitic-like in their chemical form. In general, it is very difficult to distinguish between the two types of adsorbed carbon overlayers with AES alone, so the distinction between carbide-like and graphite-like overlayers has been made with great caution and when possible with the aid of other pieces of evidence.

2.3.2 Low Energy Electron Diffraction

Low energy electron diffraction (LEED) is perhaps the most widely recognized surface science technique due to its origin in the famous work of Davisson and Germer [7]. In 1927, they demonstrated the wave-like behavior of electrons by observing the diffraction of low energy electrons from the surface of a nickel substrate. This result provided experimental evidence to support the theoretical work of de Broglie which predicted the wave-like properties of particles. The de Broglie

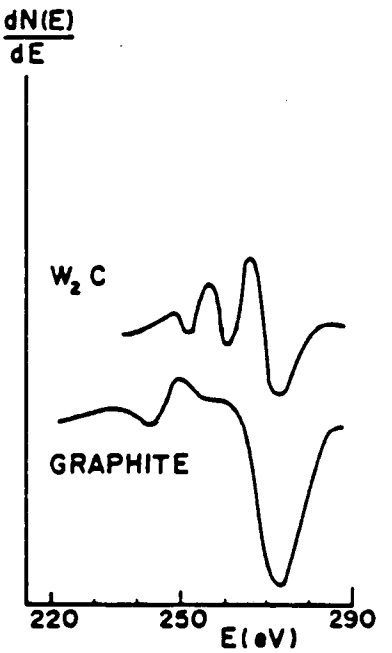

Figure 2.13: AES lineshapes for carbon in the form of graphite and tungsten carbide.

equation for the wavelength of electrons is shown below.

$$\lambda(\mathring{A}) = \sqrt{\frac{150.4}{E(eV)}}$$

Using this equation, it is easily calculated that for electron energies between 30 eV and 500 eV, the wavelength of electrons is comparable to the lattice spacings of most crystals. In addition, the mean path length of electrons in solids over this energy range is limited to a few atomic layers so backscattered electrons interact only with the outermost layers of the surface.

The theory and practice of LEED has been well described in books by Ertl and Clarke, so only general considerations are addressed here [3,8]. Diffraction of a beam of electrons from a surface results from the interaction of the periodic oscillations of the electron waves with a periodic array of scattering centers. Therefore, if a monoenergetic and parallel beam of electrons is scattered from a single crystal surface, constructive and destructive interference of elastically back-scattered electrons will occur and diffraction is observed. The diffraction condition for LEED studies with a normal incidence beam is given by the Bragg Law:

$$sin\phi = \frac{n\lambda}{d} = \frac{n}{d}\sqrt{\frac{150.4}{E(eV)}}$$

where n is an integer, d is the separation between rows of surface atoms in Ångstroms (Å) and E is the electron energy in electron volts (eV). Figure 2.14 is a schematic diagram of the LEED experiment. A normal incidence electron gun is located at the center of the LEED optics assembly and the single crystal surface is positioned at the center of curvature of the phosphor screen. A negative voltage a few volts less negative than the beam voltage is applied to the second and third grids of the LEED optics in order that only elastically backscattered electrons reach the phosphor screen. The elastically scattered electrons are post-accelerated into the screen by a positive bias of $\sim$ 5 kV placed on the phosphor

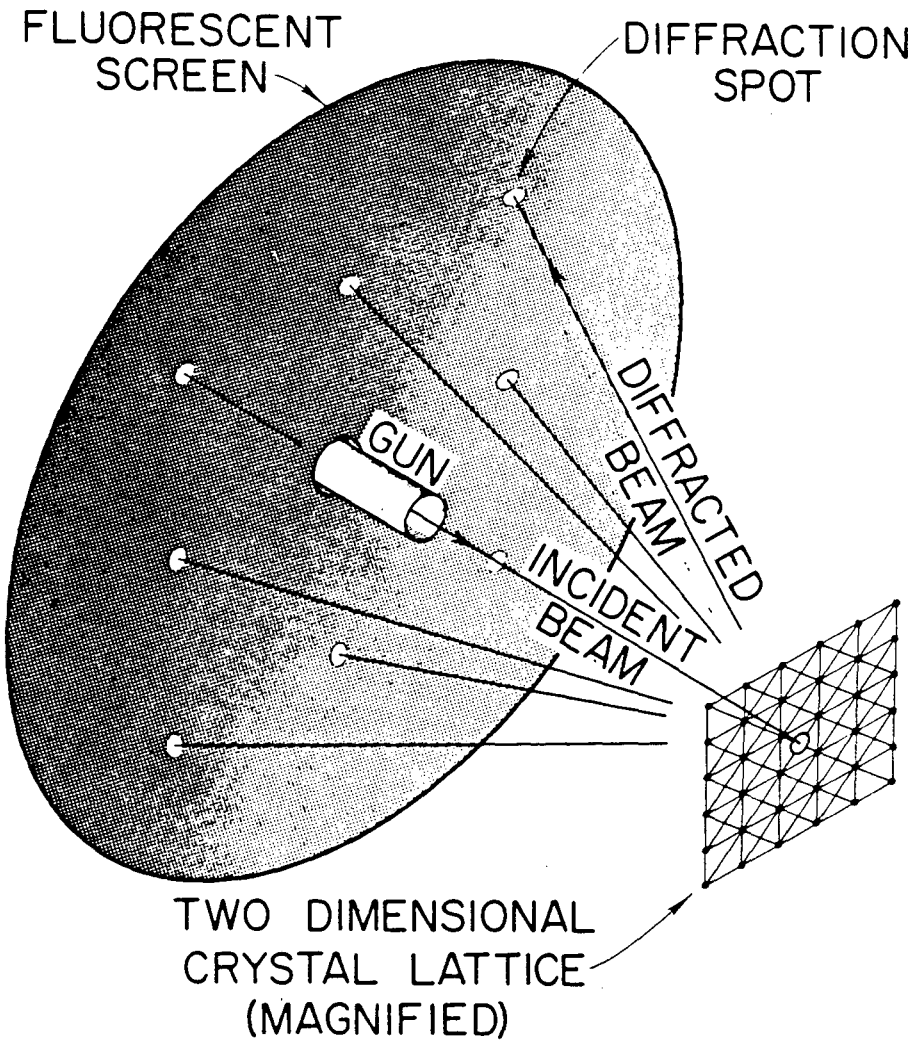

XBB 708-3583

Figure 2.14: A schematic diagram of a LEED experiment.

screen. At angles satisfying the Bragg condition, bright spots appear on the screen which can be observed directly or photographed with a camera. A photograph of a p(2×1) LEED pattern observed from a Mo(100) single crystal covered with 1 ML of sulfur is shown in Figure 2.15 along with a possible real space structure of the surface.

LEED was used in this thesis research primarily as a technique to verify the long range order of clean and adsorbate covered single crystal surfaces, to determine adsorbate coverages in combination with AES, and to determine the dimensions and symmetry of the adsorbate unit cell. LEED experiments in which the diffraction pattern is viewed and recorded at a single energy allow determination of the symmetry and dimensions of the adsorbate unit cell, but do not yield the registry of the adsorbate overlayer with the underlying substrate. More complicated and time-consuming LEED studies can be performed which yield the adsorption sites and coordinates of adsorbates as well as the unit cell information. These studies entail recording the intensity of the LEED diffraction spots as a function of the incident beam energy and then modeling the diffraction experiment with sophisticated computer calculations until the experimental and theoretical intensity versus voltage curves match.

The diffraction pattern observed in a LEED experiment is a direct representation of the reciprocal lattice of the surface. The symmetry of the surface is readily obtained from the diffraction pattern while determination of the dimensions of the surface unit cell requires transformation of the reciprocal lattice vectors into real space lattice vectors. In the case of an ordered adsorbate on a single crystal surface, it is often possible to express the lattice vectors of the overlayer lattice ($\vec{b_1}$, $\vec{b_2}$) as a linear combination of the substrate lattice vectors ($\vec{a_1}$, $\vec{a_2}$) as shown

beam energy = 125 eV

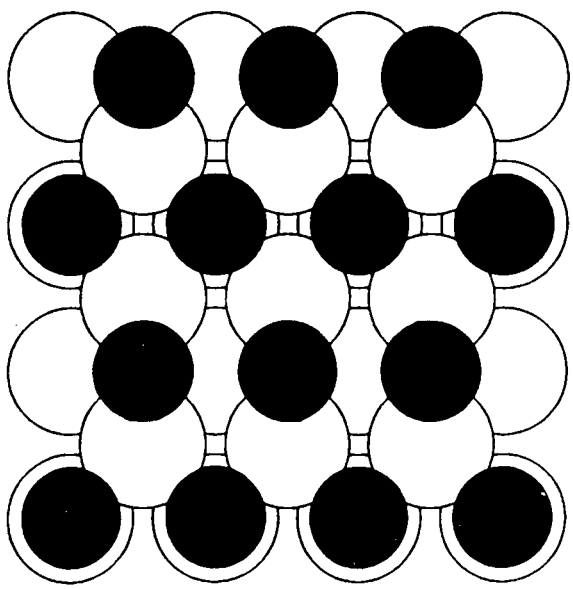

XBB 887-7310

Figure 2.15: A p(2×1) LEED pattern for 1 ML sulfur covered Mo(100) surface.

below in matrix notation.

$$\begin{pmatrix} b_1 \\ b_2 \end{pmatrix} = \begin{pmatrix} m_{11} & m_{12} \\ m_{21} & m_{22} \end{pmatrix} \begin{pmatrix} a_1 \\ a_2 \end{pmatrix}$$

or

$$\vec{b} = \mathbf{M} \cdot \vec{a}$$

If the above is true, then a corresponding relationship exists in reciprocal space.

$$\vec{b}^* = \mathbf{M}^* \cdot \vec{a}^*$$

Therefore, using the reciprocal matrix and the relation $\mathbf{M} \cdot \mathbf{M}^* = \mathbf{1}$ the real space matrix, $\mathbf{M}$, can be determined. Once $\mathbf{M}$ is known, the dimensions of the overlayer unit cell can be calculated.

2.4 Detection of Radiotracer ^{14}C and ^{35}S Overlayers

Radiotracer ^{14}C and ^{35}S were employed in this research to determine rates of hydrogenation and exchange of adsorbed carbon and sulfur overlayers under high pressure reaction conditions. Radiotracers are particularly useful in studies of heterogeneous catalysis because labelled isotopes on catalyst surfaces can be distinguished from surface species containing normal isotopes which are produced by adsorption and reaction of gas phase molecules. ^{14}C and ^{35}S are low energy beta (β^-) emitters and their half-lives and maximum energies of beta emission are shown in Table 2.1 [9]. A UHV compatible β^- detection system has been developed in this laboratory which permits radiotracer labelling studies to be carried out in conjunction with high pressure reactions and/or surface science experiments [10]. The detection system consists of a silicon surface barrier detector (Ortec TA-23-25-300) recessed in a liquid nitrogen cooled copper jacket and connected to a

Table 2.1: Beta Emission Data for ^{14}C and ^{35}S

Isotope	*Half-life (years)*	E_{max} *(keV)*
^{14}C	5.7×10^{3}	158
^{35}S	2.4×10^{-1}	167

rotatable feedthrough. A schematic diagram of the β^- detector and counting system is shown in Figure 2.16. The surface barrier detector is composed of a slice of ultrapure n-type silicon whose surface region has been depleted of free charge carriers. The detector is mounted in an insulating ring and its front and back surfaces are metallized with gold and aluminum respectively so that a voltage bias can be applied across the detector. The thicknesses of the gold window (40 μg Au/cm^{-2}) and of the silicon which has been depleted of charge carriers (300 μm) were chosen to optimize the detector efficiency for low energy beta radiation ($\sim$ 150 keV). The front side of the detector is grounded while a positive bias of 50-100 volts is applied to the backside. Free charge carriers produced in the depletion region by ionizing radiation are separated by the electric field and detected as a current pulse at the detector electrodes. Integration of the current pulse yields a signal proportional to the energy of the ionizing radiation and it is amplified and collected by a multichannel, pulse height analyzer (Tracor TN 1705). Integration of the timed spectra recorded by the pulse height analyzer yields a count rate (counts/minute) which is proportional to the amount of radioactively labelled material in the detection area.

The detector unit is located at the end of a rotatable feedthrough mounted on a six inch conflat flange. The flange is equipped with feedthroughs for a chromel-alumel thermocouple and water or liquid nitrogen cooling as shown in Figure 2.17.

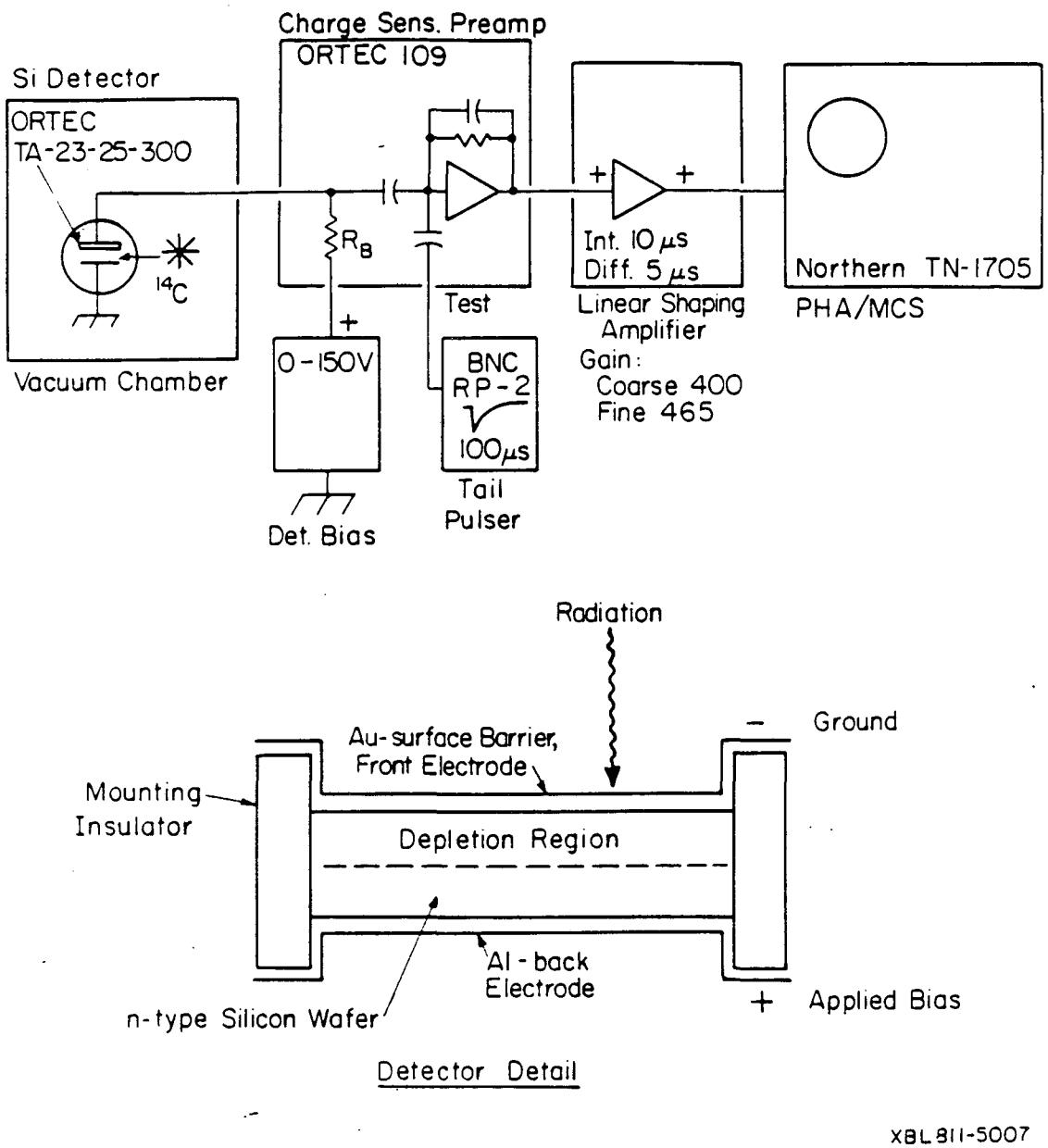

Figure 2.16: A schematic diagram of the β^- detector and counting system

The temperature of the detector must be maintained between -30° C and 30° C during the time in which the voltage bias is applied to the detector. The best β^- measurement conditions were found to be a detector temperature of -30° C to minimize the detector dark current, all filaments in the chamber off and the chamber sealed from all sources of light.

Beta emission from ^{14}C and ^{35}S overlayers on the Mo(100) surface was measured by rotating the detector in front of the single crystal and positioning the single crystal at the center of the detector at a distance of ~ 0.2 cm. A typical β^- emission spectrum from an adsorbed ^{14}C overlayer on the Mo(100) surface is shown in Figure 2.18. The detecting surface of the silicon detector has a diameter of 0.8 cm which is about the same size or smaller than the diameter of the single crystals used in the radiotracer studies. Furthermore, the detecting surface is recessed approximately 0.2 cm into the detector unit which helps screen all surfaces other than the single crystal surface from contributing to the β^- emission measurements. The background β^- emission was determined by measuring the count rate of the clean sample surface before and after a radiotracer experiment. For both the ^{14}C and ^{35}S experiments, the background contribution to the count rate was found to be ≤ 20 %.

2.5 Materials

2.5.1 Single Crystals and Polycrystalline Foils

The molybdenum and rhenium single crystals used in this research were cut by spark erosion from single crystal rods obtained from the Materials Research Corporation. The single crystals, which were on average 1 cm^2 in area and < 0.1 cm thick, were oriented to within 1° using Laue back-diffraction and polished using

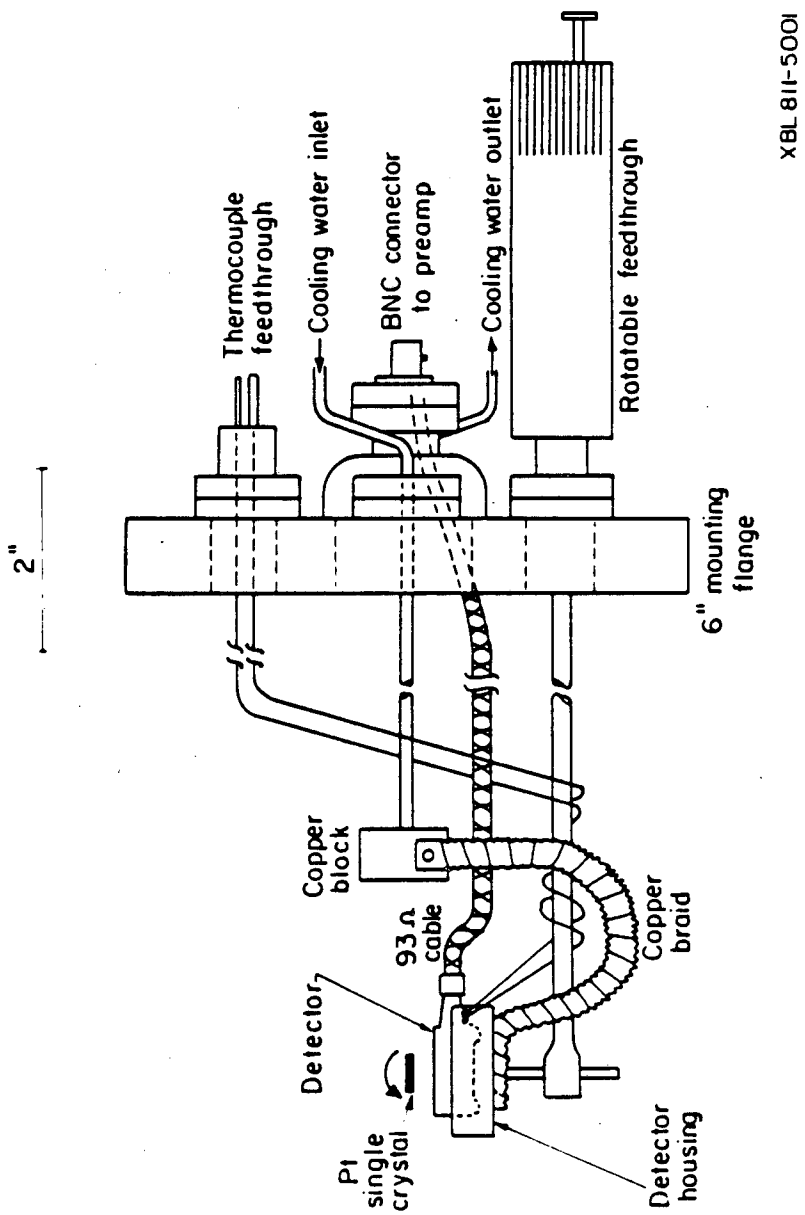

Figure 2.17: Drawing of the β^- detector and mounting flange.

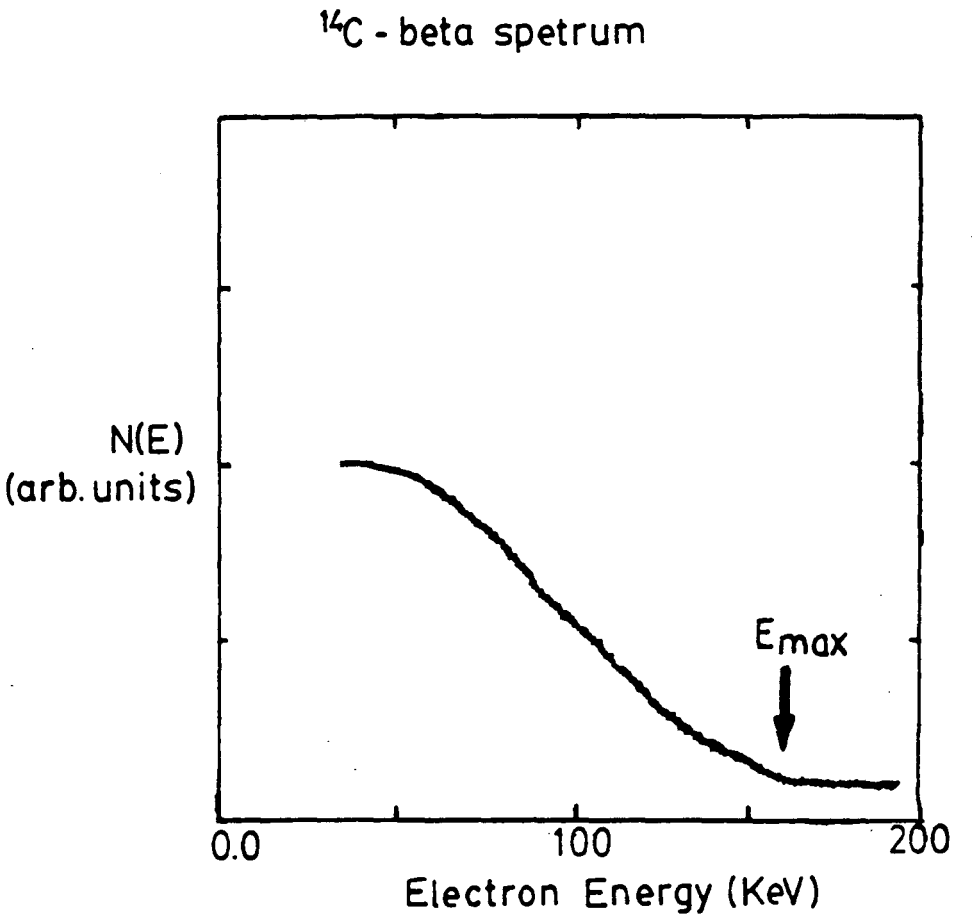

Figure 2.18: A β^- emission spectrum from adsorbed ^{14}C on the Mo(100) surface.

Table 2.2: Reagents Used in this Research

Reagent	*Source*	*Purity (%)*
Thiophene	Aldrich	99+
Butadiene	Matheson	99.0
cis-2-Butene	Matheson	95.0
Ethylene	Matheson	99.5
Hydrogen sulfide	Matheson	99.5+
Hydrogen	Matheson	99.95
Oxygen	Matheson	99.9
Argon	Matheson	99.9

successively finer grades of diamond paste until mirror finish was achieved. One should make the single crystals as thin as is practically possible to minimize the contribution of the edge area to the total surface area. The single crystals were spot-welded to short pieces of 0.020 inch Ta or Re wire which were in turn spot-welded to the sample manipulator as described in Section 2.2.2.

Molybdenum, rhenium and cobalt foils were cut from high purity sheets of the metals and inserted into the UHV chamber without further treatment. The foils had thicknesses in the range 2-5 mil (0.005-0.013 cm) and areas of 1-2 cm^2. The Mo foil was of unknown origin while the Re and Co foils were purchased from Alpha Products and the Materials Research Corporation respectively. The metal foils were mounted onto the manipulator via 0.020 inch wires of the respective metals spot-welded along the length of the foils and attached to the heating feedthroughs by spot-welds.

2.5.2 Reagents

The reagents used in this research (except the radioactive compounds) are listed in Table 2.2 along with their sources and purities. All of the reagents with the excep-

tion of thiophene were used without further purification. The "gold label" quality thiophene purchased from Aldrich contained amounts of an impurity, believed to be carbon disulfide (CS_2), sufficient to interfere with the thiophene HDS reaction. The impurity strongly deactivated both Mo and Re catalysts and its presence led to abnormally high production of methane under reaction conditions. To remove the impurity, thiophene was fractionally distilled over metallic sodium in an inert atmosphere of dry nitrogen. The distilled thiophene was further purified by repeated freeze-pump-thaw cycles before use in the catalytic reactor system.

2.5.3 Radioactively Labelled Reagents

^{14}C labelled overlayers were formed on the Mo(100) surface by decomposition of $^{14}C_2H_4$. Twenty millicuries (mCi) of ^{14}C-ethylene was obtained from the Amersham Corporation and had a radiochemical purity of 98.7 % and a specific activity of 100 mCi/mmole. The labelled ethylene was divided between two break-seal pyrex tubes and was further purified before use by freeze-pump-thaw cycles. The Lawrence Berkeley Laboratory glass shop outfitted the tubes with teflon stopcocks and pyrex-to-1/4 inch Kevlar adapters which allowed vacuum tight connection of the tubes to the UHV system using Gyro-lok fittings.

^{35}S labelled overlayers were produced on the Mo(100) surface by the decomposition of $C^{35}S_2$. The labelled CS_2 was custom synthesized by the New England Nuclear Corporation and had a radiochemical purity > 99 % and a specific activity of 100 mCi/mmole. The $C^{35}S_2$ was stored in two breakseal tubes, each containing $\sim$ 37 mCi of the radioactive material, and the tubes were outfitted in the same manner as for the labelled ethylene for use in the UHV system.

2.6 Procedures

2.6.1 Sample Cleaning

Molybdenum and rhenium are refractory metals which can be cleaned using similar methods. The major impurities in single crystals and foils of the two metals were found to be carbon, sulfur and oxygen. Sulfur was easily removed from the metal surfaces by heating the samples to 1900 K which resulted in desorption of sulfur into the vacuum. Surface oxygen can also be desorbed from molybdenum and rhenium by heating, but it is necessary to reach a temperature of 2000 K for complete oxygen removal. The platinum-platinum 10 % rhodium thermocouple used in this work melts at $\sim$ 1925 K so sample heating was limited to a maximum of 1900 K. Higher temperature thermocouples exist (e. g. tungsten-rhenium), but they are not suitable for use in high pressures of hydrogen. Residual oxygen left on the molybdenum and rhenium surfaces was removed by reaction with C_2H_4 to produce CO in UHV or by reaction during thiophene HDS to form products which have not been characterized.

Carbon was found to be the most tenacious impurity in the molybdenum and rhenium samples. Carbon was removed by reaction with oxygen ($P_{O_2} = 1\times10^{-8}$-1×10^{-5} Torr) at high temperatures (T = 1100-1575 K) to produce CO and CO_2. New single crystals required repeated oxygen treatments for many days under the most severe conditions to clean the near surface region of the samples of carbon. Removal of carbon with oxygen was closely monitored to avoid dissolving oxygen into the bulk of the samples.

The major impurities in cobalt foil samples were also found to be carbon, sulfur and oxygen. Argon ion sputtering must be employed to clean cobalt samples as they cannot be heated to temperatures sufficient to desorb sulfur and oxygen.

The sputtering conditions used were an accelerating voltage of 1000 volts, a gas mixture of 0.1 % oxygen in argon (total pressure = 5×10^{-5} Torr) and a sample temperature of 875 K. After 10-30 minutes at these conditions, the sample was sputtered at room temperature for an additional five minutes and then annealed at 800 K.

2.6.2 Preparation of Carbon and Sulfur Overlayers

Adsorbed sulfur overlayers were prepared on the Mo(100), Re(0001), Re($10\bar{1}0$) surfaces by deposition of sulfur with the electrochemical sulfur source described earlier. In all cases, sulfur was deposited with the surfaces at room temperature and saturation coverages of 1.0 ML, $\sim$ 0.7 ML, and 1.0 ML on the Mo(100), Re(0001), Re($10\bar{1}0$) surfaces respectively could be prepared in this manner. Lower coverages were produced by annealing the sulfur saturated surfaces to desorb a fraction of the adsorbed sulfur. Coverages were determined using AES calibration curves generated using the equations described in Section 2.3.1.

The AES attenuation factors for sulfur on the Re(0001) and Re($10\bar{1}0$) surfaces were determined with the aid of LEED. A ($2\sqrt{3}\times2\sqrt{3}$) LEED pattern and a p(2×2) LEED pattern are observed from the Re(0001) and Re($10\bar{1}0$) surfaces respectively at a sulfur coverage of 0.5 ML [11]. AES peak heights were measured for the S(148eV) and Re(177eV) Auger transitions for the sulfur covered and clean rhenium surfaces and the AES attenuation factors calculated assumming a linear decrease of the Re(177eV) AES peak height with coverage up to 1.0 ML. An AES calibration curve for sulfur on the Mo(100) surface has been previously determined in the UHV chamber used in this research [12].

Adsorbed carbon overlayers were formed by decomposition of ethylene (C_2H_4) on the molybdenum and rhenium single crystal surfaces. Carbon coverages up

to 0.85 ML, 0.25 ML, and 0.6 ML could be formed on the Mo(100), Re(0001), Re($10\bar{1}0$) surfaces respectively by dosing C_2H_4 on to the surfaces at room temperature followed by annealing to temperatures of 700-800 K to desorb H_2. To obtain higher coverages, it was necessary to thermally decompose C_2H_4 on the surfaces and this was achieved by heating the single crystal surfaces to 800-1100 K during dosing. Calibration curves for carbon on the Mo(100) and Re(0001) surfaces were determined in a similar manner as described above. For the Mo(100) surface, c(2×2), $\left|\begin{smallmatrix}2 & \bar{1}\\ 1 & 1\end{smallmatrix}\right|$ and p(2×2) LEED patterns at respective coverages of 0.50 ML, 0.67 ML and 1.0 ML were used to generate an AES calibration curve while the c(4×2) LEED pattern at a carbon coverage of 0.25 ML was used for the Re(0001) surface [13,14]. On the Re($10\bar{1}0$) surface, the AES attenuation factor for carbon was determined in a different manner. The surface was dosed with thiophene at room temperature followed by annealing to 700 K. Using the AES calibration curve for sulfur on the Re($10\bar{1}0$) surface, the sulfur coverage was determined to be 0.1 ML. Thiophene decomposes completely on the clean Re($10\bar{1}0$) surface with desorption of H_2 only, indicating that the carbon coverage is 0.4 ML. The C(272eV) and Re(177eV) AES peak heights were measured for this surface and the clean surface and were used to calculate the AES attenuation factor for carbon. This procedure does not take into account attenuation of the Re(177eV) peak by the coadsorbed sulfur from thiophene, but carbon coverages using this calibration are believed to be accurate within 15 % [15].

2.6.3 Preparation of ^{35}S and ^{14}C Labelled Overlayers

^{35}S and ^{14}C overlayers were prepared on the Mo(100) surface by decomposition of $C^{35}S_2$ and $^{14}C_2H_4$. In both cases, the compounds were dosed on to the metal surface at room temperature followed by heating to decompose the

molecules. The maximum sulfur coverage which could be achieved by decomposition of $C^{35}S_2$ was 0.75 ML and this was accomplished by two doses of $C^{35}S_2$ totalling 30-45$\times 10^{-9}$ Torr·sec using a leak valve equipped with a dosing tube. The Mo(100) crystal was heated to 1100 K after each dose to dissociate the $C^{35}S_2$ and to allow diffusion of carbon into the bulk. At sulfur coverages, $\theta_s \geq 0.5$ ML, coadsorbed carbon diffuses into the bulk of a Mo(100) single crystal upon heating to $\sim$ 1100 K.

^{14}C overlayers were prepared in a similar manner as for the unlabelled carbon overlayers except that dosing was always done at room temperature. Following dosing with $^{14}C_2H_4$, the single crystal was heated to 700 K to decompose the adsorbed ethylene and to desorb hydrogen. The ^{14}C covered Mo(100) surface was never annealed above 700 K to avoid diffusion of ^{14}C into the bulk of the crystal.

2.6.4 High Pressure Reactions

Atmospheric pressure reactions on single crystal and polycrystalline foil samples were carried out using the high pressure isolation cell and catalytic reactor system described in Sections 2.2.2 and 2.2.3. The single crystal and foil samples were prepared and characterized in UHV prior to closing the high pressure isolation cell. The valves isolating the cell from the reaction loop were opened and the system pressurized with reactant gases. The minor components (thiophene, butadiene, cis-2-butene, H_2S) were leaked into the reactor first at pressures in the range 0.1-5.0 Torr, followed by hydrogen and/or argon to a total pressure of 780 Torr. The gases were circulated in the system with a small circulation pump (flow rate $\approx$ 50 cm^3/minute) for 15-30 minutes prior to heating the sample to the reaction temperature to ensure complete mixing as determined by gas chromatography. The temperature of the sample was maintained at the reaction

Table 2.3: Retention Times of Thiophene and its HDS Products

Compound	*Retention Time (seconds)*
Thiophene	460
1-Butene	124
Butane	151
cis-2-butene	170
trans-2-butene	201
Butadiene	211

temperature using a temperature controller built in the Lawrence Berkeley Laboratory electronics shop. Gas samples were injected into a gas chromatograph at 15 minute intervals and components separated on a 6 foot long, 19 % picric acid on carbowax column. The temperature program of the gas chromatograph was set for a cycle of 4 minutes at 30°C followed by heating at a rate of 32°/minute to 110°C, at which temperature the column was maintained for an additional 4 minutes. C_4 hydrocarbon products were separated with the column at 30°C while the higher temperature was necessary to achieve elution of thiophene. The retention times for thiophene and its HDS products are shown in Table 2.3. The products were detected with a flame ionization detector and the peak areas determined electronically using a Spectra Physics Minigrator. The flame ionization detector was calibrated over the range of hydrocarbon pressures produced in HDS reactions using a standard CH_4/N_2 gas mixture.

Upon completion of a high pressure reaction, the single crystal or polycrystalline foil was cooled to room temperature in the flowing gas mixture followed by evacuation of the reactor using a mechanical pump. When the pressure of the reaction cell was $\leq$ 500 mTorr, it was isolated from the reaction loop and pumped with a liquid nitrogen trapped, 2 inch diffusion pump for 15-120 minutes to a

pressure $< 10^{-3}$ Torr. The high pressure cell was then opened and the crystal characterized and prepared for further experiments.

High pressure reactions involving radioactively labelled overlayers were carried out in the following manner. An overlayer of ^{14}C or ^{35}S of the desired coverage was formed on the Mo(100) surface and the β^- activity measured. The single crystal was then enclosed in the isolation cell and exposed to reactant gases as described above for normal high pressure reactions. After circulation of the gases to ensure mixing, the single crystal was heated to the desired reaction temperature for a time interval of 5-30 minutes. The crystal was then cooled, the isolation cell evacuated and opened to expose the single crystal to UHV. The β^- activity was then determined and the process repeated with the existing surface or a newly prepared surface.

References

[1] C. Wagner. *J. Chem. Phys.* **21** (1953) 1819.

[2] G. A. Somorjai. *Chemistry in Two Dimensions: Surfaces.* Cornell University Press, Ithaca, 1981.

[3] G. Ertl and J. Kuppers. *Low Energy Electrons and Surface Chemistry.* Verlag Chimie, Weinheim, 1974.

[4] D. Briggs and M. P. Seah. *Practical Surface Analysis by Auger and X-ray Photoelectron Spectroscopy.* J. Wiley and Sons, Chichester, England, 1983.

[5] F. N. Palmberg, G. E. Riach, R. E. Weber, and N. C. MacDonald. *Handbook of Auger Electron Spectroscopy.* Physical Electronics Ind., Minnesota, 1972.

[6] K. Ishikawa and Y. Tomida. *J. Vac. Sci. Technol.* **15** (1978) 1123.

[7] C. J. Davisson and L. H. Germer. *Phys. Rev.* **30** (1927) 705.

[8] L. J. Clarke. *Surface Crystallography, An Introduction to Low Energy Electron Diffraction.* J. Wiley and Sons, Chichester, England, 1985.

[9] G. Friedlander, J. W. Kennedy, and J. M. Miller. *Nuclear and Radiochemistry.* J. Wiley and Sons, New York, 1964.

[10] S. M. Davis, B. E. Gordon, M. Press, and G. A. Somorjai. *J. Vac. Sci. Technol.* **19** (1981) 231.

[11] D. G. Kelly, A. J. Gellman, M. Salmeron, G. A. Somorjai, V. Maurice, M. Huber, and J. Oudar. *Surf. Sci.,* (in press) .

[12] A. J. Gellman. PhD thesis, University of California, Berkeley, 1985.

[13] C. Guillot, R. Riwan, and J. LeCante. *Surf. Sci.* **59** (1976) 581.

[14] R. Ducros, M. Housley, M. Alnot, and A. Cassuto. *Surf. Sci.* **71** (1978) 433.

[15] D. G. Kelly. PhD thesis, University of California, Berkeley, 1987.

Chapter 3

Structure of Clean and Adsorbate (C, S) covered Molybdenum and Rhenium Single Crystal Surfaces

3.1 Introduction

The hydrodesulfurization reaction has been the basis for one of the most important catalytic processes employed in the petroleum industry for over fifty years, yet the fundamental surface chemistry of the reaction is poorly understood. As discussed in the introductory chapter, fundamental research studies of HDS have concentrated on the use of unsupported and supported metal sulfide catalysts. The failure to develop a molecular level description of the active HDS site and of the reaction mechanism is in part due to the complex and heterogeneous nature of the catalysts employed in these studies. The approach used in this thesis research and related studies in our laboratory has been to use structurally less complex, metal single crystals as model catalysts for the HDS reaction [1,2]. The well-ordered structure of single crystals permits determination of their surface structure at the atomic level and chararcterization of the interaction of adsorbate atoms and molecules with their surfaces. In this chapter, the surface structure of the single crystals used as model HDS catalysts is discussed. First, the structure of the clean metal

surfaces will be addressed, followed by a discussion of the structure of carbon and sulfur adlayers on these same surfaces.

3.2 Structure of Clean Mo and Re Surfaces

Surface science and high pressure reaction studies of thiophene hydrodesulfurization have been carried out over single crystal surfaces of molybdenum and rhenium. HDS studies over molybdenum were carried out over the (100) face; perspective and top view drawings of this surface and the (110) and (111) faces of molybdenum are shown in Figures 3.1 and 3.2. The drawings of the (110) and (111) faces have been included because results of thiophene HDS studies over these surfaces, obtained previously in this laboratory, will be compared with the results of this work over the Mo(100) surface [2]. For rhenium, thiophene HDS has been studied over four different crystallographic planes ((0001), $(10\bar{1}0)$, $(11\bar{2}0)$, $(11\bar{2}1)$) and perspective and top view drawings of these surfaces are shown in Figures 3.3 and 3.4 respectively. The surfaces depicted in Figures 3.1-3.4 are idealized representations and were drawn assuming that the surfaces are perfect truncations of the bulk metal structure. In reality, the structure of most metal surfaces deviates from what would be predicted by the bulk structure because of the absence of metal atoms for bonding on the vacuum side of the surfaces. To compensate for the anisotropic bonding environment, the top layer atoms relax from their predicted positions and contract into the bulk of the metal. This contraction is reflected in a decrease of the atom layer spacing normal to the surface. The top layer contractions have been experimentally determined for some of the Mo and Re surfaces of interest and they are listed in Table 3.1 along with other pertinent data [3,4,5,6].

Comparison of the surface atom densities and top layer contractions listed in Table 3.1 for the Mo surfaces indicates that the more open a surface, the greater

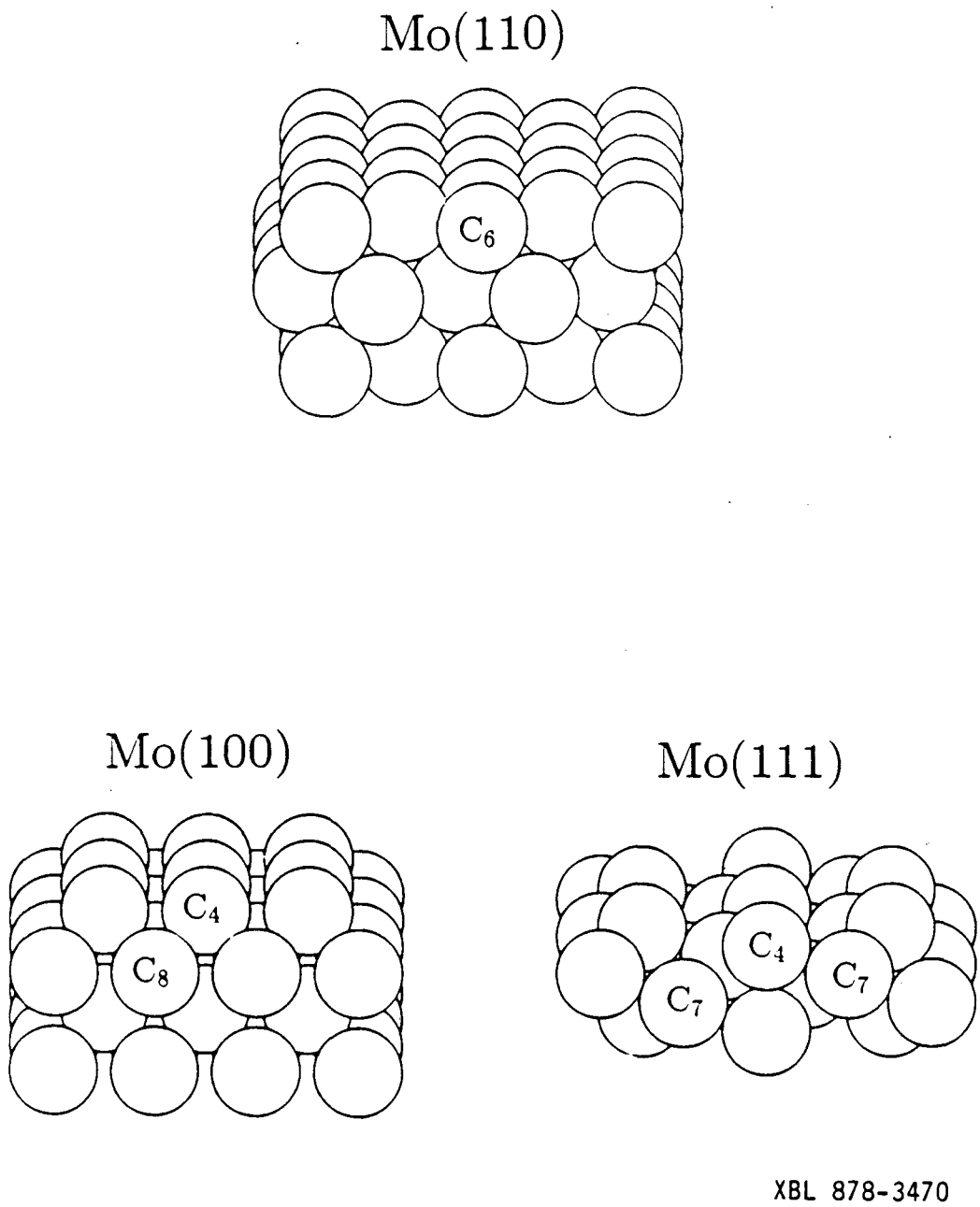

Figure 3.1: Perspective drawings of three low miller index planes of molybdenum.

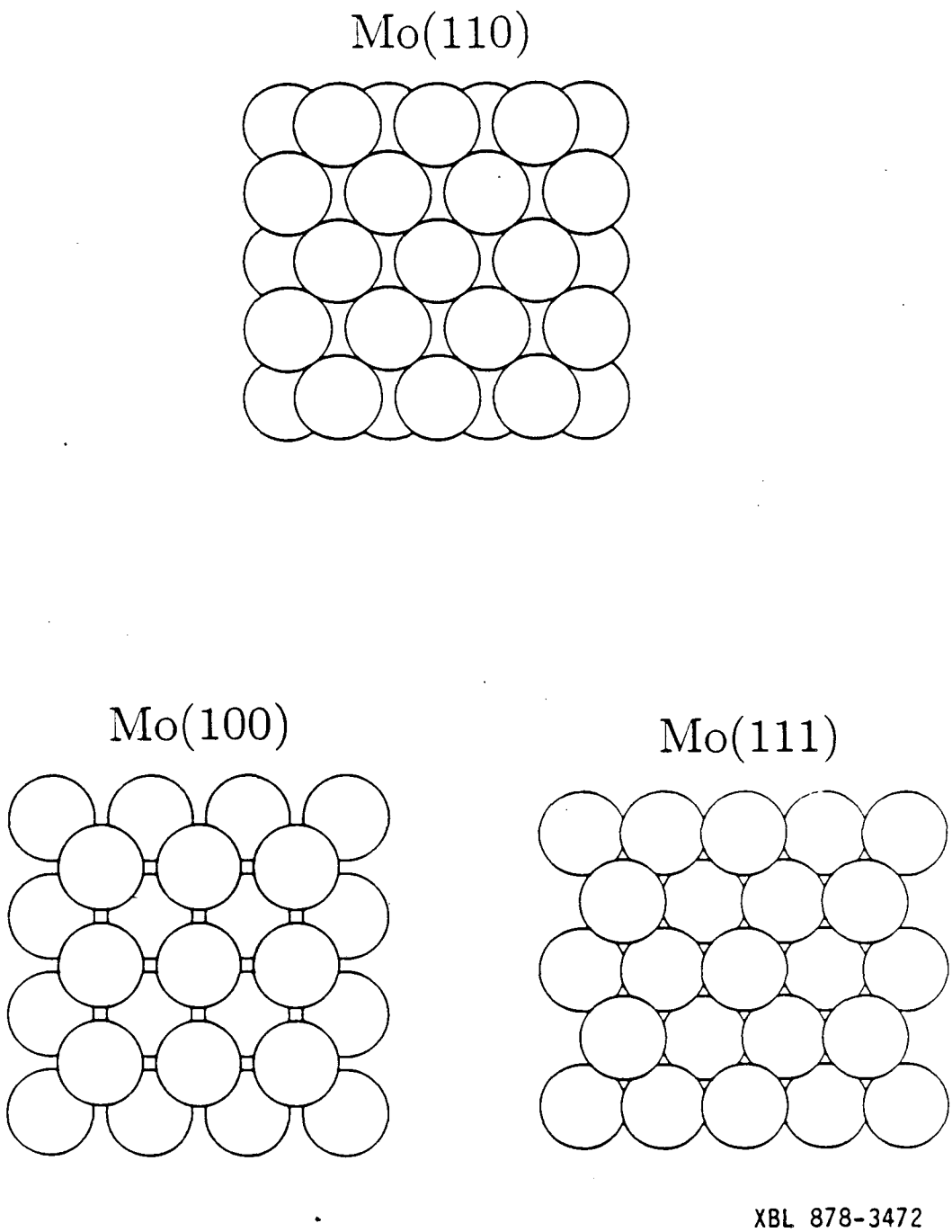

Figure 3.2: Top view drawings of the molybdenum surfaces shown in Figure 3.1.

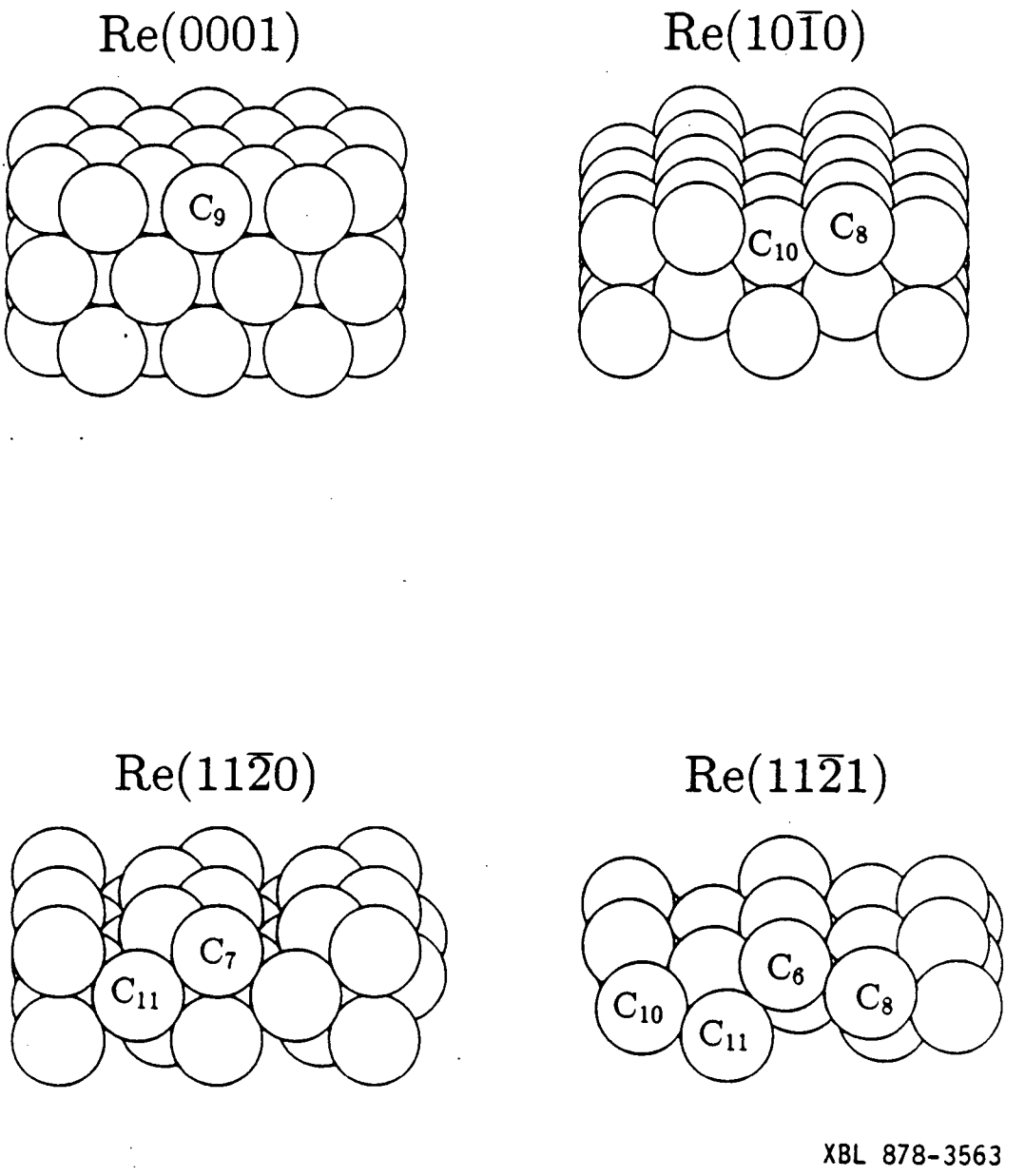

Figure 3.3: Perspective drawings of three low miller index planes of rhenium.

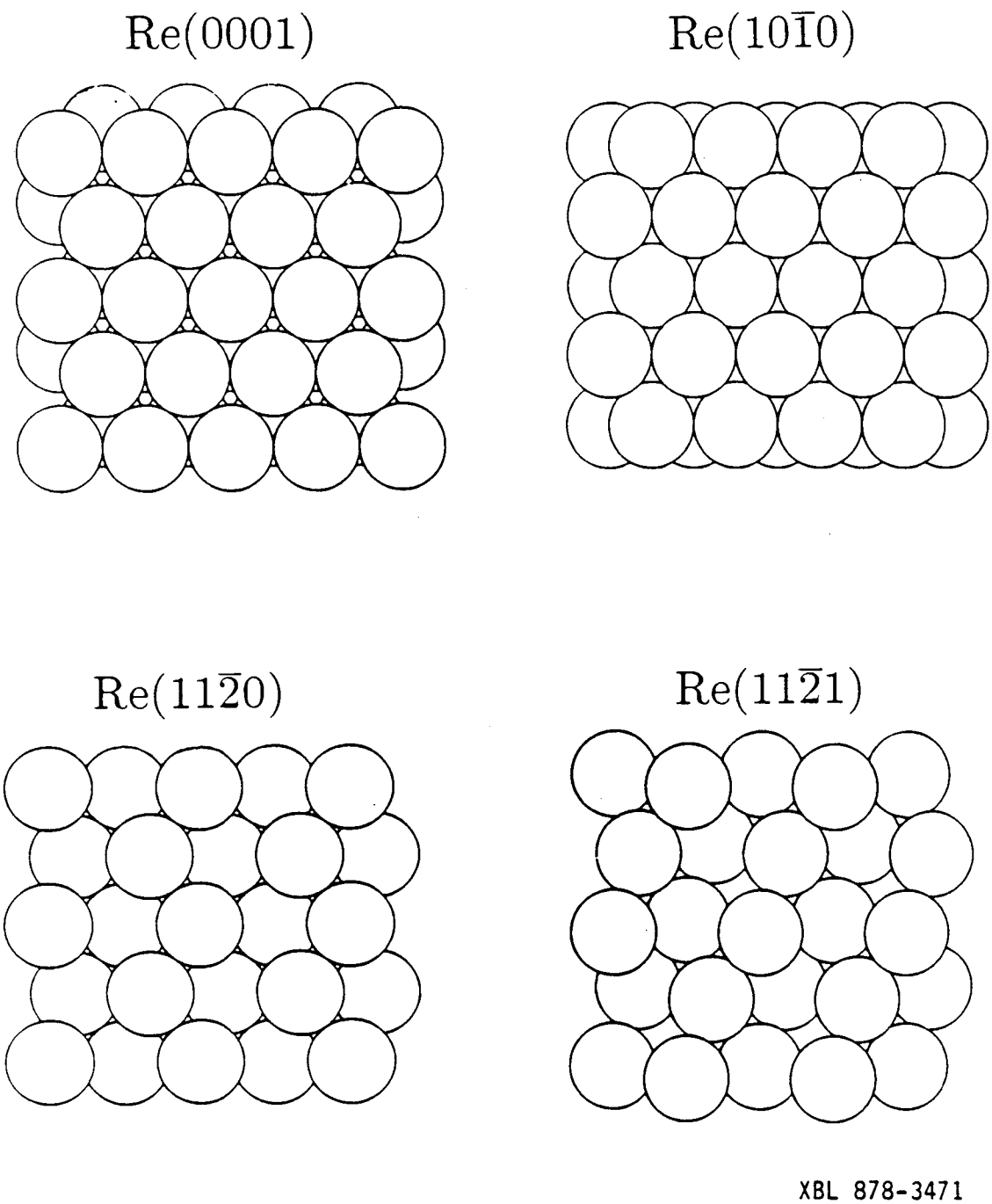

Figure 3.4: Top view drawings of the rhenium surfaces shown in Figure 3.3.

Table 3.1: Surface Atomic Densities

Surface	*Atomic Density (atoms/cm^2)*	*Relative Atomic Density*	*Top Layer Atom Coord. Number*	*Top Layer Contraction (%)*
Mo(110)	1.434 x 10^{15}	1.00	C_6	1.6
Mo(100)	1.014 x 10^{15}	0.71	C_4	9.5
Mo(111)	0.586 x 10^{15}	0.41	C_4	18
Re(0001)	1.514 x 10^{15}	1.00	C_9	—
Re(10$\bar{1}$0)	0.815 x 10^{15}	0.53	C_8	16.2
Re(11$\bar{2}$0)	0.470 x 10^{15}	0.31	C_7	—
Re(11$\bar{2}$1)	0.450 x 10^{15}	0.30	C_6	—

is the contraction of the top layer atoms. Surface atoms in open surfaces have fewer atoms with which to coordinate, so they contract further into the bulk to achieve lower energy states. It follows that the thermodynamically most stable surfaces are those in which the surface atoms are the most densely packed. The top layer atoms in these surfaces have the fewest number of dangling bonds which therefore makes the surfaces the most stable. In some cases, thermodynamically unstable surfaces undergo reconstruction to form more stable surfaces which have completely different structures from that predicted by the bulk metal structure. LEED studies of the single crystals used in this research verified that at room temperature none of the surfaces underwent reconstruction in UHV.

3.3 Structure of Carbon and Sulfur Overlayers on the Mo(100) Single Crystal Surface

3.3.1 Carbon on Mo(100)

The structure and properties of carbon overlayers on the Mo(100) surface have been the subject of numerous surface science studies [7,8,9,10]. Three ordered structures exist for the adsorbed carbon on Mo(100) system: c(2×2), $\left|\begin{smallmatrix}2 & \bar{1}\\ 1 & 1\end{smallmatrix}\right|$, and p(1×1) at coverages of 0.5 ML, 0.67 ML and 1.0 ML respectively. Ion scattering (ISS) studies of the carbon covered Mo(100) surface show carbon atoms to be adsorbed in four-fold hollow sites [8]. The ISS work and preliminary dynamical LEED studies in our group suggest that the carbon overlayer extends < 0.6 Å above the metal surface [1]. A schematic drawing of the Mo(100) surface covered with 0.5 ML of carbon is shown in Figure 3.5. In order to generate these drawings, published values of 1.36 Å and 0.77 Å were used for the atomic radii of molybdenum and carbon while the relaxation value listed in Table 3.1 was used for the Mo(100) surface [11,12]. It can be seen that the relatively small size of a carbon atom permits it to adsorb in a four-fold hollow site and extend very little, if not at all, above the plane of the metal surface.

The AES calibration curve of carbon coverage on Mo(100) which was used in this thesis work is shown in Figure 3.6 along with experimental points corresponding to ordered carbon overlayers as established using LEED. The experimentally determined AES attenuation factor for carbon on the Mo(100) surface was 0.65. The chemical form of the carbon has been previously found to be carbidic and this result has been corroborated in the present study. Figure 3.7 shows the dependence of the shape of the carbon AES transition on the the crystal annealing temperature for a surface saturated with ethylene. The AES peak shape becomes

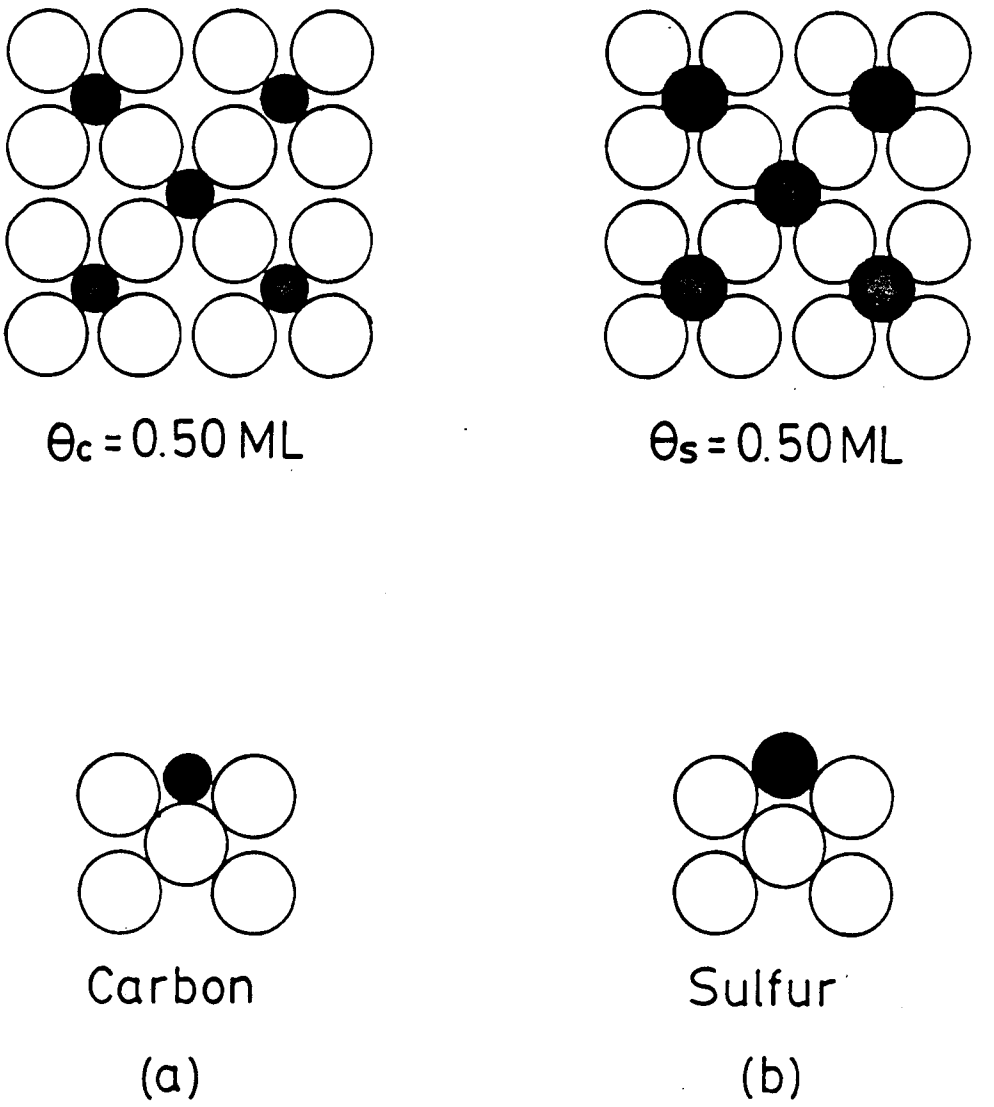

Figure 3.5: A schematic drawing of one-half monolayer of carbon and sulfur adsorbed on the Mo(100) surface.

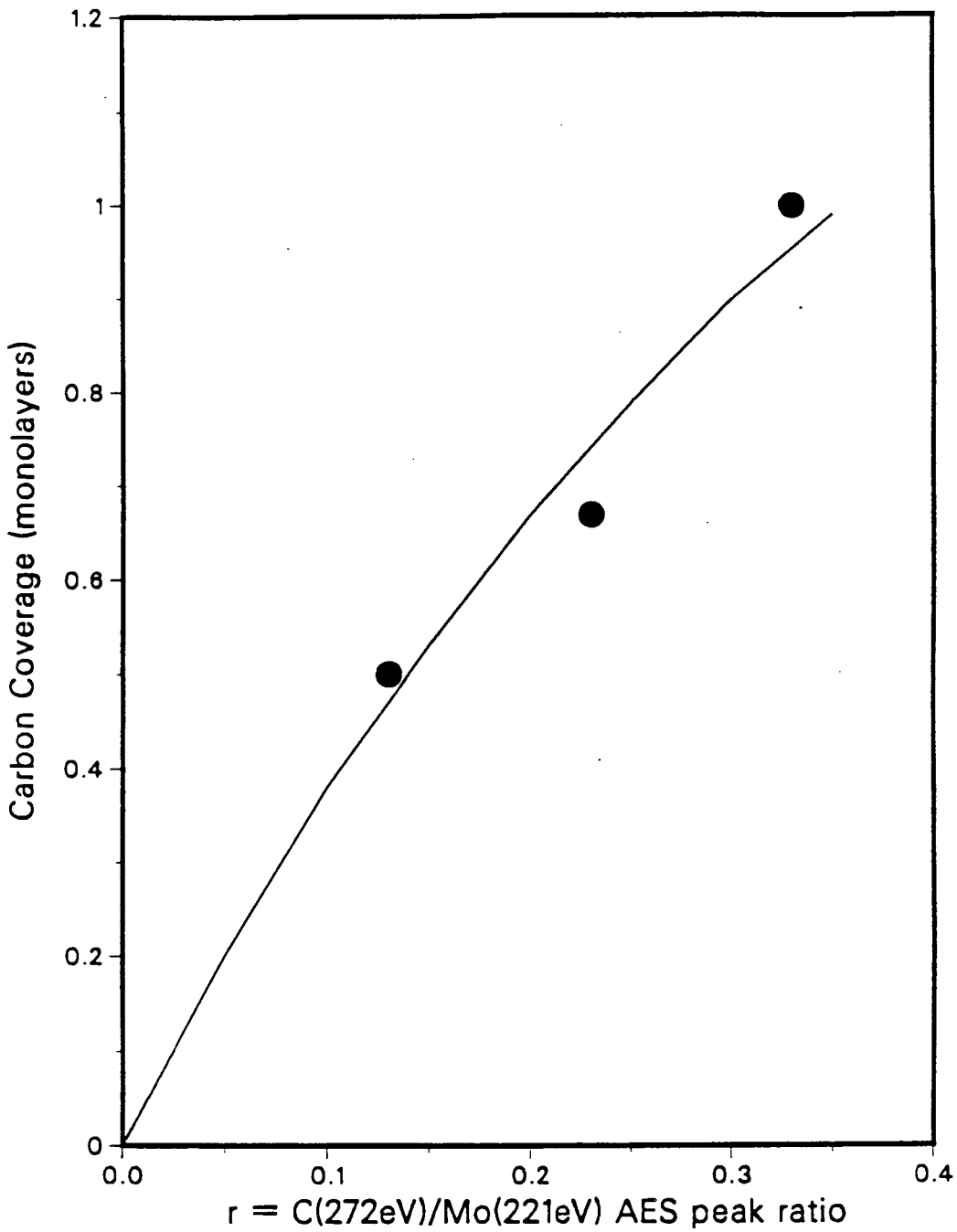

Figure 3.6: An AES calibration curve of adsorbed carbon on the Mo(100) surface.

characteristic of carbidic carbon for annealing temperatures > 500 K. Additional evidence that the overlayer is composed of atomic carbon by 500 K is found in the TPD work of Madix et al. which showed that hydrogen desorption from ethylene decomposition on Mo(100) is complete by 500 K [13]. In related work on Mo(111), Overbury found carbon overlayers, derived from ethylene, to be carbidic for annealing temperatures of 550 K and above [14]. Stair and coworkers have investigated adsorbed carbon on Mo(100) using X-ray photoelectron spectroscopy [10]. It was determined that charge transfer takes place from the metal to the carbon overlayer, leaving the surface Mo atoms in the +1 oxidation state. These XPS results provide further evidence that carbon on the Mo(100) surface is carbidic as no charge transfer is detected by XPS for graphitic carbon on metal surfaces [15].

3.3.2 Sulfur on Mo(100)

Adsorbed sulfur forms four ordered overlayers on the Mo(100) surface [16,17,18,19,20]. The ordered structures are observed by LEED to have c(2×2), $\left|\begin{smallmatrix}2 & \bar{1}\\ 1 & 1\end{smallmatrix}\right|$, c(4×2) and p(2×1) unit cells and occur at respective sulfur coverages of 0.5, 0.67, 0.75 and 1.0 ML. Clarke has carried out dynamical LEED studies of the c(2×2) sulfur structure and found best agreement between the experimental and theoretical curves for adsorbed sulfur atoms bonded in four-fold hollow sites [16]. The real space lattice is depicted in Figure 3.5 where an atomic radius of 1.04 Å is used for sulfur; the molybdenum radius and (100) relaxation value are the same as before [12]. Although sulfur and carbon atoms occupy the same adsorption sites on the Mo(100) surface at one-half monolayer coverage, there is much less exposed metal surface area on the sulfur covered surface. The atomic radius of sulfur is 35 % larger than that of carbon so it is expected to cover more of the Mo surface at a given

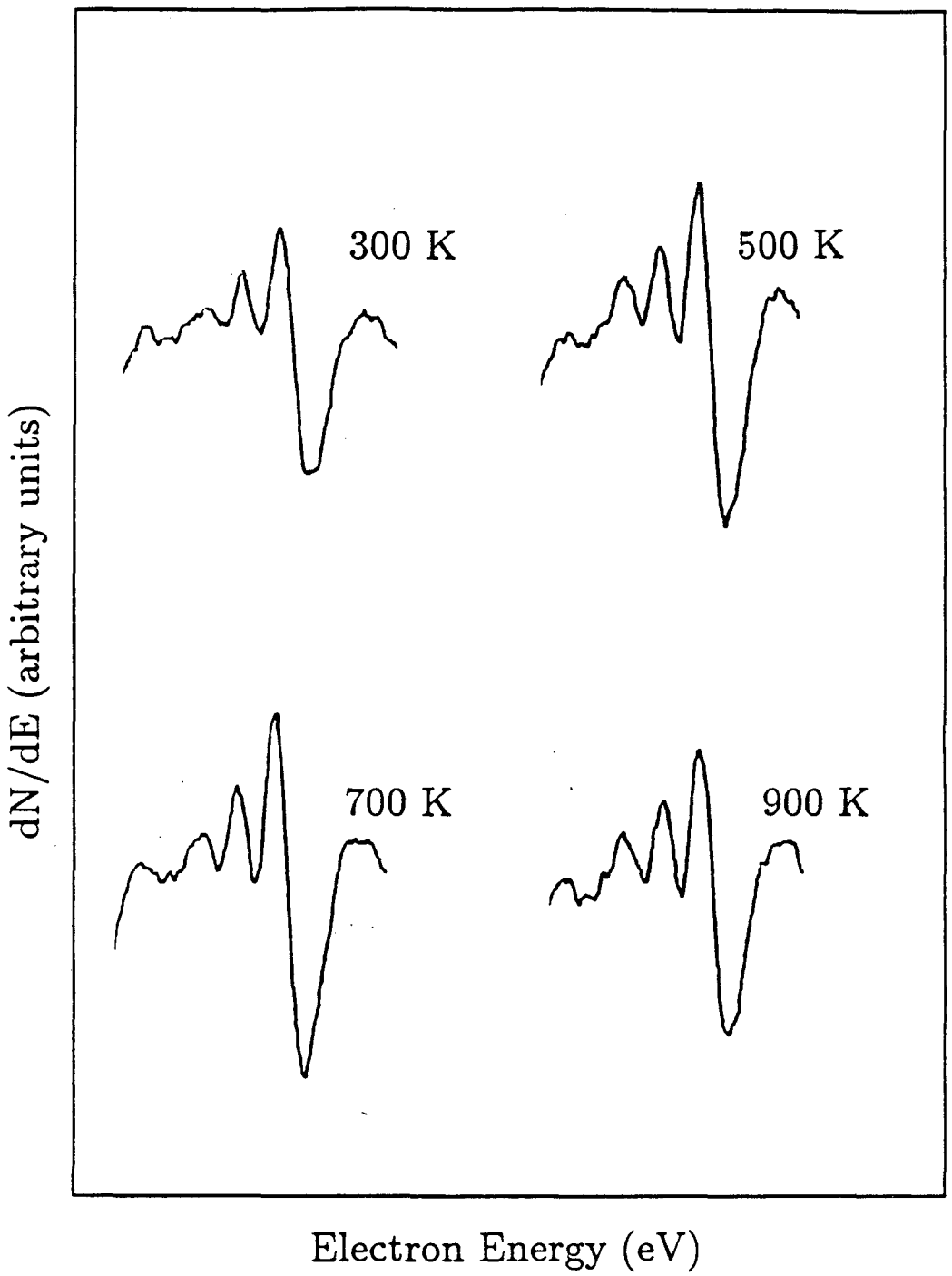

Figure 3.7: AES peak shapes for carbon on the Mo(100) surface as a function of the crystal annealing temperature.

adsorbate coverage. Carbon can penetrate further into the surface while sulfur sits above the metal plane. In fact, the larger size of sulfur is reflected in repulsive sulfur-sulfur interactions at high coverages which result in changes in the bonding of sulfur to the Mo(100) surface. Carbon atoms adsorb in four-fold hollow sites at all coverages ($0 < \theta_c \leq 1.0$) while evidence suggests that sulfur atoms at high coverages ($\theta_s > 0.67$ ML) occupy new adsorption sites in order to minimize repulsive interactions between adjacent sulfur atoms [16,2,19,21]. It has been proposed that above two-thirds of a monolayer, sulfur atoms begin to populate two-fold bridge sites. This hypothesis is supported by XPS, UPS and TDS studies which show that the Mo–S bond strength decreases for sulfur adsorbed above 0.67 ML [22,19]. As will be discussed shortly, recent scanning tunnelling microscopy (STM) studies indicate that all sulfur atoms in the p(2×1) structure are adsorbed in equivalent, but displaced, sites [23].

The bonding of sulfur on the Mo(100) surface has been investigated with numerous techniques. Thermal desorption shows sulfur to be strongly bound to the Mo(100) surface with the maximum rate of desorption at 1800 K and a low temperature shoulder at 1300-1500 K [19]. XPS and work function measurements indicate that electron transfer from molybdenum to sulfur transpires upon adsorption of sulfur on the Mo(100) surface [22,24,20]. Oudar and coworkers observed the work function to increase linearly over the coverage range $0.25 < \theta_s < 1.0$ ML and from this deduced a charge transfer of 0.044 e^- per sulfur atom, indicating that the Mo–S bond is predominantly covalent in character [20]. The XPS measurements of Gellman and coworkers in this laboratory showed that the binding energy of sulfur on the Mo(100) surface is similar to that of sulfur in MoS_2 [22]. By analogy to MoS_2, they assigned a formal oxidation state of -2 for sulfur on Mo(100).

3.3.3 STM Study of the p(2×1) Mo(100)–S System

The recently developed technique of scanning tunnelling microscopy (STM) has been used to image sulfur atoms on the Mo(100) surface with atomic resolution in air [23]. The STM experiments were carried out by Dr. Bruno Marchon and Dr. Miquel Salmerón of the Lawrence Berkeley Laboratory on sulfur covered Mo(100) surfaces prepared in this laboratory. Atomic resolution images could be recorded by the STM in air due to the chemical inertness of the Mo(100) surface when covered with one monolayer of sulfur. UHV thermal desorption studies have shown that the sulfur passivated surface is chemically inert to the most common contaminants (CO, N_2, H_2O, O_2) at room temperature [19]. To determine whether the p(2×1) Mo(100)–S surface was inert to adsorption of gas phase contaminants at ambient pressures, the surface was exposed to air (1 atm) for fourteen hours in the high pressure cell. Following evacuation, AES revealed insignificant amounts of adsorbed carbon and oxygen on the surface and no loss of adsorbed sulfur. In addition, the LEED pattern after air exposure was found to be as sharp as the initial pattern. The AES spectra and LEED patterns of the surface from before and after air exposure are shown in Figures 3.8 and 3.9.

The p(2×1) unit cell of sulfur atoms on the Mo(100) surface is clearly resolved in Figure 3.10, an STM image taken in the barrier height mode. The shortest sulfur-sulfur distance is 3.4 Å which agrees, within uncertainty, with the value of 3.1 Å predicted by Clarke [16]. Topographic imaging of the sulfur covered surface reveals all of the sulfur atoms to be at the same distance above the metal surface, suggesting that they are adsorbed in equivalent sites. Clarke has proposed two models for the real space structure and they are shown in Figure 3.11. Structure (a) has sulfur atoms adsorbed in both four-fold hollow and two-fold bridge sites. The

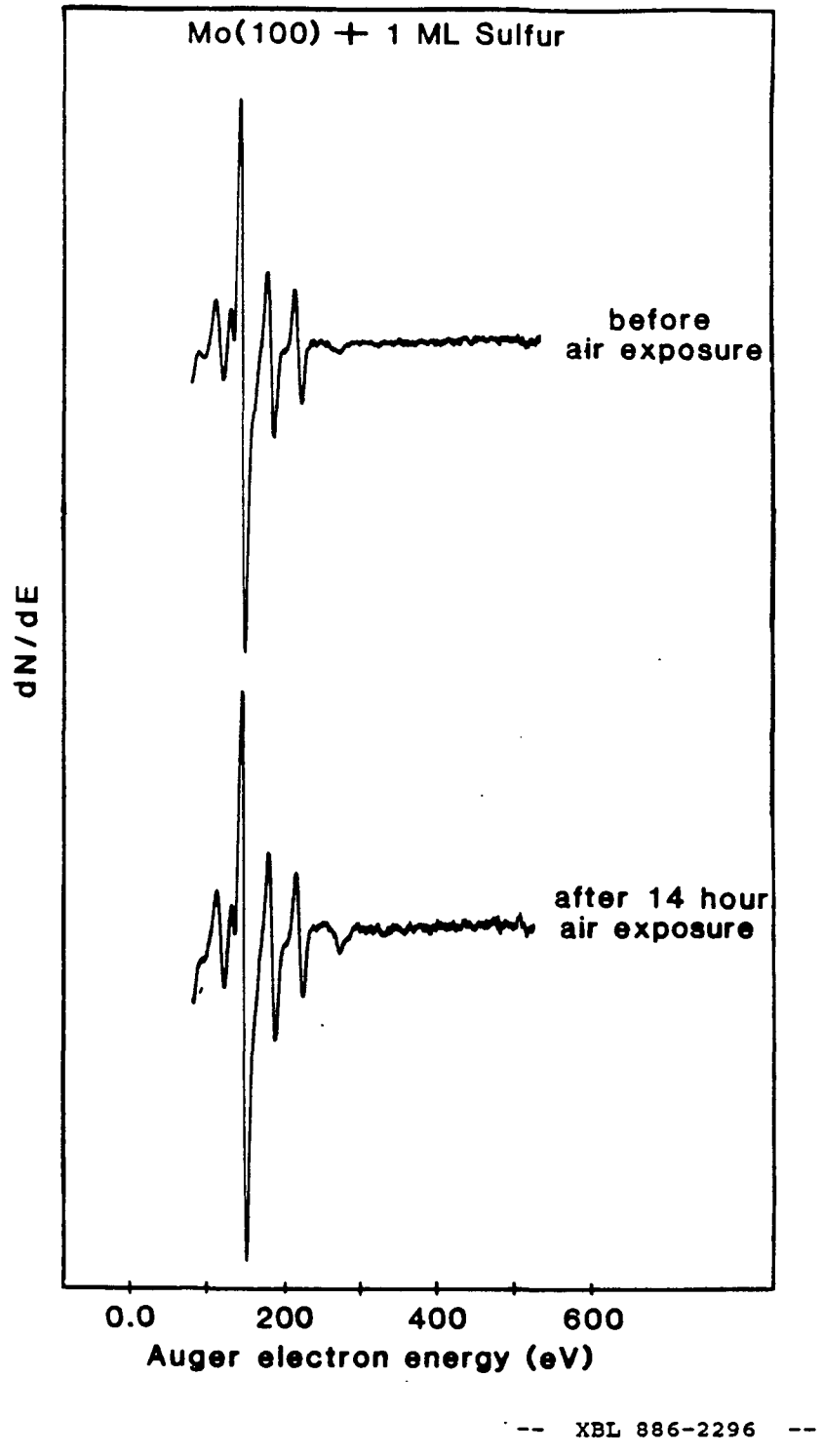

Figure 3.8: AES spectra of the p(2×1) sulfur on Mo(100) surface before and after air exposure.

before
air exposure

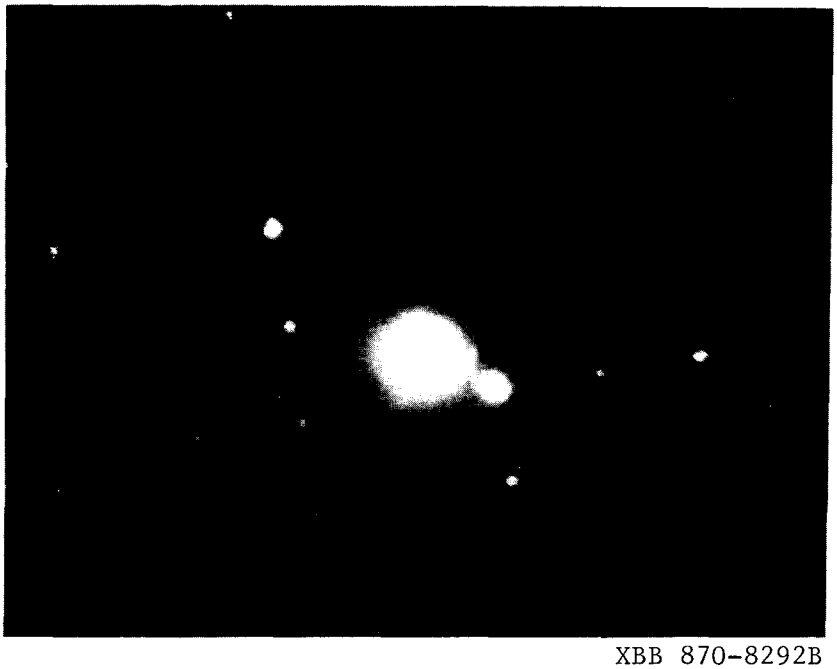

after 14 hour
air exposure

XBB 870-8292B

beam energy = 125 eV

Figure 3.9: LEED patterns of the p(2×1) sulfur on Mo(100) surface before and after air exposure.

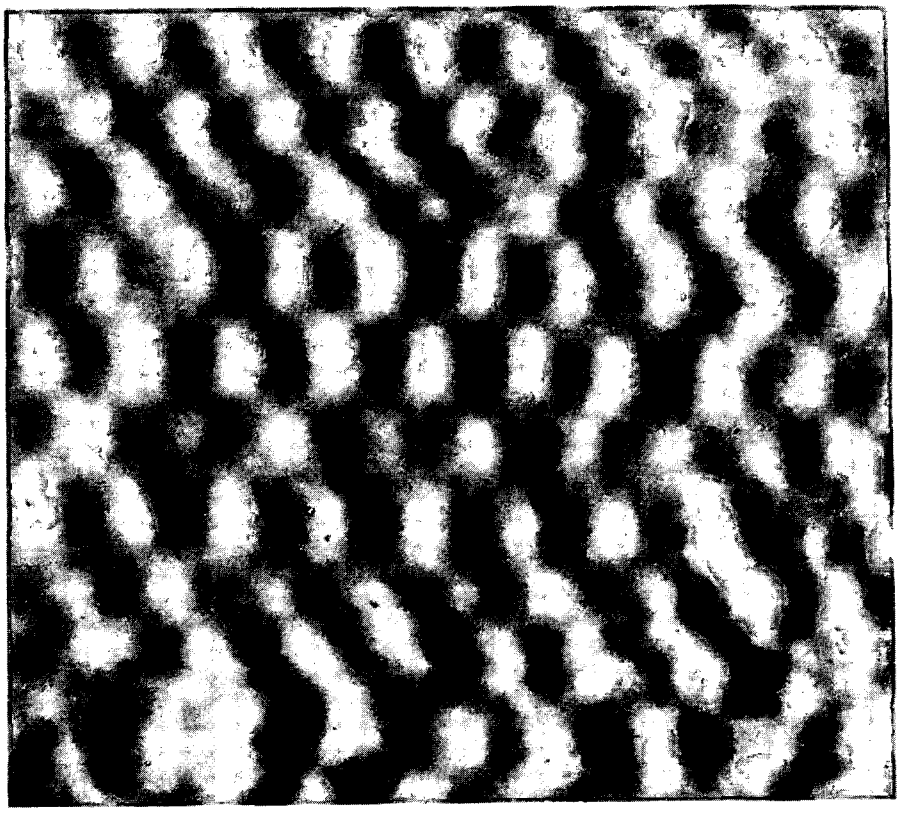

Barrier Height Image

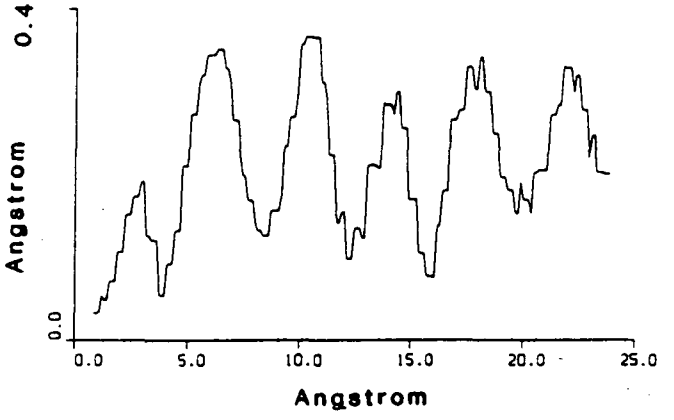

Topographic Scan

XBB 882-867

Figure 3.10: (a) A barrier height STM image of the p(2×1) Mo(100)–S surface in air. (b) A topographic scan of the same surface in the [120] direction.

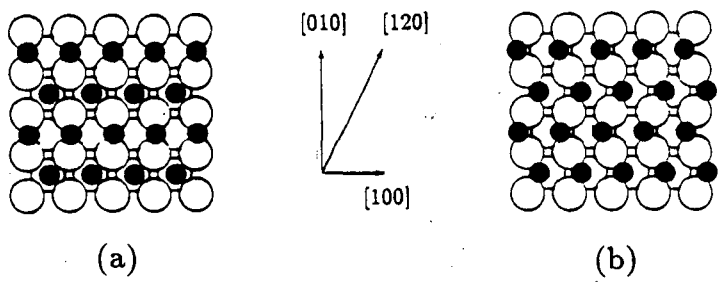

Figure 3.11: Model Structures proposed for the p(2×1) overlayer lattice of sulfur on the Mo(100) surface.

two adsorption sites are not equivalent and would result in a difference in the height of sulfur atoms in the two sites of ~ 0.8 Å. This was not observed in the STM studies. In contrast, structure (b) has all of the sulfur atoms adsorbed in equivalent sites in which the sulfur atoms are displaced laterally from the four-fold hollow and two-fold bridge sites. The structure is consistent with the STM results in that all sulfur atoms extend the same distance above the metal substrate.

Further LEED work is in progress in this laboratory to further clarify the adsorption sites of sulfur on the Mo(100) surface. LEED I-V experiments are being performed for the p(2×1) sulfur structure which will permit determination of the registry of the sulfur overlayer with the Mo(100) surface. In addition, careful observation of the p(2×1) LEED pattern will be carried out as a function of the orientation of the incident electron beam. The structural model (b) in Figure 3.11 contains a glide plane symmetry element which would cause the systematic extinction of the (0, n+1/2) diffraction spots from the p(2×1) LEED pattern at normal

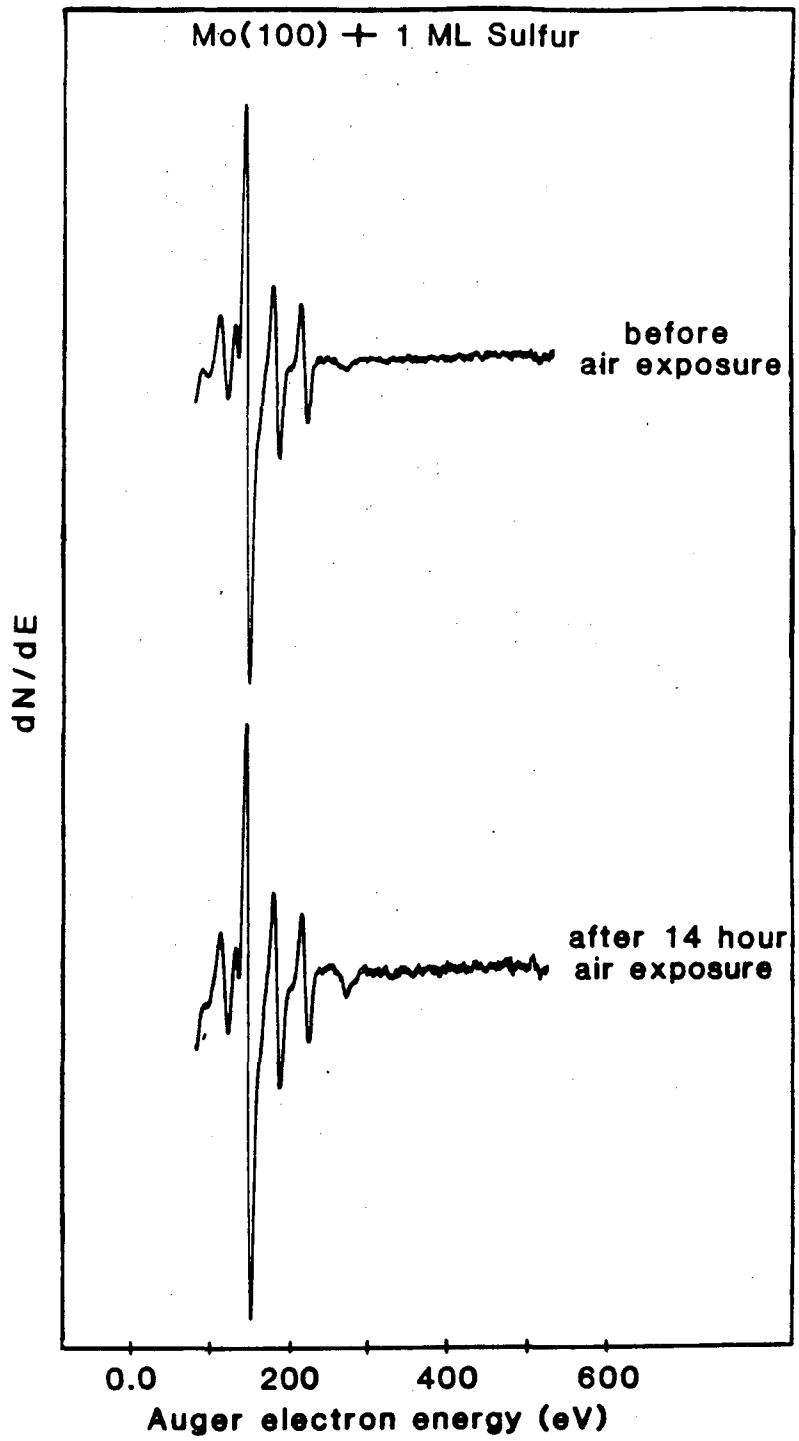

-- XBL 886-2296 --

Figure 3.8: AES spectra of the p(2×1) sulfur on Mo(100) surface before and after air exposure.

before
air exposure

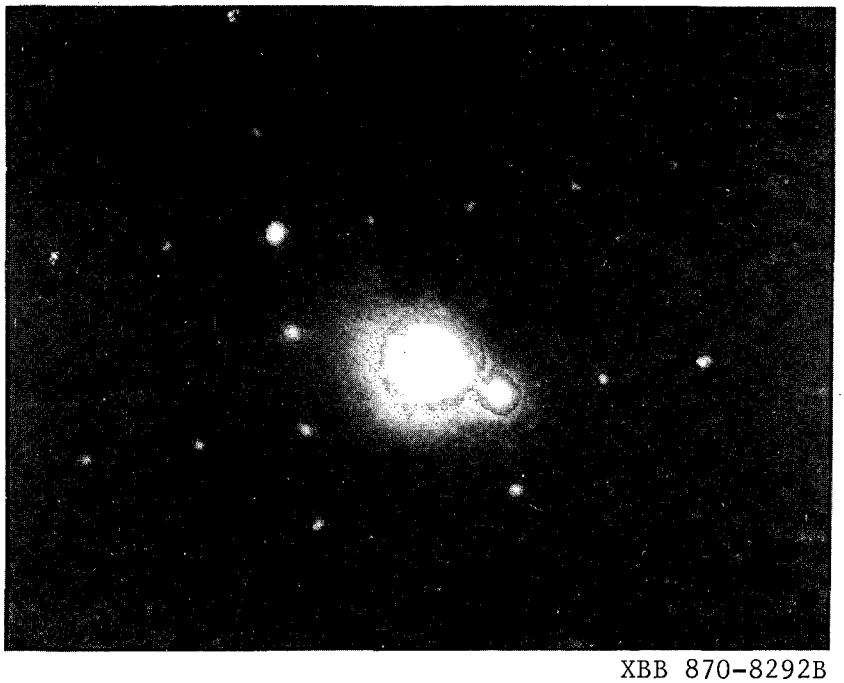

after 14 hour
air exposure

XBB 870-8292B

beam energy = 125 eV

Figure 3.9: LEED patterns of the p(2×1) sulfur on Mo(100) surface before and after air exposure.

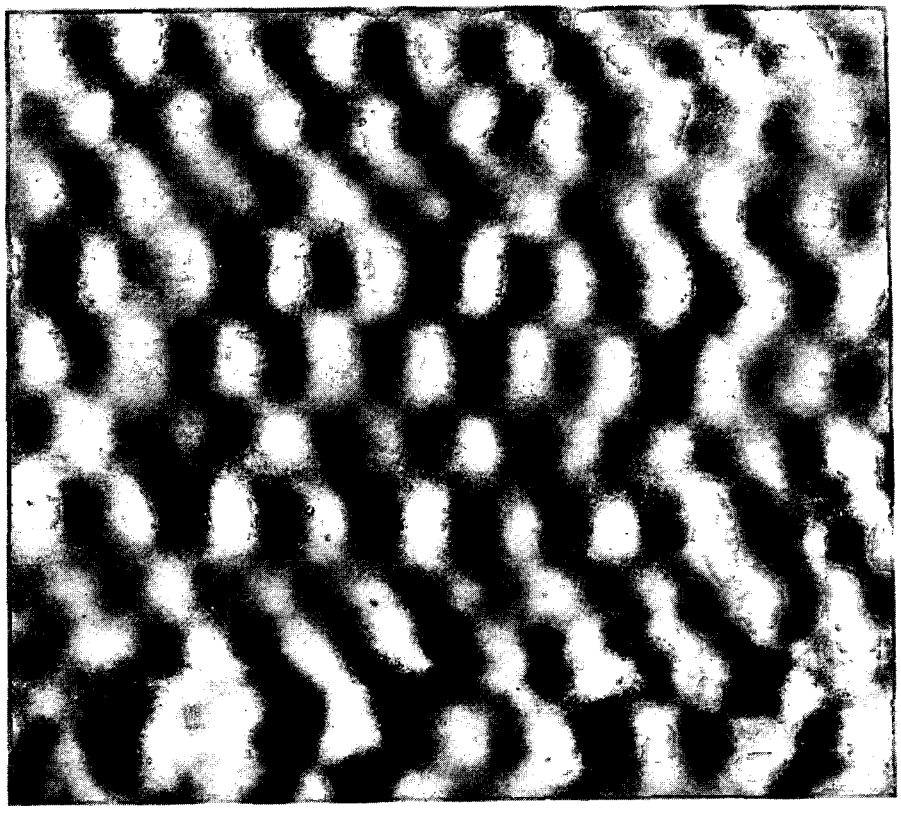

Barrier Height Image

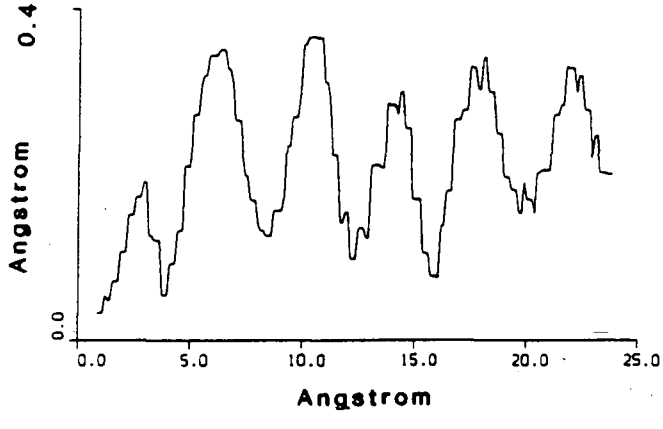

Topographic Scan

XBB 882-867

Figure 3.10: (a) A barrier height STM image of the p(2×1) Mo(100)–S surface in air. (b) A topographic scan of the same surface in the [120] direction.

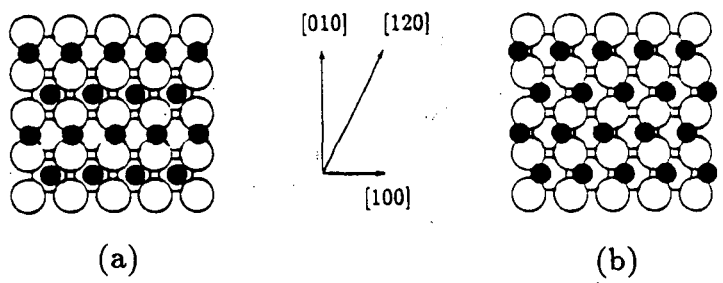

Figure 3.11: Model Structures proposed for the p(2×1) overlayer lattice of sulfur on the Mo(100) surface.

two adsorption sites are not equivalent and would result in a difference in the height of sulfur atoms in the two sites of $\sim$ 0.8 Å. This was not observed in the STM studies. In contrast, structure (b) has all of the sulfur atoms adsorbed in equivalent sites in which the sulfur atoms are displaced laterally from the four-fold hollow and two-fold bridge sites. The structure is consistent with the STM results in that all sulfur atoms extend the same distance above the metal substrate.

Further LEED work is in progress in this laboratory to further clarify the adsorption sites of sulfur on the Mo(100) surface. LEED I-V experiments are being performed for the p(2×1) sulfur structure which will permit determination of the registry of the sulfur overlayer with the Mo(100) surface. In addition, careful observation of the p(2×1) LEED pattern will be carried out as a function of the orientation of the incident electron beam. The structural model (b) in Figure 3.11 contains a glide plane symmetry element which would cause the systematic extinction of the (0, n+1/2) diffraction spots from the p(2×1) LEED pattern at normal

incidence of the electron beam [25]. This experiment will provide additional evidence for determination of the adsorption sites of sulfur on the Mo(100) surface at high coverages.

3.4 Structure of Carbon and Sulfur Overlayers on the Re(0001) and Re(10$\bar{1}$0) Single Crystal Surfaces

In contrast to the large number of papers in the literature which discuss the structure of carbon and sulfur overlayers on the Mo(100) surface, there are very few published accounts of studies of these adsorbates on rhenium surfaces. Ducros and coworkers have studied the adsorption and decomposition of acetylene and ethylene on the Re(0001) and polycrystalline foil surfaces, and Gall et al. have studied the interaction of carbon with a rhenium foil [26,27]. Recent work by Kelly and coworkers has addressed the structure and chemisorption properties of sulfur and carbon covered Re(0001) and Re(10$\bar{1}$0) surfaces [1,28,29]. In the present work, the structural results of both Kelly and Ducros have been used to calibrate sulfur and carbon coverages on the Re(0001) and Re(10$\bar{1}$0) surfaces. The AES attenuation factors determined for carbon and sulfur on the rhenium surfaces are listed in Table 3.2. The following sections of this chapter will discuss the structural

Table 3.2: AES Attenuation Factors for C and S on Rhenium

Rhenium Surface	*AES Attenuation Factors*	
	$\alpha_c = \frac{Re(\theta_c=1)}{Re(\theta_c=0)}$	$\alpha_s = \frac{Re(\theta_s=1)}{Re(\theta_s=0)}$
Re(0001)	0.60	0.50
Re(10$\bar{1}$0)	0.64	0.54

results of the studies described above as well as those of this present work.

3.4.1 Carbon on Re(0001)

Adsorbed carbon on the Re(0001) surface has been found to form one ordered overlayer structure [26]. LEED studies of acetylene and ethylene on Re(0001) revealed a c(4×2) pattern at a carbon coverage of 0.25 ML. The pattern is observed only after annealing the single crystal to 770 K to dissociate the hydrocarbons and desorb H_2 into the vacuum. The dimensions of the overlayer unit cell suggest that scission of the C–C bond of the C_2 molecules has occurred by 770 K, as the shortest carbon-carbon distance in the overlayer is 4.78 Å , considerably greater than the C–C bond length of 1.54 Å [30]. Possible adsorption sites for carbon on the Re(0001) surface are not discussed by the authors, but comparison with other adsorbates and other close-packed surfaces would suggest that carbon is adsorbed in three-fold hollow sites.

The chemical form of adsorbed carbon overlayers has been found to greatly influence the catalytic properties of metal surfaces. In general, graphitic carbon overlayers strongly deactivate catalysts while surfaces covered with carbidic carbon deposits often remain active [31,32]. In this thesis research, AES was used to study the form of adsorbed carbon overlayers on Re(0001). Figure 3.12 shows the evolution of the carbon AES peak shape as a function of the crystal annealing temperature for a Re(0001) surface saturated with ethylene. As discussed in Section 2.3.1, AES can be used to distinguish between carbidic and graphitic carbon on metal surfaces. For carbon overlayers on Re(0001) produced by decomposition of ethylene, the AES peak shape for annealing temperatures below 900 K most closely resembles that of amorphous or graphitic carbon. This suggests that at these temperatures, the surface is covered primarily with carbonaceous species

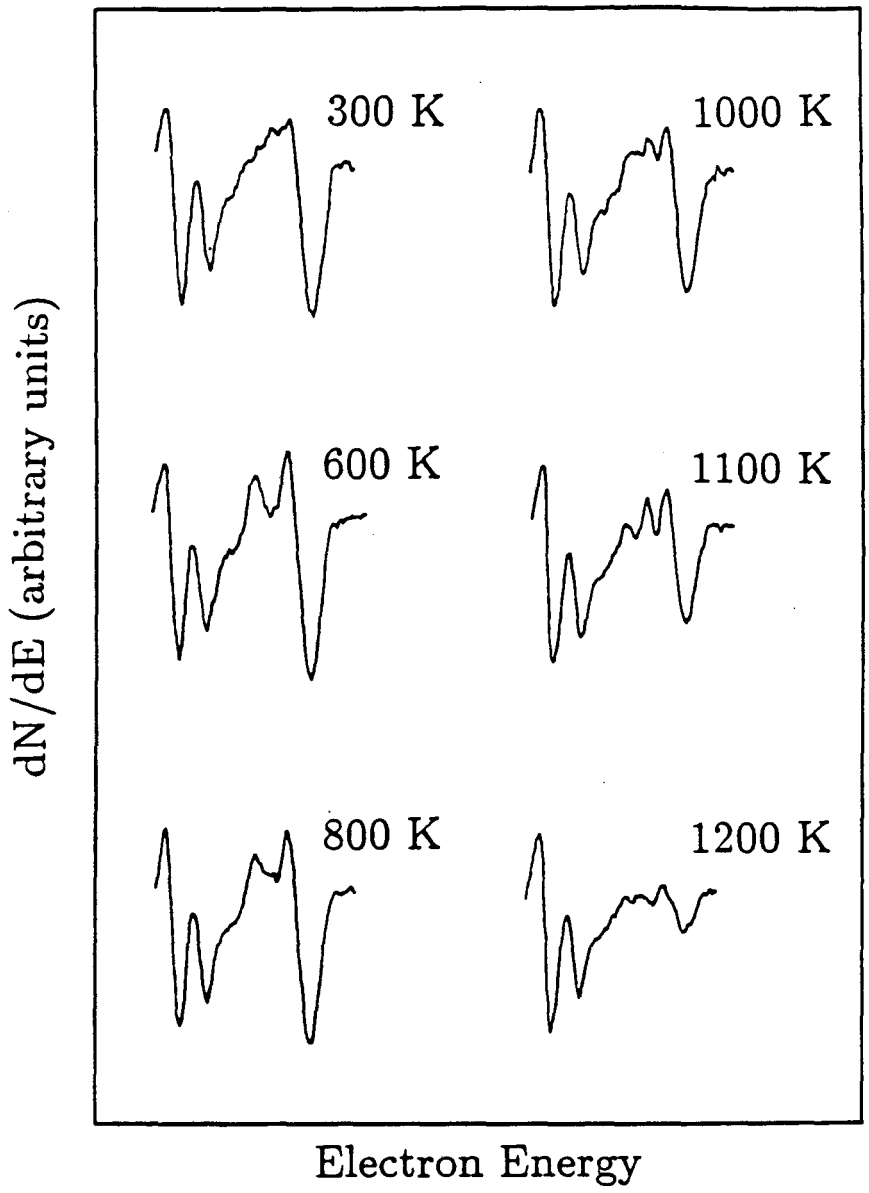

-- XBL 884-1382 --

Figure 3.12: Carbon AES peak shapes for adsorbed carbon on the Re(0001) surface.

containing C–C bonds. Following heating of the crystal to temperatures above 900 K, the carbon AES peak shape more closely resembles that of carbon in a transition metal carbide, implying that the predominant carbon species is atomic carbon bonded to rhenium. In addition to this temperature dependence of the chemical form of carbon on Re(0001), Kelly and coworkers have also observed a coverage dependence. For carbonaceous overlayers annealed to 850 K, the carbon AES peak shape was observed to become more graphite-like as the carbon coverage was increased from 0.2 ML to above 1.0 ML [1]. Kelly concluded that at low coverages, carbon atoms are widely spaced and therefore interact only weakly with each other, while at high carbon coverages they are more closely packed and interact strongly.

3.4.2 Carbon on Re(10$\bar{1}$0)

Adsorbed carbon on Re(10$\bar{1}$0) has been reported to form one ordered structure, a c(2×4) overlayer lattice in the coverage range of $0.5 < \theta_c < 1.5$ ML, but the LEED pattern was not observed in this work [1]. Carbon AES peak shapes similar to those of carbon on Re(0001)were observed on the Re(10$\bar{1}$0) surface. Two representative carbon AES spectra for overlayers formed from ethylene decomposition are shown in Figure 3.13.

3.4.3 Sulfur on Re(0001)

The adsorption and bonding of sulfur overlayers on the Re(0001) surface have been studied using AES, TDS and LEED [1,28]. Sulfur forms four ordered structures on the (0001) face of rhenium: p(2×2), $(3\sqrt{3}\times3\sqrt{3})$R 30°, $\left|\begin{smallmatrix}3 & 1\\ 1 & 3\end{smallmatrix}\right|$ and $(2\sqrt{3}\times2\sqrt{3})$R 30° at respective coverages of 0.25, 0.32-0.37, 0.39-0.44 and 0.5 ML. Three-fold hollows have been proposed as adsorption sites for sulfur based on analogy with

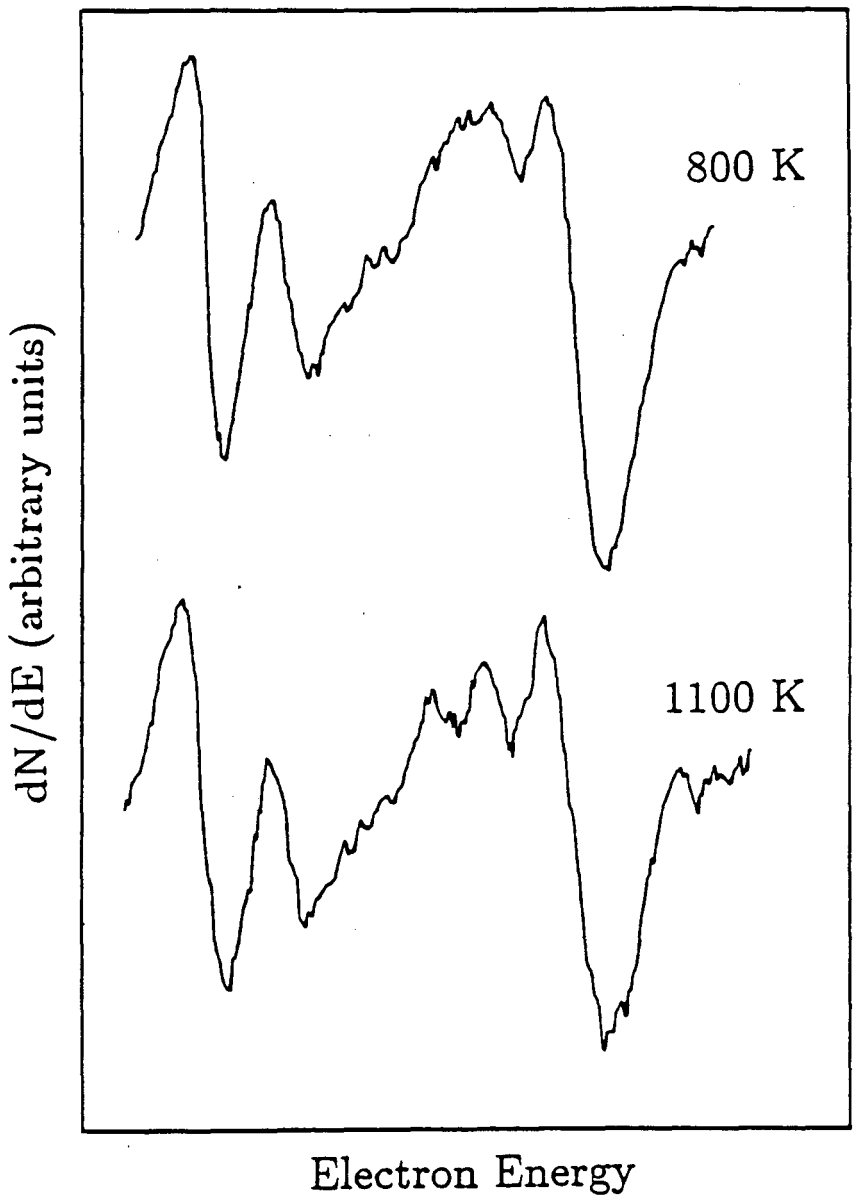

-- XBL 884-1381 --

Figure 3.13: Carbon AES peak shapes for adsorbed carbon on the Re(10$\bar{1}$0) surface.

results of dynamical LEED studies of sulfur on Pt(111) (θ_s = 0.33 ML) and Ni(111) (θ_s = 0.25 ML) [33,34]. These results suggest that, at least for low sulfur coverages ($\theta_s \leq 0.33$ ML), sulfur atoms on the Re(0001) surface are adsorbed in three-fold hollow sites.

Sulfur is strongly bound to the Re(0001) surface as attested by TDS studies which show a maximum rate of sulfur adsorption at 1600 K with low temperature shoulders at 1400 K and 900 K. The strong binding of sulfur to Re(0001) is also reflected in the stability of the $(2\sqrt{3}\times2\sqrt{3})$R 30° Re(0001)–S surface (θ_s = 0.5 ML) to exposure to the ambient atmosphere. As was observed with the p(2×1) Mo(100)–S surface, the sulfur passivated Re surface retained its ordered overlayer structure after exposure to air (1 atm) for thirty minutes and was contaminated with only small amounts of carbon and oxygen. The AES spectra and LEED patterns from before and after exposure of the single crystal to air are shown in Figures 3.14 and 3.15. The sharpness of the diffraction spots is lower and the diffuse background intensity considerably higher for the $(2\sqrt{3}\times2\sqrt{3})$R 30° Re(0001)–S surface following air exposure than for the p(2×1) Mo(100)–S surface, despite a shorter period of exposure. This may be due to the fact that the $(2\sqrt{3}\times2\sqrt{3})$R 30° ordered structure occurs at a coverage below the saturation sulfur coverage of ~ 0.7 ML, while the p(2×1) sulfur structure on Mo(100) occurs at the saturation coverage of 1.0 ML. Apparently, the $(2\sqrt{3}\times2\sqrt{3})$R 30° Re(0001)–S surface is not completely inert in an atmospheric pressure environment [1].

Scanning tunnelling microscopy study of the sulfur passivated Re surface has shown that the single crystal is not perfectly flat on the atomic scale, but is instead composed of large (0001) terraces separated by monoatomic and multiatomic steps [35]. More recent STM studies have achieved atomic resolution of sulfur on Re(0001) and preliminary analysis of the images suggest that sulfur forms hexag-

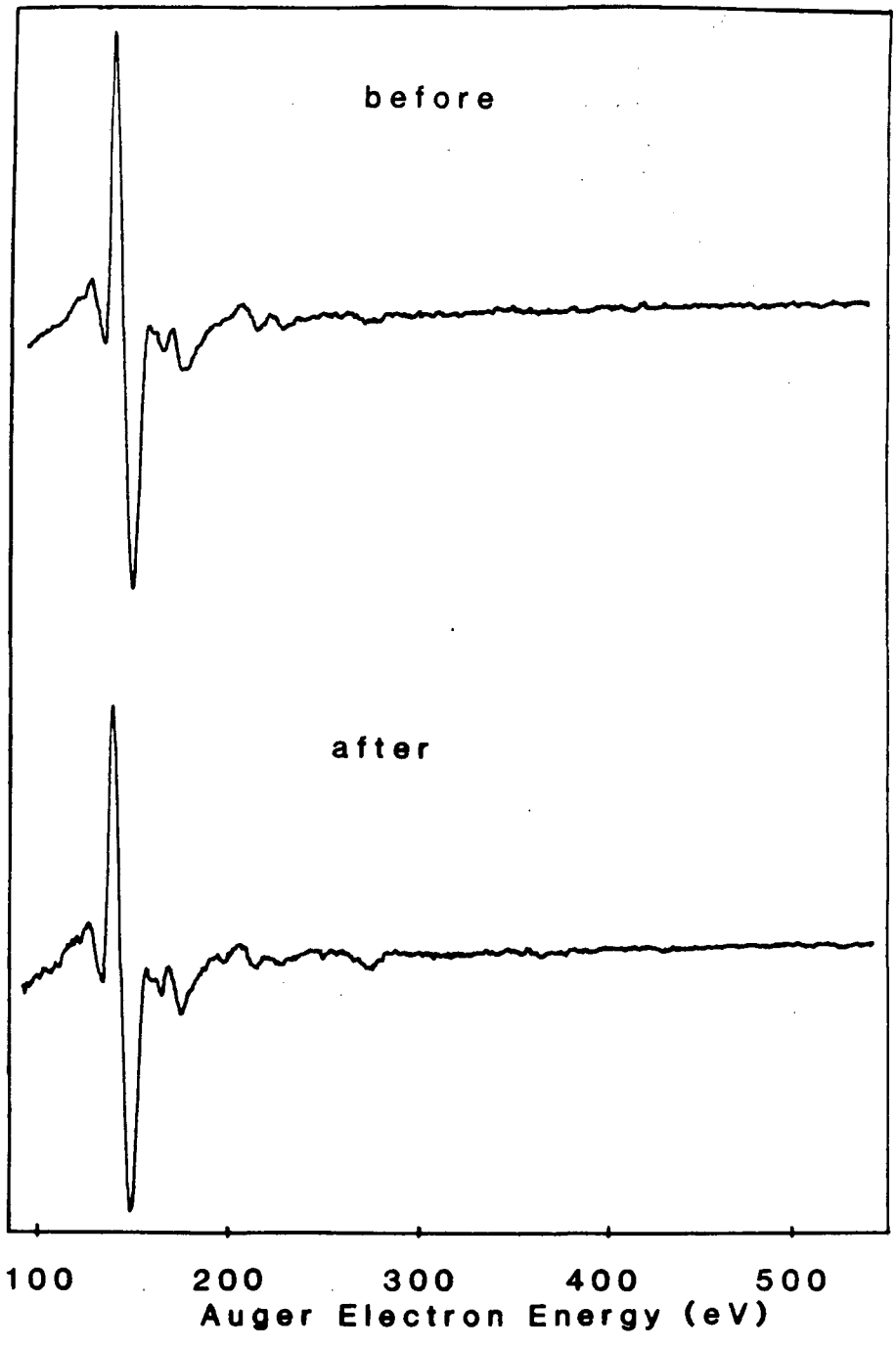

Figure 3.14: AES spectra before and after air exposure of Re(0001) covered with 0.5 ML of sulfur.

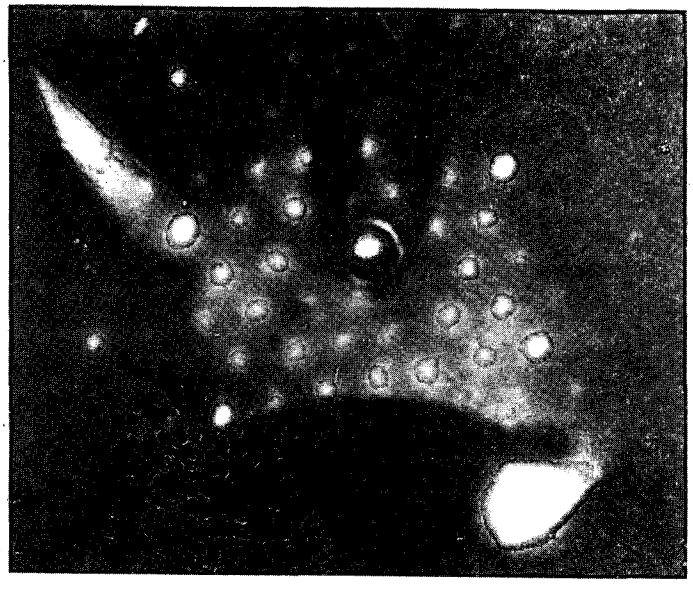

before

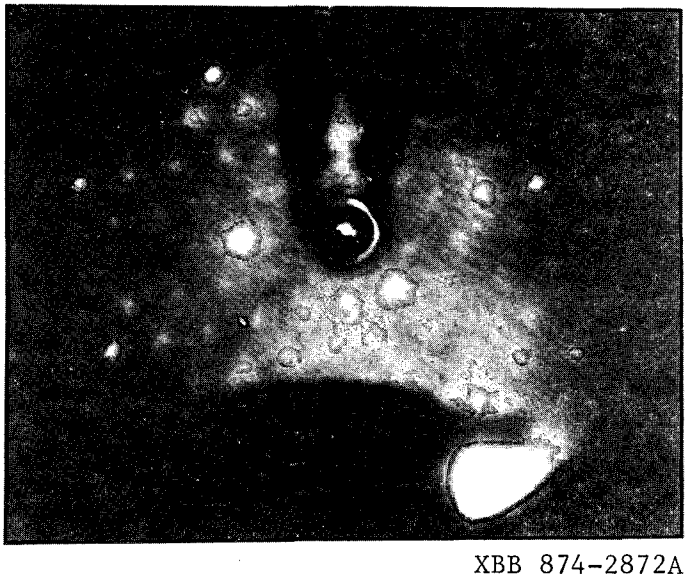

XBB 874-2872A

after

beam energy 135 eV

Figure 3.15: LEED patterns before and after air exposure of Re(0001) covered with 0.5 ML of sulfur.

onal S_6 units on the Re surface. [36].

3.4.4 Sulfur on Re(10$\bar{1}$0)

Adsorbed sulfur on the Re(10$\bar{1}$0) surface forms two ordered structures at coverages of 0.5 and 1.0 ML which have p(2×2) and p(1×2) unit cells respectively [1,28]. Kelly and coworkers have proposed three-fold adsorption sites for sulfur formed between one second layer and two top layer Re atoms. Thermal desorption studies of the bonding of sulfur on Re(10$\bar{1}$0) indicate that it is similar in strength to sulfur on the (0001) face. Sulfur desorbs from the Re(10$\bar{1}$0) surface with a maximum rate of desorption at 1700 K with a low temperature shoulder at 1500-1600 K for coverages > 0.5 ML. The higher saturation coverage of sulfur on Re(10$\bar{1}$0) than on Re(0001) arises from the fact that it is a less densely packed surface (see Table 3.2). For transition metal surfaces, it has been found that the maximum surface coverage of sulfur atoms falls in the range 0.65-1.0×10^{15} atoms/cm^2, corresponding to a sulfur-sulfur distance of the order of the van der Waals radius of sulfur [37]. On an open surface like Re(10$\bar{1}$0), Re atoms are more widely spaced than on Re(0001), so the saturation sulfur coverage ($\frac{max.\ no.\ S\ atoms/cm^2}{no.\ Re\ atoms/cm^2}$) will be higher.

3.5 Discussion

The structure of clean and adsorbate covered (C, S) molybdenum and rhenium single crystal surfaces has been studied with a number of different surface science techniques in ultrahigh vacuum. The most important results of these studies are the following:

I. The three Mo surfaces ((110), (100), (111)) and four rhenium surfaces ((0001), (10$\bar{1}$0), (11$\bar{2}$0), (11$\bar{2}$1)) of interest in this work do not undergo reconstruction at room temperature as determined by LEED.

II. Adsorbed sulfur is strongly bound on the Mo(100), Re(0001) and Re($10\bar{1}0$) surfaces with desorption energies in the range 98-110 kcal/mole for low coverages. At high coverages, low temperature shoulders appear in the sulfur TPD spectra, indicating that sulfur atoms populate adsorption sites of lower binding energy.

III. Adsorbed carbon on the Mo(100) surface is carbidic in nature for annealing temperatures $\geq$ 500 K, with carbon atoms bound in four-fold hollow sites. Carbon overlayers on the Re(0001) and Re($10\bar{1}0$) surfaces appear to be carbidic-like only for annealing temperatures $\geq$ 1100 K. For lower annealing temperatures, adsorbed carbon on the rhenium surfaces show AES features attributable to graphitic carbon.

The structural results discussed in this chapter provide information on the atomic-level structure of the clean and adsorbate covered surfaces of molybdenum and rhenium shown in Figures 3.1-3.4. The following chapters of this thesis will draw upon these studies to both help understand the catalytic behavior of thiophene HDS over the model single crystal catalysts, and to develop a molecular level description of the thiophene HDS reaction.

References

[1] D. G. Kelly. PhD thesis, University of California, Berkeley, 1987.

[2] A. J. Gellman. PhD thesis, University of California, Berkeley, 1985.

[3] L. Morales Do Garza and L. J. Clarke. *J. Phys. Chem.* **14** (1981) 5391.

[4] L. J. Clarke. *Surf. Sci.* **91** (1979) 131.

[5] S. H. Overbury. *Surf. Sci.* **175** (1986) 123.

[6] H. L. Davis and D. M. Zehner. *J. Vac. Sci. Technol.* **17** (1979) 190.

[7] C. Guillot, R. Riwan, and J. LeCante. *Surf. Sci.* **59** (1976) 581.

[8] S. H. Overbury and P. C. Stair. *J. Vac. Sci. Technol. A* **1** (1983) 1055.

[9] E. I. Ko and R. J. Madix. *Surf. Sci.* **100** (1980) L449.

[10] J. L. Grant, T. B. Fryberger, and P. C. Stair. *Surf. Sci.* **159** (1985) 333.

[11] R. Q. Barr. *Encylopedia of Chemical Technology.* Volume 15, J. Wiley and Sons, New York, 1981.

[12] C. Kittel. *Solid State Physics.* J. Wiley and Sons, New York, 1976.

[13] A. J. Gellman, M. H. Farias, M. Salmeron, and G. A. Somorjai. *Surf. Sci.* **136** (1984) 217.

[14] S. H. Overbury. *Surf. Sci.* **184** (1987) 319.

[15] G. Panzner and W. Diekmann. *Surf. Sci.* **160** (1985) 253.

[16] L. J. Clarke. *Surf. Sci.* **102** (1981) 331.

[17] M. Salmeron and G. A. Somorjai. *Surf. Sci.* **126** (1983) 410.

[18] M. Salmeron, G. A. Somorjai, and R. R. Chianelli. *Surf. Sci.* **127** (1983) 526.

[19] M. H. Farias, A. J. Gellman, G. A. Somorjai, R. R. Chianelli, and K. S. Liang. *Surf. Sci.* **140** (1984) 181.

[20] V. Maurice, L. Peralta, Y. Berthier, and J. Oudar. *Surf. Sci.* **148** (1984) 623.

[21] A. J. Gellman, W. T. Tysoe, and G. A. Somorjai. *Surf. Sci.,* (to be published)

[22] A. J. Gellman, W. T. Tysoe, F. Zaera, and G. A. Somorjai. *Surf. Sci.* **191** (1987) 271.

[23] B. Marchon, P. Bernhardt, M. E. Bussell, G. A. Somorjai, M. Salmeron, and W. Siekhaus. *Phys. Rev. Lett.* **60** (1988) 1166.

[24] Th. Baldinger and E. Bechtold. *Surf. Sci.* **159** (1985) 406.

[25] L. J. Clarke. *Surface Crystallography, An Introduction to Low Energy Electron Diffraction.* J. Wiley and Sons, Chichester, England, 1985.

[26] R. Ducros, M. Housley, M. Alnot, and A. Cassuto. *Surf. Sci.* **71** (1978) 433.

[27] N. R. Gall, S. N. Mikhailov, E. V. Rut'kov, and A. Ya. Tontegode. *Surf. Sci.* **191** (1987) 185.

[28] D. G. Kelly, A. J. Gellman, M. Salmeron, G. A. Somorjai, V. Maurice, M. Huber, and J. Oudar. *Surf. Sci.,* (in press) .

[29] D. G. Kelly, J. A. Odriozola, and G. A. Somorjai. *J. Phys. Chem.* **91** (1987) 5695.

[30] A. Streitweiser Jr. and C. H. Heathcock. *Introduction to Organic Chemistry.* Macmillan Publishing Co., New York, 1976.

[31] H. J. Krebs and H. P. Bonzel. *Surf. Sci.* **99** (1980) 570.

[32] D. W. Goodman and J. M. White. *Surf. Sci.* **90** (1979) 201.

[33] K. Hayek, H. Glassl, H. Gutmann, H. Leohard, M. Prutton, Tear. S. P., and Welton-Cook M. R. *Surf. Sci.* **152/153** (1985) 419.

[34] J. E. Demuth, D. W. Jepsen, and P. M. Marcus. *Phys. Rev. Lett.* **32** (1974) 1182.

[35] B. Marchon, D. F. Ogletree, M. Salmeron, and W. Siekhaus. *J. Vac. Sci. Technol. A* **6** (1988) 531.

[36] B. Marchon and M. Salmeron (private communication) .

[37] J. Oudar. *Catal. Rev.-Sci. Eng.* **22** (1980) 171.

Chapter 4

Thiophene Hydrodesulfurization over Molybdenum Single Crystal Surfaces

4.1 Introduction

This chapter discusses catalytic studies of thiophene hydrodesulfurization over molybdenum single crystal surfaces. The research approach used in this work, combining high pressure catalytic reactions with catalyst characterization and preparation in UHV, is unique among studies of HDS in the literature. Well-defined single crystal catalysts were characterized and modified at the atomic level and their HDS activities measured in-situ, to exclude the possibility of contamination during handling procedures.

As discussed in the introductory chapter, industrial HDS processes utilize sulfided Co-Mo/Al_2O_3 catalysts in which molybdenum is considered to be the catalyst and cobalt a promoter. Under reaction conditions, molybdenum is present on the alumina support as MoS_2 and the active sites are believed to be located along the edge planes where molybdenum cations are exposed (see Figure 1.4). In our laboratory, the active sites of molybdenum-based HDS catalysts have been modelled using molybdenum single crystals. By varying the crystallographic orientation of

the single crystals, the effects of surface structure on activity can be studied, and, by depositing known amounts of sulfur and carbon onto the surfaces in a controlled fashion, the effects of catalyst composition determined.

4.2 Thiophene HDS over Initially Clean Mo Surfaces

Catalytic studies of thiophene HDS were initiated in this laboratory using the simplest model catalysts: clean molybdenum single crystals. Gellman and coworkers measured the thiophene HDS activities of three low miller index planes of molybdenum (see Figure 3.1) and they are compared in Figure 4.1 [1]. The Mo single crystals were found to exhibit almost identical activities, indicating that thiophene HDS is a structure insensitive reaction over molybdenum [2,3]. The structure insensitivity led us to concentrate on a single crystallographic face and, as a result, the remainder of the research described in this chapter was carried out over Mo single crystals of (100) orientation. The HDS activities quoted in Figure 4.1 have been normalized per unit area (cm^2) to take into account the different surface atom densities of the single crystal catalysts. Catalytic activity can also be expressed in terms of a turnover frequency which is the activity per site, defined here to be a surface metal atom.

For the clean Mo(100) surface, a turnover frequency of 0.13 ± 0.02 mol./site·sec was measured which agrees within experimental uncertainty with the value of 0.11 ± 0.03 mol./site·sec measured by Gellman and coworkers. Typical product accumulation curves for thiophene HDS over the Mo(100) surface are shown in Figure 4.2. Only the C_4 products are shown as they comprise greater than 95 % of the total, C_1-C_3 hydrocarbons make up the remainder. The major product is 1-butene, despite the fact that thermodynamics predicts that the products should

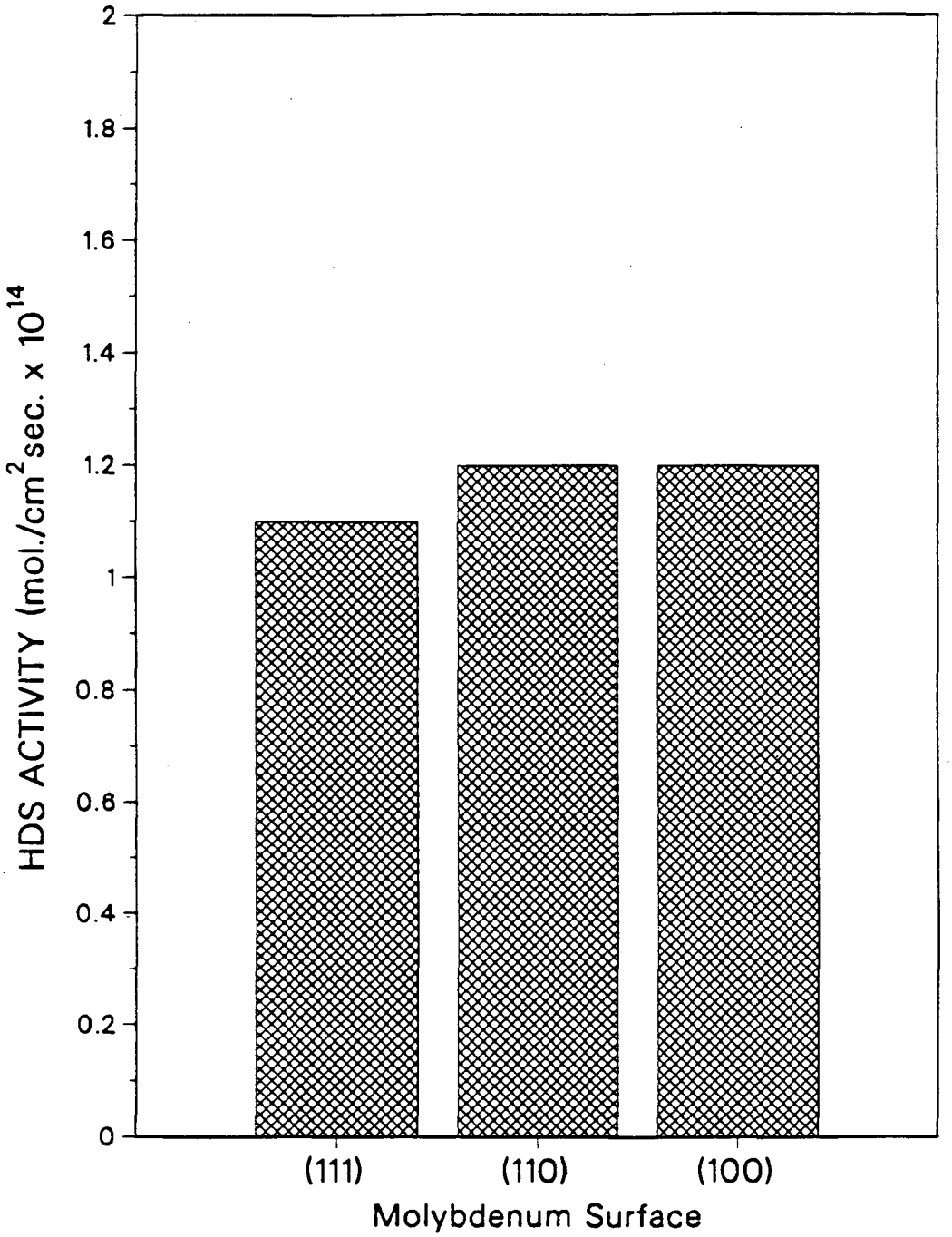

Figure 4.1: Thiophene HDS activities of three low miller index planes of molybdenum (P_{Th}=3.0 Torr, P_{H_2}=780 Torr, T=613 K).

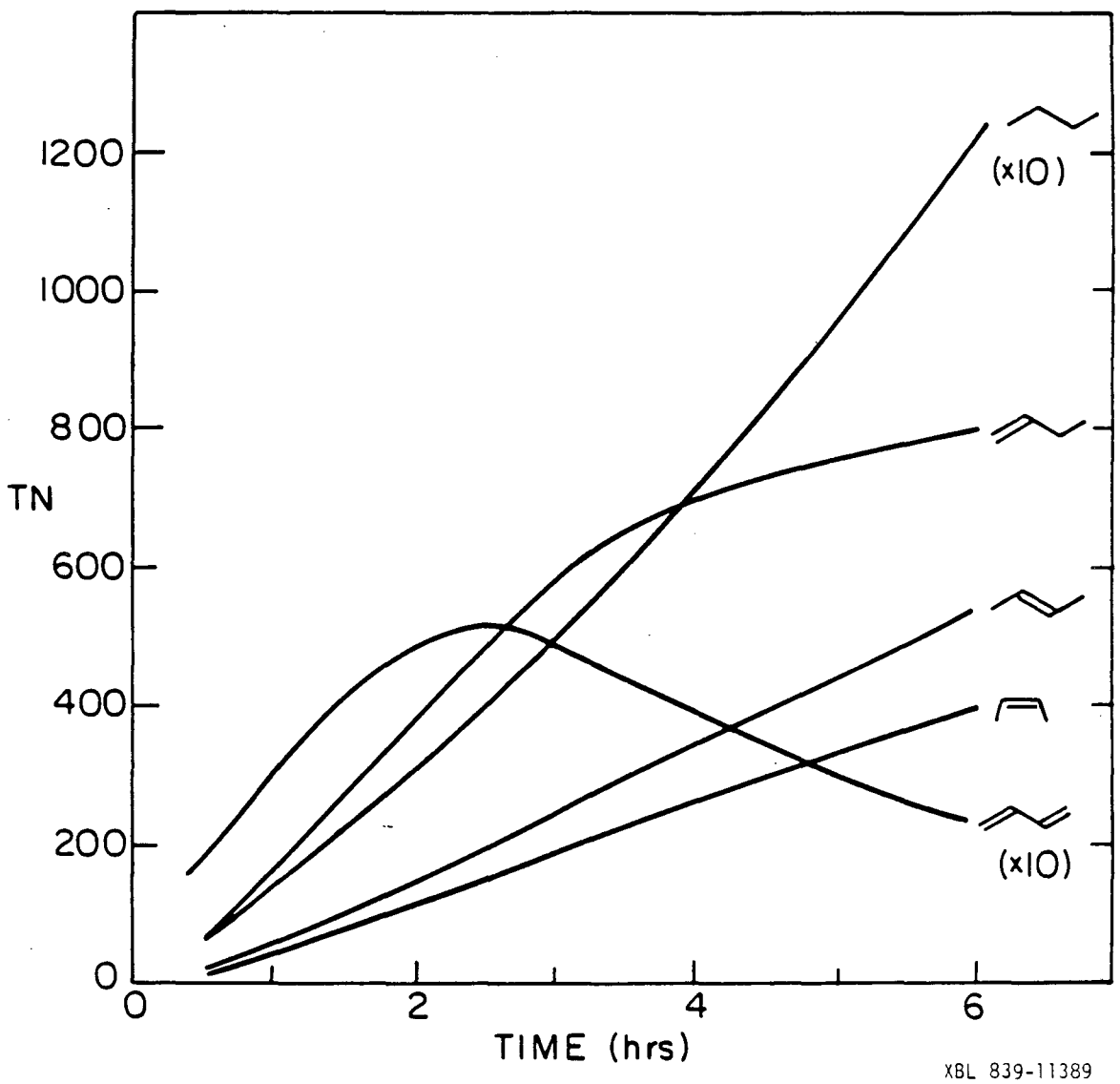

Figure 4.2: Product accumulation curves for thiophene HDS over the Mo(100) surface.

consist almost solely of butane. The fact that the butenes and butadiene make up over 90 % of the products indicates that the reaction is kinetically controlled. As shown in Figure 4.2, the yield of butadiene peaks at $\sim$ 2 hours and then decreases, indicating that it undergoes secondary reactions to give butenes and butanes. In general, deactivation of a Mo(100) single crystal begins $\sim$ 90-120 minutes into a reaction and reaches completion after about 12 hours.

4.3 Thiophene HDS over sulfided Mo(100) Surfaces

4.3.1 Effect of Adsorbed Sulfur on HDS Activity

Hydrodesulfurization catalysts are activated by sulfidation of inactive oxides (MoO_3, CoO) to produce MoS_2 and Co-Mo-S phases on the catalyst support. To determine the effect of adsorbed sulfur on the HDS activity of molybdenum, Gellman et al. carried out thiophene HDS reactions over Mo(100) surfaces covered with submonolayer amounts of adsorbed sulfur [4,1]. As shown in Figure 4.3, at low coverages ($\theta_s < 0.6$ ML), sulfur decreases the HDS activity of the Mo(100) surface while additional sulfur does not further affect catalyst activity. The lower activity of the sulfided Mo(100) surface is observed for the duration of an HDS reaction (90-120 min.), indicating that the sulfur overlayer is stable on the catalyst surface.

4.3.2 Radiotracer (^{35}S) Labelling Studies

In order to investigate the role of adsorbed sulfur in thiophene HDS over the Mo(100) surface, high pressure reactions were performed over sulfur covered surfaces labelled with ^{35}S [4,1]. Removal of ^{35}S from the Mo(100) surface was studied in both pure hydrogen (P_{H_2} = 100-780 Torr) and in the HDS gas mixture (P_{Th} = 1-5 Torr, P_{H_2} = 100-780 Torr). In pure H_2, ^{35}S can be removed from the surface only

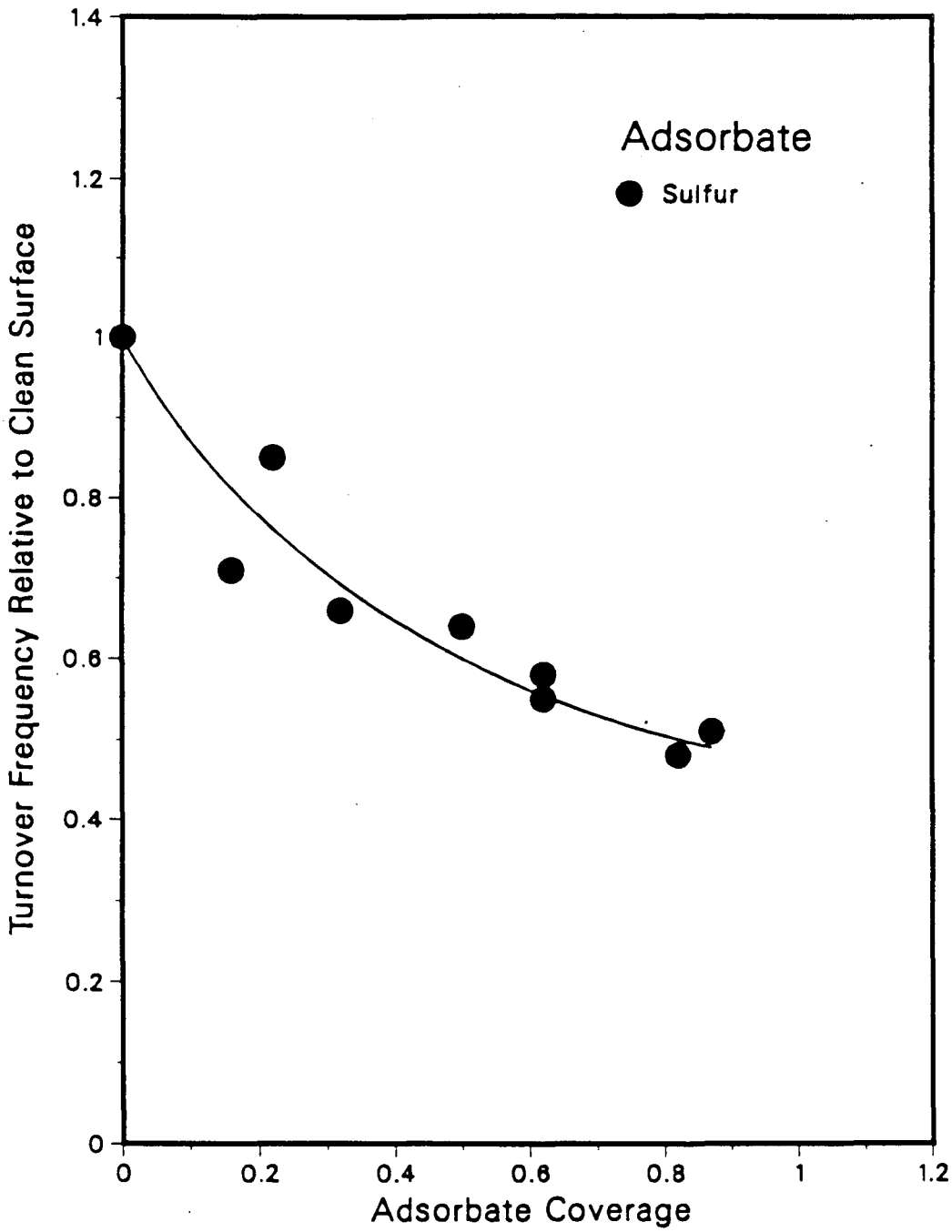

Figure 4.3: Rate of thiophene HDS as a function of the initial sulfur coverage on the Mo(100) surface.

by hydrogenation (equation 4.1), while in the HDS mixture, ^{35}S can be removed by hydrogenation and/or exchange (equation 4.2) reactions.

$$^{35}S_{(ads)} + 2\,H_{(ads)} \longrightarrow {}^{35}SH_{2(g)} \tag{4.1}$$

$$^{35}S_{(ads)} + C_4H_4S_{(ads)} \longrightarrow {}^{35}SC_4H_4(g) + S_{(ads)} \tag{4.2}$$

Starting with 0.75 ML of sulfur on the Mo(100) surface, the change in sulfur coverage was measured as a function of reaction time in one atmosphere of hydrogen (T = 800 K) and the data is shown in Figure 4.4a. If the hydrogenation of sulfur is a first order process, as represented in equation 4.3 below,

$$r_s = \frac{d\theta_s}{dt} = k \cdot \theta_s \tag{4.3}$$

then a linear relationship exists between the natural log of the coverage and the time of reaction. In this equation, r_s is the rate of ^{35}S removal, θ_s is the coverage of ^{35}S and k is a first order rate constant which contains the hydrogen partial pressure dependence. The close agreement of the data points and the straight line in Figure 4.4b indicates that the assumption of first order kinetics for sulfur hydrogenation on the Mo(100) surface is justified. The slope of the plot is the rate constant, which at a temperature of 800 K was determined to be $k = 3.0\times10^{-4}$ atom^{-1}sec^{-1}. The temperature and hydrogen partial pressure dependencies of sulfur hydrogenation on Mo(100) were determined and the data are plotted in Figures 4.5 and 4.6. The Arrhenius plot yields an activation energy of 13.9 kcal/mole over the temperature range 675-825 K, while a hydrogen partial pressure dependence of 0.34 is obtained from Figure 4.6 for hydrogen pressures between 100 and 780 Torr.

The kinetic studies discussed above were carried out on Mo(100) surfaces with initial sulfur coverages of 0.75 ML. The rate of sulfur hydrogenation was found to depend strongly on the sulfur coverage, as illustrated in Figure 4.7. For ini-

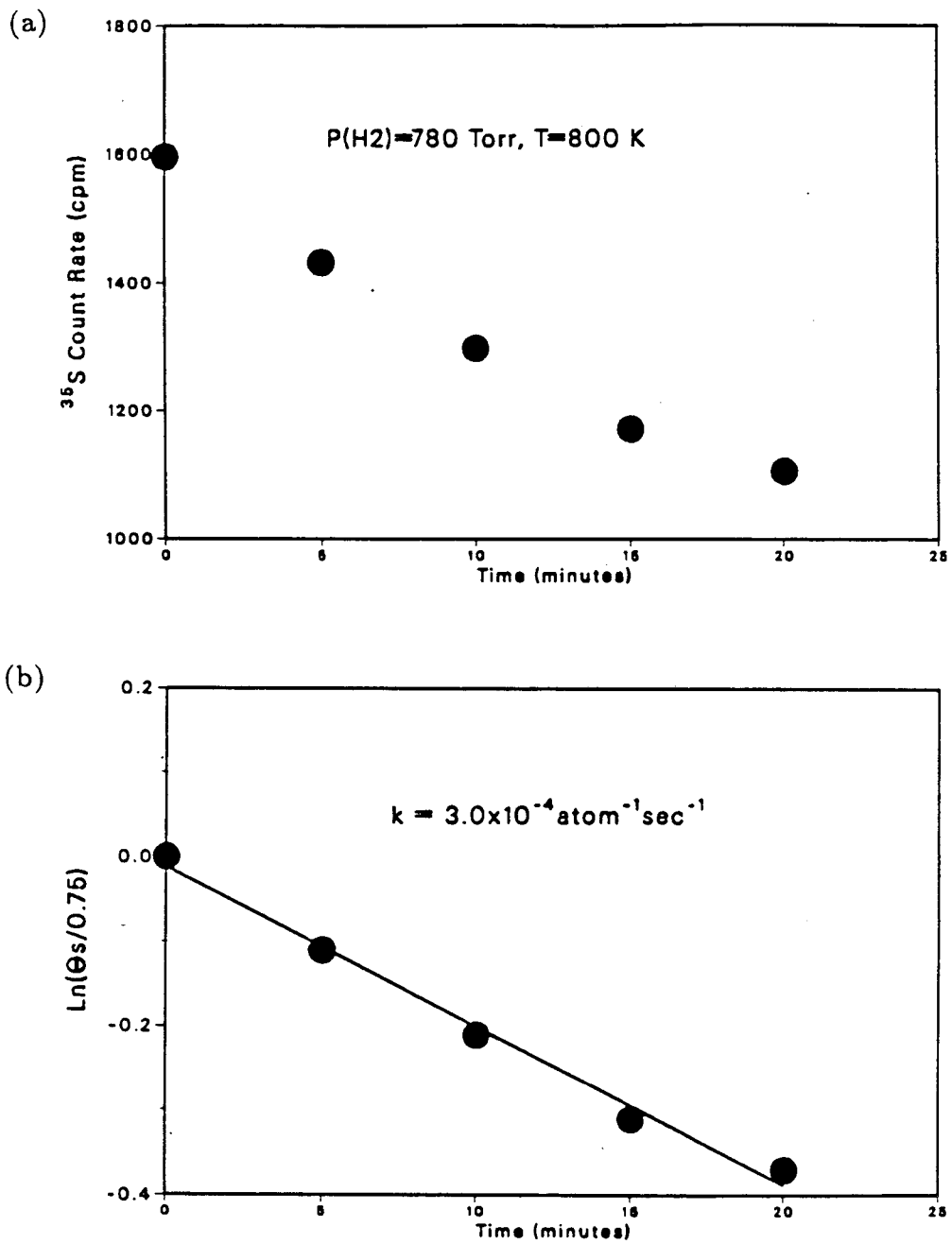

Figure 4.4: (a) Change in sulfur coverage on the Mo(100) surface as a function of reaction time in hydrogen. (b) Same data as in (a) plotted assuming first order kinetics in ^{35}S.

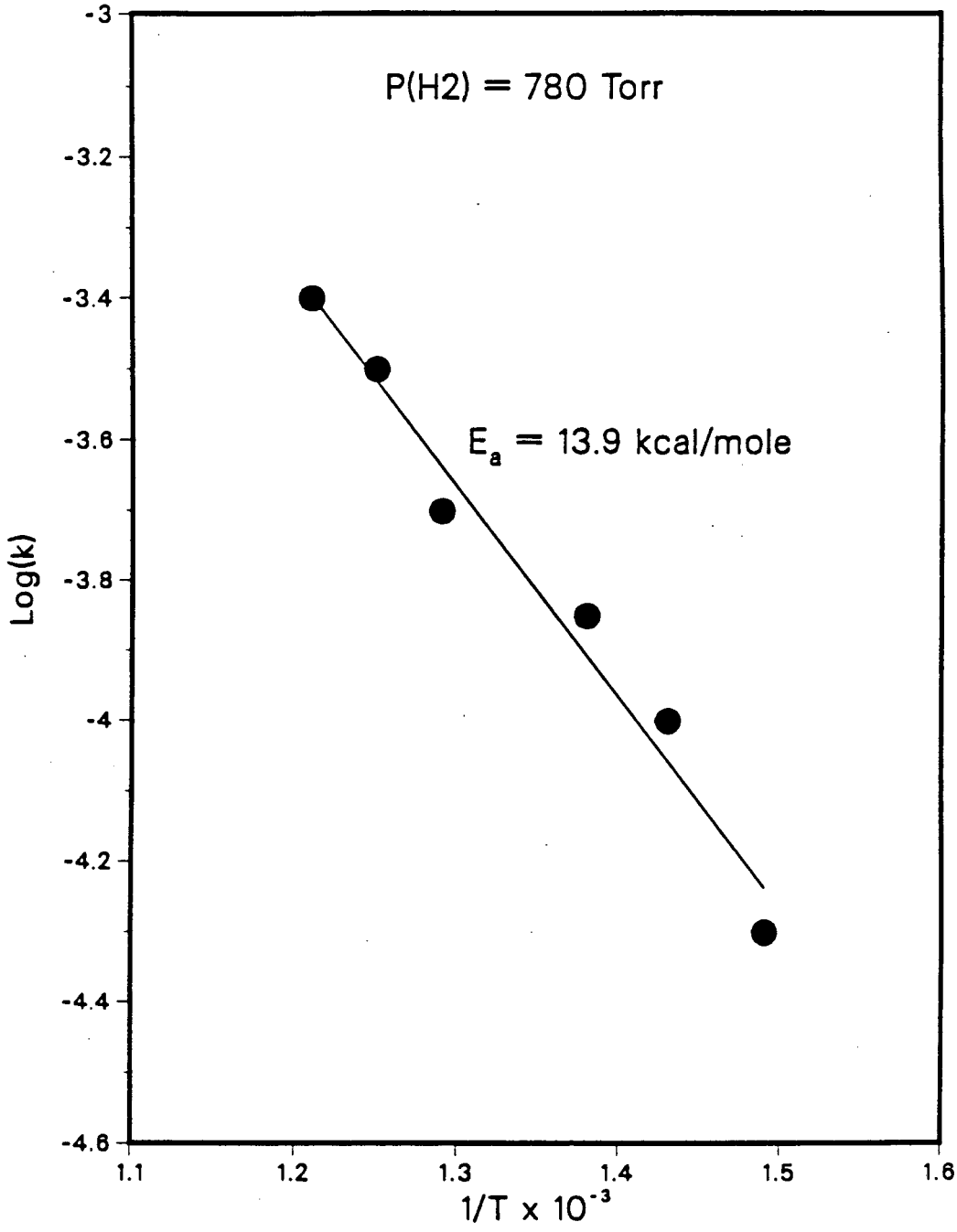

Figure 4.5: Temperature dependence of sulfur hydrogenation on the Mo(100) surface.

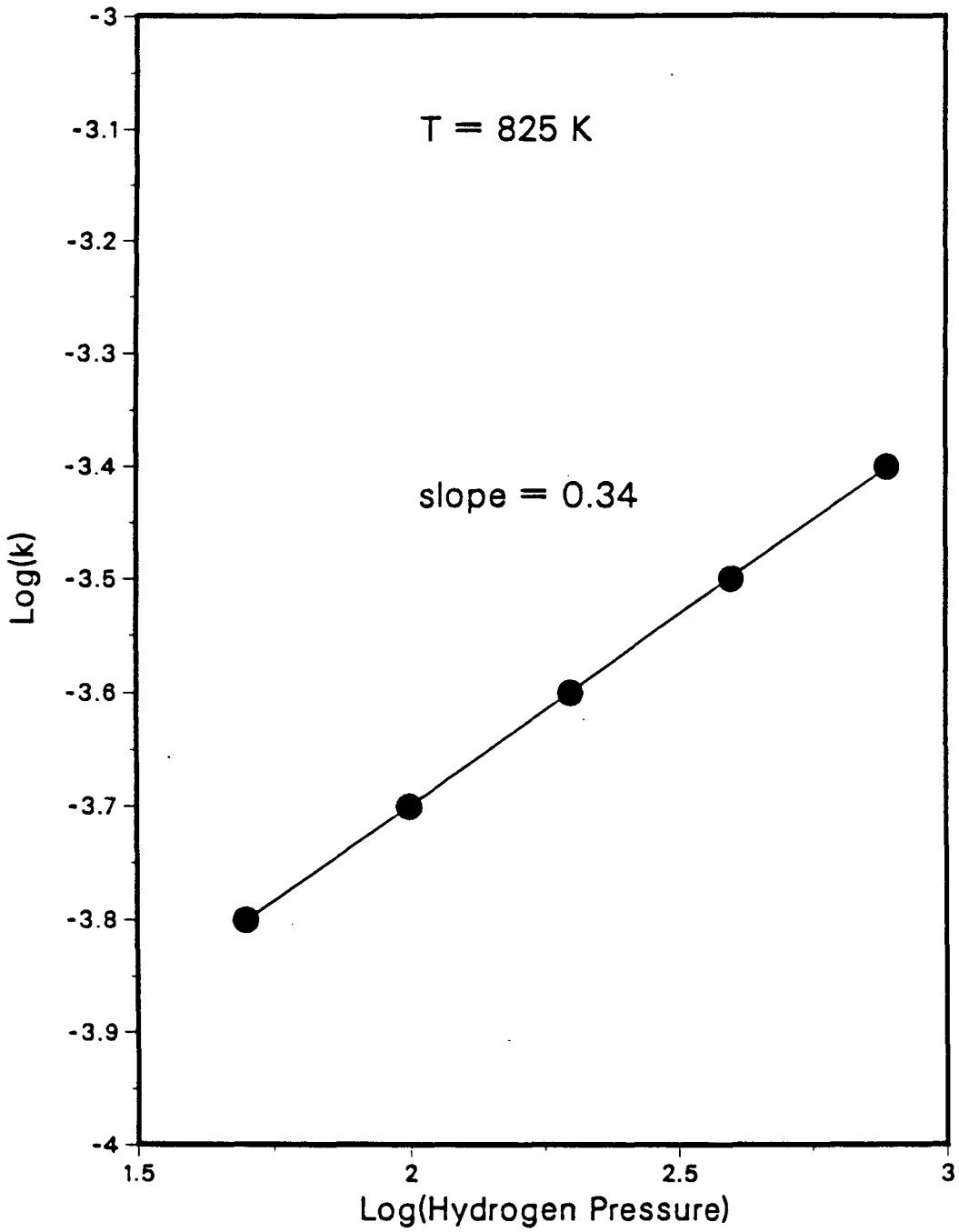

Figure 4.6: Hydrogen partial pressure dependence of sulfur hydrogenation on the Mo(100) surface.

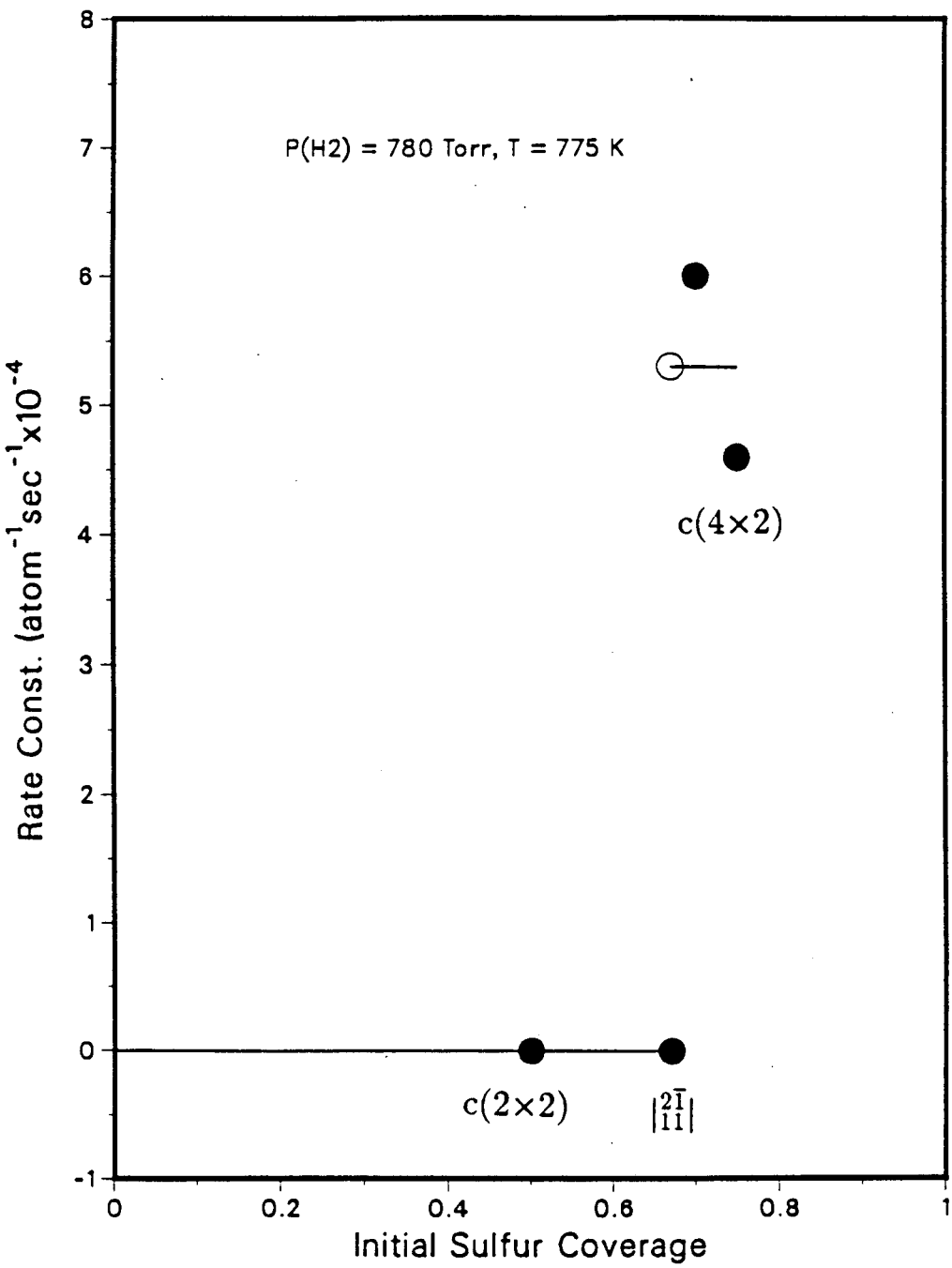

Figure 4.7: Rate of sulfur hydrogenation on the Mo(100) surface as a function of the initial sulfur coverage.

tial sulfur coverages $\leq$ 0.67 ML, no change in the sulfur coverage could be detected after five minutes of reaction at 773 K. The minimum detectable rate constant which could be measured was 2×10^{-5} atom^{-1}sec^{-1}, well below the values of k $\geq 3\times10^{-4}$ atom^{-1}sec^{-1} measured for initial sulfur coverages greater than 0.67 ML at the same temperature. Reaction times were limited to five minutes for the data plotted in Figure 4.7 in order to minimize the build-up of sulfur and carbon on the single crystal from contaminant, background gases in the reaction loop. The adsorption of these contaminants onto the single crystal over long reaction times led to the eventual loss of ^{35}S from the Mo surface.

The rate of sulfur removal from the Mo(100) surface was also determined in the thiophene HDS mixture. The addition of thiophene to the gas phase dramatically affected the rate at which ^{35}S was removed from the surface. Under the reaction conditions of P_{Th} = 1.0 Torr, P_{H_2} = 780 Torr and T = 618 K, a rate constant of 6.8×10^{-4}atom^{-1}sec^{-1} was determined which is more than 30 times greater than that calculated for sulfur removal in pure hydrogen by extrapolation of the Arrhenius plot in Figure 4.5. The temperature and partial pressure dependencies of sulfur removal from the Mo(100) surface in HDS conditions are shown in Figures 4.8 and 4.9. A clear break is exhibited in the Arrhenius plot at $\sim$ 653 K, giving activation energies of 7.2 kcal/mole for low temperatures (500-653 K) and 32.2 kcal/mole in the high temperature regime (653-713 K). Interestingly, the rate of ^{35}S removal was found to be independent of both the thiophene and hydrogen partial pressures.

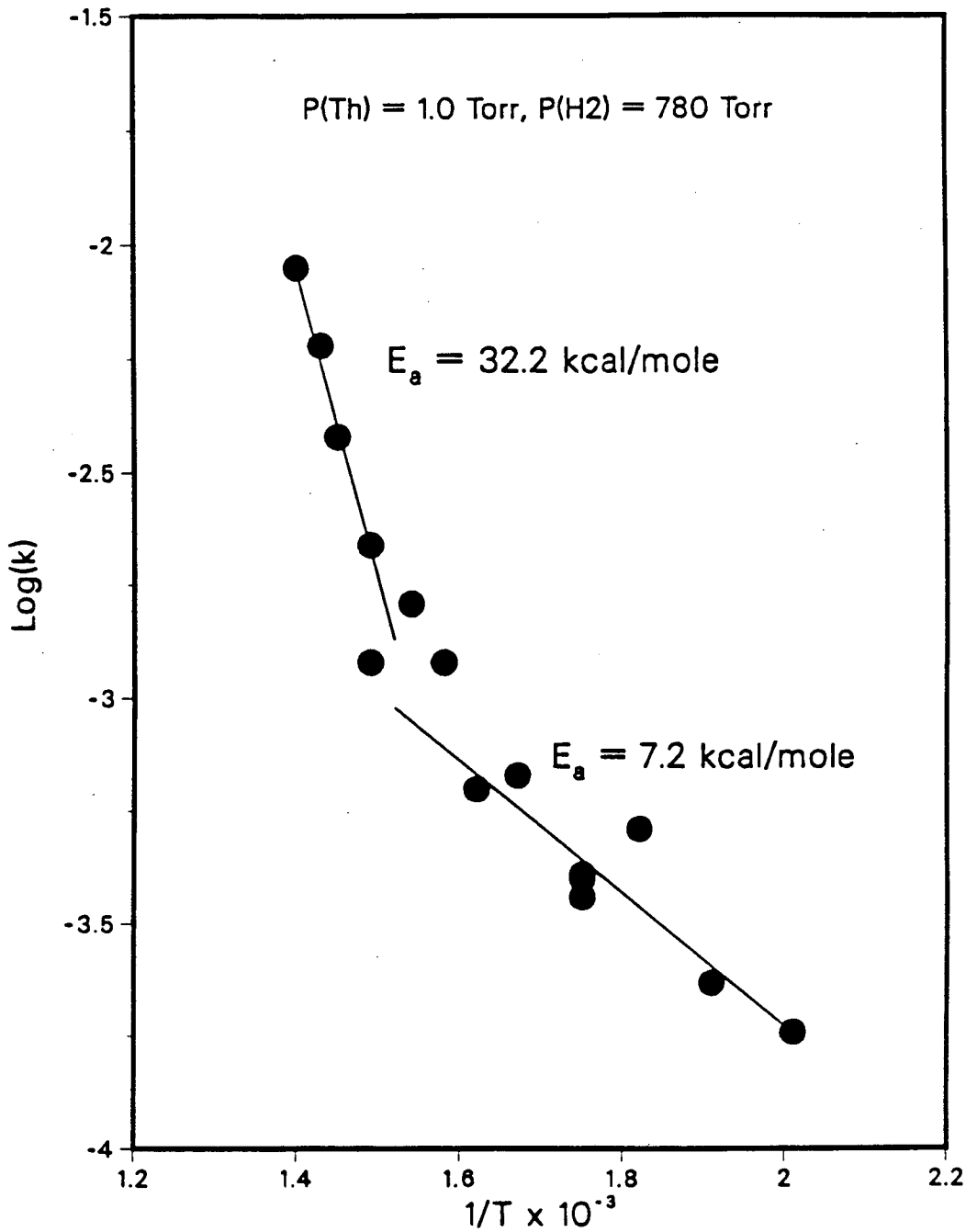

Figure 4.8: Temperature dependence of ^{35}S removal from the Mo(100) surface under HDS conditions (P_{Th} = 1.0 Torr, P_{H_2} = 780 Torr).

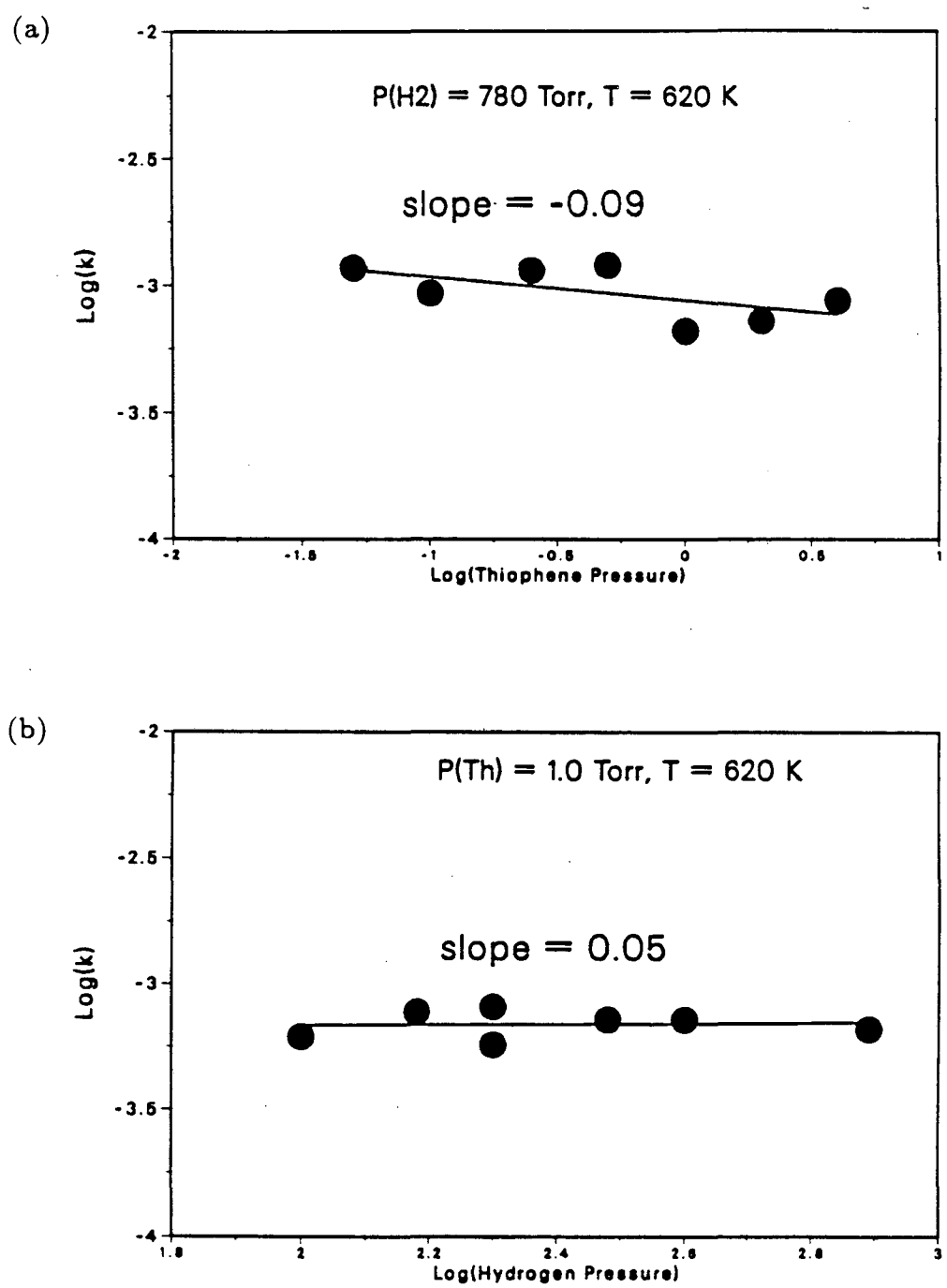

Figure 4.9: (a) Dependence of ^{35}S removal rate on thiophene pressure (P_{H_2} = 780 Torr, T = 618 K). (b) Dependence of ^{35}S removal on hydrogen pressure (P_{H_2} = 780 Torr, T = 618 K).

4.4 Thiophene HDS over Carbided Mo(100) Surfaces

4.4.1 Effect of Adsorbed Carbon on HDS Activity

Ultrahigh vacuum chemisorption studies of thiophene on the clean Mo(100) surface have shown that thiophene decomposes at temperatures $\leq$ 690 K to produce mixed overlayers of sulfur and carbon on the metal surface [5,6,7]. Therefore, in addition to investigating thiophene HDS over clean and sulfided Mo surfaces, it is important to study the catalytic properties of carbided Mo surfaces [8]. An AES spectrum of a clean Mo(100) surface exposed to the reaction mixture at 613 K showed the surface to be covered with predominantly carbon ($\theta_c \approx 0.8$ ML, $\theta_s \approx 0.2$ ML). The fine structure of the C(272) peak indicates that the carbon is carbidic (see Sections 2.3.1 and 3.3.1). After a 90 minute reaction, the carbon coverage is high ($\theta_c \approx 0.7$ ML) and the sulfur coverage has increased to $\theta_s \approx 0.9$ ML. This sulfur does not block active HDS sites suggesting that it is weakly adsorbed or adsorbs after reaction during evacuation of the isolation cell. Figure 4.10 is a plot of thiophene HDS activity as a function of initial carbon coverage on the Mo(100) surface. As will be discussed shortly, carbon adsorbed on the Mo(100) surface in UHV remains on the surface during HDS but does not lower the HDS activity of the Mo(100) catalyst. The product distribution for thiophene HDS over carbided Mo(100) surfaces is similar to the distribution obtained over an initially clean surface (see Table 4.1). Deactivation of the carbided catalysts occurred at similar conversions as for the initially clean surface as well. The deactivation of Mo(100) single crystals will be discussed in Section 4.5.

To determine whether the carbided Mo(100) surface is sensitive to poisoning by sulfur, HDS studies were carried out on carbided surfaces covered with sulfur

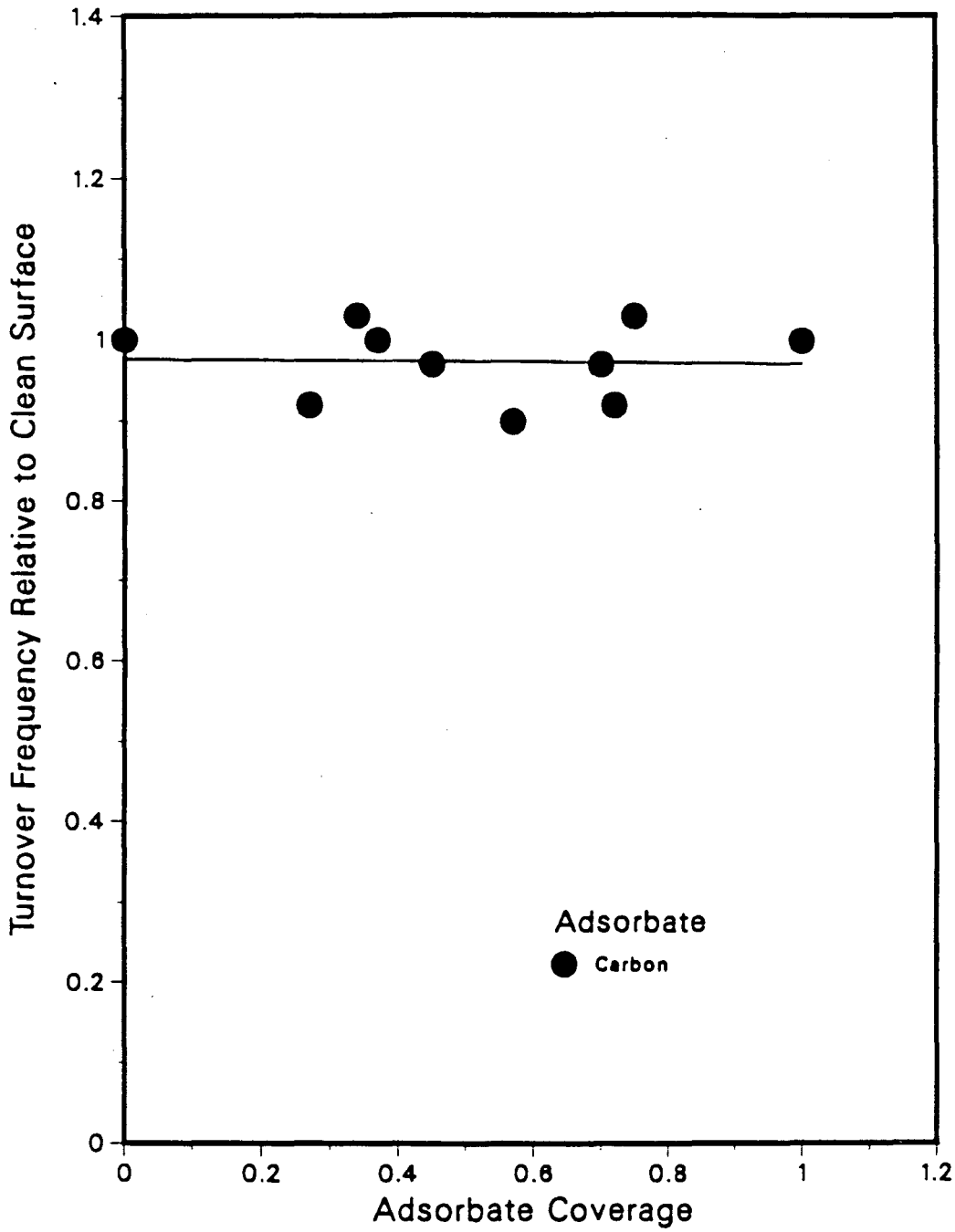

Figure 4.10: Rate of thiophene HDS as a function of the initial carbon coverage on the Mo(100) surface.

overlayers. Sulfur was deposited onto a p(1×1) Mo(100)-C surface (θ_c = 1.0 ML) at room temperature to a coverage of 0.75 ML. No observable change was apparent in the LEED pattern. Annealing to 613 K for one minute caused the (1×1) spots to become blurred with faint streaks between spots. An HDS reaction was performed over this surface and an activity of 0.076 mol./site·sec measured, well below the value of 0.13 mol./site·sec determined for a carbided Mo(100) surface. As discussed in Chapter 3, carbon atoms adsorbed on the Mo(100) surface are bound in four-fold hollow sites. Therefore, sulfur deposited onto the carbon covered surface must occupy different binding sites. The decreased HDS activity of this surface indicates that sulfur atoms need not be adsorbed in four-fold hollows to block active HDS sites. For comparison, the HDS turnover frequencies of a sulfur covered carbide surface, a sulfur covered Mo(100) surface, a carbided surface and the initially clean Mo(100) surface are shown together in Figure 4.11.

4.4.2 Radiotracer (^{14}C) Labelling Studies

Radiotracer ^{14}C was used in this work to determine the residence time of adsorbed carbon on the Mo(100) surface. The removal of ^{14}C was studied in pure hydrogen as well as in butadiene/hydrogen and thiophene/hydrogen gas mixtures. As was the case with ^{35}S, the labelled carbon could be removed from the Mo surface via hydrogenation and exchange reactions. Isotopic analysis of the products of reactions over ^{14}C labelled surfaces was not performed, so the identities of the ^{14}C containing product species are unknown. In hydrogen, the only pathway for the removal of ^{14}C from the Mo(100) surface is hydrogenation. Figure 4.12 shows the decrease in ^{14}C coverage as a function of reaction time in hydrogen at two temperatures. ^{14}C hydrogenation reactions were not carried out to times longer than fifteen minutes in pure hydrogen due to the gradual adsorption of sulfur and car-

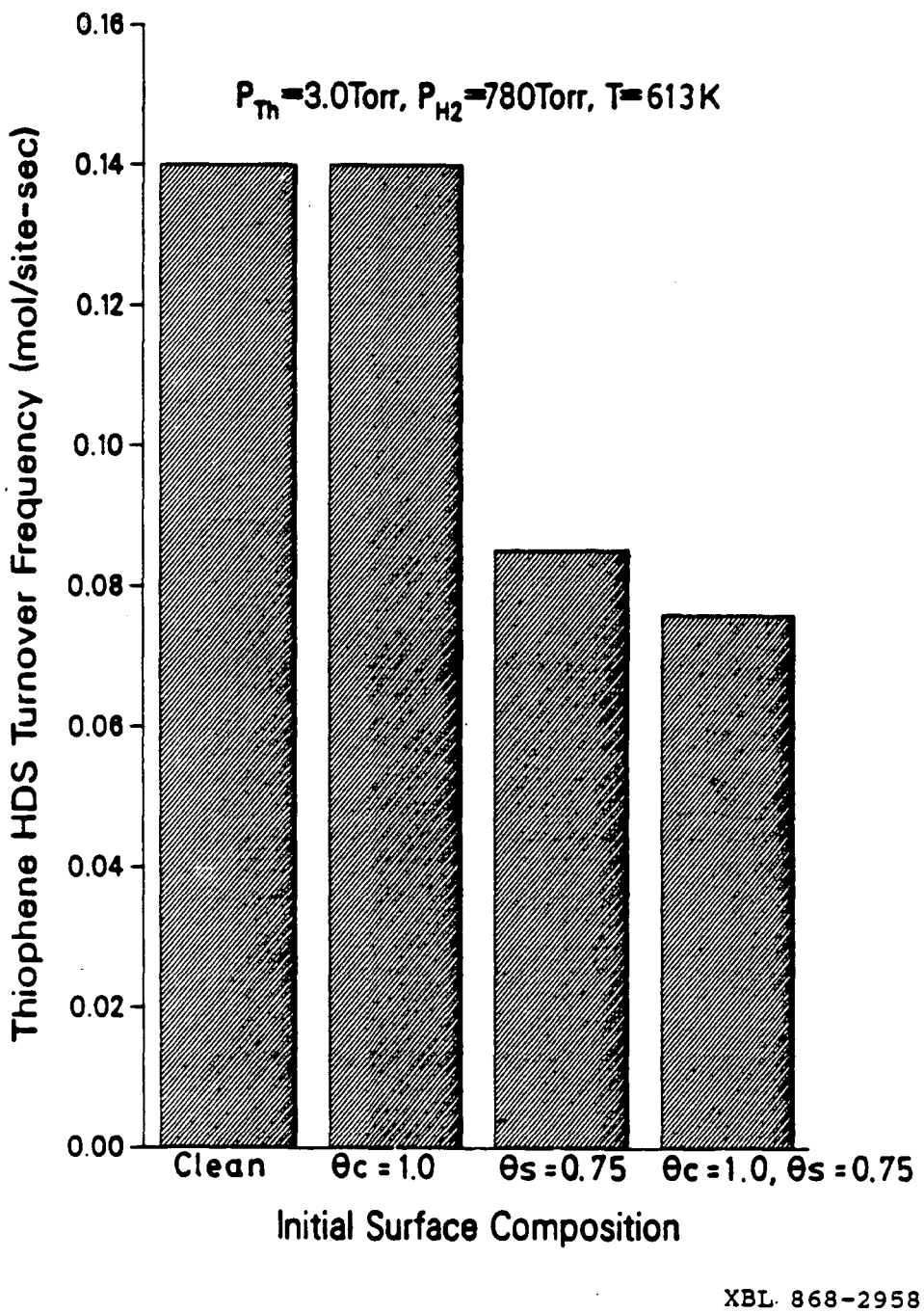

Figure 4.11: Thiophene HDS activity of Mo(100) surfaces with different initial surface compositions.

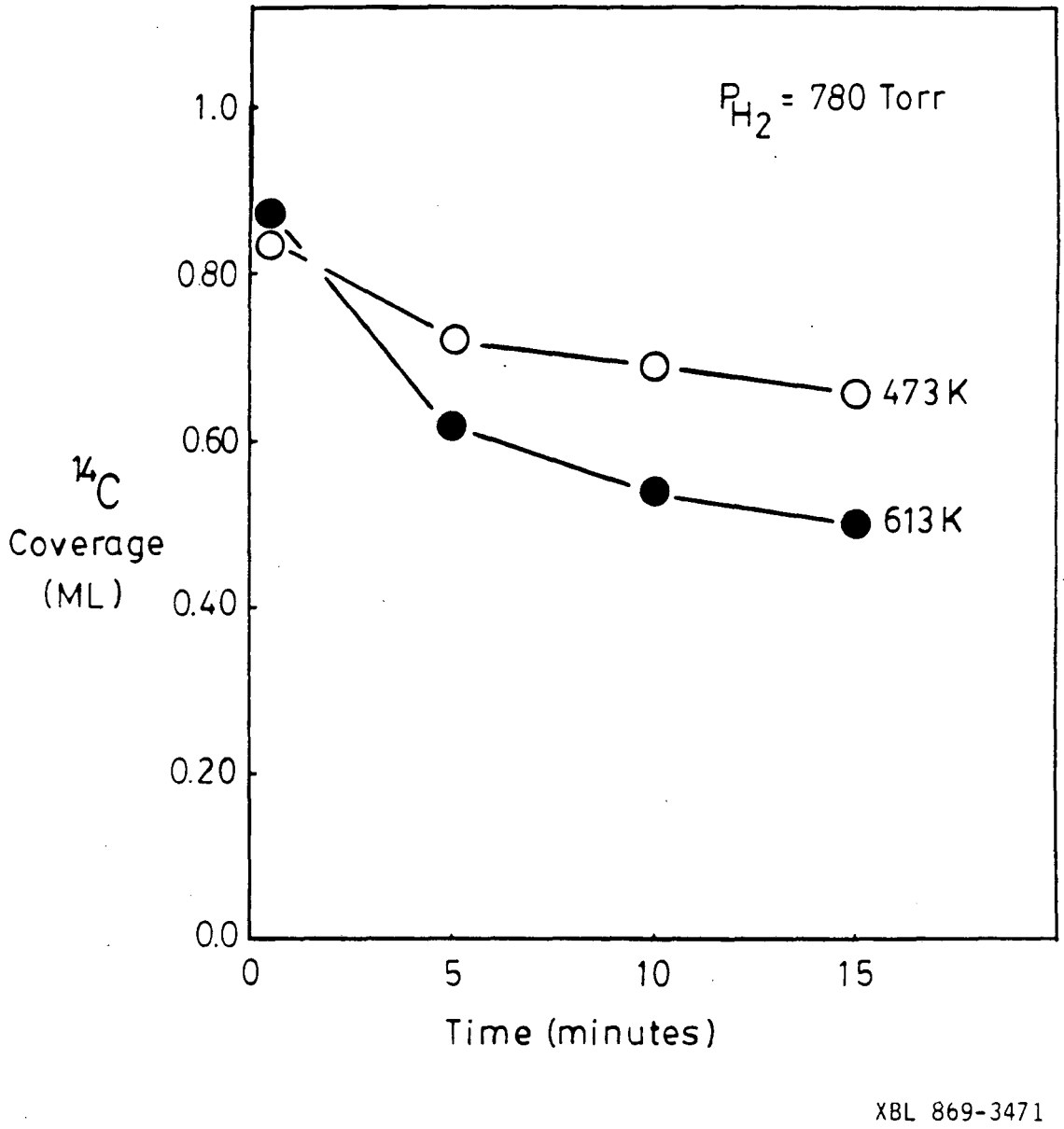

Figure 4.12: ^{14}C coverage on the Mo(100) surface as a function of the reaction time in pure hydrogen (P_{H_2} = 780 Torr).

bon onto the Mo single crystal from the reactor loop. After 15 minutes of reaction at 613 K, the carbon coverage was reduced to 65 % of its initial value of 0.85 ML. The time scale for carbon hydrogenation is much longer than for thiophene HDS over the carbided M(100) surface; over 100 thiophene molecules are desulfurized per surface Mo atom in 15 minutes at this temperature. The hydrogenation of adsorbed carbon on the Mo(100) surface was found to be independent of hydrogen pressure over the range 100-780 Torr as shown in Figure 4.13.

In Section 4.4.1, it was shown that Mo(100) surfaces initially covered with carbon overlayers have the same HDS activity as initially clean surfaces. In order to show that adsorbed carbon does not affect the HDS activity of a Mo(100) catalyst relative to an initially clean single crystal, it is necessary to show that carbon remains on the catalyst surface during reaction. The removal of adsorbed ^{14}C from the Mo(100) surface was measured in typical HDS conditions (P_{Th} = 3.0 Torr, P_{H_2} = 780 Torr, T = 613 K) as shown in Figure 4.14. Following an initial drop in ^{14}C coverage from 0.80 ML to 0.68 ML, the ^{14}C coverage decreases very slowly to 0.63 ML after 90 minutes of reaction. Over a 90 minute reaction period, the thiophene turnover number is in excess of 700. Clearly, carbon adsorbed on the Mo(100) surface in UHV remains on the surface during reaction, but does not block the active thiophene HDS sites.

Butadiene has been shown to be an intermediate in thiophene HDS over the Mo(100) surface [9]. It is of interest to investigate the influence of the hydrocarbons produced in thiophene HDS on the removal of adsorbed carbon in the absence of sulfur. Figure 4.15 compares the removal of ^{14}C in a butadiene/hydrogen mixture, in the HDS gas mixture and also in pure hydrogen at a temperature of 573 K. The decrease in ^{14}C coverage in the butadiene hydrogenation mixture is very similar to that observed in pure hydrogen, and greater than in the case of the thiophene

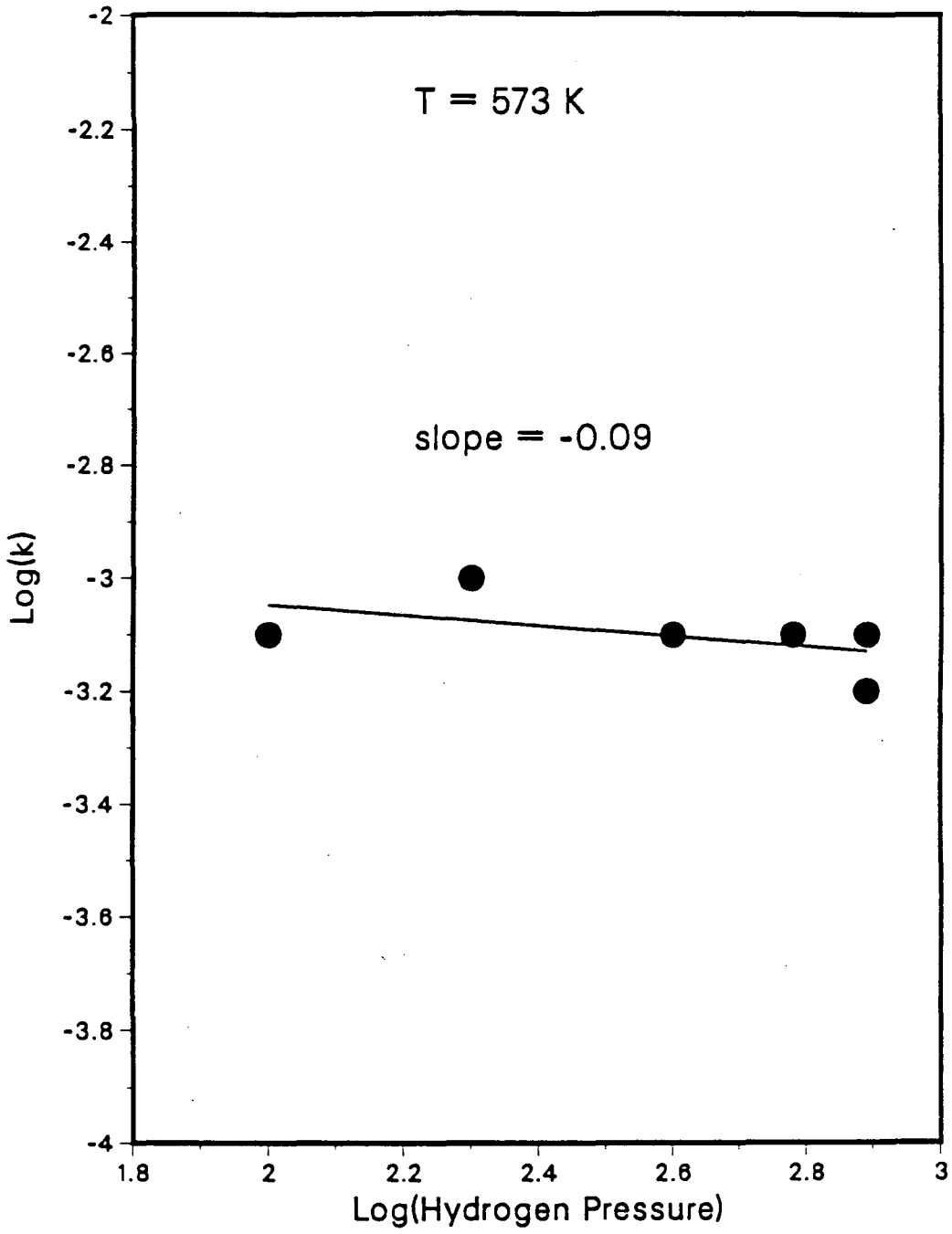

Figure 4.13: Hydrogen pressure dependence of carbon hydrogenation on the Mo(100) surface.

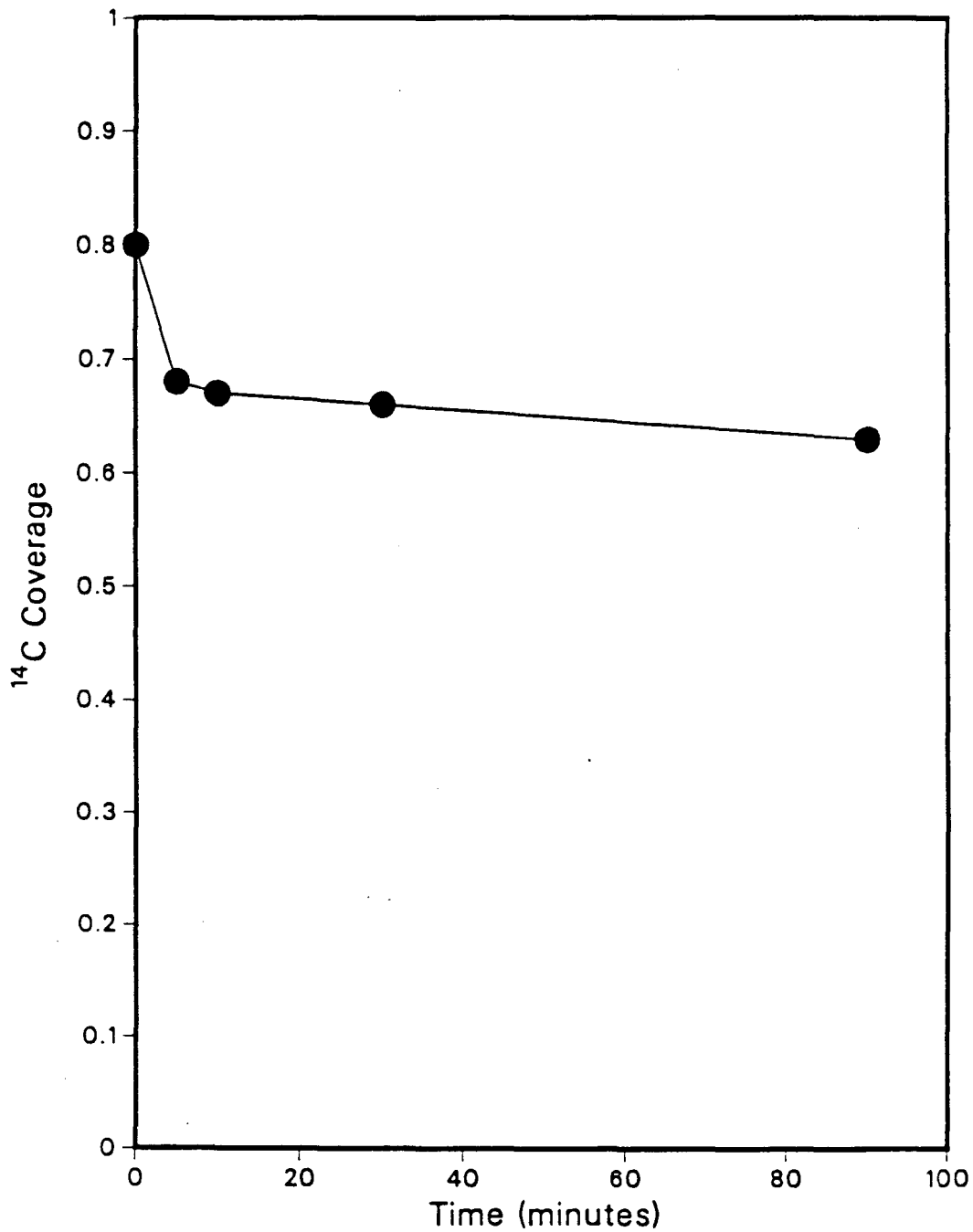

Figure 4.14: Change in ^{14}C coverage as a function of reaction time in the HDS reaction mixture.

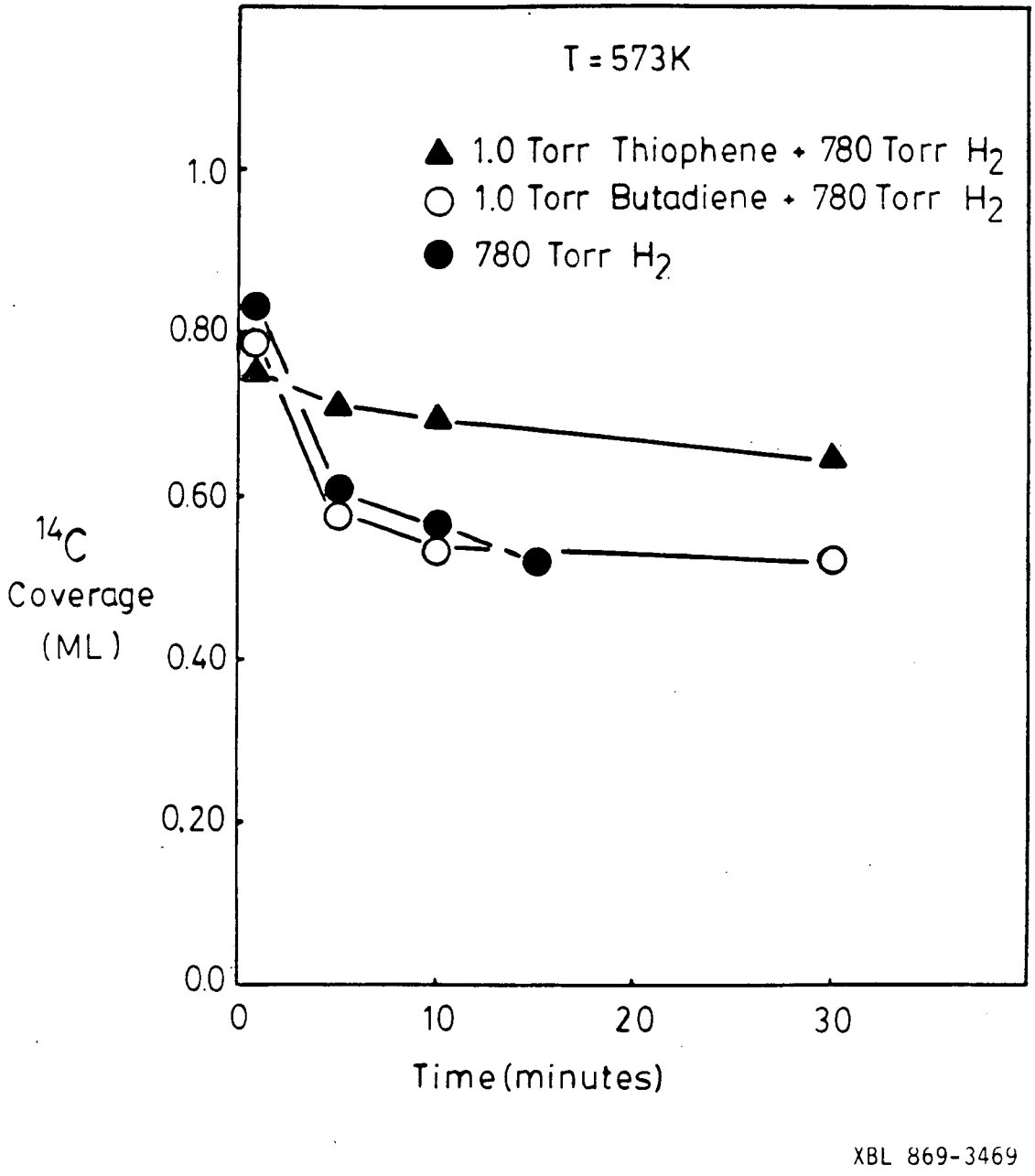

Figure 4.15: Change in ^{14}C coverage in pure hydrogen and in gas mixtures of butadiene and hydrogen, and thiophene and hydrogen at 573 K.

HDS mixture. Apparently, butadiene and the hydrogenated products produced (butenes, butane) have no effect on the rate or extent of ^{14}C removal, while thiophene (and/or the H_2S produced) decreases the rate and amount of adsorbed carbon which is removed from the Mo(100) catalyst.

4.5 The Influence of Products (H_2S, cis-2-butene) on HDS Activity of Mo(100) Surfaces

Figure 4.16 shows the effect of H_2S and cis-2-butene on the thiophene HDS activity of a Mo(100) single crystal. The partial pressures of product used in these experiments were chosen to correspond to the pressures of H_2S and C_4 hydrocarbon present when catalyst deactivation occurs (5-10 % conversion). Cis-2-butene has a very small influence on the HDS activity of the catalyst; we do not believe the increase in activity observed is significant. Hydrogen sulfide strongly decreases the activity of the catalyst. At a partial pressure of 300 mTorr of H_2S, an HDS turnover frequency of 0.053 mol./site·sec was measured, less than one-half the activity in the absence of H_2S. After pumping the reaction loop to a pressure $\leq 10^{-3}$ Torr, the reactor loop was repressurized with a fresh mixture of thiophene (3.0 Torr) and hydrogen (780 Torr). The activity of the catalyst was measured to be 0.12 mol./site·sec showing that the inhibition of HDS on the Mo(100) surface by H_2S is reversible. This indicates that it is molecular H_2S which blocks active HDS sites instead of a species which decomposes to form strongly bound sulfur that cannot be removed by evacuation.

4.6 Discussion

There are five primary points which can be made that help to understand the surface chemistry of thiophene HDS over the Mo(100) surface.

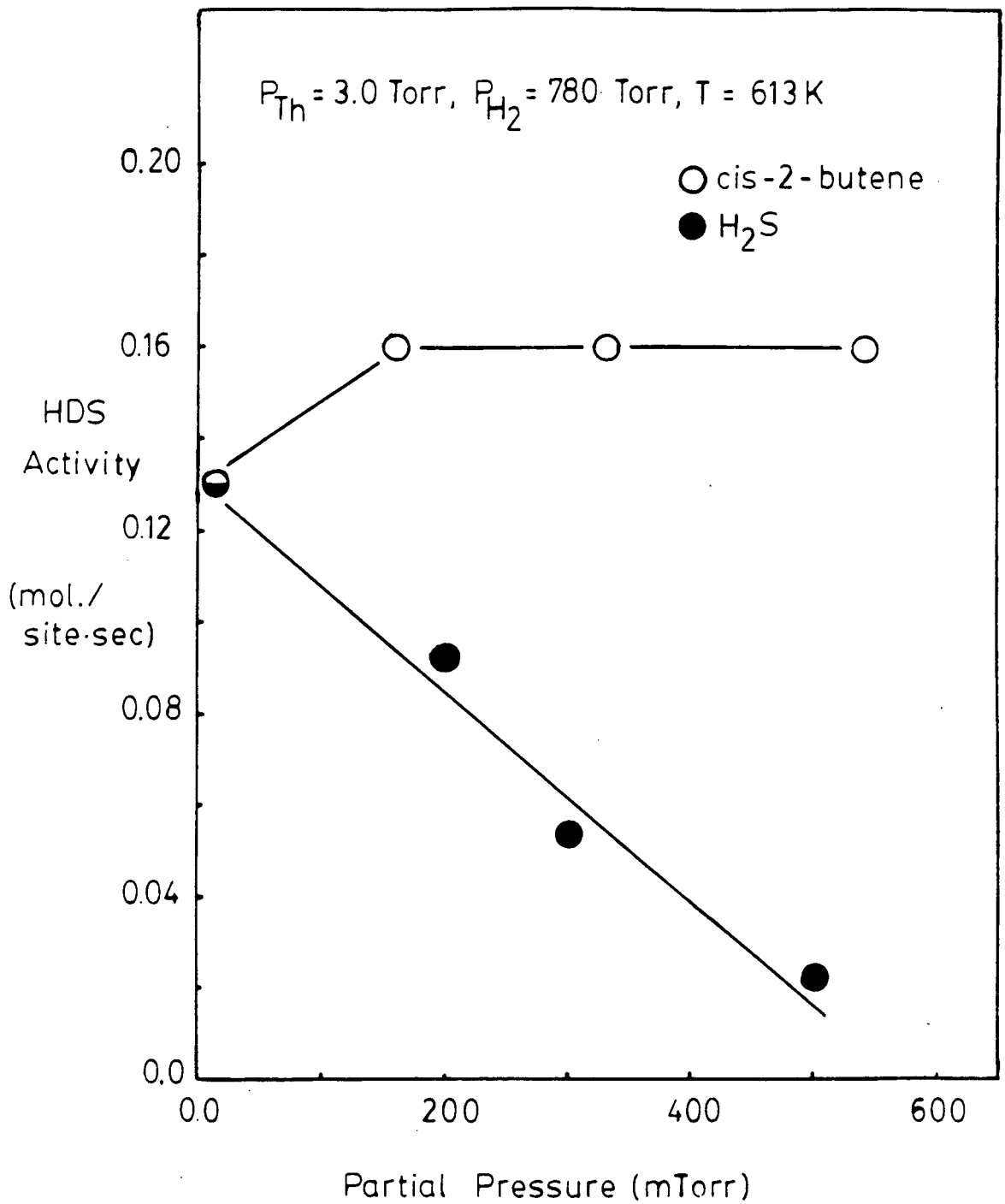

XBL 869-3470

Figure 4.16: HDS activity of an initially clean Mo(100) single crystal as a function of the partial pressure of product (H_2S or cis-2-butene) in the gas mixture (P_{Th} = 3.0 Torr, P_{H_2} = 780 Torr, T = 613 K).

I. Thiophene hydrodesulfurization is a structure insensitive reaction over molybdenum single crystal surfaces. The HDS turnover frequencies, product distributions and poisoning of Mo single crystal catalysts are similar to those observed for sulfide catalysts [10,11,12].

II. Carbon adsorbed on Mo(100) remains on the surface during HDS but does not block the active thiophene HDS sites, while adsorbed sulfur decreases the activity of the catalyst.

III. The active catalytic surface is covered with adsorbed carbon. An initially clean Mo(100) single crystal catalyst becomes covered with predominantly carbon from thiophene decomposition.

IV. Deposition of atomic sulfur onto either the metal or carbon covered surface does not occur during thiophene HDS. Apparently, the thiophene desulfurization step is a concerted process in which S–H bonds are formed at the same time that C–S bonds are broken.

V. Deactivation of the Mo(100) catalyst in a batch reactor occurs by reversible adsorption of H_2S onto the active catalytic sites. The hydrocarbon product cis-2-butene does not significantly alter the activity of the catalyst.

4.6.1 Thiophene Hydrodesulfurization over Clean Molybdenum Single Crystal Surfaces

Thiophene hydrodesulfurization has been investigated over three molybdenum single crystal faces and been found to be a structure insensitive reaction [2,3,1]. The Mo single crystals are active catalysts for thiophene hydrodesulfurization as attested by turnover numbers greater than one. In addition, thiophene HDS over

Mo metal surfaces exhibits many similarities to thiophene HDS over sulfide catalysts. In Table 4.1, the product distribution from thiophene HDS over a Mo(100) single crystal is compared with that obtained over an unsupported MoS_2 catalyst [9,11]. The similarity of the product distributions for the Mo(100) surface

Table 4.1: Thiophene HDS Product Distributions.

Product	[a]*Mo(100)*	[b]*MoS_2*
Butadiene	5.6%	6.3%
1-Butene	52.8	41.7
trans-2-Butene	19.4	22.8
cis-2-Butene	13.9	17.8
Butane	8.1	11.5

[a]P_{Th} = 2.5 Torr, P_{H_2} = 780 Torr, T=558 K
[b]P_{Th} = 20. Torr, P_{H_2} = 780 Torr, T=558 K

and the MoS_2 catalyst suggests that the HDS reaction pathway is the same over the two catalysts. Butadiene hydrogenation over the Mo(100) surface produces an almost identical distribution of products, indicating that thiophene HDS proceeds via butadiene as an intermediate, and its hydrogenation determines the product distribution [9]. Comparing their HDS activities, a Mo(100) single crystal (HDS activity = 3.2×10^{13} mol./cm^2·sec) is two orders of magnitude more active than the powdered MoS_2 catalyst (HDS activity = 1.4×10^{11} mol./cm^2·sec). However, it should be noted that HDS activities of MoS_2 catalysts do not correlate with their BET surface areas so this comparison is not valid [13]. The BET method measures the total surface area of a catalyst instead of the active surface area, so the lower activity of the MoS_2 catalyst is not surprising. Chianelli and coworkers have recently developed an optical absorption technique using photothermal deflection spectroscopy which can be used to measure the edge area of MoS_2 crystallites [10].

If the edge area, the distribution of edge planes and the density of Mo atoms in the edge planes are known, then the number of sites can be calculated. Using this method, the authors determined a turnover frequency of 0.079 mol./site·sec for dibenzothiophene HDS (623 K) over small MoS_2 crystallites, close to the turnover frequency measured for Mo(100) at 613 K in this work. Dibenzothiophene is more difficult to desulfurize than thiophene, so the lower turnover frequency of Chianelli and coworkers is expected. The similarity of the product distributions and turnover frequencies for an initially clean Mo(100) single crystal and unsupported MoS_2 suggest that metal single crystals are good model catalysts for the HDS process and that further studies of HDS over single crystal surfaces are warranted.

4.6.2 The Role of Adsorbed Sulfur in Thiophene HDS over the Mo(100) Surface

Atomic sulfur adsorbed on the Mo(100) surface in ultrahigh vacuum has been found to decrease its thiophene HDS activity under high pressure conditions [1,4]. This observation, first recorded by Gellman et al. and reproduced in this work, has significant ramifications for the mechanism of thiophene hydrodesulfurization. Firstly, this observation suggests that adsorbed sulfur is stable on Mo(100) under reaction conditions and blocks active sites for thiophene HDS. ^{35}S labelling experiments in fact verify that the residence time of adsorbed sulfur on Mo(100) is long compared to the turnover time of thiophene to products. Secondly, this result implies that the sulfur produced via the desulfurization of thiophene is not deposited into strong binding adsorption sites on Mo(100), unlike sulfur adsorbed on the Mo(100) surface in UHV which has binding energies $\geq$ 75 kcal/mole [14].

As shown in Figure 4.3, the thiophene HDS activity decreases in an approximately linear fashion over the coverage range $0 < \theta_s < 0.6$ ML, while additional

sulfur does not further affect the activity. An initially clean Mo(100) surface maintains its high HDS activity (about two times higher than a sulfided surface) for the duration of an HDS reaction of 90-120 minute length, indicating that the coverage of adsorbed sulfur is very low for the entirety of the HDS reaction. For Mo(100) surfaces with sulfur coverages $\leq$ 0.6 ML, sulfur atoms adsorbed on the metal surface block active sites which is reflected in a lowered HDS activity. For Mo surfaces with sulfur coverages > 0.6 ML, only a fraction of the adsorbed sulfur affects the activity of the catalyst. This result can be explained in two ways: 1) sulfur atoms adsorbed at coverages > 0.6 ML occupy different adsorption sites not involved in HDS; or 2) the high coverage sulfur species are unstable under reaction conditions and are rapidly removed from the catalyst surface, leaving the steady state sulfur coverage approximately equal to 0.6 ML. Our ^{35}S studies of sulfur hydrogenation on the Mo(100) surface support the latter explanation. As shown in Figure 4.7, the hydrogenation of sulfur on Mo(100) is coverage dependent. Sulfur at coverages > 0.67 ML could be hydrogenated from the Mo(100) surface at a measurable rate, while for sulfur coverages $\leq$ 0.67 ML, no detectable change in the ^{35}S coverage was measured. The existence of two types of sulfur species on the Mo(100) surface has also been proposed based upon spectroscopic and TPD measurements. As discussed in Chapter 3, TPD and XPS studies of sulfur adsorbed on Mo(100) indicate that when the coverage exceeds 0.67 ML, sulfur atoms occupy adsorption sites of lower binding energy than sulfur at lesser coverages [14,15]. A TPD desorption energy of 110 kcal/mole was determined for sulfur at coverages < 0.67 ML, while sulfur above this coverage was found to have a binding energy in the range 75-90 kcal/mole. These results suggest that a break in the plot of HDS activity versus sulfur coverage plot would come at θ_s = 0.67 ML, close to the coverage of 0.6 ML determined from the catalytic studies.

The radiotracer labelling experiments using ^{35}S have shown unambiguously that adsorbed sulfur is stable on the Mo(100) surface under HDS conditions. Sulfur atoms adsorbed in the low and high coverage adsorption sites are removed from the surface at rates well below the thiophene HDS turnover frequency. The rate of ^{35}S removal from the Mo(100) surface at initial coverages of 0.75 ML in pure hydrogen and in the HDS reaction mixture are compared to the rate of thiophene HDS in Figure 4.17. The thiophene HDS turnover frequency is over two orders of magnitude greater than the rate of sulfur removal from the Mo(100) surface under HDS conditions. In other words, during the time that one sulfur atom is removed from an adsorption site on Mo(100), over 100 thiophene molecules are desulfurized per surface molybdenum atom. If mechanisms for thiophene HDS are considered, those that include desulfurization steps which lead to the production of atomic sulfur on the metal surface can be rejected. Figure 4.18 shows two possible mechanisms for the desulfurization of thiophene. The top pathway depicts the desulfurization step of the thiophene HDS mechanism proposed by Lipsch and Schuit (see Figure 1.6a) [16]. Clearly, this cannot be the thiophene desulfurization pathway on the Mo(100) surface since the rate of the second step, removal of sulfur from an adsorption site on the metal surface, has been found to be over two orders of magnitude lower than the overall HDS rate. Alternatively, the bottom pathway is proposed for the desulfurization of thiophene on the Mo(100) surface. In this mechanism, the sulfur removed from thiophene is never adsorbed on the molybdenum surface in the atomic state. Two possibilities for the desulfurization step are the following: 1) a concerted process in which S–H bonds are formed at the same time that the C–S bonds of thiophene are broken, leaving butadiene and H_2S on the catalyst surface; and 2) a modified Lipsch-Schuit mechanism in which sulfur removed from thiophene is deposited into a weak binding site on the

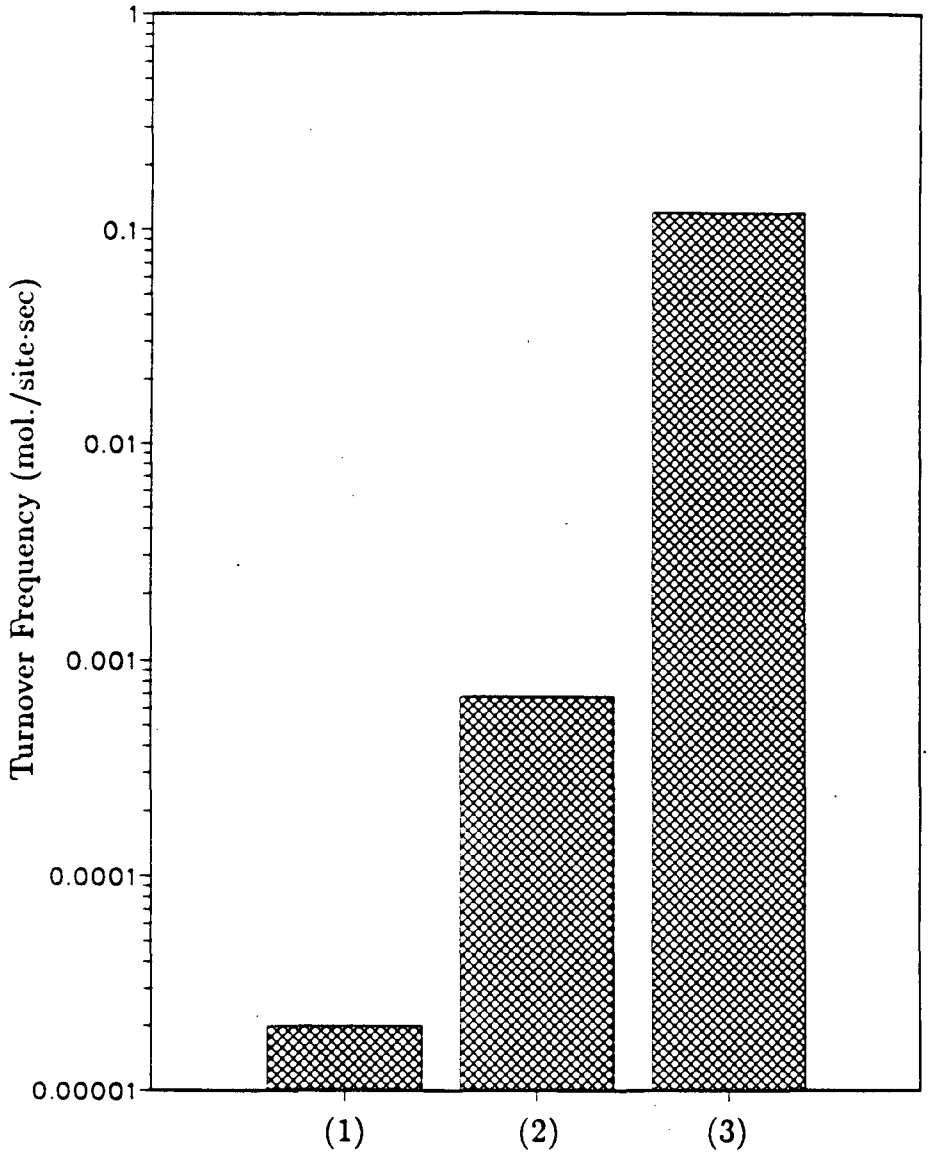

(1) ^{35}S removal: P_{H_2}=780 Torr, T=613 K

(2) ^{35}S removal: P_{Th}=2.5 Torr, P_{H_2}=780 Torr, T=613 K

(3) Thiophene HDS: P_{Th}=2.5 Torr, P_{H_2}=780 Torr, T=613 K

Figure 4.17: Comparison of the rates of ^{35}S removal in pure H_2 (P_{H_2} = 780 Torr, T = 613 K) and in the HDS mixture (P_{Th} = 2.5 Torr, P_{H_2} = 780 Torr, T = 613 K) with the thiophene HDS turnover frequency (P_{Th} = 2.5 Torr, P_{H_2} = 780 Torr, T = 613 K).

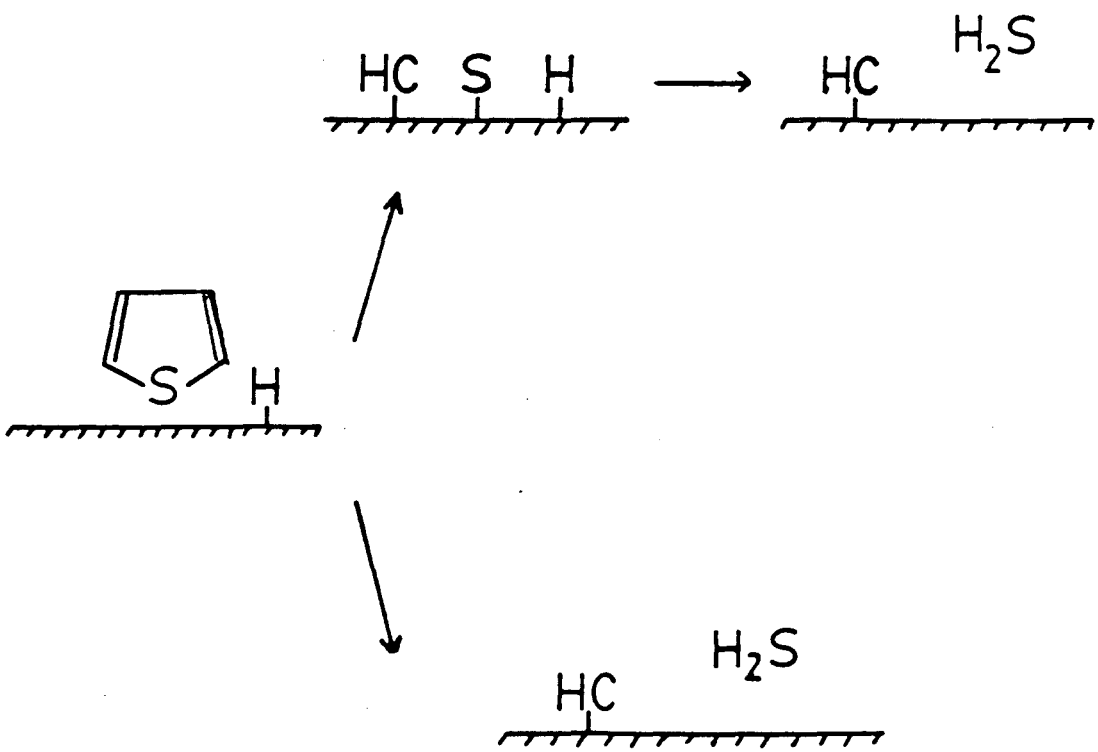

-- XBL 862-478 --

Figure 4.18: Two possible mechanisms for the desulfurization step of thiophene HDS.

catalyst surface which is not populated during sulfur adsorption on Mo(100) in UHV.

Kolboe has proposed an HDS mechanism in which thiophene desulfurization is a concerted process that produces adsorbed H_2S and a highly unsaturated species, diacetylene, on the catalyst surface (see Figure 1.6b) [11]. Thiophene is desulfurized in an intramolecular dehydrosulfurization step in which β-hydrogens are transferred to the thiophenic sulfur as the C–S bonds are broken. Diacetylene has not been detected on the catalyst surface, it would probably be immediately hydrogenated to butadiene, but there is other work in the literature which supports such a mechanism. Catalytic studies have shown that HDS of deuterated thiophene (C_4D_4S) in pure H_2 produces only D_2S and HDS of normal thiophene (C_4H_4S) in D_2 produces only H_2S [17,18]. Both studies implicate thiophene as the source of hydrogen for hydrogenation of sulfur. Evidence also exists that supports a modified Lipsch-Schuit mechanism in which the sulfur removed from thiophene is adsorbed on weak binding sites on the catalyst surface. ^{35}S labelling studies by Gachet and coworkers using an industrial Co-Mo/Al_2O_3 catalyst suggest that there are labile and fixed sulfur species on the catalyst surface [19]. The labile species consists primarily of sulfur removed from thiophene and is rapidly turned over on the catalyst surface while the fixed sulfur species does not participate in the reaction. Unfortunately, the complex nature of the Co-Mo/Al_2O_3 catalyst made it impossible to characterize the adsorption sites of the different sulfur species on the catalyst surface.

4.6.3 Evidence that the Active Surface is Covered with Adsorbed Carbon

To prove that the active Mo(100) surface is carbon covered it is necessary to show that adsorbed carbon remains on the Mo(100) surface during thiophene HDS and that carbided surfaces are active for thiophene HDS. Using the β^- emitter ^{14}C, it was found that 80 % of a carbidic overlayer prepared in UHV remained on the surface following 90 minutes of thiophene HDS in typical reaction conditions (P_{Th} = 3.0 Torr, P_{H_2} = 780 Torr, T = 613 K). As discussed earlier, there are two mechanisms by which ^{14}C can be removed from the Mo(100) surface during thiophene HDS: 1) exchange with carbon atoms from thiophene and/or hydrocarbon products, and 2) direct hydrogenation (discussed in detail below). The former process causes no net change in the carbon coverage while the latter will result in a decrease in carbon coverage. The ^{14}C coverages measured represent a lower bound for the actual carbon coverage on the Mo(100) surface during HDS. Our results show that adsorbed carbon remains on the Mo(100) surface during thiophene hydrodesulfurization.

The HDS activity measured for carbon covered Mo(100) surfaces was found to be the same as for initially clean Mo(100) single crystals. The identical turnover frequencies and product distributions for thiophene HDS over initially clean and carbon covered Mo(100) surfaces suggest that the steady state surface composition for the surfaces is similar during reaction. The fact that adsorbed carbon remains on the surface in reaction conditions points to the active surface being covered with a carbidic overlayer. Decomposition of thiophene on the clean surface could produce an adsorbate overlayer on the metal surface which is composed primarily of adsorbed carbon. AES of a Mo(100) surface following thermal desorption of a saturated monolayer of thiophene shows the surface to be covered with sulfur

and carbon from thiophene decomposition. Zaera and coworkers have found the saturation thiophene coverage in UHV to be 0.3 thiophene molecules per surface Mo atom which gave a sulfur coverage of 0.3 ML following thermal decomposition of thiophene [7]. No desulfurized hydrocarbon products desorb from the thiophene saturated surface upon heating, indicating that carbon coverage must be high as each thiophene molecule has four carbon atoms [5,6]. In this work, thiophene decomposition on the clean Mo(100) surface at 613 K in the typical HDS gas mixture (P_{Th} = 3.0 Torr, P_{H_2} = 780 Torr) gave a surface composition of $\theta_c \approx 0.8$ ML of carbidic carbon and ≈ 0.2 ML of coadsorbed sulfur following evacuation of the reactant gases. This indicates that the initially clean Mo(100) catalyst is covered with predominantly adsorbed carbon at the beginning of a thiophene HDS reaction. After 90 minutes of reaction, the carbon coverage remains high ($\theta_c \approx 0.7$ ML), while the amount of coadsorbed sulfur has increased to $\theta_s \approx 0.9$ ML. This coadsorbed sulfur does not block active HDS sites suggesting that it is weakly bound to the surface or adsorbs onto the catalyst surface during evacuation of the isolation cell. Clearly, it is not bound to the surface in the strong binding sites populated when sulfur is adsorbed onto the clean or carbided Mo(100) surface in UHV, as this sulfur decreases the activity of the catalyst.

4.6.4 Explanation of the Different Effects of C and S on Thiophene HDS over the Mo(100) Surface

Both sulfur ($\theta_s \leq 0.67$ ML) and carbon atoms ($\theta_c \leq 1.0$ ML) bond to the Mo(100) surface in high coordination four-fold hollow sites. The dissimilar sizes of the two adsorbates, however, suggest that the amount of exposed molybdenum on the adsorbate covered surfaces is quite different (see Figure 3.5). Carbon's smaller size (atomic radius = 0.77 Å [20]) makes it possible for it to adsorb in a four-fold hollow

without extending above the top layer molybdenum atoms, while sulfur (atomic radius = 1.04 Å [20]), on the other hand, extends above the surface Mo atoms when adsorbed in a four-fold hollow. In fact, due to its larger size, a sulfur atom experiences repulsive interactions with neighboring sulfur atoms which force some sulfur atoms to occupy weaker binding sites at high coverages ($\theta_s \geq 0.67$ ML).

An experimental and theoretical study of CO chemisorption on sulfur, oxygen and carbon covered Fe(100) surfaces by Benziger and Madix indicates that sulfur attenuates the reactivity of the metal surface more than carbon because of its larger size [21]. Carbon and sulfur have similar electronegativities and should cause similar shifts in the Fermi level of the metal. The authors' calculations indicate that sulfur is a stronger poison for CO chemisorption because sulfur atoms sit high above the plane of the metal and therefore interact strongly with CO molecules (decreasing CO chemisorption). Carbon, however, sits in the plane of the surface, and CO interactions with carbon atoms are much less than with sulfur.

In an unrelated study, MacLaren and coworkers also found a relationship between the strength of catalyst poisoning by an adsorbate and its height above the substrate surface [22]. Using the change in the local density of states (LDOS) as a measure of catalyst poisoning, they found that adsorbed sulfur, which sits 1.3 Å above the metal plane, strongly poisons a Ni(100) catalyst while carbon, which sits just 0.1 Å above the top layer nickel atoms, only weakly affects the LDOS. However, if the height of the adsorbed carbon atoms above the nickel substrate is artificially increased to 1.3 Å, the same height as for sulfur, a dramatic increase in poisoning is observed. Both this study and the work of Benziger and Madix indicate that the tendancy for an adsorbate to poison a catalytic reaction is related to its height above the metal substrate on which it is adsorbed.

The difference in site blocking potential of sulfur and carbon is reflected in the

interactions of sulfur and carbon covered surfaces with thiophene and hydrogen. Kelly et al. showed that adsorbed sulfur on the Mo(100) surface blocks thiophene decomposition and that no molecular adsorption states other than the physisorbed state exist on this surface. Carbon adsorbed on the Mo(100) surface blocks thiophene decomposition as well, but this surface also has new molecular chemisorption states for thiophene [6]. Thiophene desorbs from the carbided Mo(100) surface at temperatures of 300 K and 360 K, well above the temperature of 170 K as observed on the sulfided Mo(100) surface.

Zaera and coworkers have investigated hydrogen chemisorption on the clean and sulfided Mo(100) surface [23]. They suggest that hydrogen adsorbs at bridge sites and find that dissociative adsorption of hydrogen is blocked at a sulfur coverage of 0.5 ML. At this coverage there are sulfur atoms adjacent to all of the bridge sites, suggesting that sulfur in four-fold hollows can block dissociative adsorption of hydrogen at bridge sites. Adsorbed carbon also blocks dissociative adsorption of hydrogen but total suppression does not occur until the carbon monolayer is complete [24]. These results show that the interaction of thiophene and hydrogen is greater on the carbided than the sulfided surfaces, suggesting that the carbided Mo(100) surface may be a better HDS catalyst.

4.6.5 Hydrogenation of Adsorbed Carbon and Sulfur on the Mo(100) Surface: The Effect of Hydrocarbons

Hydrogenation of adsorbed carbon on metal surfaces has been the subject of surface science investigation in the past. Carbon hydrogenation on the Pt(111) surface was studied by Davis and coworkers in our laboratory and Krebs and Bonzel investigated carbon hydrogenation on an iron foil [25,26]. For both the Pt

and Fe surfaces there are two stages of reaction: an initial stage in which adsorbed carbon is hydrogenated rapidly, followed by a second phase in which hydrogenation is much slower. This two stage behavior has been attributed to two kinds of carbon adsorbed on the surfaces: 1) carbidic carbon and 2) graphitic carbon. Both Davis and Krebs concluded that the former type of carbon is reactive and rapidly hydrogenated, while graphitic carbon is quite stable under the hydrogenation conditions investigated. In the case of the Mo(100) surface, hydrogenation of the ^{14}C overlayer does not show a clear break in the ^{14}C coverage versus reaction time curves which would suggest two kinds of carbon on the surface. This result is supported by AES studies which showed the adsorbed carbon to be carbidic in nature.

Introduction of butadiene into the hydrogen atmosphere has no effect on the rate of ^{14}C hydrogenation on the Mo(100) surface. Apparently, butadiene and the hydrogenated products (butenes, butane) do not alter the bonding of adsorbed carbon or significantly change the amount of adsorbed hydrogen available for ^{14}C hydrogenation. Thiophene, on the other hand, does influence the removal of adsorbed carbon from the surface. Including thiophene in the gas mixture decreases the rate and extent of ^{14}C removal from the crystal surface. Adsorbed thiophene may decrease the hydrogen coverage by blocking hydrogen dissociation sites or simply compete with the carbidic overlayer for available hydrogen on the surface. Previously published results from our laboratory indicate that the hydrogen coverage is low during thiophene HDS while the work reported here suggests that hydrogen saturates a carbon covered surface in a pure hydrogen atmosphere [9].

In contrast to the inhibitory effect of thiophene on the rate of ^{14}C removal, the radiotracer sulfur studies showed that thiophene enhanced ^{35}S removal by a factor of approximately 30 compared to a pure hydrogen atmosphere [4]. This

may be due to repulsive interactions between adsorbed thiophene molecules and ^{35}S atoms which decrease the Mo-^{35}S bond strength, making adsorbed sulfur more labile to hydrogenation. This effect would be expected for adsorbed sulfur which extends well above the metal surface and to a lesser extent for carbon which does not extend above the top layer Mo atoms. If weakening of the Mo-^{35}S bond by thiophene was responsible for the increased ^{35}S removal rate and the mechanism of ^{35}S removal was the same, then a lower activation energy would be expected for sulfur hydrogenation in the presence of thiophene. However, over a similar temperature range, the activation energy for sulfur removal was actually found to increase when thiophene was included in the gas mixture. The different kinetic parameters for ^{35}S removal in pure hydrogen and in the HDS gas mixture suggest that the mechanism of sulfur hydrogenation changes upon introduction of thiophene into the reaction mixture (see Section 4.3.2). The positive hydrogen partial pressure dependence of 0.34 for sulfur removal indicates that hydrogen does not saturate the sulfur covered Mo(100) surface for hydrogen pressures less than one atmosphere. Thiophene, or hydrocarbon intermediates, may increase the rate of ^{35}S removal by providing an additional source of hydrogen or by acting as a hydrogen transfer agent. Kinetic studies by Gellman have shown that the catalyst surface is saturated by partially hydrogenated intermediates of C_4H_7 and C_4H_9 stoichiometry [9]. If these species provide hydrogen for removal of ^{35}S from the molybdenum surface, then the zero order partial pressure dependencies of ^{35}S removal on hydrogen and thiophene can be understood. C_4H_7 and C_4H_9 intermediates have also been implicated as hydrogen sources for the hydrogenation of sulfur on the Pt(110) surface [27].

4.6.6 Deactivation of the Mo(100) Surface at High Conversions

Adsorbed sulfur on the clean and carbided Mo(100) surfaces has been shown to decrease the thiophene HDS activity of the catalysts by approximately one-half. This observation allows the following conclusions to be made. Bonding interactions between sulfur and the carbided surface stabilize the sulfur such that it is not hydrogenated from the surface during reaction. Sulfur atoms must occupy lower coordination sites on the carbided surface as carbon atoms are adsorbed in the four-fold hollows, yet the decreased catalyst activity indicates that the sulfur remains on the surface and blocks HDS sites. This excludes the possibility that adsorbed carbon keeps the Mo(100) surface active by blocking sulfur deposition into strong binding adsorption sites. Adsorption sites for sulfur exist on the carbon covered surface from which sulfur is not removed in the reaction conditions used. This allows us to conclusively rule out a thiophene desulfurization mechanism in which atomic sulfur is deposited into binding sites on the metal or carbide surface. It also allows us to rule out deposition of atomic sulfur onto the catalyst as the pathway by which catalyst deactivation occurs as the deactivation process has been found to be reversible; atomic sulfur does not desorb from the surface upon evacuation. Likewise, carbon deposition from thiophene decomposition is not involved in deactivating the catalyst as adsorbed carbon does not affect catalyst activity.

Deactivation of the Mo(100) surface is caused by reversible adsorption of molecular H_2S on the catalyst surface. Catalyst activity begins to fall after about 5 % conversion and complete deactivation occurs by a conversion of approximately 10 % under normal HDS conditions (P_{Th} = 3.0 Torr, P_{H_2} = 780 Torr, T = 613 K). This deactivation is reversible as catalyst activity can be restored to close to its initial

value by replacing the gases in the reactor with a fresh mixture of thiophene and hydrogen. The C_4 hydrocarbons produced during thiophene HDS do not compete with thiophene for adsorption sites as indicated by cis-2-butene having no effect on catalyst activity. Hydrogenation of butadiene and butenes apparently occurs on different sites than the desulfurization sites. The inhibitory effect of H_2S and the insignificant effect of butenes on thiophene HDS activity has been observed previously [12,28]. In both cases the catalysts employed were industrial cobalt molybdate catalysts. The similar effect of products on the activity of a Mo(100) single crystal and industrial HDS catalysts suggests that the active sites on the two catalysts are the same.

4.6.7 Nature of the Active Site for Thiophene HDS on Mo(100)

Consideration of the surface structure of the clean, carbided and sulfided Mo(100) surface along with the catalytic results described in this thesis allow us to draw some conclusions on the nature of the active site for thiophene HDS. Atomic sulfur on both the clean and carbon covered Mo(100) surface is strongly bound and blocks active HDS sites. However, in the hydrogenated state (H_2S), the bonding of sulfur to the catalyst surface is moderated and catalyst activity is maintained as H_2S desorbs from the surface following scission of the C-S bonds. The key feature to the thiophene HDS mechanism appears to be that the sulfur removed from thiophene is not present on the surface as atomic sulfur. These results allow us to rule out high symmetry metal sites, four-fold hollows and bridge sites, as the active sites for thiophene HDS as these sites dissociate H_2S and bind atomic sulfur very strongly to the metal surface. The active HDS site is proposed to be a mixed molybdenum-carbon site on which decomposition of H_2S to atomic

sulfur and hydrogen does not occur. The clean Mo(100) surface is too reactive to carry out the selective cleavage of only the C-S bonds of thiophene. Instead, indiscriminate bond breaking occurs on the clean surface leaving it covered with an overlayer composed primarily of adsorbed carbon. In the carbided state, the reactivity of the Mo(100) surface is moderated and the more gentle and desirable chemistry, C-S bond cleavage, supercedes thiophene decomposition as the major reaction pathway.

References

[1] A. J. Gellman. PhD thesis, University of California, Berkeley, 1985.

[2] M. E. Bussell, A. J. Gellman, and G. A. Somorjai. *J. Catal.* **110** (1988) 423.

[3] M. E. Bussell, A. J. Gellman, and G. A. Somorjai. *Catal. Lett.,* (submitted for publication) .

[4] A. J. Gellman, M. E. Bussell, and G. A. Somorjai. *J. Catal.* **107** (1987) 103.

[5] A. J. Gellman, M. H. Farias, M. Salmeron, and G. A. Somorjai. *Surf. Sci.* **136** (1984) 217.

[6] D. G. Kelly, M. Salmeron, and G. A. Somorjai. *Surf. Sci.* **175** (1986) 465.

[7] F. Zaera, E. B. Kollin, and J. L. Gland. *Surf. Sci.* **184** (1987) 75.

[8] M. E. Bussell and G. A. Somorjai. *J. Catal.* **106** (1987) 93.

[9] A. J. Gellman, D. Neiman, and G. A. Somorjai. *J. Catal.* **107** (1987) 92.

[10] C. B. Roxlo, M. Daage, A. F. Ruppert, and R. R. Chianelli. *J. Catal.* **100** (1986) 176.

[11] S. Kolboe. *Can. J. Chem.* **47** (1969) 352.

[12] C. N. Satterfield and G. W. Roberts. *AICHE J.* **14** (1968) 159.

[13] S. J. Tauster, T. A. Pecoraro, and R. R. Chianelli. *J. Catal.* **63** (1980) 515.

[14] M. H. Farias, A. J. Gellman, G. A. Somorjai, R. R. Chianelli, and K. S. Liang. *Surf. Sci.* **140** (1984) 181.

[15] A. J. Gellman, W. T. Tysoe, F. Zaera, and G. A. Somorjai. *Surf. Sci.* **191** (1987) 271.

[16] J. G. Lipsch and G. L. A. Schuit. *J. Catal.* **15** (1969) 179.

[17] R. J. Mikovsky, A. J. Silvestri, and H. Heinemann. *J. Catal.* **34** (1974) 324.

[18] K. F. McCarty and G. L. Schrader. *J. Catal.* **103** (1987) 261.

[19] C. G. Gachet, E. Dhainaut, L. de Mourges, Candy J. P., and P. Fouilloux. *Bull. Soc. Chim. Belg.* **90** (1981) 1279.

[20] R. Q. Barr. *Encylopedia of Chemical Technology.* Volume 15, J. Wiley and Sons, New York, 1981.

[21] J. B. Benziger and R. J. Madix. *Surf. Sci.* **94** (1980) 119.

[22] J. M. MacLaren, J. P. Pendry, and R. W. Joyner. *Surf. Sci.* **165** (1986) L80.

[23] F. Zaera, E. B. Kollin, and J. L. Gland. *Surf. Sci.* **166** (1986) L149.

[24] E. I. Ko and R. J. Madix. *Surf. Sci.* **109** (1981) 221.

[25] S. M. Davis, F. Zaera, B. E. Gordon, and G. A. Somorjai. *J. Catal.* **92** (1985) 240.

[26] H. J. Krebs and H. P. Bonzel. *Surf. Sci.* **99** (1980) 570.

[27] C.-M. Pradier, E. Margot, Y. Berthier, and J. Oudar. *Appl. Catal.* **31** (1987) 243.

[28] P. J. Owens and C. H. Amberg. *Adv. Chem. Ser.* **33** (1961) 182.

Chapter 5

Thiophene Hydrodesulfurization over Rhenium Surfaces

5.1 Introduction

The composition of hydrodesulfurization catalysts has changed little in the fifty years since the advent of the industrial HDS process despite the knowledge that many transition metal sulfides exhibit superior activity compared to MoS_2 and WS_2. This paradox is a result of the fact that molybdenum and tungsten sulfide are relatively inexpensive and have adequate HDS activities, therefore removing the incentive to develop new catalysts based on more active sulfides. However, the prospect of processing crude oil fractions of poorer quality in the coming years has recently generated interest in developing more active and resistant HDS catalysts.

As discussed in the introductory chapter, exploratory work by Chianelli, and more recently Ledoux, has shown that the HDS activity of the second and third row transition metal sulfides shows a volcano-like dependence upon the position of the metal in the periodic table [1,2]. However, in considering the results of these studies, it should be pointed out that it is very difficult to measure the "active" surface area of sulfide catalysts and, therefore, the turnover frequency. HDS studies by Tauster over MoS_2, for example, indicate that the HDS activity

of MoS_2 catalysts does not correlate with their BET surface areas but does vary linearly with their O_2 chemisorption capacities [3]. The relationship between O_2 chemisorption and the active HDS sites is not well understood, however, and the O_2 chemisorption studies have not been extended to other transition metal sulfides. In their work, Pecoraro and Chianelli also note that the HDS activities of the sulfides do not correlate with the their BET surface areas and instead normalize their HDS activities per millimole or gram of metal. It is far from obvious that either of these quantities accurately measures the active surface area of a catalyst. Ledoux and coworkers assume unit dispersion of the metal on the carbon support and that the dispersion remains constant during the presulfidation process. The similarity of the volcano type curves obtained in the two studies indicates that the relative trends in activity are most likely correct, but it is not clear that quantitative comparisons between the activites of different sulfides can be made. Without turnover frequencies, comparison of the activities of two catalysts cannot be made with confidence. The approach used in this thesis work, using metal single crystals as model HDS catalysts, has the distinct advantage of allowing the accurate measurement of the active surface area of the catalysts.

To determine the effect of periodic position on the surface chemistry of the HDS reaction, HDS studies parallel to those with molybdenum were undertaken using rhenium single crystal catalysts. Chianelli and Pecoraro found rhenium disulfide (ReS_2) to be about four times more active than MoS_2 while Ledoux and coworkers found ReS_2 supported on carbon to be about two times more active than MoS_2 on the same support [1,2]. Rhenium was chosen for this study because of the significantly higher activity of ReS_2 and because of the similarity in structure of the two sulfides. Both ReS_2 and MoS_2 have lamellar structures and it is expected that differences in their HDS activities are primarily due to electronic differences.

To this end, the HDS activities of four initially clean rhenium single crystals of different crystallographic orientation ((0001), $(10\bar{1}0)$, $(11\bar{2}0)$, $(11\bar{2}1)$) were measured and the effects of adsorbed overlayers of carbon and sulfur determined for the least active (Re(0001)) and most active (Re$(10\bar{1}0)$) surfaces. In addition, the kinetics and poisoning mechanisms of the thiophene HDS reaction have been investigated over a rhenium foil catalyst.

5.2 Thiophene HDS over Initially Clean Rhenium Surfaces

The thiophene HDS activities of four rhenium single crystals of different crystallographic orientation (see Figure 3.3) and a polycrystalline foil are compared in Figure 5.1. The HDS of thiophene is a structure sensitive reaction over rhenium with a six-fold variation in activity for the single crystal surfaces studied. Typical product accumulation curves for thiophene HDS over the Re(0001) surface are shown in Figure 5.2. The product distribution obtained from thiophene HDS over a Re(0001) single crystal is shown in Table 5.1 and is similar to the distributions observed for the other rhenium surfaces. Small amounts of C_1 to C_3 hydrocarbons were produced by hydrogenolysis but their contribution to the product distribution was always less than 5 %.

Following a 90 min. reaction and evacuation of the reaction cell, AES showed the single crystal catalysts to be covered with substantial quantities of sulfur (Re(0001): $\theta_s = 0.5$, Re$(10\bar{1}0)$: $\theta_s = 0.7$) but only small amounts of adsorbed carbon. However, this sulfur probably adsorbs during evacuation of the high pressure cell as the high activity of the catalysts after 90 min. of reaction indicates that they are not covered with irreversibly bound sulfur. The temperature dependence of the total thiophene HDS activity was measured for a Re$(10\bar{1}0)$ single

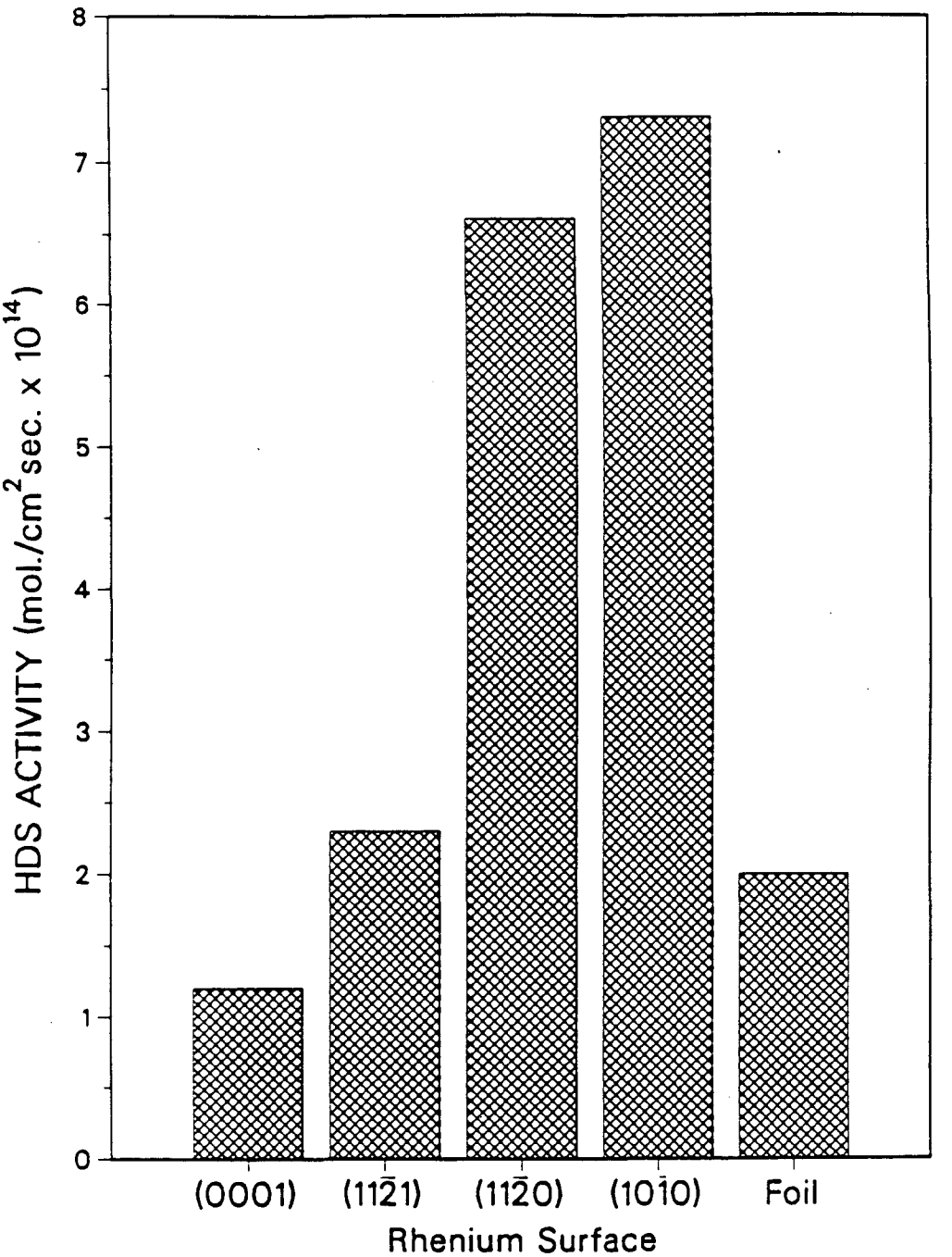

-- XBL 884-1380 --

Figure 5.1: Thiophene HDS activities of four low miller index planes of rhenium and a polycrystalline rhenium foil (P_{Th} = 3.0 Torr, P_{H_2} = 780 Torr, T = 613 K).

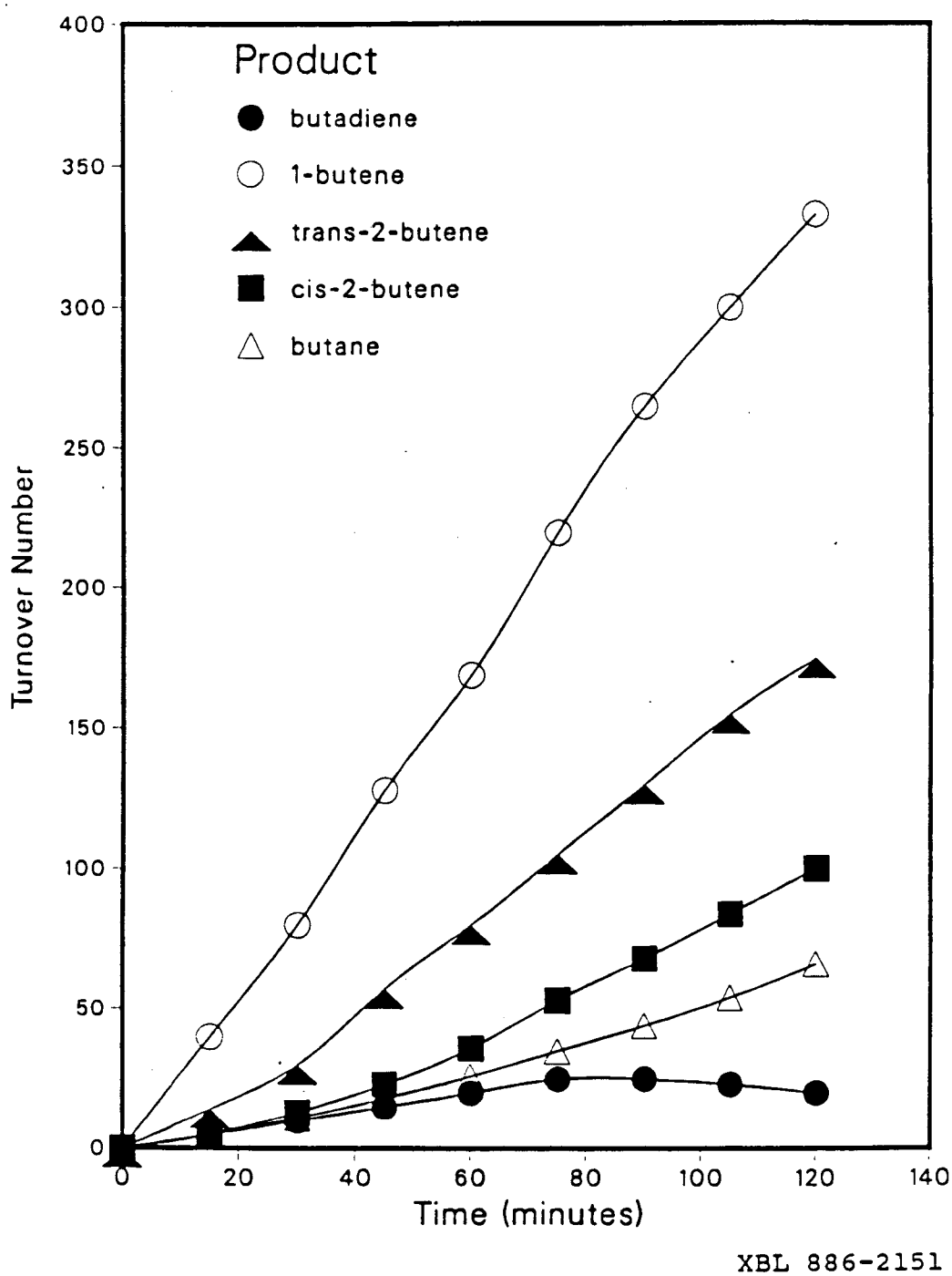

Figure 5.2: Product accumulation curves for thiophene HDS over the Re(0001) surface (P_{Th} = 3.0 Torr, P_{H_2} = 780 Torr, T = 613 K).

Table 5.1: Product Distributions for Thiophene HDS and Butadiene Hydrogenation.

Product	*Fractional Yield (%)*		
	Thiophene HDS		*Butadiene + H_2*
	[a]*Re(0001)*	[a]*Mo(100)*	[b]*Re Film*
Butadiene	4.4	5.6	—
1-Butene	49.7	52.8	49
trans-2-Butene	23.5	19.4	31
cis-2-Butene	13.9	13.9	11
Butane	4.4	8.1	9

[a](P_{Th} = 3.0 Torr, P_{H_2} = 780 Torr, T = 613 K)
[b](P_B = 5.0 Torr, P_{H_2} = 10. Torr, T = 423 K) [4]

crystal and a polycrystalline foil over the temperature range from 493-653 K and the data is plotted in Figure 5.3. Identical activation energies of 9.4 kcal/mole were measured for these two rhenium surfaces. The temperature dependence data is plotted for the products individually in Figure 5.4. Cis- and trans-2-butene exhibit similar temperature dependence behavior to 1-butene and are therefore not included in the figure. As can be seen from the 1-butene curve, butene production shows a negative deviation from Arrhenius behavior for temperatures $\geq$ 673 K. The butenes comprise 87 % of the total products, so the overall thiophene HDS rate shows concomitant non-linearity for temperatures of 673 K and above.

AES analysis of the Re foil surface after reactions at temperatures above 673 K shows the catalyst surface to be covered with an overlayer of graphitic carbon. The dependence of the HDS activity of a Re foil on the partial pressures of thiophene and hydrogen was determined and the data is shown in Figures 5.5 and 5.6. The HDS rate is one-half order in thiophene and first order in hydrogen over the pressure ranges studied. The thiophene and hydrogen partial pressure dependencies of the individual products are displayed in Figures 5.7 and 5.8.

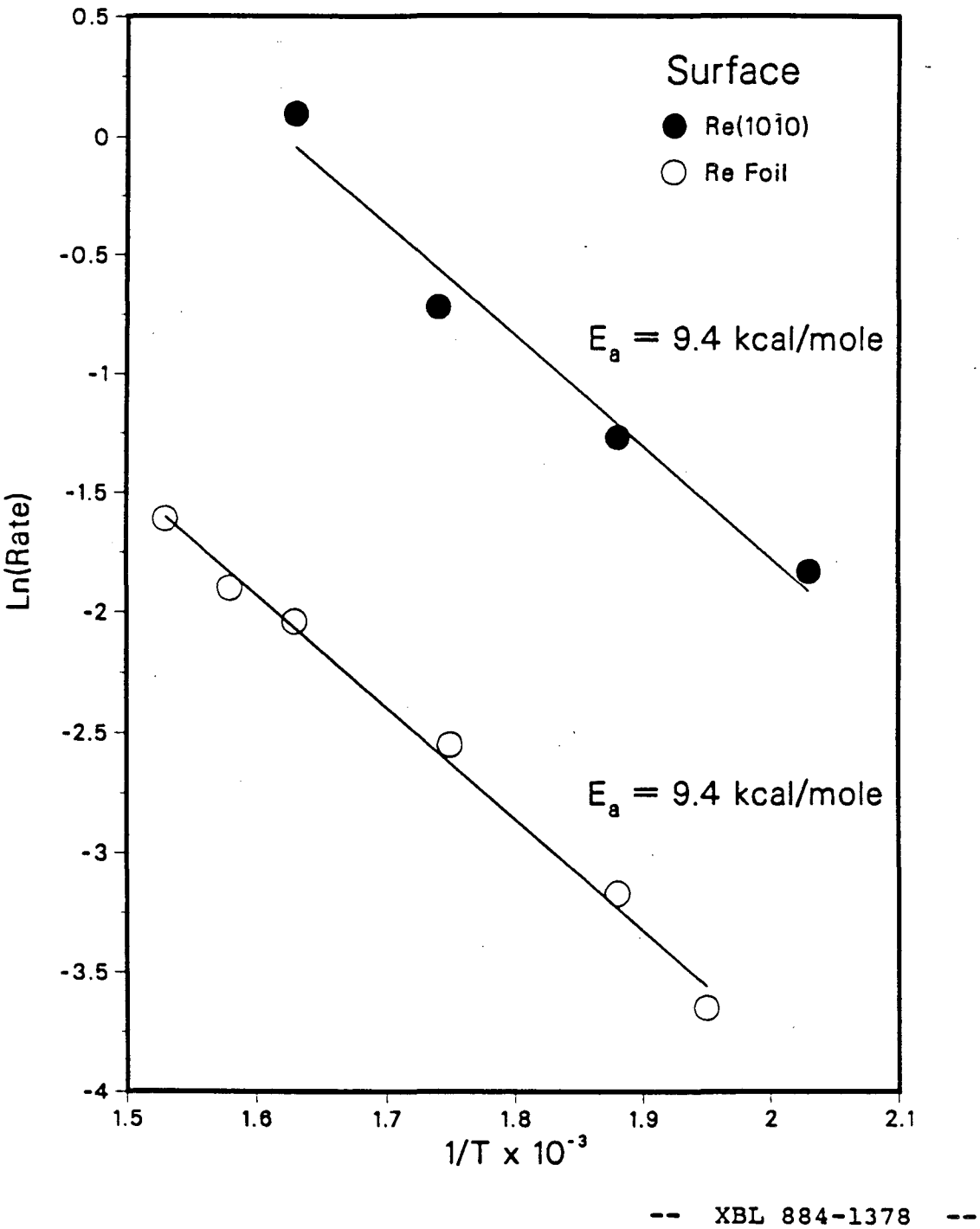

Figure 5.3: Temperature dependence of Thiophene HDS over Re(0001) and a polycrystalline Re foil ($P_{Th} \doteq 3.0$ Torr, $P_{H_2} = 780$ Torr).

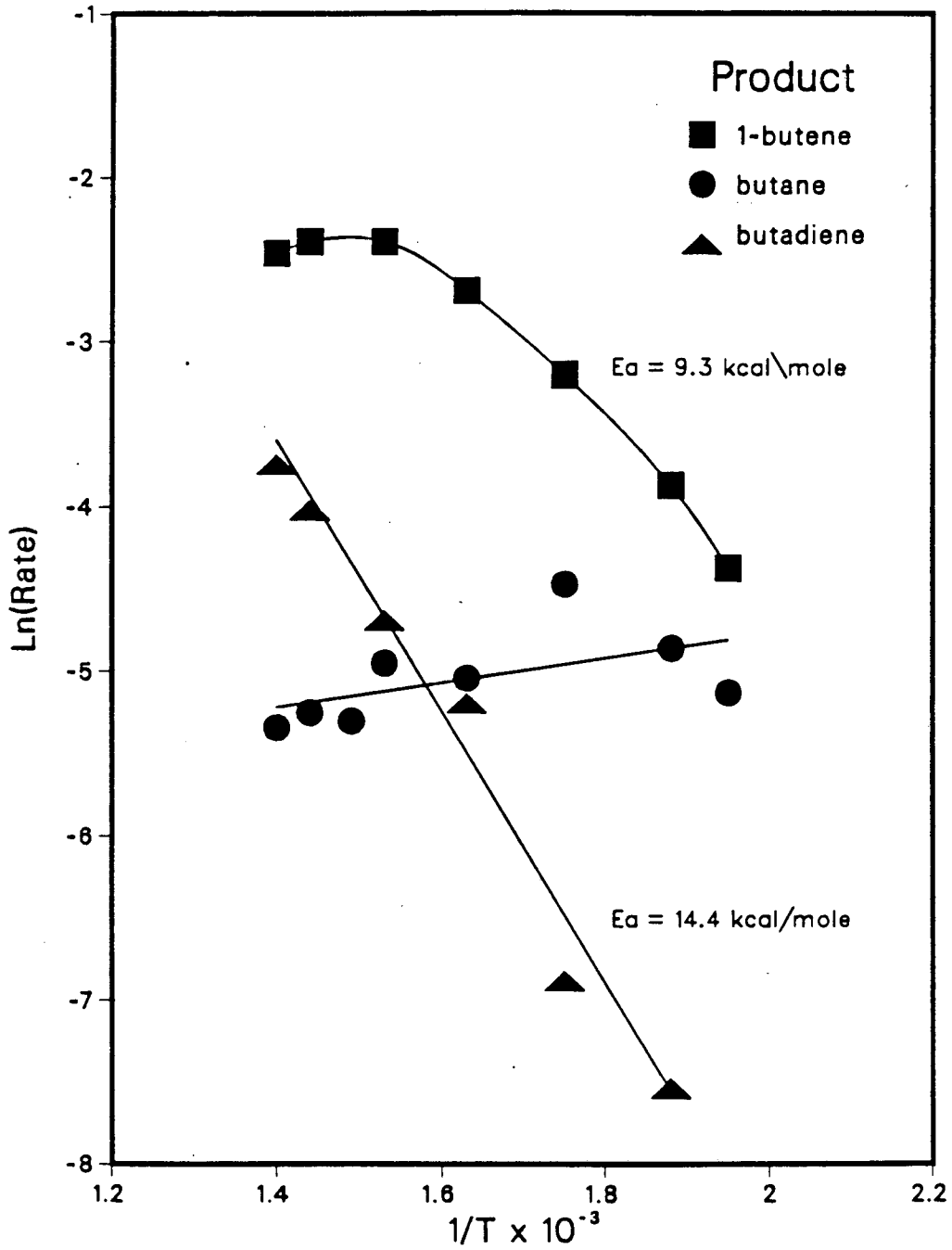

Figure 5.4: Temperature dependence of Thiophene HDS over a Re Foil for the products individually (P_{Th} = 3.0 Torr, P_{H_2} = 780 Torr).

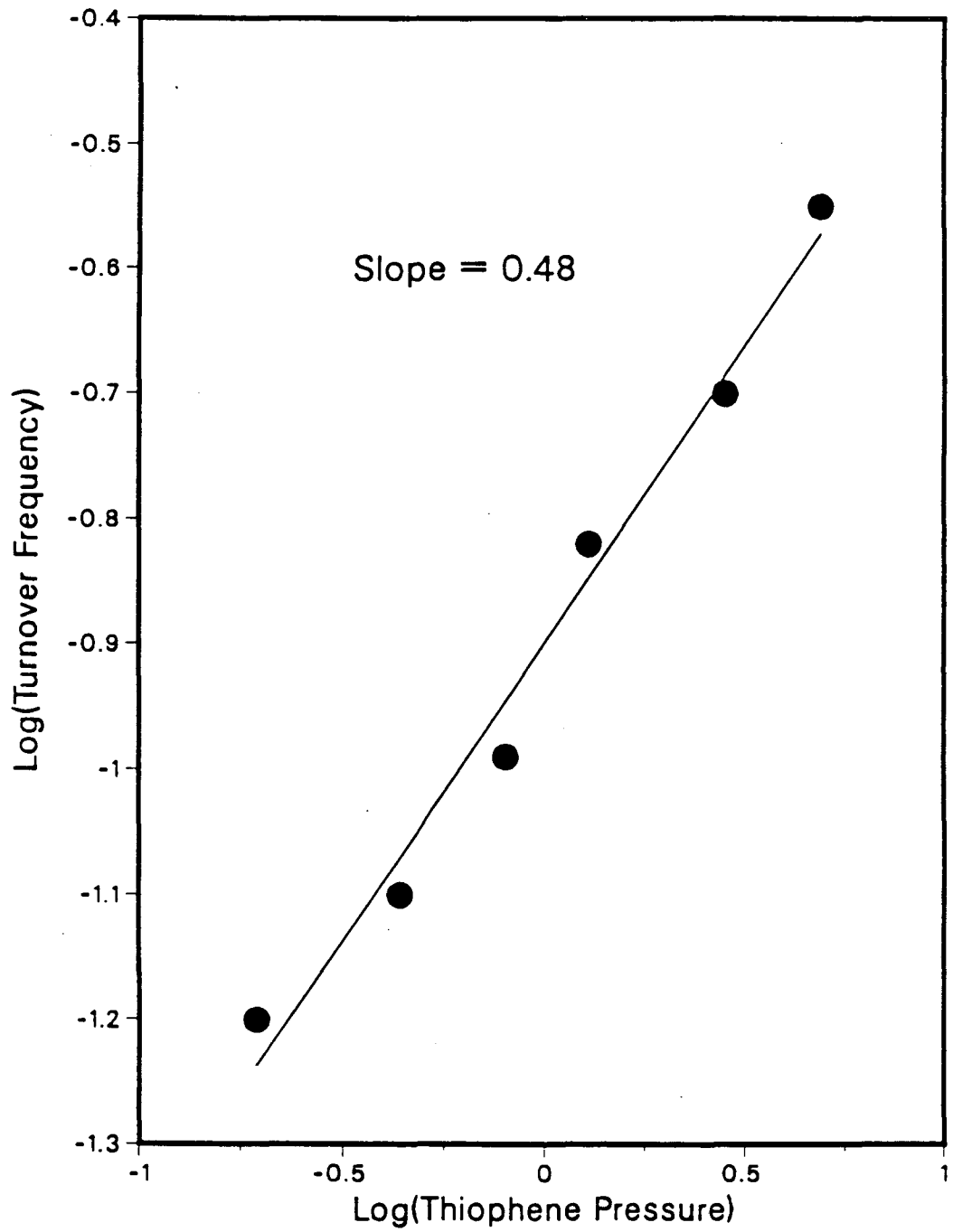

Figure 5.5: Thiophene partial pressure dependence of HDS over a Re foil (P_{H_2} = 780 Torr, T = 613 K).

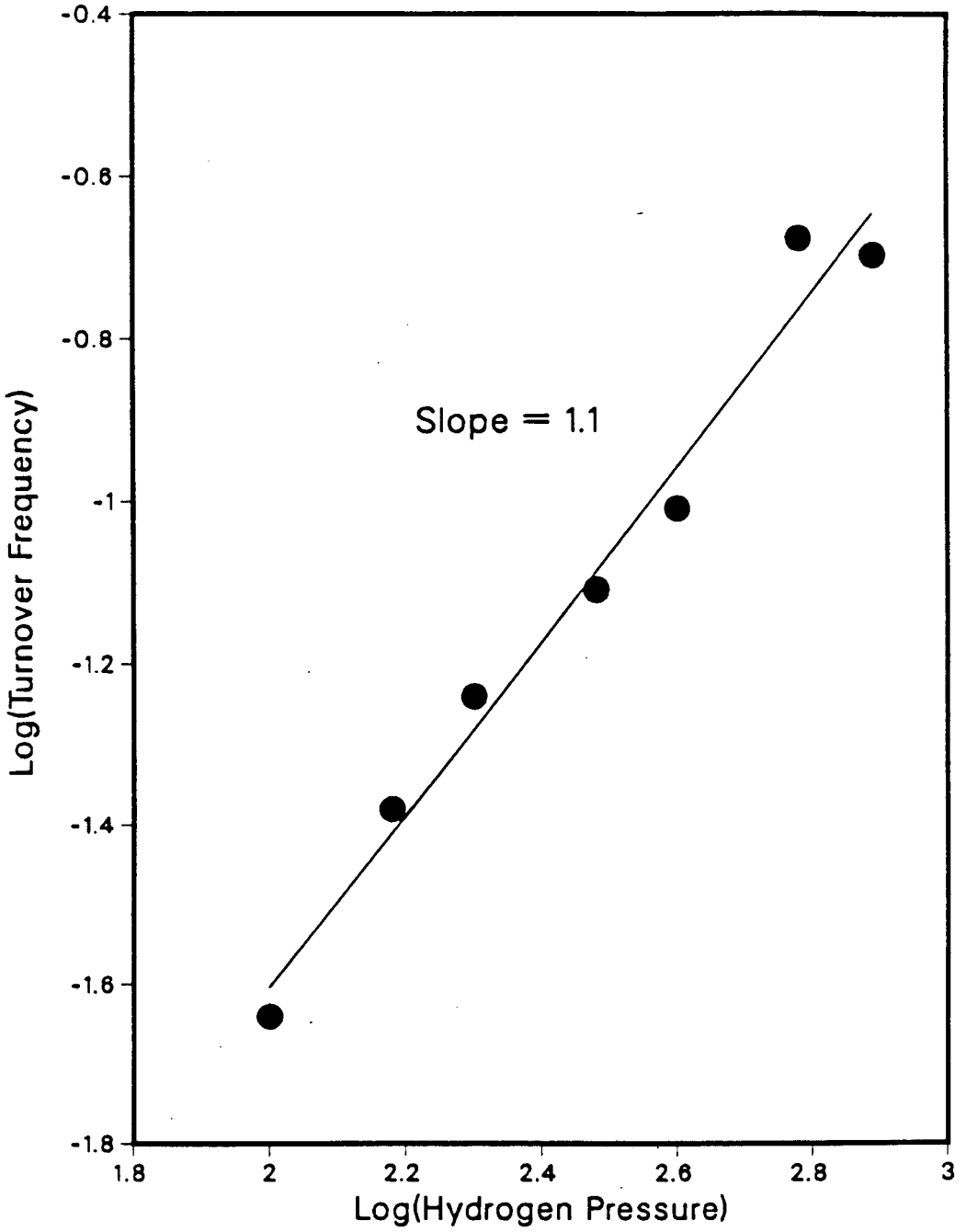

Figure 5.6: Hydrogen partial pressure dependence of HDS over a Re foil (P_{Th} = 3.0 Torr, T = 613 K).

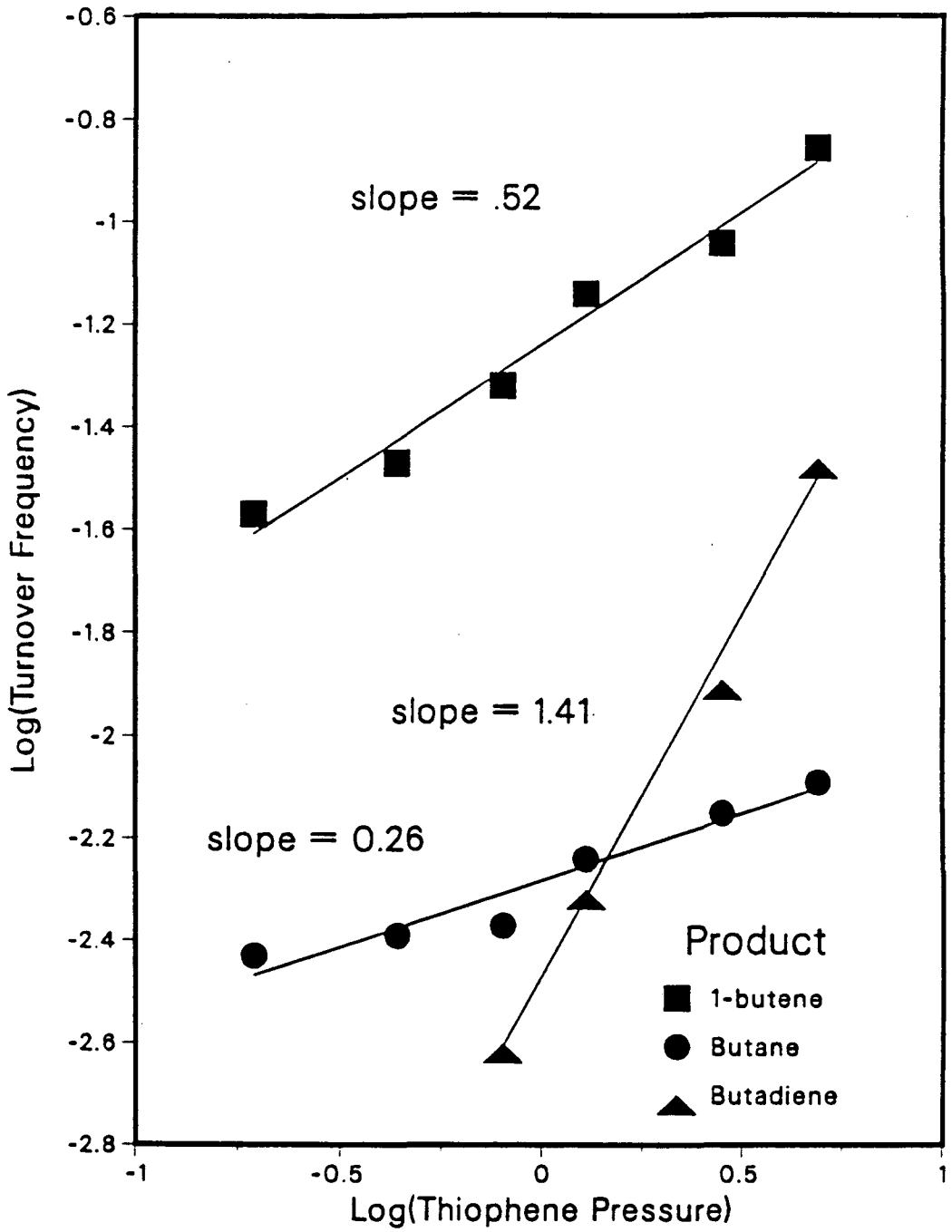

Figure 5.7: Thiophene partial pressure dependence of HDS over a Re foil for the individual products (P_{H_2} = 780 Torr, T = 613 K).

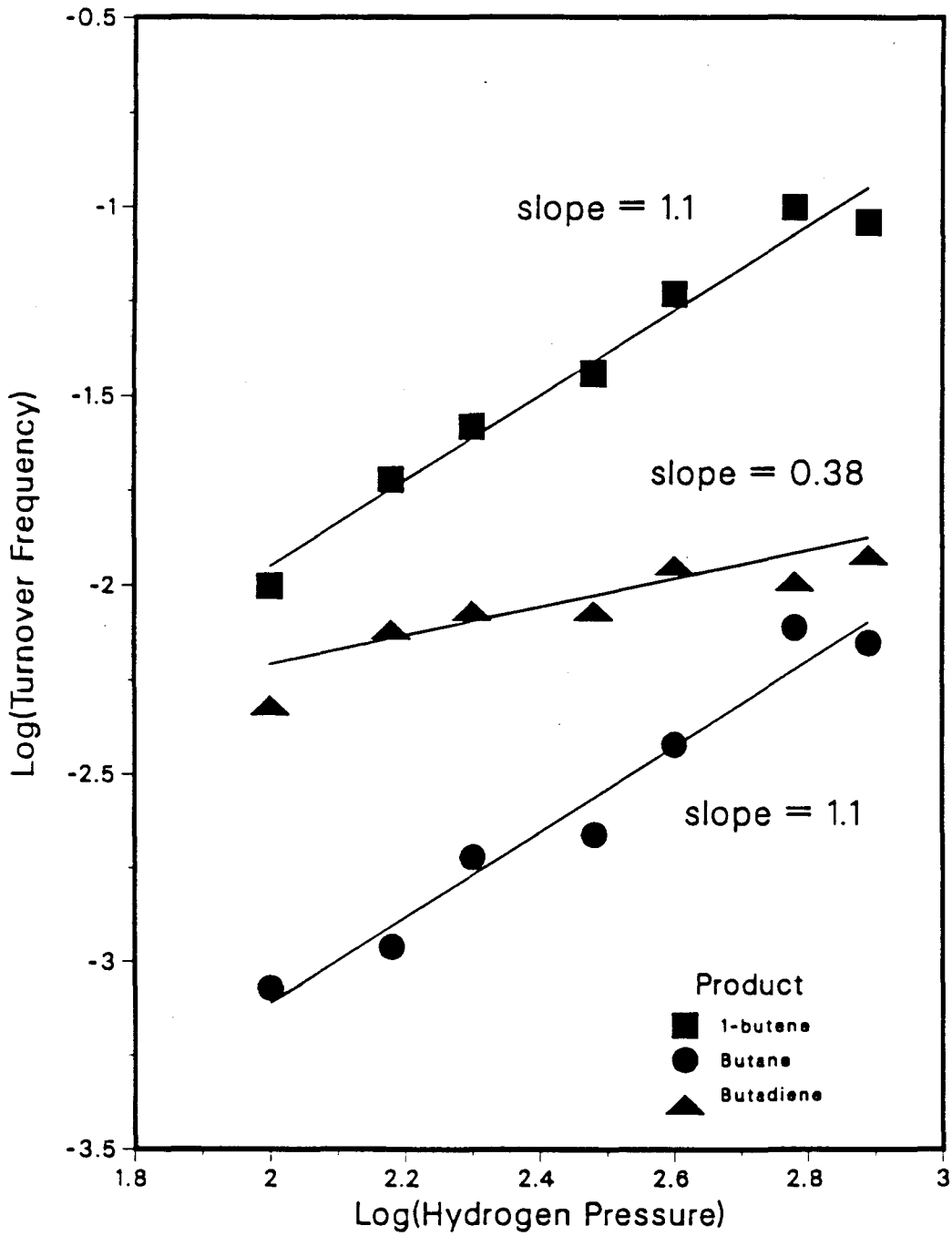

Figure 5.8: Hydrogen partial pressure dependence of HDS over a Re foil for the individual products (P_{Th} = 3.0 Torr, T = 613 K).

5.3 Thiophene HDS over Sulfided Rhenium Single Crystal Surfaces

In Figures 5.9 and 5.10, the effects of adsorbed carbon and sulfur on the HDS activity of the least active (Re(0001)) and most active (Re(10$\bar{1}$0)) of those rhenium surfaces studied are shown. Adsorbed sulfur decreases the activity of both single crystal surfaces compared to the initially clean single crystals. The activity of the (0001) face is markedly decreased at low sulfur coverages ($\theta_s \leq 0.25$), while additional sulfur is a much weaker poison of HDS activity. At a sulfur coverage of 0.5 ML (close to the saturation coverage of 0.6-0.7 ML), the HDS activity is about 70 % of that of the initially clean surface. On the more active Re(10$\bar{1}$0) surface, adsorbed sulfur is a stronger poison; at a sulfur coverage of 0.75 ML, the HDS activity is about 40 % of the initially clean surface value. As with the Re(0001) surface, adsorbed sulfur at high coverages ($\theta_s > 0.6$) is a weaker poison of active HDS sites.

5.4 Thiophene HDS over Carbon Covered Rhenium Single Crystal Surfaces

As shown in Figures 5.9 and 5.10, adsorbed carbon on the Re(0001) and Re(10$\bar{1}$0) single crystal surfaces markedly decreases their HDS activity. Indeed, carbon is a stronger poison than sulfur. In contrast to the non-linear decrease in HDS activity caused by increasing coverages of adsorbed sulfur on these surfaces, the decrease in activity induced by carbon is linear as a function of coverage and the curves tend to zero activity at the full monolayer coverage. These results indicate that each adsorbed carbon atom blocks an active HDS site on the catalysts for all coverages, while this is true for adsorbed sulfur only at low coverages. As discussed in Chap-

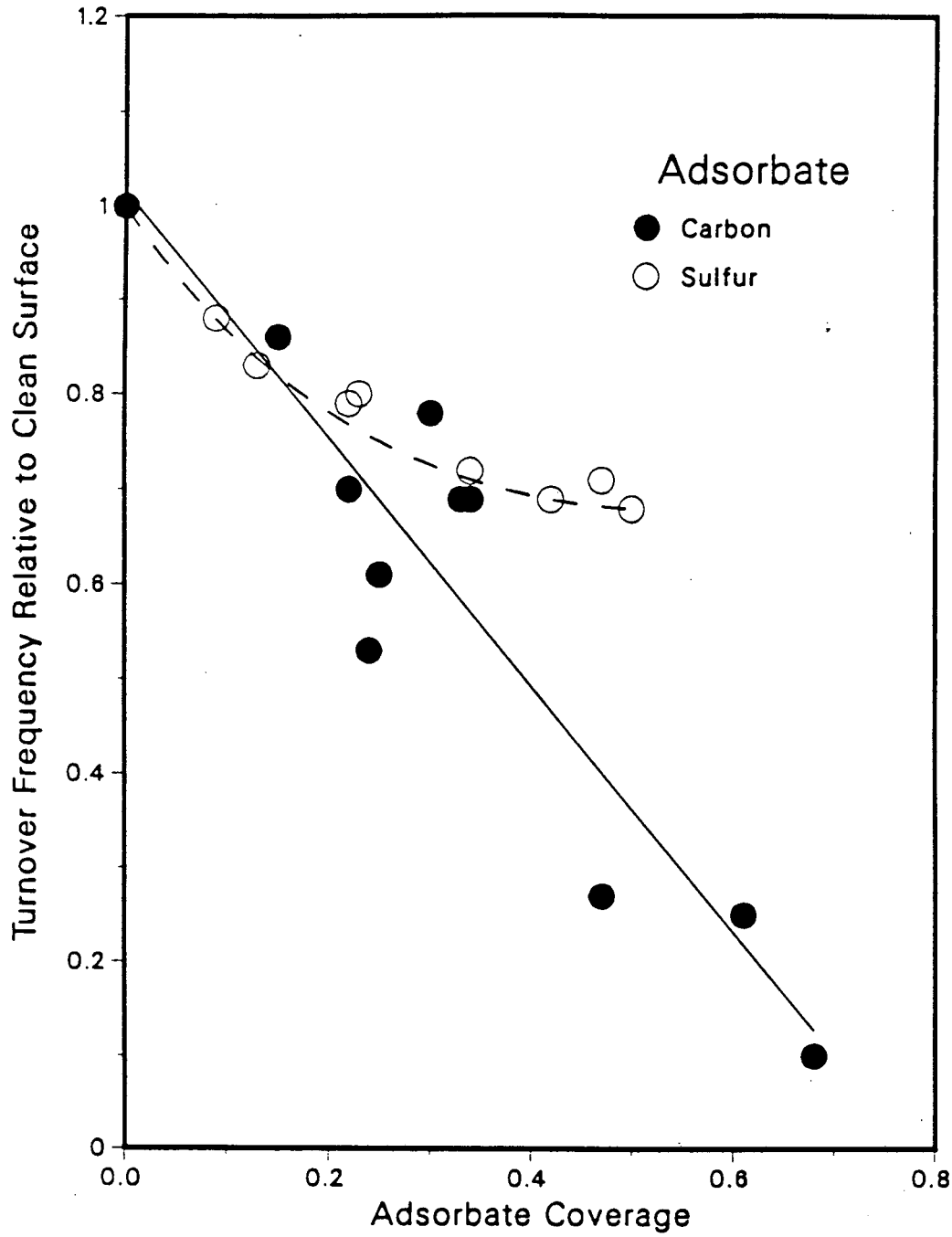

- XBL 8712-5348 -

Figure 5.9: Thiophene HDS activity of a Re(0001) single crystal as a function of the initial sulfur (o) and carbon (•) coverage (P_{Th} = 3.0 Torr, P_{H_2} = 780 Torr, T = 613 K).

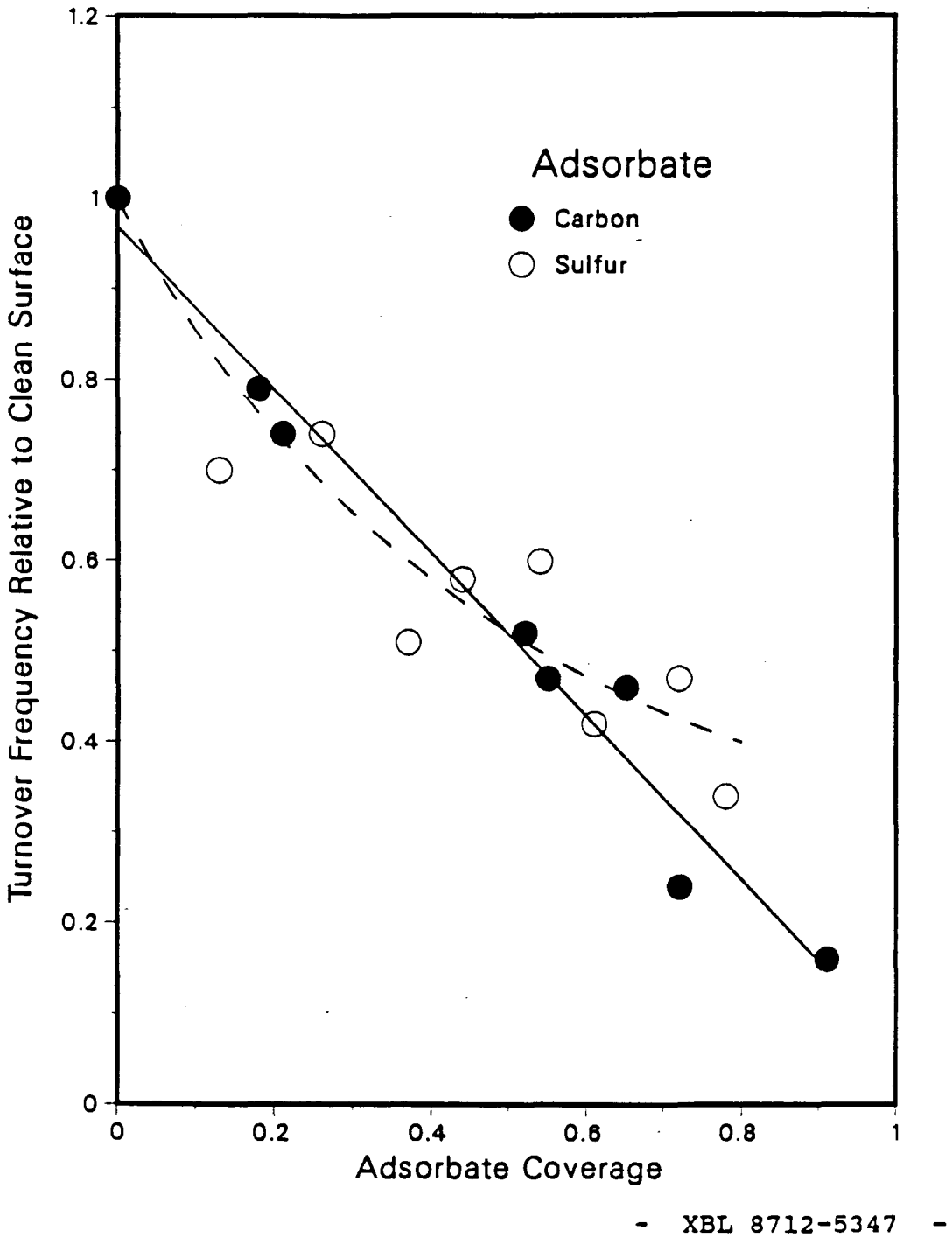

Figure 5.10: Thiophene HDS activity of a Re(10$\bar{1}$0) single crystal as a function of the initial sulfur (o) and carbon (•) coverage (P_{Th} = 3.0 Torr, P_{H_2} = 780 Torr, T = 613 K).

ter 3, the structure and bonding of adsorbed carbon overlayers on transition metal surfaces has been shown to change as a function of temperature [5]. Figures 3.12 and 3.13 show the carbon AES peak shapes for different annealing temperatures of ethylene overlayers on the Re(0001) and Re(10$\bar{1}$0) surfaces. The AES spectra indicate that for annealing temperatures below 900 K, the carbonaceous overlayers are graphite-like while for annealing temperatures greater than 900 K, adsorbed carbon appears to be more carbidic in nature on the two rhenium surfaces. In order to determine whether the form of the adsorbed carbon overlayers affects the HDS activity of the Re(0001) and Re(10$\bar{1}$0) surfaces, reactions were carried out over carbon covered surfaces annealed to 800 K and 1100 K in UHV prior to enclosure in the high pressure cell. The HDS activities of the clean Re(0001) surface and carbon covered Re(0001) surfaces annealed to the two different temperatures are shown in Figure 5.11. For both this and the (10$\bar{1}$0) single crystal surface, the annealing temperature of the carbon overlayers had no effect on the HDS activity of the catalysts. Hence, the initial state of the carbon does not appear to be important for the rhenium surfaces studied.

5.5 The Influence of Products (H_2S, cis-2-butene) on the HDS Activity of a Rhenium Foil

The deactivation of the model rhenium HDS catalysts was studied by carrying out extended HDS reactions over a rhenium foil. The HDS activity of the polycrystalline Re foil was found to remain constant for the first three hours of reaction but then to decline steadily with complete deactivation occurring after 9-12 hours (corresponding to 10-15 % total conversion). The role of product poisoning in deactivation of the Re foil was examined by including hydrogen sulfide and cis-2-butene in the initial reaction mixture at partial pressures corresponding to 5-15 %

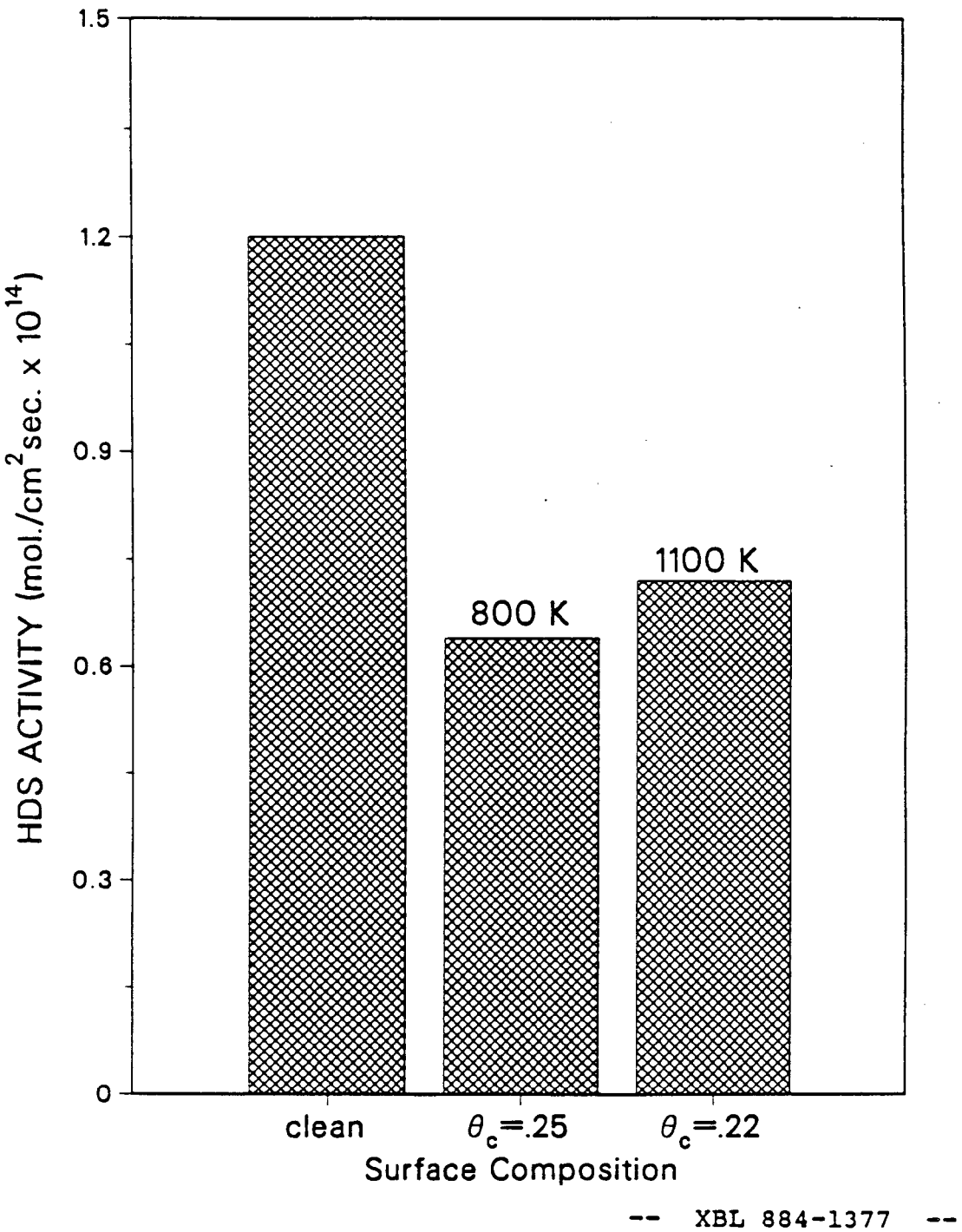

Figure 5.11: Thiophene HDS activity for the initially clean Re(0001) surface and for carbon covered surfaces annealed in UHV to 800 K and 1100 K prior to reaction (P_{Th} = 3.0 Torr, P_{H_2} = 780 Torr, T = 613 K).

thiophene conversion. Cis-2-butene had no effect on the activity of a rhenium polycrystalline foil while H_2S strongly decreased the activity of the catalyst as shown in Figure 5.12. Following the reaction in which 600 mTorr was included in the HDS mixture, the reaction loop was evacuated and then repressurized with a fresh mixture of thiophene and hydrogen. The HDS activity increased from 0.021 mol./site·sec to 0.11 mol./site·sec. This latter activity is close to the value of 0.13 mol/site·sec measured for an initially clean Re foil.

5.6 Discussion

Rhenium single crystals and polycrystalline foils have been found to be active catalysts for the hydrodesulfurization of thiophene. The most important results of this work are the following:

I. Rhenium is a more active HDS catalyst than molybdenum, in agreement with previous studies using sulfide catalysts [1,2].

II. Adsorbed sulfur and carbon overlayers decrease the activity of rhenium single crystal catalysts toward thiophene HDS.

III. Thiophene HDS is a structure sensitive reaction over rhenium single crystals.

5.6.1 Thiophene HDS over Initially Clean Rhenium Surfaces

The lack of reliable techniques for the measurement of catalyst surface areas which can distinguish between active and inactive adsorption sites on metal sulfide catalysts has hampered the ability of researchers to compare reaction rates of different

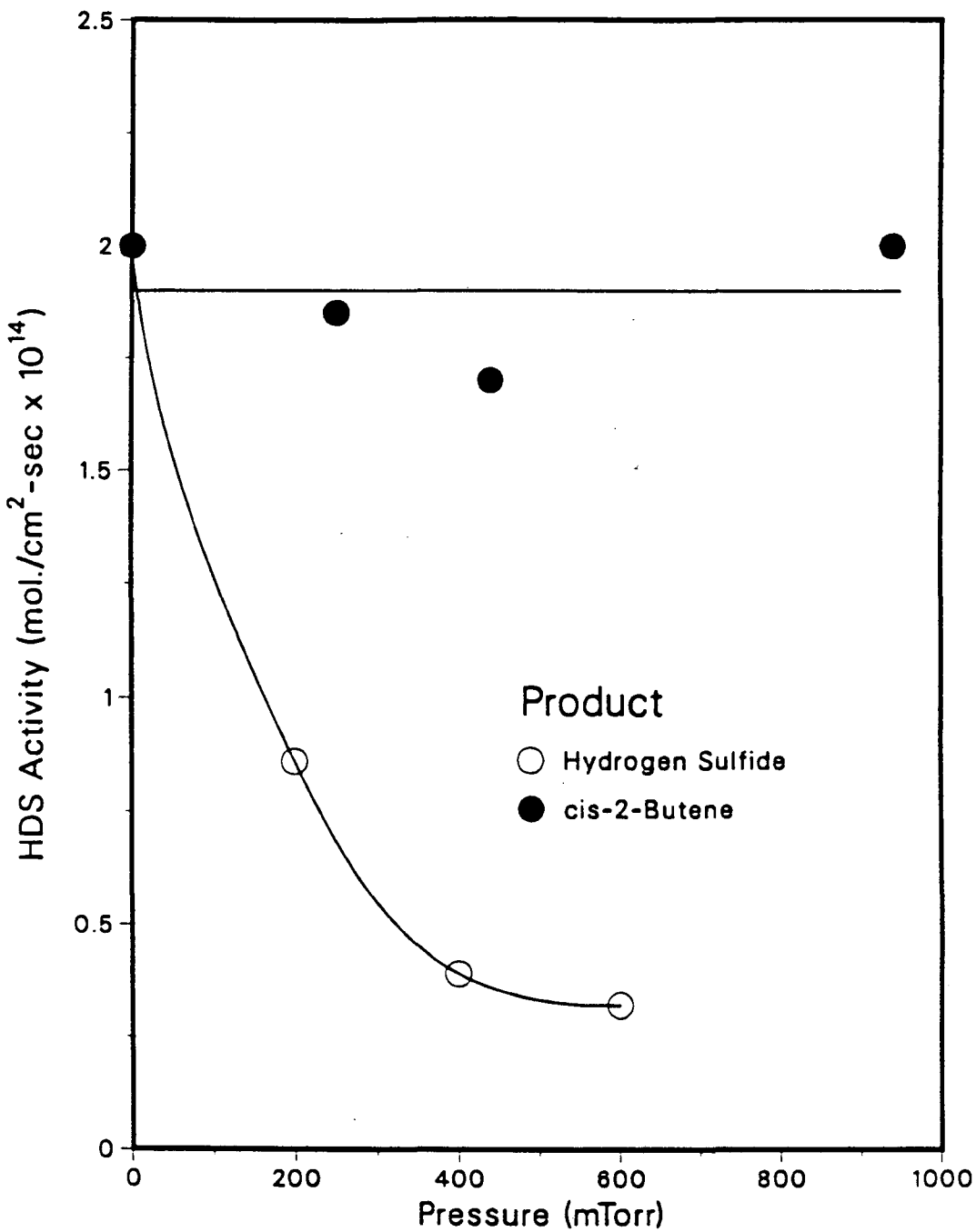

-- XBL 884-1379 --

Figure 5.12: HDS activity of an initially clean Re foil as a function of the partial pressure of product (H_2S or cis-2-butene) in the gas mixture (P_{Th} = 3.0 Torr, P_{H_2} = 780 Torr, T = 613 K).

catalysts with confidence. The use of single crystals as catalysts allows one to measure the turnover frequencies of catalysts per unit area of the active metal, and therefore facilitates direct comparison of activities for different transition metal catalysts. The results of this study, in conjunction with previous work in our laboratory, show that rhenium single crystal catalysts are up to six times more active for thiophene HDS than molybdenum single crystals, depending on the crystallographic orientation of the rhenium single crystals [6,7,8]. This difference in HDS activities is similar to that measured for unsupported as well as supported molybdenum and rhenium disulfide catalysts (see Section 5.1). The similarity of these results is significant because it indicates that the HDS activities measured in the studies described above are suitably normalized to reflect the activity per unit of active surface area and most importantly that metal single crystals can indeed be used as model catalysts to study the surface chemistry of the hydrodesulfurization process.

The product distribution obtained for thiophene HDS over the rhenium catalysts, shown in Table 5.1 for Re(0001), was found to be independent of the crystallographic orientation of the rhenium surface. This indicates that the reaction mechanism is the same, despite differences in the surface structure of the catalysts. It might have been expected that different adsorption geometries of thiophene on surfaces of dissimilar structure would lead to different reaction mechanisms. Based upon our results, however, this does not appear to be the case. Similar behavior has been observed by Lang and Masel on Pt surfaces [9]. They investigated the desulfurization of thiophene in UHV on the Pt(100), Pt(111) and Pt(210) surfaces using TPD, EELS and XPS and found the desulfurization of thiophene to be identical on the three surfaces. Thiophene adsorbs in a parallel configuration at 170 K, but assumes a tilted geometry at higher temperatures due to the developing Pt-S

bond. Desulfurization is complete by 350 K, leaving a tilted butadiene-like species on the platinum surfaces.

The temperature dependence studies of thiophene HDS over the Re(10$\bar{1}$0) surface and a polycrystalline rhenium foil also support the conclusion that the reaction mechanism is the same over the different Re surfaces (i.e. the mechanism is insensitive to the catalyst surface structure). Identical activation energies of 9.4 kcal/mole were measured for the two surfaces. A Re foil has been shown to consist primarily of crystallites of the thermodynamically most stable (0001) face following high temperature annealing [10]. The low HDS activity of the rhenium foil indicates that this is the case. The similarity of the activation energies over a Re(10$\bar{1}$0) single crystal and a rhenium foil provides further evidence that the reaction mechanism is the same over the different rhenium surfaces.

5.6.2 Effect of Adsorbed Sulfur on HDS Activity

Overlayers of sulfur adsorbed on the Re(0001) and Re(10$\bar{1}$0) single crystal surfaces decrease the thiophene HDS activity of the catalysts. As discussed in Chapter 1, Kelly et al. have investigated the UHV chemisorption of thiophene on the clean and sulfided Re(0001) and Mo(100) surfaces using temperature programmed desorption (TPD) [11,12]. On the clean single crystal surfaces, the major reaction pathway for adsorbed thiophene is decomposition to yield adsorbed carbon, sulfur and hydrogen, with the latter desorbing into the vacuum as H_2. Adsorbed sulfur on these surfaces was found to decrease their reactivity towards thiophene decomposition; as the coverage of sulfur is increased, the fraction of adsorbed thiophene that decomposes on the surface decreases. Instead, thiophene interacts very weakly with the sulfur covered surfaces and desorbs at temperatures below 200 K, indicative of physisorption. Clearly, the addition of sulfur to the Re(0001)

and Mo(100) single crystal surfaces weakens their interaction with thiophene in the UHV environment to the extent that thiophene desorption is favored over bond cleavage. Our catalytic results also indicate that adsorbed sulfur weakens the interaction between thiophene and the single crystal surfaces. Adsorbed sulfur blocks active HDS sites on the rhenium surfaces and as a result, the HDS activities of the sulfur covered surfaces are lower.

The poisoning effect of sulfur is not transient but instead remains constant for the entire reaction, strongly suggesting that the sulfur overlayer is stable under reaction conditions. However, sulfur adsorbed at low coverages (Re(0001): $\theta_s \leq 0.25$, Re(10$\bar{1}$0): $\theta_s \leq 0.6$) appears to be better able to block active sites than the additional sulfur present at higher coverages. This suggests that the high coverage sulfur is more readily removed from the catalyst surface under reaction conditions. This data can be usefully compared with the effect of pre-adsorbed sulfur on the HDS behavior of Mo(100) surfaces. As discussed in the previous Chapter, sulfur adsorbed on the Mo(100) surface at coverages above 0.67 ML is bound more weakly than sulfur at lower coverages. Apparently, the high coverage sulfur does not decrease the HDS activity of the Mo(100) surface because it is removed from the catalyst surface under reaction conditions. TPD studies of sulfur adsorbed on the Re(0001) and Re(10$\bar{1}$0) surfaces and our catalytic results indicate similar phenomena for these surfaces as for the Mo(100) surface [13]. On the Re(0001) surface, adsorbed sulfur at low coverages ($\theta_s \leq 0.25$) desorbs in a single peak at 1600 K. As the coverage is increased, low temperature shoulders appear in the TPD spectrum at 1400 K ($\theta_s > 0.3$) and 900 K ($\theta_s > 0.5$). On the more open Re(10$\bar{1}$0) surface, sulfur desorbs at 1700 K at low coverages ($\theta_s \leq 0.5$), and a low temperature shoulder at 1500-1600 K appears above 0.5 ML. The coverages at which sulfur begins to populate the more weakly bonding adsorption sites corre-

spond approximately to the coverages above which the effectiveness of additional adsorbed sulfur in poisoning the HDS reaction on Re surfaces is decreased. As mentioned above, this is consistent with previous results on the Mo(100) surface for which the coverage at which a low temperature shoulder appeared in the TPD spectrum coincided with the coverage above which additional sulfur did not affect the HDS activity.

It is important to note that during HDS reactions over the rhenium single crystal catalysts, sulfur is not deposited into the strong binding sites populated when sulfur is pre-adsorbed on the single crystals in UHV. Sulfur bonded in these adsorption sites lowers the HDS activity of the catalyst, while the initially clean single crystals maintain high catalytic activities for up to three hours. Well over 1000 thiophene molecules are desulfurized per surface rhenium atom in three hours; yet if sulfur was deposited in these strong binding sites during reaction, the surface would become covered with sulfur in a few seconds and the HDS activity would fall to that of a sulfur covered surface. The high catalyst activities of the initially clean single crystals indicate that this is not the case. The results suggest, as was the case with the Mo(100) surface, that the thiophene HDS mechanism does not include a step in which the C-S bonds are cleaved to give a hydrocarbon and a sulfur atom directly bonded to the metal surface [14].

5.6.3 Effect of Adsorbed Carbon on HDS Activity

Overlayers of adsorbed carbon on the Re(0001) and Re($10\bar{1}0$) surfaces strongly decrease the HDS activity of the single crystal catalysts. As discussed in Section 3.2, the linearity of the plots of HDS activity versus carbon coverage indicate that each adsorbed carbon atom blocks an active HDS site on the catalyst surfaces. These results are distinctly different from those for the the Mo(100) surface; adsorbed

carbon had no effect on the HDS activity of this surface [15]. The form of the adsorbed carbon overlayers on the Mo and Re surfaces was investigated using Auger electron spectroscopy. On the Mo(100) surface, carbon overlayers produced by adsorption of ethylene and heating to T $\geq$ 500 K give AES line shapes characteristic of a metal carbide (see Figure 3.7). Carbon atoms are adsorbed in four-fold hollow sites and penetrate into the surface such that they extend less than 0.6 Å above the metal surface [16,17]. For the Re(0001) and Re(10$\bar{1}$0) surfaces, carbon overlayers formed in the same manner and annealed at temperatures < 900 K give AES line shapes which resemble those of graphite and amorphous carbon (see Figures 3.12 and 3.13). For a graphitic or amorphous carbon overlayer, the interaction between the overlayer and the metal substrate is considerably weaker than for a carbidic overlayer, as strong bonds are formed between neighboring carbon atoms and not with metal atoms in the substrate. This is reflected in the increased height of the carbon overlayer above the metal plane. Using surface extended energy loss fine structure spectroscopy (SEELFS), Rosei et al. determined that a graphitic overlayer sits 2.8 $\pm$ 0.08 Å above the Ni(111) surface [18]. The Re(0001) face is also a close packed surface and the Re(10$\bar{1}$0) has only a weak corrugation, so it is expected that a graphitic or amorphous carbon overlayer would extend well above these surfaces as well.

The differences in the structure of the carbon overlayers on the Mo(100) and Re(0001) surfaces are reflected in how they influence thiophene chemisorption. As mentioned earlier, adsorbed carbon on the Mo(100) surface blocks thiophene decomposition and creates new molecular adsorption states from which thiophene desorbs at 310 K and 360 K [11]. On the (0001) face of rhenium, adsorbed carbon also blocks thiophene decomposition, but thiophene interacts very weakly with this surface giving rise to molecular desorption peaks at 180 K and 230 K [12]. As

discussed in Chapter 4, theoretical calculations by MacLaren et al. also suggest that the height of an adsorbate above the metal surface influences its poisoning effect [19]. Their calculations of the local density of states (LDOS) indicate that as the height of an adsorbed carbon atom is increased from 0.4 Å to 1.3 Å, the LDOS at the surface, and therefore the predicted catalytic activity, decreases strongly. This provides further evidence that carbon's poisoning effect is dependent upon its overlayer structure. In summary, at normal temperatures for thiophene HDS reactions (500-700 K), adsorbed carbon is carbidic on the Mo(100) surface and does not block active sites for thiophene HDS. For the Re(0001) and Re($10\bar{1}0$) surfaces on the other hand, adsorbed carbon is graphitic-like and strongly poisons their HDS activity.

As shown is Figures 3.12 and 3.13, the AES line shapes for carbon on the Re(0001) and Re($10\bar{1}0$) surfaces change with temperature. The line shape evolves from one resembling most closely graphitic and amorphous carbon at low annealing temperatures to a peak shape most similar to carbon in a metal carbide after annealing above 900 K. These changes suggest that the form of the carbon overlayers becomes more carbidic in nature following annealing at high temperatures. On the basis of the preceding discussion, this change would be expected to coincide with a higher thiophene HDS activity. The results presented in Figure 5.11 show that this is <u>not</u> the case as carbon covered surfaces annealed at 800 K and 1100 K were found to have similar turnover frequencies for HDS.

The interaction of carbon with rhenium surfaces has also been investigated by other researchers. Ducros et al. studied ethylene decomposition on the Re(0001) surface and found that dehydrogenation of ethylene is complete by 700 K and that C-C bond cleavage occurs by 800 K [10]. This latter conclusion is based upon observation of a c(4×2) LEED pattern following heating of an ethylene

saturated surface to 770 K. TPD of ethylene indicates that the carbon coverage is 0.25 ML, hence the spacing between carbon atoms in the unit cell requires that scission of the C-C bonds has occurred. Our AES studies, however, indicate that the structure of the carbon overlayers is graphitic-like up to 900 K, above which it resembles carbidic-type carbon. Gall and coworkers have also investigated the structure of carbon overlayers on rhenium [20]. They used AES and TPD to study the interaction of carbon with a polycrystalline rhenium ribbon and report carbon AES line shapes similar to those shown in Figures 3.12 and 3.13. In addition, they observed a stable rhenium carbon surface phase formed at $T \geq 1500$ K which persisted to $T \geq 2600$ K. Although the rhenium-carbon phase diagram shows no carbide phases, the authors believe the stable phase observed is a surface carbide. The reactivity of the carbon covered rhenium surfaces was probed using the UHV dissociation of CsCl as a test reaction. Clean rhenium, the surface carbide and carbon covered surfaces annealed between 800-1100 K were found to be active towards CsCl dissociation while a graphite covered surface was inactive.

In this work, AES indicates that carbon overlayers annealed to 800 K are more graphitic in nature while overlayers annealed to 1100 K are more carbidic-like. The results of Gall et al. indicate that carbon overlayers formed on the Re(0001) and Re($10\bar{1}0$) surfaces by adsorption of hydrocarbons and annealed between 800 K and 1100 K are intermediary between a surface carbide and an overlayer of graphite. The most important point, however, is that carbon species produced at the two annealing temperatures are both strong poisons of HDS activity. This suggests that the carbon overlayers sit well above the rhenium metal plane and therefore block active sites for HDS. This is in contrast to the Mo(100) surface for which adsorbed carbon sits in the plane of the metal and does not decrease the activity of the catalyst.

5.6.4 Deactivation of a Rhenium Foil at High Conversions

As discussed in Chapter 4, hydrogen sulfide was found to poison the Mo(100) surface while cis-2-butene had no effect on catalyst activity, both results being consistent with HDS studies over industrial Co/Mo catalysts [15]. At H_2S and cis-2-butene partial pressures corresponding to 5-15 % thiophene conversion, H_2S also strongly decreases the activity of a Re foil catalyst while the effect of cis-2-butene is negligible (see Figure 5.12). The observation that cis-2-butene does not affect the HDS rate indicates that it does not compete with thiophene for adsorption sites on the catalyst surface and that desulfurization and hydrogenation occur on different sites. As in the case of a Mo(100) single crystal catalyst, the poisoning of a Re foil is reversible as the activity of the catalyst could be restored to its initial clean surface value by removing the H_2S from the reactor. This indicates that H_2S does not dissociate on the catalyst surface under reaction conditions to give strongly bound sulfur similar to that formed by prior deposition in UHV.

5.6.5 Kinetics and Mechanism of Thiophene HDS over Rhenium Surfaces

The product distributions from thiophene HDS over the Re(0001) and Mo(100) surfaces as well as from butadiene hydrogenation over a rhenium film are shown in Table 5.1 [21,4]. The similarity of the three product distributions leads us to conclude that the HDS pathway is essentially the same over Re and Mo surfaces and that butadiene is an intermediate in the reaction. This indicates that thiophene must be desulfurized on the catalyst surface prior to hydrogenation of its ring since tetrahydrothiophene HDS produces a different product distribution over Mo(100) [21]. Apparently, the desulfurization of thiophene on the catalyst surface yields adsorbed butadiene and its hydrogenation then determines the product

distribution. The reaction is clearly kinetically controlled as thermodynamics predicts that under the conditions used the products should consist almost entirely of butane.

The complexity of the thiophene HDS reaction makes it very difficult to formulate a reaction mechanism based upon kinetic studies. The temperature and partial pressure dependence data presented in Section 5.2 do, however, permit a number of observations to be made about the reaction. The positive dependence of the overall HDS rate on the thiophene and hydrogen pressures indicates that neither reactant saturates the rhenium surface under the reaction conditions studied. In addition, thiophene and hydrogen do not compete for the same adsorption sites as is the case for many hydrogenation reactions for which negative order dependence of the rate on hydrocarbon pressure is observed. This is consistent with the result that HDS and hydrogenation occur on different sites on the catalyst surface as arrived at in Section 5.6.4.

The non-Arrhenius behavior of thiophene HDS over rhenium for $T \geq 673$ K can be understood if the temperature dependence data of the individual products is considered. The products which exhibit large deviation from Arrhenius behavior, the butenes and butane, are those whose rates depend strongly on the hydrogen pressure. For surface catalyzed reactions, negative deviation from the Arrhenius equation is usually caused by depletion of the surface in one of the reactants. The kinetic data suggests that the surface becomes depleted in hydrogen at temperatures of 673 K and above. The observation with AES of graphite overlayers on the rhenium foil surface following high temperature reactions suggests that the low coverages of surface hydrogen under these reaction conditions causes dehydrogenation of hydrocarbon intermediates to graphite to be favored over hydrogenation to products which desorb from the catalyst surface.

5.6.6 Explanation of the Structure Sensitivity

Re(0001) and Re($10\bar{1}0$) surfaces maintain higher HDS activities when they are initially clean than when they are covered with predeposited overlayers of sulfur or carbon. This indicates that the initially clean rhenium single crystals do not become covered with strongly bound overlayers of sulfur or carbon under reaction conditions. Instead the single crystal surfaces are apparently covered with only reversibly bound species which either desorb into the gas phase or are hydrogenated to products. This suggests that HDS of thiophene does indeed occur directly on the metal surface and not on an adsorbate overlayer, in contrast to the Mo(100) surface for which it was found that thiophene HDS occurred on an overlayer of adsorbed carbon [15]. Consequently, thiophene's interaction with the rhenium surfaces is not moderated by an adsorbate overlayer and the structure of the different crystal faces influences their HDS activity.

The trend of increasing HDS activity of the rhenium surfaces determined in this work (0001)<($11\bar{2}1$)<($11\bar{2}0$)<($10\bar{1}0$) does not mirror the trend of increasing surface openness (0001)<($10\bar{1}0$)<($11\bar{2}0$)<($11\bar{2}1$) as measured by the surface atomic density. This indicates that surface openness is not the determining factor in catalyst activity. Another reaction which exhibits structure sensitivity is the ammonia synthesis reaction over iron and rhenium single crystal surfaces which has been found to be very structure sensitive [22,23]. Again, the activity of the different surfaces could not be correlated to their openess but instead could be related to the density of highly coordinated atoms (Fe: C_7 sites, Re: C_{10}, C_{11} sites) exposed at the surface of the single crystals. Theoretical calculations by Falicov and Somorjai suggest that the highly coordinated metal atoms exposed at the surface have high catalytic activity because these sites experience the largest

charge fluctuations in the solid [24]. However, steric effects must also be examined when considering the catalytic activity of a site. For a surface atom to be catalytically active, it must be accessible for adsorption of the reactant species. It is generally accepted that dissociation of molecular nitrogen is the rate limiting step in the ammonia synthesis reaction. N_2 is a relatively small molecule (van der Waal's radii = 1.5 Å) and is expected to be able to interact with exposed second and third layer metal atoms at the surface. These are believed to be the most active sites for ammonia synthesis as they are the most highly coordinated surface atoms and are still accessible for adsorption of the reactant molecules.

In the HDS reaction, thiophene's relatively large size (vertical adsorption: v.d.W. radius = 1.85 Å, horizontal adsorption: v.d.W. radius = 3.5 Å) probably limits its accessibility to metal atoms in only the topmost layer of the surface. Using this assumption, examination of the coordination numbers of the top layer atoms of the surfaces studied may help explain the observed trend in activity. In Figure 5.13, the HDS activity of the rhenium single crystal catalysts is plotted as a function of the coordination number of the top layer rhenium atoms (see Figure 3.3). The "volcano" shaped curve shown in Figure 5.13 is common throughout heterogeneous catalysis and can be understood by relating the catalytic activity to the chemisorption energy of species involved in the reaction [25]. If we assume that the active sites for thiophene HDS on the rhenium surfaces are composed of the top layer rhenium atoms, the trend in activity can be explained. On the left side of the curve, a C_6 surface atom is the most coordinately unsaturated compared to the other top layer surface atoms and would be expected to bind species involved in the reaction the most strongly. Although the coverage of reactant and intermediate species will be high, the species may be so stable that they do not decompose into products, therefore causing the Re$(11\bar{2}1)$ surface to have a

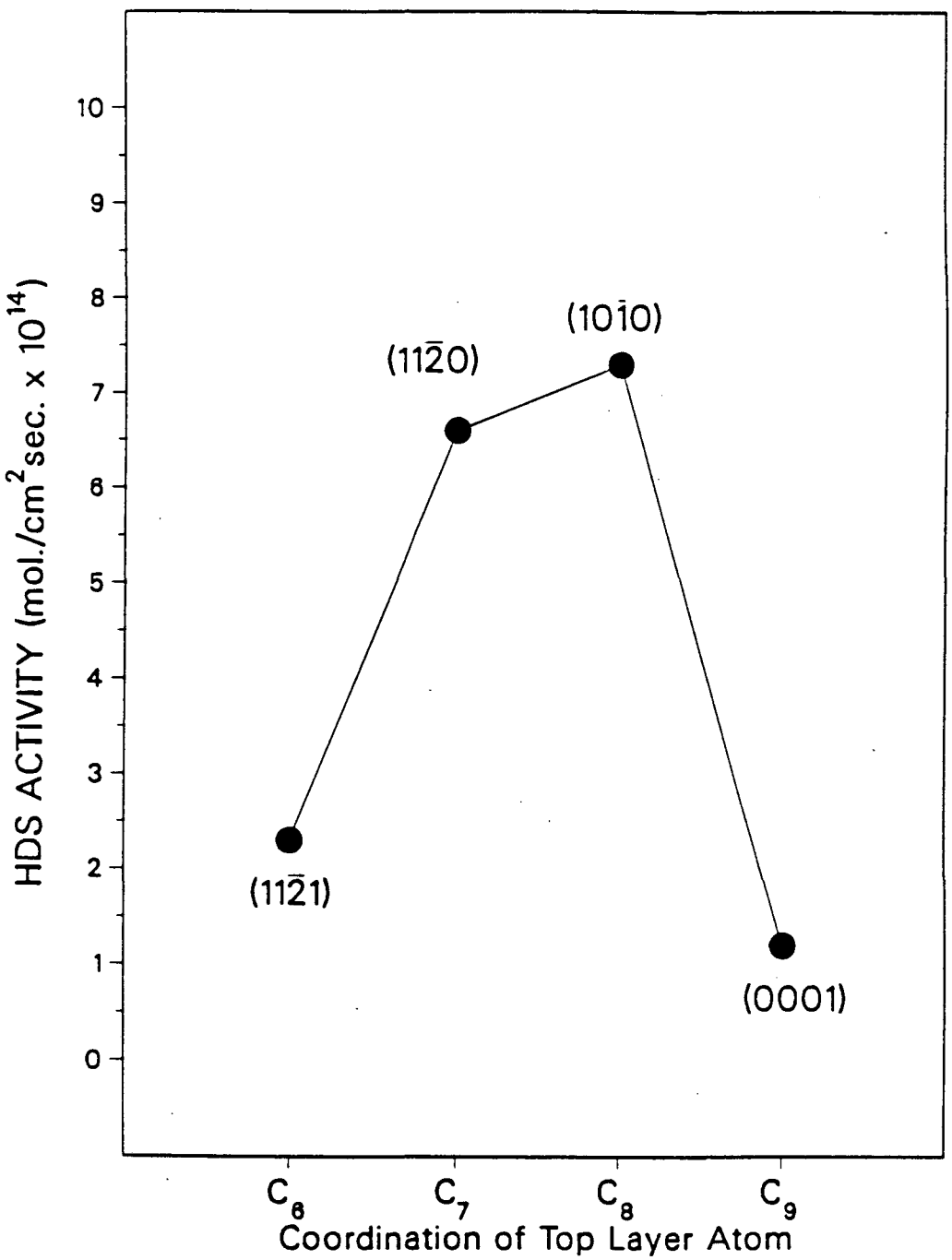

XBL 879-3761

Figure 5.13: HDS activity of the rhenium single crystal surfaces studied as a function of the top layer atom coordiantion numbers.

relatively low activity. In addition, this surface is the most likely to experience product inhibition due to strong binding of product molecules on the active sites. At the other extreme, a C_9 surface atom is the most coordinately saturated and will therefore be expected to interact the weakest with species involved in the reaction. As a result, the coverage of reactant and intermediate species will be lower and the surface will be less able to "activate" thiophene molecules. Therefore the turnover frequency of the Re(0001) surface would also be expected to be low. In addition the close-packed structure of this surface may sterically hinder adsorption of reactant species. The most active surfaces, the Re($10\bar{1}0$) and Re($10\bar{2}0$) surfaces, are those which have top layer atoms with coordination numbers (C_7, C_8) intermediary between the two extremes described above. Unfortunately, it is not possible to directly determine the chemisorption energies of thiophene on the different surfaces since thiophene decomposes to carbon, sulfur and hydrogen instead of desorbing molecularly. However, desorption energies have been determined for sulfur on the Re(0001) and Re($10\bar{1}0$) surfaces. At low coverages, sulfur desorbs from Re(0001) at 1600 K (E_d = 98 kcal/mole) and from Re($10\bar{1}0$) at 1700 K (E_d = 104 kcal/mole) [13]. Sulfur is believed to be adsorbed on three-fold sites formed betweem three C_9 atoms on the Re(0001) surface and on three-fold sites formed between two top layer C_8 atoms and one second layer C_{10} atom on the Re($10\bar{1}0$) surface. Clearly, sulfur chemisorbs more strongly on Re($10\bar{1}0$) which may indicate that thiophene and other species in the reaction pathway also bind more strongly to this surface.

References

[1] T. A. Pecoraro and R. R. Chianelli. *J. Catal.* **67** (1981) 430.

[2] M. J. Ledoux, O. Michaux, G. Agostini, and P. Panissod. *J. Catal.* **102**

(1986) 275.

[3] S. J. Tauster, T. A. Pecoraro, and R. R. Chianelli. *J. Catal.* **63** (1980) 515.

[4] J. Grant, R. B. Moyes, and P. B. Wells. *J. Catal.* **51** (1978) 355.

[5] J. B. Benzinger and R. E. Preston. *Surf. Sci.* **161** (1985) 373.

[6] M. E. Bussell, A. J. Gellman, and G. A. Somorjai. *J. Catal.* **110** (1988) 423.

[7] M. E. Bussell, A. J. Gellman, and G. A. Somorjai. *Catal. Lett.*, (submitted for publication) .

[8] A. J. Gellman. PhD thesis, University of California, Berkeley, 1985.

[9] J. F. Lang and R. I. Masel. *Surf. Sci.* **183** (1987) 44.

[10] R. Ducros, M. Housley, M. Alnot, and A. Cassuto. *Surf. Sci.* **71** (1978) 433.

[11] D. G. Kelly, M. Salmeron, and G. A. Somorjai. *Surf. Sci.* **175** (1986) 465.

[12] D. G. Kelly, J. A. Odriozola, and G. A. Somorjai. *J. Phys. Chem.* **91** (1987) 5695.

[13] D. G. Kelly, A. J. Gellman, M. Salmeron, G. A. Somorjai, V. Maurice, M. Huber, and J. Oudar. *Surf. Sci.*, (in press) .

[14] A. J. Gellman, M. E. Bussell, and G. A. Somorjai. *J. Catal.* **107** (1987) 103.

[15] M. E. Bussell and G. A. Somorjai. *J. Catal.* **106** (1987) 93.

[16] S. H. Overbury and P. C. Stair. *J. Vac. Sci. Technol. A* **1** (1983) 1055.

[17] D. G. Kelly. PhD thesis, University of California, Berkeley, 1987.

[18] R. Rosei, M. De Crescenzi, F. Sette, C. Quaresima, A. Savoia, and P. Perfetti. *Phys. Rev. B* **28** (1983) 1161.

[19] J. M. Maclaren, J. B. Pendry, R. W. Joyner, and P. Meehan. *Surf. Sci.* **175** (1986) 263.

[20] N. R. Gall, S. N. Mikhailov, E. V. Rut'kov, and A. Ya. Tontegode. *Surf. Sci.* **191** (1987) 185.

[21] A. J. Gellman, D. Neiman, and G. A. Somorjai. *J. Catal.* **107** (1987) 92.

[22] D. R. Strongin, J. Carazza, S. R. Bare, and G. A. Somorjai. *J. Catal.* **103** (1987) 213.

[23] M. Asscher, J. Carrazza, M. M. Khan, K. B. Lewis, and G. A. Somorjai. *J. Catal.* **98** (1986) 277.

[24] L. M. Falicov and G. A. Somorjai. *Proc. Nat. Acad. Sci.* **82** (1985) 2207.

[25] R. P. H. Gasser. *Introduction to Chemisorption and Catalysis by Metals*, pages 185–190. Clarendon Press, Oxford, 1985.

Chapter 6

Thiophene Hydrodesulfurization over Transition Metal Foils

6.1 Introduction

The final chapter of this thesis concerns the investigation of thiophene hydrodesulfurization over polycrystalline foils of cobalt, molybdenum and rhenium metals. Foils were employed in this work in addition to single crystals for the following reasons:

1. The polycrystalline nature of foils suggests that they more closely model the heterogeneous structure of an industrial catalyst than do single crystals which are relatively flat on the atomic scale. The density of surface defects is much higher for a metal foil than for a well-polished single crystal. Therefore, catalytic studies over metal foils allow one to establish the importance of structural defects in determining the catalytic activity of a surface.

2. Cobalt undergoes a phase transition from face centered cubic to hexagonal close-packed structure at $\sim$ 693 K. If a cobalt single crystal is heated above 693 K and then cooled below the transition temperature, the sample is usually rendered polycrystalline. Hence, it is impractical to use cobalt sin-

gle crystals as model HDS catalysts as they are extremely difficult to clean below 693 K.

The disadvantage of using polycrystalline foils as model catalysts is that they are difficult to characterize structurally with surface science techniques that are routinely available. Accordingly, the work described in this thesis has focussed on single crystals as model catalysts, and the results obtained over Mo and Re foils have been obtained primarily for the purpose of making comparisons with single crystals.

Thiophene HDS has been investigated over a cobalt foil since Co is used as a promoter in industrial HDS catalysts. The surface chemistry of hydrodesulfurization will not be completely understood until the role of cobalt is fully elucidated. As discussed in the first chapter, the addition of cobalt to molybdenum catalysts results in an increased activity of the catalyst for the HDS of thiophene and other sulfur containing compounds [1]. The ratio of molybdenum to cobalt is always greater than one and cobalt is therefore considered to be a promotor. For this reason, molybdenum has received more attention than cobalt in this thesis. However, it has been proposed in the literature by Prins and De Beer that a sulfided cobalt phase actually comprises the active phase of the catalyst and that MoS_2 simply serves as a secondary support to keep the cobalt dispersed and from diffusing into the alumina support [2,3]. The evidence which supports this proposal is based upon the observation that sulfided cobalt supported on an inert carbon support displays superior activity than sulfided molybdenum on the same support. In addition, the so-called Co-Mo-S phase identified by Topsoe and coworkers to be the active component of industrial HDS catalysts was also observed to exist in a carbon supported cobalt catalyst [4,3]. In other words, De Beer et al. suggest that molybdenum need not be present to produce the active component of the catalyst.

The catalytic results of Prins and De Beer, however, are not in agreement with the work of the groups of Chianelli and Ledoux [5,6]. Chianelli found unsupported molybdenum and cobalt sulfides to have similar activities while Ledoux found MoS_2 to be almost three times more active than cobalt sulfide when the sulfides are supported on carbon. To help resolve this disagreement and to initiate a surface science and catalytic study of cobalt promotion of molybdenum catalysts, thiophene HDS activities were measured for cobalt and molybdenum foils. These results are discussed in the remaining sections of this chapter along with HDS over a rhenium foil.

6.2 Thiophene HDS over Co, Mo and Re Foils

The thiophene HDS activities of polycrystalline foils of cobalt, molybdenum and rhenium metals are shown in Figure 6.1. The reaction conditions were identical to those used for HDS activity measurements over single crystal surfaces (P_{Th} = 3.0 Torr, P_{H_2} = 780 Torr, T = 613 K). The product distributions differ significantly for the three metals and are compared in Table 6.1.

Table 6.1: Product Distributions for Thiophene HDS.

	Metal Foil		
Product	*Cobalt*	*Molybdenum*	*Rhenium*
Butadiene	11.%	2.5%	7.0%
1-Butene	44.	55.	47.
trans-2-Butene	24.	19.5	23.6
cis-2-Butene	13.5	12.	13.9
Butane	7.5	11.	8.5

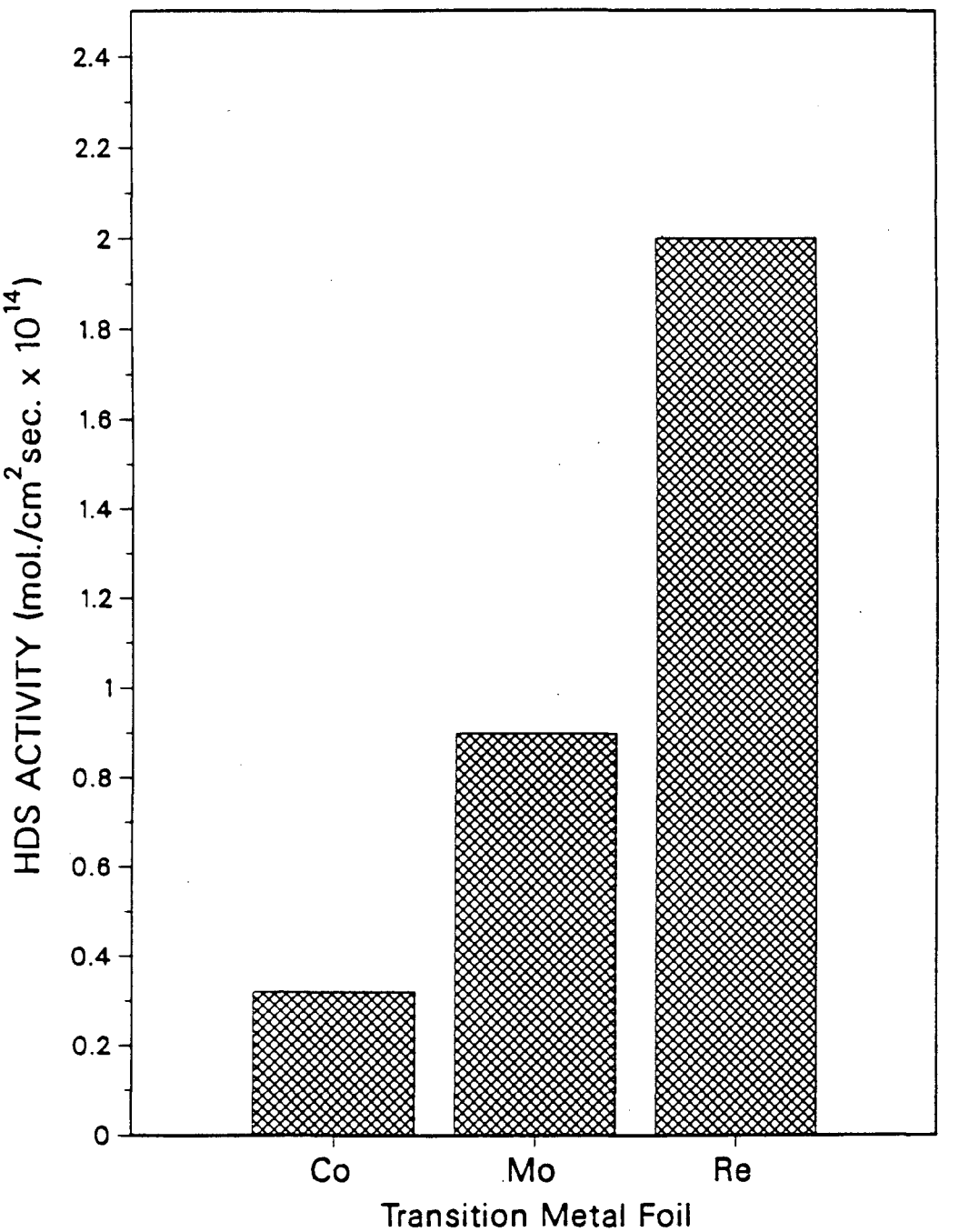

Figure 6.1: Thiophene HDS activities of cobalt, molybdenum and rhenium foils (P_{Th} = 3.0 Torr, P_{H_2} = 780 Torr, T = 613 K).

6.3 Discussion

6.3.1 Trend of HDS Activities of Co, Mo and Re foils

The ratio of the HDS activities measured in this work for the three metals are compared in Table 6.2 with those for the same metals in sulfides as taken from the studies of Ledoux, Chianelli and Prins [5,6,2]. It is clear that the trend of

Table 6.2: Comparison of HDS activities.

Study	*Cobalt*	*Molybdenum*	*Rhenium*
[a]This work	1.0	2.8	6.3
[b]Ledoux	1.0	2.2	4.3
[c]Chianelli	1.0	1.0	4.3
[d]Prins	1.0	0.25	3.8

[a]Metal foils.
[b]Metal sulfides supported on carbon [6].
[c]Unsupported metal sulfides [5].
[d]Metal sulfides supported on carbon [2].

HDS activities measured for Co, Mo and Re foils is in best agreement with that observed by Ledoux and coworkers [6]. Close agreement with the trend in activity measured by Chianelli is not expected as the only method by which the authors measured the surface area of their catalysts was the BET method which does not distinguish between active and inactive sites in a metal sulfide [5]. Therefore, the similarity in acitivities measured for cobalt sulfide and molybdenum sulfide in Chianelli's work could be coincidental.

The biggest discrepancy among the four studies is the higher activity for cobalt than molybdenum measured by Prins and coworkers [2]. This is especially surprizing since comparison of the catalyst preparation methods used by Prins and Ledoux do not reveal the existence of major differences in the composition or

structure of their catalysts. In any case, the results presented here support the observation that molybdenum is more active than cobalt. Therefore, it appears that the role of cobalt is to promote molybdenum HDS catalysts instead of cobalt itself being the active component. As discussed in Chapter 1, the promotional effect of cobalt is not well understood and deserves the attention of a combined surface science and catalysis study. The general agreement of the trend in HDS activities measured here for metal surfaces with those for metal sulfides in the literature suggests that this approach would be well worth undertaking.

6.3.2 Importance of Surface Defects in Thiophene HDS over Metal Surfaces

Comparison of the HDS activities of Mo and Re foils with those of single crystals of the same metals indicates that the orientation of the crystal face exposed at the surface is more important than the presence of surface defects. A molybdenum foil was found to have an HDS activity of 0.9×10^{14} mol./cm^2·sec compared to activities of $(1.1\text{-}1.2)\times10^{14}$ mol./cm^2·sec determined for the low miller index planes of molybdenum. If defect sites exhibited a far higher activity than sites found on a homogeneous surface than the activity of the foil would be expected to be higher than that of a low miller index single crystal. Clearly, surface defects are not a major factor in determining the activity of molybdenum metal surfaces for thiophene HDS. Similar results to those over molybdenum were also observed for rhenium. An activity of 2.0×10^{14} mol./cm^2·sec was measured for a rhenium foil, while single crystals of rhenium had activities in the range $(1.2\text{-}7.3)\times10^{14}$ mol./cm^2·sec. The fact that the Re foil has an activity between the extremes measured for the single crystals indicates that the foil surface is composed of a distribution of crystallite faces, with the predominant one being the thermodynamically most stable (0001)

face.

References

[1] R. Prins, V. H. J. de Beer, and G. A. Somorjai. *to be published.*

[2] V. H. J. De Beer, J. C. Duchet, and R. Prins. *J. Catal.* **72** (1982) 369.

[3] A. M. Van De Kraan, M. W. J. Craje, E. Gerkema, W. L. T. M. Ramselaar, and V. H. J. De Beer. *Appl. Catal.* **39** (1988) L7.

[4] H. Topsoe and B. S. Clausen. *Catalysis and Surface Science*, pages 95–120. Volume 21, Marcel Dekker, New York, 1985.

[5] T. A. Pecoraro and R. R. Chianelli. *J. Catal.* **67** (1981) 430.

[6] M. J. Ledoux, O. Michaux, G. Agostini, and P. Panissod. *J. Catal.* **102** (1986) 275.

LAWRENCE BERKELEY LABORATORY
CENTER FOR ADVANCED MATERIALS
1 CYCLOTRON ROAD
BERKELEY, CALIFORNIA 94720